TUDelft

Delft University of Technology

Electrolysers, Fuel Cells and Batteries
Analytical Modelling

Haverkort, J.W.

Important note
To cite this publication, please use the final published version (if applicable).
Please check the document version above.

Electrolysers, Fuel Cells and Batteries: Analytical modelling

J.W. Haverkort

TU Delft OPEN

Electrolysers, Fuel Cells and Batteries

analytical modelling

J.W. Haverkort

Preface

Prerequisites

This book was written to accompany the lectures of the M.Sc. course ME45203: Electrolysers, Fuel Cells and Batteries at Delft University of Technology. Its main aim is to create an understanding of the mathematical description of the relationship between current and voltage in electrochemical devices. A solid background in physical transport phenomena is assumed, while some training in electrochemistry, batteries or fuel cells is highly beneficial. Reading and re-reading the first chapter before continuing with the other chapters may be advisable when this is lacking.

Reader guidelines

Important equations will be boxed

$$\boxed{j_\perp = j_* \left(e^{\eta/b_a} - e^{-\eta/b_c} \right).}$$
(1)

We will indicate logical steps that are important but perhaps not immediately obvious, and may require one or a few lines of derivation, with the blue "exercise figure": ⅄. The student is encouraged to work out these steps independently. Footnotes, appendices, and sections denoted with * are optional additional reading material and are not part of the curriculum of ME45203.

Content

The first three chapters of the book explore the fundamental concepts related to electrochemistry, transport, and porous electrodes, respectively. The final four chapters are named after particular applications: batteries, fuel cells, electrolysers, and redox flow batteries, respectively. However, from the perspective of analytical modelling, there are more similarities than differences between these devices, so these chapters focus on those aspects that are distinctively associated with these applications. For batteries, treated in chapter 4, a distinctive feature is that their porous electrodes are involved in the reaction as products or reactants. Chapter 5 on fuel cells focuses on the management of water produced in the reaction. This includes how to model the

multiphase flow in diffusion layers or gas diffusion electrodes and inside a flooded catalyst layer. While these aspects are perhaps most often associated with fuel cells, they can be equally important for proton exchange membrane electrolysers or CO_2 electrolysers, for example. In chapter 6 on electrolysers we examine the effects of gas bubbles. Contrary to the previous chapters, the direction normal to the current is modelled here. Finally, in chapter 7 on redox flow batteries, both directions parallel and normal to the current are considered in a quasi-two-dimensional model that considers the flow of reactants through a flow field.

Acknowledgements

Delft, April 2024   J.W. (Willem) Haverkort

Contents

Nomenclature

Dimensionless variables

$\bar{c}$	Concentration c/c_0	
$\mathcal{B}$	Bruggeman's coefficient in $\tau^2 \approx \epsilon^{-\mathcal{B}}$	
$\mathcal{E}$	Electrode effectiveness factor	
$\bar{\phi}$	Electrolyte potential $F\phi/\mathcal{R}T$	
r	Reaction order	
s	Liquid water saturation	
S	Transfer coefficient, inverse mass transfer resistance	
$\mathrm{S_{oC}}$	State of charge	
t_i	transference/transport number of ion i	
X	Conversion $(c_{\mathrm{in}} - c_{\mathrm{out}})/c_{\mathrm{in}}$	
z	Ion charge number	

Constants

e	Elementary charge $1.602176634 \cdot 10^{-19}$	[C]
F	Faraday constant 96485.3329	[C/mol]
k_{B}	Boltzmann constant $1.38064852 \cdot 10^{-21}$	[J/K]
N_{A}	Avagadro constant $6.02214076 \cdot 10^{23}$	[-]
$\mathcal{R}$	Gas constant 8.31446	[J/mol$_{\mathrm{g}}$/K]

Dimensionless numbers

Gz	Graetz number $\langle w \rangle l^2/hD$	
M	Thiele modulus $1/\mathcal{E} \to 0$	
Pe	Péclet number $\langle w \rangle l/D$	
Re	Reynolds number wl/ν	

Sh   Sherwood number $Nl/D\Delta c$

Greek variables

α	Charge transfer coefficient	[-]
δ	Boundary layer thickness	[m]
ϵ	Porosity	[-]
η	Activation overpotential $\Phi - \phi - \left(\Phi - \phi\right)_{\text{eq}}$	[V]
γ	Surface tension	[N/m]
κ	Effective electrolyte conductivity	[S/m]
λ	Pore size distribution parameter	[-]
μ	Dynamic viscosity	[Pa s]
ν	Kinematic viscosity	[m^2/s]
Φ	Electrostatic potential in electrode	[V]
ϕ	Electrostatic potential in electrolyte	[V]
ρ	Density	[kg/m^3]
ρ_q	Charge density	[C/m^3]
σ	Effective electrode conductivity	[S/m]
τ	Tortuosity	[-]
ε	Gas fraction	[m$^3_{\text{g}}$/m^3]
φ_{e}	Voltage efficiency	[-]

Lower case roman

a	Volumetric surface area	[m$^2_{\text{s}}$/m^3]
b	Tafel slope $RT/\alpha F$	[V]
c	Concentration	[mol m^{-3}]
c_{m}	Cup mixing concentration $\frac{1}{\langle w \rangle l} \int_0^l wc\,dx$	[mol m^{-3}]
h	Flow channel height	[m]
j	Magnitude of total current density	[A/m^2]
j_*	Superficial exchange current density	[A/m$^2_{\text{s}}$]
k	Areal reaction rate constant	[mol^{1-r} s^{-1} m^{3r-2}]
n	Electrons per reactant/product molecule	[mol$_{\text{e}-}$/mol]
p	Pressure	[Pa]
q	Electric charge	[C]
r	Pore radius [m]	

t	Time	[s]
x	Coordinate in the direction of the main current	[m]
y	Coordinate normal to x and z	[m]
z	Coordinate parallel to flow, normal to main current	[m]
z	Charge number q/e	[-]

Mathematical operators

cosh x Hyperbolic cosine $\frac{1}{2}(e^x + e^{-x})$

ln x Natural logarithm $e^{\ln x} = x$

sinh x Hyperbolic sine $\frac{1}{2}(e^x - e^{-x})$

tanh x Hyperbolic tangent sinh x/cosh x

Notation

′   A spatial derivative d/dx ($d/d\bar{x}$ dimensionless)

‾   Overbars denote dimensionless quantities

Δ   Difference right minus left, or after minus before

$\hat{n}$ Unit vector, normal to a surface into the fluid

⟨.⟩   Spatial average, $\frac{1}{x}\int_0^x .dx$ or $\frac{1}{z}\int_0^z .dz$ in one dimension

D/Dt Material derivative $\frac{\partial}{\partial t} + \boldsymbol{u} \cdot \nabla$

opt   Optimised for energy efficiency

Subscripts

⊥   Normal to a surface, into the fluid

∥   Parallel to particle/parcel trajectory

i Species index

x, y, z Vector component in the x- y- or z-direction

+   Positively charged ions, cations

-   Negatively charged ions, anions

0,L At $x = 0$ or $x = L$

a   Anode

c   Cathode

cap   Capillary

d   Discharge/discharged

diff   Diffusion (superscript)

eq   Equilibrium

fl	Fluid	
g	Gas	
in,out	At the inlet $z = 0$ or outlet $z = h$, respectively	
l	Liquid	
lim	Limiting	
lin	Linear	
m	Molecular / material	
mig	Migration (superscript)	
O	Oxidation	
opt	Optimal with respect to energy efficiency	
R	Reduction	
ref	Reference	
s	Solid/Surface	
tn	Thermoneutral	
tot	Total	

Upper case roman

A	Projected electrode area	[m^2]
AR	Areal resistance	[Ωm^2]
C_p	Heat capacity, at constant pressure	[J kg^{-1} K^{-1}]
D	Effective diffusion coefficient	[m^2 s^{-1}]
E	Electrode potential	[V]
$\mathcal{E}_a$	Activation energy	[J]
G	Gibbs free energy	[J/mol]
I	Current	[A]
J_*	Total superficial exchange current density aLj_*	[A/m^2]
J_κ	Characteristic current density $b\kappa/L$	[A/m^2]
l	Flow channel thickness	[m]
L	Electrode thickness	[m]
$\mathcal{M}$	Mobility, u/F in equilibrium	[s/kg]
M	Molar mass	[kg mol^{-1}]
N	Molar flux	[mol m^{-2} s^{-1}]
R	Radius of a particle or bubble	[m]
S	Source term	[something/m^3/s]

T	Temperature	[K]
$\mathcal{U}$	Potential energy	[J]
V	Voltage	[V]
$\mathcal{V}$	Volume	[m^3]
$\mathcal{V}_{\mathrm{m}}$	Molar volume M/ρ	[m^3/mol]

Vectors

$\boldsymbol{A}$	Area, normal to surface	[m^2]
$\boldsymbol{E}$	Electric field	[V/m]
$\boldsymbol{F}$	Force	[N]
$\boldsymbol{I}$	Current	[A]
$\boldsymbol{i}$	Electronic current density	[A m^{-2}]
$\boldsymbol{j}$	Ionic current density	[A m^{-2}]
$\boldsymbol{N}$	Molar flux	[mol m^{-2} s^{-1}]
$\boldsymbol{U}$	Superficial velocity with components U, V, W	[m/s]
$\boldsymbol{u}$	Interstitial velocity with components u, v, w	[m/s]

Other conventions

1. The cathode is the electrode at which the reduction occurs, and oxidation occurs at the anode.

2. Cell potentials are that of the cathode minus that of the anode $E_{\mathrm{cell}} = E_{\mathrm{c}} - E_{\mathrm{a}}$, so positive for Galvanic cells and negative for electrolytic cells.

3. We will draw the cathode on the right and the anode on the left.

4. Surface local fluxes $N_\perp$ and $j_\perp$ are always directed from the solid surface into the electrolyte, so $j_\perp$ is positive on the anode and negative on the cathode.

5. Since anodic currents are positive, the overpotential will also be positive on the anode, and negative on the cathode.

6. Tafel slopes b will be used on an e-folding basis, rather than per decade.

7. The number of electrons $n > 0$ transferred in the reaction $O + n\mathrm{e}^- \rightarrow R$; per number of reactant or product molecules as indicated.

Chapter 1

Electrochemistry

This introductory chapter constitutes a refresher of the basic electrochemical terminology and notation necessary for the subsequent chapters. In this chapter, the basic foundations are laid in terms of electrostatics, equilibrium thermodynamics, and electrochemical kinetics culminating in a simplified cell model.

1.1 Electrostatics

An electric charge q [C] in an electric field E [V/m] experiences an electrostatic force

$$F = qE. \tag{1.1}$$

Since this is a conservative force, the electric field can be expressed in terms of an electrostatic potential ϕ as

$$E = -\nabla \phi. \tag{1.2}$$

Combining these two equations, we get $F = -q\nabla\phi$, where we see that a positive charge moves down along a potential gradient while a negative charge moves up in potential. The electric potential energy of a charge is the negative of the work done by an electric field in moving the charge within such a field

$$\mathcal{U} = -\int F \cdot dx = q\Delta\phi, \tag{1.3}$$

where $\Delta\phi$ is ϕ at the end minus the start of the path that the charged particle traverses. Positively charged particles thus increase their potential energy when the potential increases, while negatively charged particles increase their potential energy when the potential decreases. Note that in all these equations only *differences* in potential, termed *voltages*, are physically relevant.

19

1.2 Current and resistance

When thinking of conduction and current we usually think about the movement of electrons. While this is most relevant inside metals, electrochemistry is also concerned with the flow of charged molecules, or ions. Media that conduct ions are called electrolytes. In general, we can define current as the flow of *charge*, regardless of whether the *charge carriers* are electrons, ions, or other charged particles. The movement of ion charge in the form of a current I [C/s=A] through an area A constitutes a current density i [A/m^2]

$$i = \frac{I}{A}. \tag{1.4}$$

Since the flow of ions is not constrained to any preferential direction, in general, the ionic current density $\boldsymbol{i}$ is a vector field that can have a different direction and magnitude at each location.

Often, there is an approximate proportionality between the current density $\boldsymbol{i}$ and the electric field, expressed through[1]

$$\boxed{\boldsymbol{i} = \kappa \boldsymbol{E}.} \tag{1.5}$$

In the next chapter, we will get into why this is often the case and also when it does not hold. The constant of proportionality is the *conductivity* κ [S/m = Ω^{-1}m^{-1}], which is the inverse of the *resistivity*. These material properties depend strongly on the charge carrier and physical parameters, such as temperature, and can differ widely between materials. Metals, for example, typically conduct electrons very well. Aqueous salt solutions, on the other hand, are typically insulating for electrons but conduct ions well. We will refer to such ionic conductivity with the symbol κ, while reserving the symbol σ for the conductivity of a material towards electrons. When speaking of conductivity, it is therefore important to specify with respect to what particle. We will also use a different symbol $\boldsymbol{j}$ for the electronic current density so that Ohm's law for electrons reads $\boldsymbol{j} = \sigma \boldsymbol{E}$. Since the ionic current is converted to electronic at the electrode, charge conservation gives $j = I/A$ as well. We will typically use the symbol j for the current density unless explicitly referring to the current density magnitude inside the electrolyte.

Referring to Figure 1.1, we consider the case in which there is a difference in potential $\Delta \phi \equiv \phi(L) - \phi(0) < 0$ between the back and front of a block of material of thickness L. The average electric field strength in the x-direction is obtained by integrating Eq. (1.2) to give $E_x = -\Delta\phi/L$, which after inserting in Eq. (1.5) gives the positive current density in the x-direction,

$$i_x = -\frac{\kappa \Delta \phi}{L} \tag{1.6}$$

---

[1]This is the continuum formulation of Ohm's law.
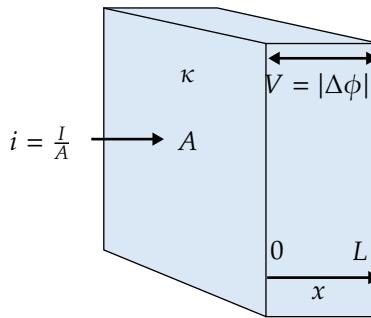
Figure 1.1: *A schematic to illustrate Ohm's law $V = IR$ and Pouillet's law $R = L/\kappa A$ in a planar domain with ion conductivity κ.*

Multiplying with the area A and taking the absolute value with $I = |i_x|A$ and $V = |\Delta\phi|$ we obtain 🏃

$$I = \frac{V}{R}, \quad \text{where } R = \frac{L}{A\kappa}. \tag{1.7}$$

The first of these equations is **Ohm's law**, while the second is referred to as **Pouillet's law**. The latter relates resistance to geometry and the material property κ in a logical way. The larger the distance ions have to travel or the lower the electrolyte conductivity, the larger the resistance. The area appears only because we introduced the current. Dividing Eq. (1.7) by the area A, we obtain an expression for the current density magnitude:

$$i = \frac{V}{AR}, \quad \text{where } AR = \frac{L}{\kappa} \tag{1.8}$$

Here the *area-specific resistance* (ASR) AR [Ωm^2] may be viewed as a separate new symbol or as the product of area and resistance.

Since the rate at which a desirable product is made in an electrochemical device scales with the current I, and the cost of electrodes, membranes, etcetera scale with area A the ratio $j = I/A$, the current density, is a good performance metric. Electrochemical processes are usually only commercially attractive above a certain current density. A high current density allows for a large amount of product to be made per unit area of the cell components used.

On the other hand, the potential drop V has to be maintained by a power source, for which the power consumption is given by $P = IV$ [W].

Often, a balance has to be found between maximising the current density i and minimising the required potential drop V. From Eq. (1.8), minimising the area-specific resistance is therefore crucial. This means that the distance L that the charge has to travel has to be as small as possible, through a medium with conductivity as large as possible. Therefore, electrodes have to be positioned as close together as
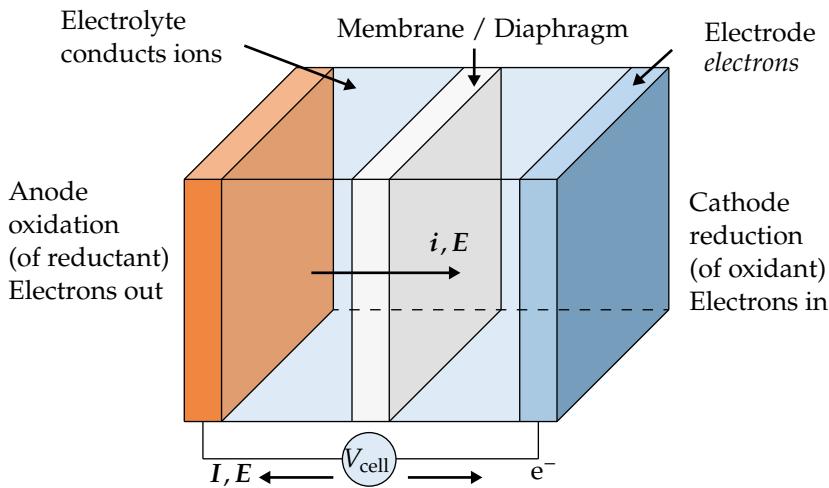
Figure 1.2: *A schematic of a general electrochemical cell. Often, but not always, the anode is depicted on the left and the cathode on the right. Electrons move through a metal from the anode, where the oxidation reaction takes place, to the cathode, where reduction occurs.*

possible. For this reason, electrodes are often directly placed next to a gas-separating membrane, in a *zero-gap* configuration or *membrane-electrode assembly* (MEA).

1.3 An electrochemical cell

A typical electrochemical cell, schematically shown in Figure 1.2, consists of at least the following functional parts:

1. An electric connection ($\kappa = 0$, $\sigma \neq 0$) between the electrodes via a power source or load

2. An *electrolyte*, conducting ions but not electrons ($\kappa \neq 0$, $\sigma = 0$)

3. Two *electrodes*, an anode and a cathode. The function of the electrodes is two-fold: they should conduct electrons *and* be catalytically active for the desired reaction.[2] Only in the case of batteries does the electrode material itself actually participate in the reaction. In this case, the reaction stalls when the electrodes are used up.

1.3.1 Redox reactions

The reactions taking place at electrodes are *redox* (reduction-oxidation) reactions in which electrons are transferred

---

[2]Sometimes, these functions of an electrode are split, in which case there is a catalyst support and a catalyst layer, for example, in the form of spray-coated catalyst nanoparticles.

1. **Reduction** takes place at the **cathode**[3], where an electron (e^-) is transferred *to an oxidant* (O)

2. **Oxidation** takes place at the **anode**, where an electron is transferred *from a reductant* (R)[4]

Such a reaction can be schematically depicted as

$$O + ne^- \leftrightarrow R. \tag{1.9}$$

We will consider the stoichiometric coefficient n to be a positive integer and will use it somewhat flexibly to denote the total number of electrons transferred in a redox reaction, or, depending on the context, the number of electrons per reactant or product molecule, respectively.

The reactants may be solids, as in the case of *batteries*. Alternatively, reactants may be dissolved in a liquid electrolyte, or the liquid itself may be the reactant, for example, in a *water electrolyser* or in various redox flow batteries. Finally, gases may also be brought in contact with the electrodes as in the case of *fuel cells*.

Figure 1.2 shows the anode on the left and the cathode on the right, a convention we will adhere to in this book but is not always followed in the literature. Electrons generated in an oxidation reaction at the anode move through the external circuit to the cathode where the reduction reaction takes place. To avoid negative charge accumulation at the cathode, negative ions (*anions*) move back through the electrolyte to the anode. Alternatively, positive ions (*cations*) move from anode to cathode. Either way, an electric field is set up and directed from the anode to the cathode to transport this charge.

1.3.2 Thermodynamics

Electrochemists often use the symbol E to denote the potential of an electrode.[5] We hope that this will cause no confusion with the magnitude of the electric field.

Neglecting ohmic losses in the external circuitry and the electrodes for now, the *cell voltage* V_{cell} reads

$$V_{cell} = E_c - E_a, \tag{1.10}$$

---

[3]To avoid renaming an electrode depending on whether a battery is charging or discharging, for a battery this naming convention only holds during discharging. During charging the oxidation reaction takes place at the cathode.

[4]Other terms for an oxidant are oxidiser/oxidising agent/electron acceptor. Other terms for a reductant are reducer/reducing agent/electron donor. Reduction refers to a reduction in charge, so the addition of electrons. Some chemists may insist it is rather the oxidation state or oxidation number that is reduced. This hypothetical charge is usually +1 for hydrogen and -2 for oxygen. The sum of oxidation states of a molecule equals its charge, in units of electron charge, which is called the charge number or valence.

[5]This notation derives from the electromotive force (EMF), a term used to describe the transformation from a different type of energy (like chemical bonding energy) to electrical energy. Electrode potentials are actually voltages since they are measured relative to some reference electrode; see the optional section 1.3.4 for more information. Sometimes the terminology cell potential is used, for which we will consistently use cell voltage.

where the subscripts a stand for anode and c for cathode, respectively. If we switch off the current, the oxidation and reduction reactions proceed at an equal rate at the equilibrium cell voltage $V_{eq} = V_{c,eq} - V_{a,eq}$.[6] From equilibrium thermodynamics, it follows that the amount of useful work that can be done at constant temperature and pressure is given by (minus) the Gibbs free energy [J] of the reaction. Per mole of product [mol_p] we will denote this as $-\Delta G$ [J/mol_p]. Upon slightly opening the circuit, an infinitesimal amount of current will run that does electrical work, given by Eq. (1.3) as qV_{eq} [J].

For one mole of product, we convert a charge $q = nF$, with n [mol_{e^-}/mol_p] here representing the number of moles of electrons per mole of product. Here, $F \approx 96485$ C/mol_{e^-} is Faraday's constant, which gives the charge of a mole of electrons.[7] Combining this gives

$$\Delta G = -nFV_{eq}. \tag{1.11}$$

1. Spontaneous reactions have $\Delta G < 0$, so such *galvanic* or *voltaic* cells have $V_{eq} > 0$.[8]

2. Non-spontaneous reactions have $\Delta G > 0$, so such *electrolytic* cells have $V_{eq} < 0$.

Besides useful work, at a finite current, there are also various types of losses. For example, the collisions of electrons and ions result in resistive heating. In defining energy efficiency, we will compare the total energy consumption by the cell to the amount of useful work.

For a galvanic cell the useful work that can be done per mole of product is $-\Delta G = nFV_{eq}$, while dissipation lowers the cell voltage to $0 < V_{cell} < V_{eq}$, leaving nFV_{cell} for useful work. Hence we define the energy efficiency or voltage efficiency as

$$\varphi_e = \frac{V_{cell}}{V_{eq}}. \tag{1.12}$$

For an electrolytic cell, dissipation makes that a more negative cell voltage $V_{cell} < V_{eq} < 0$ is needed to drive a current. Hence, the voltage efficiency, in this case, reads

$$\varphi_e = \frac{V_{eq}}{V_{cell}}. \tag{1.13}$$

---

[6]This open-circuit voltage (OCV) may be different when side-reactions like corrosion determine the cell voltage. Here we consider that an equilibrium of the desired reactions prevails.

[7]With $e = 1.602(..) \cdot 10^{-19}$ C the elementary charge and N_A Avogadro's number, or the number of particles in a mole, we have $F = eN_A$.

[8]This is a consequence of the second law of thermodynamics that states that the entropy of the universe increases. We have $\Delta G = \Delta H - T\Delta S$ where $\Delta S > 0$ is the entropy increase in the reaction and $\Delta H/T > 0$ is entropy *decrease* of the environment due to heat and work. The Gibbs free energy, therefore, gives the total entropy decrease, which is negative for a spontaneous process. For a non-spontaneous process, it can be positive, but this requires an entropy increase elsewhere in the system.

1.3.3   *Example: alkaline water electrolysis* *

As an example, we consider in this section the reactions taking place in an *alkaline* water electrolyser producing hydrogen and oxygen. The word alkaline here refers to a pH>7. Note also that this process is named *water* electrolysis for the reactant rather than for the products hydrogen and oxygen. The overall reaction $2H_2O \rightarrow 2H_2 + O_2$, proceeds through two redox reactions. The reduction reaction at the cathode, the hydrogen evolution reaction (HER), reads

$$2H_2O + 2e^- \rightarrow H_2 + 2OH^-. \tag{1.14}$$

The pre-factors for each term in this reaction are called stoichiometric coefficients. The hydrogen gas forms bubbles that leave the electrolyte. Hydroxide ions (OH-) take over the transfer of current from electrodes and move to the anode, where they take part in the oxidation reaction, the oxygen evolution reaction (OER):

$$4OH^- \rightarrow 4e^- + O_2 + 2H_2O. \tag{1.15}$$

At the anode, the current is continued by the transport of electrons in the electrodes. A power source closes the circuit and gives the electrons enough Gibbs free energy to participate in the reactions. Note that water is consumed at the cathode but formed at the anode. However, of course, more water molecules are consumed at the cathode than are produced at the anode so that, overall, water is consumed. The equilibrium voltage of the water electrolysis reactions

$$V_{eq} = -\frac{\Delta G}{nF} \approx \frac{237 \text{ kJ/mol}}{2 \cdot 9.65 \cdot 10^4 \text{ C/mol}} \approx 1.23 \text{ V}. \tag{1.16}$$

When $V_{cell} \approx V_{eq}$ the process will be endothermic, causing local cooling, which is resupplied by heat drawn from the environment. This additional heat is taken into account in the enthalpy of reaction $\Delta H = \Delta G + T\Delta S$. Here ΔS is the entropy of reaction, associated with the higher entropy of the produced gases compared to those of the consumed liquid. The cell voltage at which this additional heat is produced by internal dissipation

$$V_{tn} = -\frac{\Delta H}{nF} \approx \frac{286 \text{ kJ/mol}}{2 \cdot 9.65 \cdot 10^4 \text{ C/mol}} \approx 1.48 \text{ V}, \tag{1.17}$$

is called the *thermoneutral voltage*. At higher voltages, the process becomes exothermic, as more heat and entropy are produced than is required for the reaction. To create gaseous hydrogen and oxygen bubbles requires a further small heat/enthalpy of vaporisation.

The equilibrium voltage of Eq. (1.16) at standard conditions can be found in tables of standard electrode potentials, like Table. 1.1 in the next section. The energies of reaction ΔG and ΔH are referred to as the lower and higher heating values, respectively. In the combustion of hydrogen, this difference arises due to the additional energy required to vaporize the product water.

Often, instead of ΔG as was used in Eqs. (1.12) and (1.13), ΔH is used to define the energy efficiency of water electrolysis. In this way of bookkeeping, only the electrical energy is used for the minimum required energy, and the required heat is assumed to be freely available. This makes for a maximum efficiency $\frac{\Delta H}{\Delta G} \approx 118\%$, that can be reached for the non-spontaneous reaction, by using heat from the environment. For the spontaneous reactions of hydrogen and oxygen in a fuel cell, the reverse of Eqs. (1.14) and (1.15), on the other hand, a maximum efficiency of $\frac{\Delta G}{\Delta H} \approx 85\%$ can be reached. The generated heat is then discarded as not being useful enough to contribute to energy efficiency. This reasoning has some logic, although so does having 100% as a maximum efficiency.[9]

Note that, however we define it, at low enough current density the reactions can, in theory, be performed back and forth with 100% efficiency in an electrochemical cell. This is in stark contrast with the energy efficiency of producing work from the heat released in burning hydrogen, which is limited by the Carnot efficiency. Therefore, at ambient or moderate temperatures, the energy efficiency of electrochemical cells easily beats their mechanical equivalents.

1.3.4 *Reduction potentials* *

An electrode potential E is defined as the cell voltage $E_{\text{right}} - E_{\text{left,SHE}}$ measured when the left electrode is a reference electrode, often a *standard hydrogen electrode* (SHE). This is a theoretical, idealised, electrode but can be approximated by bubbling pure hydrogen past a platinum electrode in an acidic solution at ambient conditions. The term "standard" here refers to the *standard conditions* of 25°C, 1 atm, 1 M of all reactants, or actually, to account for non-ideal behaviour, an *activity* of 1. Electrode potentials at standard conditions are typically dressed with a superscript 0 (or sometimes $\ominus$) so that a standard hydrogen electrode has $E^0 = 0$ by definition. For other reactions, the *standard electrode potentials* can be looked up in tables.

These potentials are usually given as reduction potentials; for reduction reactions examples are shown in Table 1.1

Rows of Table 1.1 can be combined to give new reactions. For example, the final line follows by subtracting twice the second line from the one before it. Also, the potential follows from subtracting -0.83 from 0.4 to give 1.23 V. However, this is fortuitous, as, in general, we have to realise that Gibbs' free energy can be added in this way and not the potential. By Eq. (1.11), the factor n must be corrected when adding potentials.

---

[9]The EU in its "harmonized protocols for testing of low temperature water electrolysis" advises a definition also propagated in Ref. [16], which amounts to $\varphi_e = \frac{V_{\text{tn}}}{V_{\text{cell}} + V_{\text{tn}} - V_{\text{eq}}}$. Note that in this definition too, the maximum cannot exceed 100 %.

Reduction reaction	E^0 [V]
$Li^+ + e^- \rightarrow Li$	-3.04
$2H_2O + 2e^- \rightarrow H_2 + 2OH^-$	-0.83
$2CO_2 + 2H^+ + 2e^- \rightarrow CO + H_2O$	-0.52
$2H^+ + 2e^- \rightarrow H_2$	0
$O_2 + 2H_2O + 4e^- \rightarrow 4OH^-$	0.4
$O_2 + 4H^+ + 4e^- \rightarrow 2H_2O$	1.229

Table 1.1: *An example list of reduction reactions and their reduction potentials. All values are relative to SHE.*

1.4   Kinetics

We conclude this chapter in section 1.5 with a simple cell model relating the cell voltage V_{cell} to the current density j and various geometrical and material parameters of the cell. Two important elements, the equilibrium voltage V_{eq} and the ohmic losses IR have already been described. In this section, we introduce a final important ingredient, the activation overpotential.

1.4.1   Faraday's law

Consider a redox reaction taking place at an electrode. Such a surface reaction is called a heterogeneous reaction because of the two or more phases involved. We will use a *normal-to* symbol $\perp$ to denote vector components of the molar flux normal to this surface in the direction **away from the surface into the fluid**:

$$N_\perp = \hat{n} \cdot N \tag{1.18}$$

Here N is the molar flux [mol/m^2/s] and $\hat{n}$ is a unit normal vector directed into the electrolyte. Since reactants move towards the electrode surface in the $-\hat{n}$-direction, $N_\perp$ [mol/m^2/s] is negative for reactants. Product fluxes are always positive because products move away from the electrode in the direction of $\hat{n}$.

In the case of the redox reaction of Eq. (1.9), for each mole of products made or reactants consumed, n mole of electrons are used. This proportionality between charge and flux is referred to as *Faraday's law* and can be expressed as

$$j_\perp = nFN_{\perp,O}, \tag{1.19}$$

This equation relates the molar flux $N_{\perp,O}$ of oxidants to the charge flux $j_\perp = \hat{n} \cdot j$, or current density. A positive local current density $j_\perp$ is directed from the electrode into the electrolyte. In a reduction reaction, oxidants move towards the electrode so that $N_{\perp,O} < 0$ and $j_\perp < 0$, so *cathodic currents are negative*. Conversely, in an oxidation reaction oxidants move away from the electrode so that $N_{\perp,O} > 0$ and $j_\perp > 0$, so *anodic currents are positive*.
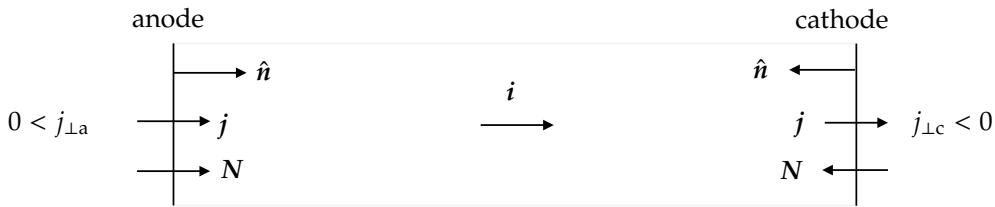
Figure 1.3: *The local electronic current density $j_\perp$, product flux N, ionic current density i, and wall-normal unit vector n.*

1.4.2 Activation energy

To have a chemical reaction proceed at a significant rate, an *activation energy* $\mathcal{E}_a$ [J/mol] usually has to be supplied. This additional energy that molecules should have to overcome the reaction energy barrier is schematically depicted in Figure 1.4. This schematic shows a spontaneous reaction, for which the Gibbs free energy of reaction $\Delta G < 0$. The energy of the molecules in their final state is below that of the energy of their initial state.

This activation energy is associated with overcoming repulsive interactions between the reactants before the attractive binding energies can take over. The activation energy can be lowered using a suitable catalytic surface. The right catalyst binds the reactant not too strongly but neither too weakly and may also align the reactants for the reaction to proceed more easily. This results in a lower activation energy barrier, as is illustrated with the dashed blue curve in Figure 1.4.

Consider a reaction at the surface of an electrode, immersed in a liquid electrolyte. For many reactions, the product flux $N_\perp$ [mol/m^2/s] can approximately be written as

$$N_\perp = kc^r, \tag{1.20}$$

where c [mol/m^3] is the reactant concentration, k [mol^{1-r} s^{-1} m^{3r-2}] the reaction *rate constant* and r is the reaction order. For first-order reactions $r = 1$ and the reaction rate is proportional to the reactant concentration. The rate constant often approximately satisfies the semi-empirical Arrhenius equation

$$k \propto e^{-\frac{\mathcal{E}_a}{\mathcal{R}T}}. \tag{1.21}$$

Here, $\frac{\mathcal{E}_a}{\mathcal{R}T}$ is the ratio between the activation energy and the characteristic kinetic energy $\mathcal{R}T$ for a mole of reactants.[10] The higher the temperature, the larger the kinetic energy of the reactants, and the faster the reaction proceeds. This is the reason that chemical reactors typically operate at high temperatures. They often also operate at a high pressure to increase the concentration c of gaseous or dissolved reactants, further increasing the reaction rate. Finally, often a catalyst helps to lower $\mathcal{E}_a$. These are the main means available to accelerate chemical reactions.

---

[10]The characteristic kinetic energy per particle is $k_B T$, with k_B the Boltzmann constant. The gas constant can be written as $\mathcal{R} = N_A k_B$, with N_A Avogadro's constant.
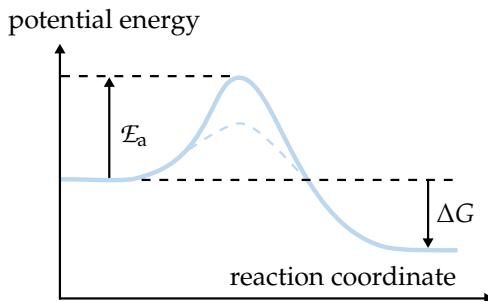
Figure 1.4: *The activation energy $\mathcal{E}_a$ "barrier" for a spontaneous reaction ($\Delta G < 0$) to proceed from left to right along the reaction coordinate, which may be seen as a re-scaled time coordinate. For a chemical reaction, the height of this barrier can be lowered using a better catalyst (dashed curve).*

Electrochemical reactions, however, have an additional "knob" that can be used to speed up a reaction, which allows them to proceed rapidly even at low temperatures $T \ll \mathcal{E}_a/\mathcal{R}$. This has to do with the potential energy of Eq. (1.3). By lowering the potential of the cathode E_c, the potential energy of electrons is increased. The most energetic electrons, at the *Fermi energy*, can then transition to a lower energy state by participating in a reduction reaction.

Similarly, by increasing the anode potential E_a relative to the potential ϕ of the adjacent electrolyte,[11] The potential energy of electrons in the anode is lowered. This facilitates electrons from oxidation reactions near the surface to enter the anode. As argued by a geometrical argument in the caption of Figure 1.5 an increase in electrode potential E, relative to that of the electrolyte, lowers the activation energy for an oxidation reaction by adding $-\alpha_O F (E - \phi)$.[12]

Here, the charge-transfer coefficient α_O for the oxidation reaction is typically around ½, and adds up to unity when combined with that for the reverse reduction reaction:

$$\alpha_O + \alpha_R = 1. \tag{1.22}$$

We consider a first-order, single-electron transfer oxidation reaction so that $n = r = 1$. As argued above, an increase in the anode potential E will decrease the activation energy $\mathcal{E}_a$ by adding $-\alpha_O F (E - \phi)$. Inserting into Eqs. (1.19), (1.20) and

---

[11]We take here the electrostatic potential in the electrolyte, measured using an electrode made of the same material as that used to measure the electrode potential. The measurement position should be very close to the electrode to exclude any ohmic drops or concentration differences over the distance to the electrode. So, it should be well within any diffusion layer thickness, but we consider it outside the electric double layer (EDL). At high electrolyte concentrations, this layer can be as thin as a few molecules, much smaller than the continuum scales considered in this book.

[12]If you have never seen this derivation before, the present exposition may be too short to appreciate the intricacies involved. In that case, you are recommended to study Fig. 1.5 and its caption in detail and/or consult electrochemistry textbooks like [3]. However, the details here will not be crucial to appreciate and apply the final results, so you may also skim over some technicalities.
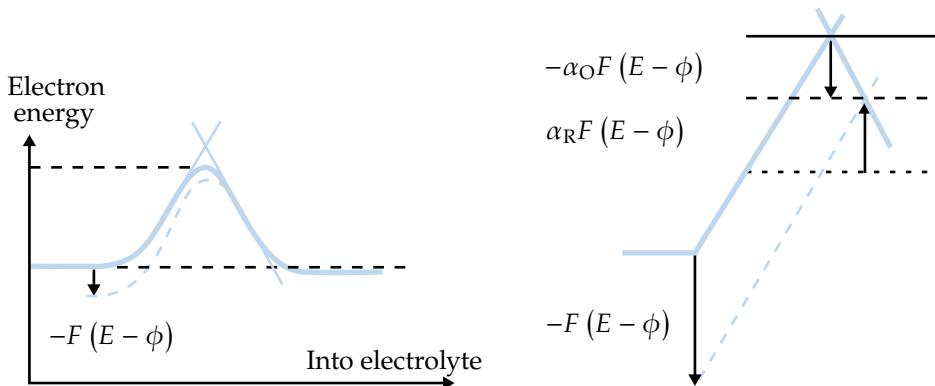
Figure 1.5: *Left: a schematic depiction of the energy landscape for a general single-electron transfer redox reaction $a\text{A} + \text{e}^- \rightarrow \text{B}$. The x-axis is a reaction coordinate, which may be seen as a sequence of reaction steps like adsorption, reorientation of molecules, the breakup of bonds, etcetera. Heuristically, it may also be seen as a re-scaled spatial coordinate from the anode into the electrolyte. The energy barrier of Figure 1.4 is decreased by increasing the potential E of the metal electrode relative to the electrolyte ϕ. This would lower the potential energy of electrons, accelerating oxidation reactions. Right: the activation barrier is approximated by two lines under an angle. Lowering the left line while keeping the right one fixed increases the peak by $\alpha_\text{R} F (E - \phi)$ as seen from the left but decreases it by $-\alpha_\text{O} F (E - \phi)$ as seen from the right. This decrease makes it easier for electrons to move to the left into the electrode, accelerating the oxidation reaction. Since these changes add up to $-F (E - \phi)$ we have $\alpha_\text{O} + \alpha_\text{R} = 1$. The exact values depend on the angle between the two lines, but $\alpha_\text{O} = \alpha_\text{R} = 1/2$ for a symmetric peak.*

Eq. (1.21) gives for the positive anodic current ⍟

$$j_\perp = k_O F c \, e^{\frac{\alpha_O F (E-\phi)}{\mathcal{R}T}}, \tag{1.23}$$

where the oxidation rate constant $k_O \propto e^{-\mathcal{E}_{a,O}/\mathcal{R}T}$. Simultaneously, reduction reactions will also take place at the anode, but at a much lower rate than the oxidation reactions. An increase in anode potential E will increase the activation energy $\mathcal{E}_a$ by adding $\alpha_R F (E - \phi)$. Inserting this into Eqs. (1.19), (1.20) and Eq. (1.21) adds a negative reduction current so that

$$j_\perp = k_O F c_R e^{\frac{\alpha_O F (E-\phi)}{\mathcal{R}T}} - k_R F c_O e^{-\frac{\alpha_R F (E-\phi)}{\mathcal{R}T}}. \tag{1.24}$$

At the anode, the first term will be referred to as the "forward" reaction and will exceed the second "reverse reaction" term so that $j_{\perp a} > 0$. At the cathode a similar expression will hold, although the kinetic parameters k_O, k_R, α_O, and α_R will generally be different when different cathode materials are used. At the cathode, the second term in Eq. (1.23) will dominate giving $j_{\perp c} < 0$. Note that for smooth planar electrodes, by charge conservation $j_{\perp a} = -j_{\perp c} = j$.

1.4.3   Current-overpotential relations

Nernst equation

Under equilibrium conditions $j_\perp = 0$ and Eq. (1.24) gives the single electron transfer Nernst-equation describing the equilibrium electrode potential ⍟

$$E_{eq} = E^{0\prime} + \frac{\mathcal{R}T}{nF} \ln\left(\frac{c_{O,eq}}{c_{R,eq}}\right), \tag{1.25}$$

where $E^{0\prime} = \phi_{eq} + \frac{\mathcal{R}T}{F} \ln\left(\frac{k_R}{k_O}\right)$ is the *formal potential* and $n = 1$, since we consider a single-electron transfer reaction. In 1.A, we consider the more general case of several reaction steps, which gives again Eq. (1.25), but now with n, the total number of electrons transferred in the reaction and a different formal potential. If the reaction is extremely fast, we speak of a reversible or Nernstian process for which this equilibrium equation can be used.

Butler-Volmer equation

We define the *activation overpotential* or *surface overpotential*

$$\eta \equiv (E - \phi) - (E - \phi)_{eq} \tag{1.26}$$

as the difference between the potential E in the electrode and the potential ϕ in the electrolyte, relative to that same difference in equilibrium. Therefore, under equilibrium conditions at zero current, the activation overpotential vanishes by definition.

You may wonder where in the electrode and in the electrolyte we take these potentials. At the high electrolyte concentrations used in most applications, the change in electrostatic potential from E inside the metal to ϕ in the electrolyte takes place over a distance of the order of a few molecules: the electric double layer (EDL).[13]

Using Eq. (1.26) in Eq. (1.24), we obtain the Butler-Volmer equation

$$j_\perp = j_* \left(\overbrace{\frac{c_R}{c_{R,eq}} e^{\frac{\alpha_O F \eta}{\mathcal{R} T}}}^{\text{oxidation}} - \overbrace{\frac{c_O}{c_{O,eq}} e^{-\frac{\alpha_R F \eta}{\mathcal{R} T}}}^{\text{reduction}} \right). \tag{1.27}$$

Here the exchange current density $j_* \equiv nF \left(k_O c_{R,eq} \right)^{\alpha_R} \left(k_R c_{O,eq} \right)^{\alpha_O}$.

The Butler-Volmer equation, Eq. (1.27), cannot, in general, be inverted analytically to give an exact expression for the overpotential η as a function of current density $j_\perp$.

Tafel equation

A noteworthy case in which an explicit expression for the overpotential can be obtained is when one of the exponentials dominates. When $j_\perp \gg j_*$ or $\eta \gg \frac{\mathcal{R} T}{F} \ln \left(\frac{c_O}{c_{O,eq}} \frac{c_{R,eq}}{c_R} \right)$, the oxidation reaction dominates over the reduction reaction and we obtain the Tafel equation

$$j_\perp = j_* \frac{c_R}{c_{R,eq}} e^{\eta_a / b_a}. \tag{1.28}$$

Solving for η gives the concentration-dependent Tafel equation

$$\boxed{\eta_a = b_a \ln \left(\frac{j_\perp}{j_*} \frac{c_{R,eq}}{c_R} \right).} \tag{1.29}$$

Here the anodic Tafel slope $b_a \equiv \mathcal{R} T / \alpha_O F$ is around 0.05 V at ambient temperature when $\alpha_O = 1/2$. This means that as long as $c_R \approx c_{R,eq}$ we can increase the current by an order of magnitude with an anodic activation overpotential of only $\eta_a = b_a \ln(10) \approx 120$ mV[14].

---

[13]This thin region near any surface in an electrolyte consists of a layer of ions that are chemically adsorbed to the surface and a layer of ions of opposing charge that are attracted to this surface charge. Hence the name electric double layer. This second layer screens the surface charge over the *Debye length* and is at relevant electrolyte concentrations $\lesssim 1$ nm thick. It is also sometimes called the diffuse layer. This is not to be confused with the diffusion layer. This boundary layer where diffusion dominates over advection, typically $10 - 100$ μm, is many orders of magnitude thicker.

[14]Tafel slopes are often reported in this way, per decade rather than per e. If this is the case, the value mentioned in the literature has to be divided by $\ln(10) \approx 2.3$ to obtain Tafel slopes as defined here.
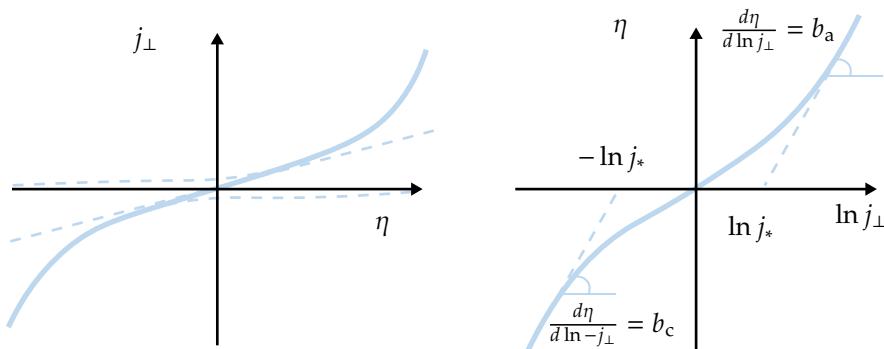
Figure 1.6: *A plot of current density $j_\perp$ versus activation overpotential η as described by the concentration-independent Butler-Volmer equation $j_\perp = j_* \left(e^{\eta/b_O} - e^{-\eta/b_R} \right)$ on a linear scale (left) and a lin-log plot with the logarithm of the current density on the x-axis (right). From this latter* Tafel *plot, the Tafel slopes $b_O = \frac{RT}{\alpha_O F}$ and $b_R = \frac{RT}{\alpha_R F}$ can be obtained as the slope of the linear sections. The intercept with the horizontal axis gives the exchange current density j_*.*

Concentration overpotential

Using $\ln ab = \ln a + \ln b$ we can write Eq. (1.29) as

$$\eta_a = \overbrace{b_a \ln\left(\frac{j_\perp}{j_*}\right)}^{\text{surface overpotential}} + \overbrace{b_a \ln\left(\frac{c_{R,eq}}{c_R}\right)}^{\text{concentration overpotential}} . \tag{1.30}$$

The surface overpotential is independent of concentration and describes purely kinetic activation losses.[15] The second part, the concentration overpotential, increases as the reactant concentration c_R decreases.

Similarly, we obtain for the reverse reduction reaction, in terms of the cathodic Tafel slope $b_c \equiv RT/\alpha_R F$:

$$\eta_c = -b_c \ln\left(\frac{-j_\perp}{j_*}\frac{c_{O,eq}}{c_O}\right). \tag{1.31}$$

At the cathode, both $j_\perp$ and η_c are negative quantities.

Concentration-independent symmetric kinetics

When there are no appreciable concentration gradients throughout the cell so that $\frac{c_R}{c_{R,eq}} = \frac{c_O}{c_{O,eq}} = 1$, we obtain in the concentration-independent Butler-Volmer equation

---

[15]Sometimes another convention is used in which part of the concentration effect is attributed to the surface overpotential, see the end of 1.B.2.

$$j_\perp = j_* \left(e^{\eta/b_a} - e^{-\eta/b_c} \right). \tag{1.32}$$

Figure 1.6 illustrates the shape of this curve and how to use it to derive b_a, b_c, and j_*. In case of equal charge transfer coefficients $\alpha_O = \alpha_R = 1/2$ we can use the definition $\sinh x \equiv \frac{1}{2}(e^x - e^{-x})$ of the hyperbolic sine, to write Eq. (1.32) as $j_\perp = 2j_* \sinh\left(\frac{\eta}{b}\right)$ using $b = \frac{2\mathcal{R}T}{F}$. This may be referred to as the symmetric concentration-independent Butler-Volmer equation. Inverting it gives[16] 𖠿

$$\eta = b \, \text{asinh}\left(\frac{j_\perp}{2j_*}\right). \tag{1.33}$$

At high current densities $j_\perp \gg j_*$ we have $b \, \text{asinh}(j_\perp/2j_*) \approx b \ln j_\perp/j_*$ so that Eq. (1.33) reduces to the Tafel equation.[17]

Linear kinetics

For most applications $j_\perp \gg j_*$ so that Tafel kinetics is an appropriate approximation. For some particularly facile reactions, like hydrogen oxidation on platinum, the exchange current density j_* is so high that $|j_\perp| < j_*$. Using the first-order Taylor expansion $e^x \approx 1 + x$ for $x \ll 1$, Eqs. (1.32) and (1.22) give the equation for linear kinetics 𖠿

$$\eta = AR j_\perp \quad \text{with} \quad AR = \frac{\mathcal{R}T}{F j_*}. \tag{1.34}$$

Here, in analogy with Eq. (1.8), we introduced an area-specific resistance AR. Note that linear kinetics only holds for very low activation overpotentials $\eta \lesssim \mathcal{R}T/F \sim 25$ mV.

1.5 Simplified cell model

In this section, we integrate the various elements discussed in this chapter into a first cell model.

Figure 1.7 shows typical profiles of both the electronic and the electrolyte potentials through an electrochemical cell in equilibrium during electrolysis ($V_{cell} < V_{eq} < 0$) and galvanic operation ($0 < V_{cell} < V_{eq}$), respectively. The figure is slightly complicated by including the increase in potential inside the cables and electrodes in the direction of the electron flow but it does not have to be fully comprehended at this point. In case of negligible electronic resistance, the picture would be slightly simpler.

---

[16]Here the inverse hyperbolic sine can be written as $\text{asinh}(x) = \ln\left(x + \sqrt{1+x^2}\right)$ so that for $x \gg 1$ we have $\text{asinh}(x) \approx \ln(2x)$

[17]For low current densities $j_\perp \ll j_*$ we have $b \, \text{asinh}(j_\perp/2j_*) \approx b \, j_\perp/2j_*$, which is consistent with Eq. (1.34).
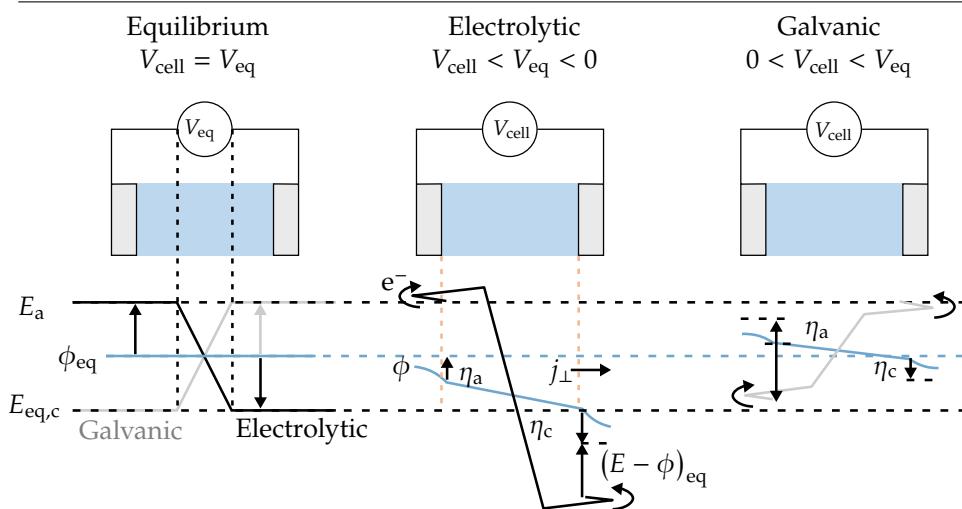
Figure 1.7: *The electronic potential (black for an electrolytic cell, grey for a galvanic cell) and electrolyte potential ϕ (blue) profiles throughout the cell and inside the external circuit. In an electrolytic cell $V_{cell} < V_{eq} < 0$. The electronic potential is locally multi-valued to show both variations inside the porous electrode and the cables. The electrolyte potential ϕ shows a constant slope in the electrolyte, which is assumed to have a constant conductivity. The "entrance" of the porous electrodes is indicated in the middle picture with the orange vertical dashed lines to guide the eye. Beyond this point, a gradually decreasing slope inside the (porous) electrodes can be seen towards the back where the ionic current and hence this slope vanishes.*

For completeness, and to anticipate what lies ahead in chapter 3, we also considered the electrodes to be porous. In this case, the overpotential $\eta = E - \phi - (E - \phi)_{eq}$ is not a constant, but varies throughout the electrode, further complicating the picture.

Often, the electronic conductivity of the electrodes is high enough to assume constant electrode potentials E_a and E_c. However, for generality, we include here an ohmic potential drop ΔV, which receives contributions from electrons moving through the electrode material, current collectors, and cables before arriving at the load or source. Note that in a galvanic cell ΔV decreases the positive cell voltage, while in an electrolytic cell ΔV makes the negative cell voltage more negative. Both efficiencies thus decrease as a result of the electronic ohmic losses ΔV.

We will define the electrolyte potentials ϕ_a and ϕ_c at the electrode-electrolyte interface so that $\Delta\phi \equiv \phi_a - \phi_c > 0$ gives the ohmic drop between the electrodes, which vanishes in equilibrium $\Delta\phi_{eq} = 0$. With the definition of Eq. (1.26) and $V_{eq} = E_{eq,c} - E_{eq,a}$ we can then write 🏃

$$\boxed{V_{cell} = V_{eq} + \eta_c - \eta_a - \Delta\phi - \Delta V.} \tag{1.35}$$

This important result gives the cell potential as a sum, or an equivalent series circuit,

of the equilibrium potential. All terms on the right act to reduce V_{eq} and may be referred to as voltage losses, or overpotentials. These losses consist of activation overpotentials $\eta_a > 0$ and $-\eta_c > 0$ as well as ohmic losses due to ions $\Delta\phi$ and electrons ΔV.

We conclude this chapter by inserting expressions for these losses obtained from the previous section, assuming:

1. An electrolyte with constant conductivity between the anode and cathode, so we can insert Eq. (1.6) for the electrolyte potential drop $\Delta\phi = jL/\kappa$.

2. An ohmic resistance R for the electronic circuit, so we can use Eq. (1.8) for the electronic potential drop $\Delta V = jAR$.

3. Concentration-independent Tafel kinetics for the anode, where $j_\perp = j > 0$, so we can use Eq. (1.32) to write $\eta_a = b_a \ln(j/j_{*a})$.[18]

4. Similarly, at the cathode $j_\perp = -j$, so we can use Eq. (1.31) to write $\eta_c = -b_c \ln(j/j_{*c})$.

Inserting these expressions into Eq. (1.35) gives

$$V_{cell} = V_{eq} - \left(b_c \ln\left(\frac{j}{j_{*c}}\right) + b_a \ln\left(\frac{j}{j_{*a}}\right) + \frac{jL}{\kappa} + jAR \right). \tag{1.36}$$

All voltage losses between brackets are positive as they should be. Figure 1.8 illustrates this expression using values that are typical for a common alkaline water electrolyser. For low current densities, the logarithmic activation overpotentials dominate,[19] while for the higher current densities, their contribution increases only very slowly. Therefore, the linear ohmic losses dominate the slope of the cell voltage at higher current densities.

The electrochemical engineer aims to minimise the voltage losses in an electrochemical cell while keeping the system costs to a minimum. Economic viability usually requires the use of high current densities to get as much product as possible for as little cell material as possible. More expensive catalysts may be used to reduce activation and voltage losses, but alternatively, using a larger surface area may be more cost-effective. Therefore, porous electrodes with a large internal surface area are often used. Also, additional phenomena like mass transport and multiphase flow phenomena start to play a role and impact the cell voltage. Creating an understanding of all these factors of influence, providing a mathematical description, and, where possible, providing optimised design parameters will be the main goal of the remainder of this book.

---

[18]For many applications this is a reasonable approximation for intermediate current densities that are large enough for Tafel kinetics to hold ($j \gtrsim 2j_*$) but small enough for concentration effects to be neglected. When smaller currents $j \lesssim j_*$ should also be included, Eq. (1.33) shows we can replace $\ln\left(\frac{j}{j_*}\right)$ with $\operatorname{asinh}\left(\frac{j_\perp}{2j_*}\right)$. Strictly speaking, this is only exactly valid for symmetric kinetics with $\alpha = 1/2$.

[19]We replaced $\ln x$ with $\operatorname{asinh}\frac{x}{2}$ in Eq. (1.36), as in Eq. (1.33). This gives approximately the same result for $x \gg 1$ but avoids the negative values that arise for $x < 1$ for which the Tafel approximation is invalid.
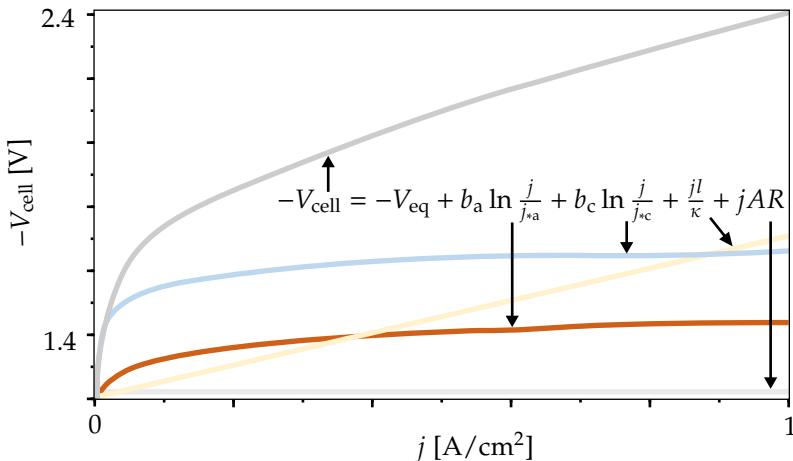
Figure 1.8: *The negative of the cell voltage $-V_{cell}$ of an electrolytic cell as a function of current density j as described by Eq. (1.36) using $V_{eq} = -1.23$ V, $b_a \approx b_c \approx 50$ mV, $j_{*c} = 10^{-2}$ A/cm^2, $j_{*a} = 10^{-4}$ A/cm^2, an electrolyte area-specific resistance $\kappa/L = 0.5$ Ω cm^2 and electronic area-specific resistance $AR = 0.01$ Ωcm^2. The logarithmic activation overpotentials mostly increase the voltage losses at low current densities but hardly vary for higher values, where the linear ohmic losses dominate the slope.*

1.6   Summary

- The ionic current density in an electrochemical cell often approximately follows Ohm's law $\boldsymbol{i} = \kappa\boldsymbol{E} = -\kappa\nabla\phi$. It is oriented in the direction of the electric field from anode, where the oxidation reaction releases electrons, to cathode, where electrons are consumed in the reduction reaction $O + ne^- \leftrightarrow R$, Eq. (1.9), through a potential drop $\Delta\phi = ARj = jL/\kappa$.

- The cell voltage $V_{cell} = E_c - E_a = V_{cell} + \eta_c - \eta_a - \Delta V$ of Eq. (1.10) is positive in a galvanic cell and related to voltage efficiency as $\varphi_e = \frac{V_{cell}}{V_{eq}}$, Eq. (1.12). It is negative in an electrolytic cell and related to efficiency as $\varphi_e = \frac{V_{eq}}{V_{cell}}$, Eq. (1.13).

- For first-order kinetics, the current density $j_\perp = nFN_\perp$ from anode to cathode can often be described by the Butler-Volmer equation $j_* \left(\frac{c_R}{c_{R,eq}} e^{\frac{\alpha_O F\eta}{\mathcal{R}T}} - \frac{c_O}{c_{O,eq}} e^{-\frac{\alpha_R F\eta}{\mathcal{R}T}} \right)$, Eq. (1.27), which can be reduced to

  - the Tafel equation, $j_\perp = j_* \frac{c_R}{c_{R,eq}} e^{\eta_a/b_a}$, (1.28) for high overpotentials $\eta = (E - \phi) - (E - \phi)_{eq}$, or $j_\perp \gg j_*$

  - linear kinetics, with an areal resistance $AR = \frac{\mathcal{R}T}{Fj_*}$ for low overpotentials, and

– the Nernst equation $E_{eq} = E^{0\prime} + \frac{RT}{nF}\ln\left(\frac{c_{O,eq}}{c_{R,eq}}\right)$, where n appears when considering multiple reaction steps near equilibrium (1.C.49).

1.7 Exercises

Exercise 1.1

The exchange current density and charge transfer coefficient of an electrochemical reaction at a cathode are $j_* = 0.01$ mA/cm^2 and $\alpha_R = 0.65$, respectively. Give an approximate value for the activation overpotential on the cathode at ambient conditions, at a current density $j_\perp = -20$ mA/cm^2, assuming $C_O \approx C_{O,eq}$.

Exercise 1.2

Consider the simple cell model

$$V_{cell} = V_{eq} - \eta - jAR$$

. Assume that the current density j is high enough for the activation overpotential η to be approximately independent of current density. The useful power output of a galvanic cell is given by $P = jAV_{cell}$. Give an expression for the current density j for which this quantity is maximised.

Exercise 1.3

Consider a cell in which both anode and cathode follow concentration-independent Tafel kinetics, with the anodic and cathodic activation overpotentials given by

$$\eta_a = b_a \ln\left(\frac{j}{j_{*a}}\right) \text{ and } \eta_c = -b_c \ln\left(\frac{j}{j_{*c}}\right). \tag{1.37}$$

Combine both overpotentials in a single expression for the total activation overpotential $\eta_a - \eta_c = b \ln(j/j_*)$.

a. What is the combined Tafel slope b?

b. If $b_a = \mathcal{R}T/\alpha_a F$ and $b_c = \mathcal{R}T/\alpha_c F$ give the combined charge transfer coefficient $\alpha = \mathcal{R}T/bF$ in terms of α_a and α_c

c. What is the combined exchange current density j_*?

Exercise 1.4

A consortium of companies is developing a new wind park integrated with water electrolysers. The combined nominal electrolyser power is chosen to be 50 MW. As the available space is important, the electrolysers have to be as small as possible. We assume a distance between the electrodes of 500 μm with an effective electrolyte conductivity 20 S/m, with $b_c = b_a = 0.05$ V, $j_{*a} = 10^2$ A/m^2 and $j_{*c} = 1$ A/m^2. We neglect any ohmic losses in the electrical connections and electrodes and any effect of bubbles.

a. If a voltage efficiency of 60% with respect to 1.23 V is required, how much an-ode plus cathode electrode area do you need? **Hint**: You might need to use a numerical solver to get to the solution.

b. Someone in your company finds out that heating the electrolyte to 100 °C increases the ionic conductivity to 70 S/m. With the same electrode area and electrolyser power, what will the new efficiency be?

Exercises 1.5-1.9

Fill in the missing steps in the main text, indicated by the symbol ⋏.

*Appendices *

1.A *Multiple reaction steps*

Often, electrochemical reactions involve several subsequent steps, including mass transfer, adsorption, desorption, redox reactions, and sometimes chemical reactions. Usually one of the steps is much slower than the rest,[20] which is then referred to as the rate-determining step (rds). Parsons [20] considered how to deal with multi-step reactions in a rather general way. Considering a process consisting of n_{preO} electron-transfer steps before a rate-determining oxidation step and n_{postO} after, he found that the effective charge transfer coefficients becomes $\alpha_{\text{effO}} = n_{\text{preO}} + n_{\text{rdsO}}\alpha_{\text{O}}$, and similarly $\alpha_{\text{effR}} = n_{\text{postO}} + n_{\text{rdsO}}\alpha_{\text{R}}$. Inserting these effective values in Eq. (1.27) gives

$$j_\perp = j_* \left(\frac{c_{\text{R}}}{c_{\text{R,eq}}} e^{(n_{\text{preO}}+n_{\text{rds}}\alpha_{\text{O}})\frac{F\eta}{\mathcal{R}T}} - \frac{c_{\text{O}}}{c_{\text{O,eq}}} e^{-(n_{\text{postO}}+n_{\text{rds}}\alpha_{\text{R}})\frac{F\eta}{\mathcal{R}T}} \right). \tag{1.A.38}$$

Here $n_{\text{rdsO}} = 1$ since the rate-determining step almost always involves the transfer of a single electron [3] or $n_{\text{rdsO}} = 0$ when the rate-determining step is not a charge-transfer step. The sum of the rate-determining step charge transfer coefficients $\alpha_{\text{O}}+\alpha_{\text{R}} = 1$ as indicated in Eq. (1.22) so that $\alpha_{\text{effO}} + \alpha_{\text{effR}} = n_{\text{preO}} + n_{\text{postO}} + n_{\text{rdsO}}(\alpha_{\text{O}}+\alpha_{\text{R}}) = n$, the total number of electrons transferred

Note that the rate-determining step for the reverse reduction reaction does not have to be the same as that of the forward oxidation reaction. In this case we have $\alpha_{\text{effR}} = n_{\text{preR}} + n_{\text{rds}}\alpha_{\text{R}}$ and $\alpha_{\text{effO}} = n_{\text{postR}} + n_{\text{rds}}\alpha_{\text{O}}$ where n_{preR} is not necessarily equal to n_{postO} and n_{postR} is not necessarily equal to n_{preO}, unless the rate-determining step is the same.

Electron-transfer steps preceding the rate-determining step thus act to increase the effective transfer coefficient and reduce the Tafel slope. When the rate-determining step is the first single-electron transfer step $\alpha_{\text{eff}} = \alpha \approx 1/2$, while if there is a preceding electron transfer step $\alpha_{\text{eff}} = 1 + \alpha \approx 3/2$, or there are two preceding electron transfer steps and the rsd does not involve an electron transfer $\alpha_{\text{eff}} = 2 + 0 = 2$. The latter is thus beneficial in the sense that it gives a lower Tafel slope, and measurement of the Tafel slope under controlled conditions gives insight into the reaction mechanism.

---

[20]As all steps take place subsequently, they must all proceed at the same rate. What is meant here is that the step has a much lower rate constant. In the case of an electrochemical reaction, it requires much more overpotential than the others to proceed at the same rate.

Take, for example, the hydrogen evolution reaction in which, according to the Volmer mechanism, the rate-determining step can be the first electron transfer step. With $\alpha_R = 1/2$ this gives at room temperature a Tafel slope $b_c = \mathcal{R}T/\alpha_R F \approx 50$ mV, or $\ln 10 b_c \approx 2.3 b_c \approx 120$ mV per decade. In case the *Heyrovski step* is rate-determining, $\alpha_{effR} = 3/2$ and the Tafel slope becomes 40 mV per decade. Finally, a Tafel step involving the desorption of oxygen or hydrogen but no electron transfer can be rate-determining, in which case $\alpha_{effR} = 2$ and the Tafel slope reduces further to only 30 mV. The oxygen evolution reaction involves more electron transfer steps so even smaller Tafel slopes can be observed. Note that a Tafel slope of 120 mV does not automatically imply the Volmer mechanism [23]. Also, transport phenomena can significantly influence the Tafel slope, which we will consider in Chapter 3.

1.B *Alternative Butler-Volmer formulations*

1.B.1 *Changing reference concentrations*

Eq. (1.27) uses the equilibrium concentrations of the oxidants and reductants. These are the concentrations associated with a zero current density. Sometimes, it can be convenient to use different reference concentrations $c_{R,ref}$ and $c_{O,ref}$. In terms of these we can rewrite Eq. (1.27), after some algebra, as

$$j_\perp = j_{*ref}\left(\frac{c_R}{c_{R,ref}}e^{\frac{\alpha_O F}{\mathcal{R}T}(E-E_{ref})} - \frac{c_O}{c_{O,ref}}e^{-\frac{\alpha_R F}{\mathcal{R}T}(E-E_{ref})}\right). \tag{1.B.39}$$

Here $E - E_{ref} = \eta + \ln\left(\frac{c_{R,ref}}{c_{R,eq}}\right) - \frac{\alpha_R}{\alpha_O}\ln\left(\frac{c_{O,ref}}{c_{O,eq}}\right)$ and $j_{*ref} = j_*\left(\frac{c_{R,ref}}{c_{R,eq}}\right)^{\alpha_R}\left(\frac{c_{O,ref}}{c_{O,eq}}\right)^{\alpha_O}$, as can be verified by inserting Eq. (1.22). Choosing $c_{R,ref} = c_{O,ref} = 1$ M we can write

$$j_\perp = nFk^0\left(c_R e^{\frac{\alpha_O F}{\mathcal{R}T}(E-E^{0'})} - c_O e^{-\frac{\alpha_R F}{\mathcal{R}T}(E-E^{0'})}\right), \tag{1.B.40}$$

in terms of the intrinsic or *standard rate-constant* k^0 and *formal potential* $E^{0'}$ as is done in, for example, Ref. [3]. The associated Nernst equation obtained for $j_\perp = 0$ reads $E = E^{0'} + \frac{\mathcal{R}T}{F}\ln\frac{c_{O,eq}}{c_{R,eq}}$. The exchange current density follows, inserting this back in Eq. (1.27) as $j_* = nFk^0 c_{R,eq}^{\alpha_R} c_{O,eq}^{\alpha_O}$.

1.B.2 *Changing overpotentials*

The overpotential $\eta = (E - \phi) - (E - \phi)_{eq}$ in Eqs. (1.27) and (1.B.39) is relative to different but fixed reference concentrations. When the current is switched on these concentrations will change: the reactant concentration will decrease while the product concentration increases. Both effects will increase the overpotential required to sustain the current. To quantify this effect we transform Eq. (1.A.38), with some

algebra, into the following form

$$j_\perp = j_{*\mathrm{s}} \left(e^{\frac{\alpha_{\mathrm{effO}} F \eta_{\mathrm{s}}}{\mathcal{R}T}} - e^{-\frac{\alpha_{\mathrm{effR}} F \eta_{\mathrm{s}}}{\mathcal{R}T}} \right), \tag{1.B.41}$$

where the effective exchange current density $j_{*\mathrm{s}}$ depends on the concentration according to

$$j_{*\mathrm{s}} = j_* \left(\frac{c_\mathrm{R}}{c_{\mathrm{R,eq}}} \right)^{\frac{\alpha_{\mathrm{effR}}}{n}} \left(\frac{c_\mathrm{O}}{c_{\mathrm{O,eq}}} \right)^{\frac{\alpha_{\mathrm{effO}}}{n}} \tag{1.B.42}$$

and $\eta_\mathrm{s} \equiv \eta - \eta_\mathrm{c}$ where the *concentration overpotential*

$$\eta_\mathrm{c} = \frac{\mathcal{R}T}{nF} \left[\ln \left(\frac{c_\mathrm{O}}{c_{\mathrm{O,eq}}} \right) + \ln \left(\frac{c_{\mathrm{R,eq}}}{c_\mathrm{R}} \right) \right] \tag{1.B.43}$$

At the anode, the reactant C_R will decrease, making a positive contribution to the concentration overpotential. The product C_O increases, also making a positive contribution. So both effects increase the total overpotential η, and similarly for a cathode.

In this new formulation, the Butler-Volmer equation (1.B.41) has seemingly become concentration-independent. The concentration-dependence has now entered the new exchange current density $j_{*\mathrm{s}}$ and the associated surface overpotential η_s is now only one component of the full overpotential $\eta = \eta_\mathrm{s} + \eta_\mathrm{c}$, with the other part being the concentration overpotential. This makes it possible to determine which part of the overpotential should be attributed to concentration and which part is due to kinetics, where we note that the kinetics is furthermore influenced by the concentration through the new exchange current density $j_{*\mathrm{s}}$.

In case of a symmetric reaction with $\alpha_\mathrm{O} = \alpha_\mathrm{R}$ we can solve Eq. (1.B.41) analytically as in Eq. (1.33) to give

$$\eta = \overbrace{b \, \mathrm{asinh} \left(\frac{j_\perp}{2j_{*\mathrm{s}}} \right)}^{\text{surface overpotential}} + \overbrace{\frac{\mathcal{R}T}{F} \ln \left(\frac{c_\mathrm{O}}{c_{\mathrm{O,eq}}} \frac{c_{\mathrm{R,eq}}}{c_\mathrm{R}} \right)}^{\text{concentration overpotential}} \tag{1.B.44}$$

where $b = \frac{2\mathcal{R}T}{F}$.

We may further simplify by assuming an anode where the reactant concentration c_R changes significantly while the product concentration $c_\mathrm{O} \approx c_{\mathrm{o,eq}}$ remains fairly constant. An example is the anode in alkaline water electrolysis at low electrolyte concentrations where the reactant is hydroxide and the product is water. In this case

$$\eta = \frac{\mathcal{R}T}{F} \left[2 \, \mathrm{asinh} \left(\frac{j_\perp}{2j_{*\mathrm{s}}} \right) + \ln \left(\frac{c_{\mathrm{R,eq}}}{c_\mathrm{R}} \right) \right]. \tag{1.B.45}$$

Another relevant limit is the Tafel limit, in which one of the terms in the Butler-Volmer equation (1.27) dominates over the other. For definiteness let us assume an anode, in which case Eq. (1.B.41) can be solved to give

$$\eta_\mathrm{s} = b_\mathrm{a} \ln \left(\frac{j_\perp}{j_{*\mathrm{s}}} \right) = b_\mathrm{a} \ln \left(\frac{j_\perp}{j_*} \right) - \frac{\mathcal{R}T}{F} \left[\frac{\alpha_\mathrm{R}}{\alpha_\mathrm{O}} \ln \left(\frac{c_\mathrm{R}}{c_{\mathrm{R,eq}}} \right) + \ln \left(\frac{c_\mathrm{O}}{c_{\mathrm{O,eq}}} \right) \right] \tag{1.B.46}$$

where $b_a = \mathcal{R}T/\alpha_O F$ and we inserted Eq. (1.B.42). The final term exactly cancels with the first term of Eq. (1.B.43). The first term between the square brackets combines with the second term of Eq. (1.B.43), using $1 - \alpha_R = \alpha_O$ to give $\frac{\mathcal{R}T}{F} \ln\left(\frac{c_R}{c_{R,eq}}\right)$.

1.C *The Nernst equation*

Next, we aim to derive the Nernst equation for the equilibrium potential. For this purpose, we use the form of the Butler-Volmer equation of Eq. (1.B.39), which in equilibrium gives

$$\frac{c_{rdsO,eq}}{c_{rdsR,eq}} = e^{\frac{Fn_{rdsO}}{\mathcal{R}T}\left(E_{eq}-E^{0\prime}_{rds}\right)}. \tag{1.C.47}$$

The non-rate-determining steps will usually be fast enough compared to the rate-determining step, so they can be considered in equilibrium [1]. When the n_{preO} charge-transfer steps before and n_{postO} after the rate-determining step are in equilibrium:

$$\frac{c_{O,eq}}{c_{rdsO,eq}} = e^{\frac{n_{preO}F}{\mathcal{R}T}\left(E_{eq}-E^{0\prime}_{preO}\right)} \text{ and } \frac{c_{rdsR,eq}}{c_{R,eq}} = e^{\frac{n_{postO}F}{\mathcal{R}T}\left(E_{eq}-E^{0\prime}_{postO}\right)}. \tag{1.C.48}$$

This gives $\frac{c_{O,eq}}{c_{R,eq}} = e^{\frac{n_{preO}F}{\mathcal{R}T}\left(E_{eq}-E^{0\prime}_{preO}\right)}e^{\frac{F}{\mathcal{R}T}\left(E_{eq}-E^{0\prime}_{rds}\right)}e^{\frac{n_{postO}F}{\mathcal{R}T}\left(E_{eq}-E^{0\prime}_{postO}\right)} = e^{\frac{nF}{\mathcal{R}T}\left(E_{eq}-E^{0\prime}\right)}$ where $E^{0\prime} = \frac{n_{preO}E^{0\prime}_{preO}+n_{rdsO}E^{0\prime}_{rds}+n_{postO}E^{0\prime}_{postO}}{n}$ when used in Eq. (1.C.47). This leads to the general multi-electron transfer **Nernst equation**

$$E_{eq} = E^{0\prime} + \frac{\mathcal{R}T}{nF}\ln\left(\frac{c_{O,eq}}{c_{R,eq}}\right). \tag{1.C.49}$$

Solving Eq. (1.B.39) for $j_\perp = 0$, with α_O and α_R replaced with α_{effO} and α_{effR}, gives $E = E_{eff} + \frac{\mathcal{R}T}{nF}\ln\left(\frac{c_{O,eq}c_{R,ref}}{c_{O,ref}c_{R,eq}}\right)$, another form of the multi-electron transfer Nernst equation.

Chapter 2

Transport

Starting from a general conservation equation, the conservation of mass, heat, momentum, and charge are described. The mass transport equations are used to calculate the concentration overpotential. The Boltzmann distribution and Einstein relations are used to derive the Nernst-Planck equation, which describes the transport of ions. A mathematical description of a binary electrolyte, with and without a surplus of supporting electrolyte, is provided. Finally, a time-dependent solution to the mass transport equations is used to describe the concentration overpotential and the associated limiting current density as a function of time.

2.1 Conservation equations

A general conservation equation can be written in differential form as

$$\frac{\partial c}{\partial t} = -\nabla \cdot N + S, \tag{2.1}$$

where c is the concentration [something/m^3] of a conserved quantity. This can be for example the mass density ρ [kg/m^3] or the charge density ρ_q [C/m^3]. The final term S is a source, and N [something/m^2/s] is the flux related to c. We will use the symbol c [mol/m^3] to represent the molar concentration of a species in a gas or dissolved in a liquid. If the fluid moves with a velocity u, the flux associated with a low concentration c can be approximately written as

$$N = cu - D\nabla c. \tag{2.2}$$

The first term cu is the convective flux. The concentration at a location can increase or decrease because of a higher or lower concentration upstream, respectively. In the absence of flow, $N = -D\nabla c$ is called Fick's law and describes diffusive transport proportional to the diffusivity or diffusion coefficient D [m^2/s].[1] Inserting Eq. (2.2)

---

[1]In this book we will assume dilute concentrations so we can neglect the impact of mass transport of a species on the flow velocity. See appendix 2.B for a simple 1D example in which this effect is included.

in Eq. (2.1) gives, with $\nabla \cdot (c\boldsymbol{u}) = c\nabla \cdot \boldsymbol{u} + \boldsymbol{u} \cdot \nabla c$ and assuming incompressible flow, $\nabla \cdot \boldsymbol{u} = 0$ as discussed in Appendix 2.A.1, and constant D: ⟨icon⟩

$$\frac{Dc}{Dt} = D\nabla^2 c + S.$$ (2.3)

Here $\frac{Dc}{Dt} \equiv \frac{\partial c}{\partial t} + \boldsymbol{u} \cdot \nabla c$ is the *material derivative*. It represents the time variation of c, while moving along a streamline of the flow. Equation (2.3) is referred to as an advection-diffusion-reaction equation, in case S represents a reaction.

Integrating Eq. (2.1) over a fixed volume $\mathcal{V}$ we obtain ⟨icon⟩

$$\frac{d \int c \, d\mathcal{V}}{dt} = -\int \boldsymbol{N} \cdot d\boldsymbol{A} + \int S \, d\mathcal{V},$$ (2.4)

where we used the divergence theorem, also known as Gauss' theorem, to write $-\int \nabla \cdot \boldsymbol{N} \, d\mathcal{V} = -\int \boldsymbol{N} \cdot d\boldsymbol{A}$.[2]

2.1.1 Charge transport

The flux of electric charge is the current density, for which we use the symbols $\boldsymbol{j}$ and $\boldsymbol{i}$ [A/m^2], depending on whether we describe electrons or ions, respectively. Except in the electric double layer, with length scales of the order of a few molecules near a surface, electrolytes contain an equal density of positive and negative ions so that the charge density ρ_q [C/m^3] vanishes. Nonetheless, we can create a conservation equation for charge by replacing c in Eq. (2.1) with ρ_q and $\boldsymbol{N}$ with $\boldsymbol{i}$ to give

$$\frac{\partial \rho_q}{\partial t} = -\nabla \cdot \boldsymbol{i} + S_q,$$ (2.5)

where S_q [C/s/m^3] is a volume source of charge. Assuming zero charge density:[3]

---

[2]The infinitesimal area vector $d\boldsymbol{A}$ is directed outwards of the integration volume. Equation (2.4) shows the change in time by influx ($d\boldsymbol{A} \cdot \boldsymbol{N} < 0$) or outflux ($d\boldsymbol{A} \cdot \boldsymbol{N} > 0$), sources ($S > 0$) or sinks ($S < 0$).

[3]Gauss's law from electrostatics relates the divergence in the electric field to charge density

$$\nabla \cdot \boldsymbol{E} = \rho_q / \varepsilon_r \varepsilon_0$$ (2.6)

where $\varepsilon_r \varepsilon_0$ is the electrical permittivity of the material under consideration, with $\varepsilon_0 = 8.85 \cdot 10^{-12}$ C/V/m that of the vacuum and ε_r the relative permittivity. Comparing Eq. (2.6) with Eq. (1.1), we may interpret $\rho_q / \varepsilon_r \varepsilon_0$ as the source of some constant quantity for which the electric field is the flux. Inserting Ohm's law, Eq. (1.5), into Eq. (2.5) and using Eq. (2.6), assuming constant κ and no sources or sinks, we obtain

$$\frac{\partial \rho_q}{\partial t} = -\frac{\kappa}{\varepsilon_r \varepsilon_0} \rho_q.$$ (2.7)

The solution to Eq. (2.7) will be $\rho_q(t) = \rho_q(0)e^{-\frac{t}{\varepsilon_r \varepsilon_0 / \kappa}}$. In the previous chapter, we argued that good performance of electrochemical devices requires high conductivity, usually $\kappa \gtrsim 1$ S/m. The resulting characteristic time-scale, $\varepsilon_0 / \kappa \ll 10^{-11}$ s, is extremely small. This implies that any small charge imbalance will be restored almost instantaneously to give $\rho_q = 0$. Therefore, we can safely assume electroneutrality.

$$\rho_q = 0, \tag{2.8}$$

equation (2.5) gives:

$$\nabla \cdot \boldsymbol{i} = S. \tag{2.9}$$

Thus, in the absence of charge sources, the current is divergence-free. In Appendix 2.A, three more examples of conservation equations for mass, heat, and momentum are provided for readers needing more practice or familiarity.

2.2 Concentration overpotential

In the previous chapter we considered the concentration-dependent Tafel equations (1.29) and (1.31) for an oxidation and reduction reaction respectively. To avoid having to specify whether we describe an anode or a cathode we will use a general reactant concentration c and the current density magnitude j.[4] We can then write Eqs. (1.29) and (1.31) as

$$\eta = b\ln\left(\frac{j}{j_*}\frac{c_{\mathrm{eq}}}{c}\right) = b\ln\left(\frac{j}{j_*}\right) + b\ln\left(\frac{c_{\mathrm{eq}}}{c}\right). \tag{2.10}$$

The final term, the *concentration overpotential* introduced already in Eq. (1.30), increases when the concentration c at the surface of the electrode drops below the equilibrium concentration c_{eq}. This will generally happen as the reaction proceeds and the reactant concentration c locally decreases. The concentration difference with the unaltered bulk concentration, $c_{\mathrm{eq}} - c$, will drive the supply of fresh reactants to the electrode by diffusion.

Consider a steady-state without a concentration volume source, $S = 0$, so that Eq. (2.1) becomes $0 = -\nabla \cdot \boldsymbol{N}$. Here $\boldsymbol{N}$ is the molar flux of reactant with concentration c that is consumed at the electrode surface. Close to this electrode we can consider a one-dimensional approximation and introduce an x-coordinate normal to an electrode, with the electrode surface at $x = 0$, and positive values for x extending into the the electrolyte as shown in Fig. 2.1, so

$$\frac{\mathrm{d}N}{\mathrm{d}x} = 0. \tag{2.11}$$

Equation (2.2) in the x-direction, in the absence of flow, gives $N = -D\frac{\mathrm{d}c}{\mathrm{d}x}$. Inserting this into Eq. (2.11) shows that for constant diffusivity D, the concentration gradient $\mathrm{d}c/\mathrm{d}x$ is a constant, as depicted in Figure 2.1. Usually, at some distance from an electrode, the fluid flows can no longer be neglected due to intentional stirring, forced flow, gas bubbles, or natural convection due to concentration or temperature

---

[4]In case of a catalyst-coated or rough surface there may be a difference between the local current density $j_\perp$ and the overall current density magnitude j. We can take this into account by redefining or measuring the exchange current density j_* with respect to the macroscopic surface area.
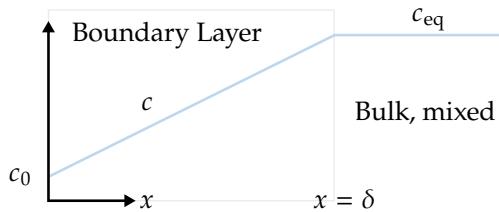
Figure 2.1: *A schematic of an idealised boundary layer concentration profile near an electrode. Within a distance $x < \delta$ no flow is assumed, giving a constant concentration gradient. Beyond $x > \delta$ exists a perfectly mixed bulk solution with reactant concentration c_{eq}.*

gradients. Beyond this distance, mixing will ensure a more or less constant bulk concentration. We will assume this to be equal to the concentration before the current was switched on so that we can use the equilibrium concentration c_{eq}.

Figure 2.1 depicts the often-used boundary layer idealisation that results from our assumptions, in which the domain is split into a no-flow region close to the electrode surface and a perfectly mixed bulk at a distance $x = \delta$ from the electrode. This is sometimes referred to as a Nernst layer, Nernst diffusion layer, or simply diffusion layer. This should not be confused with the electric double layer (EDL), which is typically several orders of magnitude thinner.

With this idealisation, the constant concentration gradient can be written as $\frac{dc}{dx} = \frac{c_{eq} - c_0}{\delta}$, with c_0 the concentration at the position of the electrode at $x = 0$. Faraday's law (1.19) gives for the electric current density magnitude $j = nF|N|$ or

$$j = nF\frac{D(c_{eq} - c_0)}{\delta} = j_{lim}\left(1 - \frac{c_0}{c_{eq}}\right). \tag{2.12}$$

Here the *limiting current density*

$$j_{lim} \equiv nF\frac{Dc_{eq}}{\delta}, \tag{2.13}$$

represents the maximum possible current, corresponding to the situation where $c_0 = 0$. A higher current density will not be possible with this boundary layer thickness δ, since diffusion cannot supply reactants at a higher rate. Inserting Eq. (2.12) into Eq. (2.10) gives

$$\eta = b\ln\left(\frac{j/j_*}{1 - j/j_{lim}}\right) = b\ln\left(\frac{j}{j_*}\right) + b\ln\left(\frac{1}{1 - j/j_{lim}}\right). \tag{2.14}$$

As j approaches the limiting current density j_{lim}, the concentration overpotential, represented by the last term in Eq. (2.14), diverges. As long as $j \ll j_{lim}$ the concentration at the electrode surface will remain relatively close to the equilibrium
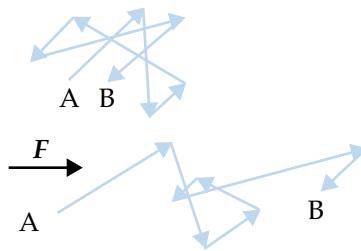
Figure 2.2: *Some particle trajectories of a molecule from A to B, where the changes in direction are due to collisions with other molecules, without a net force acting (top) and with a net force (bottom). An average drift velocity $\boldsymbol{u}_\text{d} = \mathcal{M}\boldsymbol{F}$ can be associated with the force $\boldsymbol{F}$.*

concentration. In this case, the concentration overpotential will be well below the Tafel slope (typically of the order $b \sim 50$ mV) and can often be neglected.

In case the reactant is an ion, we will have to consider the effect of the electric force, which will be the topic of the next section.

2.3 Transport of charged species

Transport of ions is governed by the Nernst-Planck equation, which is a slight generalisation of the conservation equation (2.1) with the flux expression (2.2). By Newton's second law, the force on a charged particle in an electric field leads to a constant acceleration. In an electrolyte, these accelerating charged particles undergo frequent collisions with each other or other species, as illustrated in Figure 2.2. The combined effect of the acceleration in the direction of the electrical force $\boldsymbol{F}$ and these frequent collisions is a constant effective *drift velocity* in the direction of the force:

$$\boldsymbol{u}_\text{d} = \mathcal{M}\boldsymbol{F}. \tag{2.15}$$

The constant of proportionality is called the mobility $\mathcal{M}$ [m/s/N]=[s/kg]. Also, macroscopic particles can have a mobility. This results from collisions with molecules observed as friction. This is considered, for the interested reader, in more detail in Appendix 2.C.

2.3.1 Boltzmann distribution

Not all molecules in a gas or a liquid move with the same velocity. In equilibrium thermodynamics, the probability of finding a particle with potential energy $\mathcal{U}$ is proportional to the Boltzmann factor $\text{e}^{-\frac{\mathcal{U}}{k_\text{B}T}}$, where the thermal energy $k_\text{B}T$ is a measure of the average kinetic energy per particle.[5]

---

[5]The probability of finding a molecule with an energy between E and $E + dE$ is given by $f(E)dE$ with the probability density distribution $f(E)$ given by Boltzmann distribution $f(E) = \text{e}^{-E/k_\text{B}T}/k_\text{B}T$,
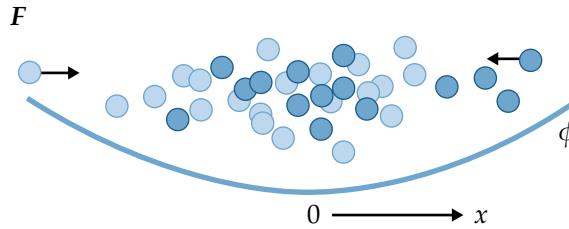
Figure 2.3: *Positively charged particles in thermal equilibrium near a minimum $\phi = 0$ in the electrical potential are distributed according to a Boltzmann distribution $\mathrm{e}^{-z\bar{\phi}}$. Exponentially fewer particles have sufficient kinetic energy to be found far away from the location where ϕ is a minimum, for example, near $x = 0$ when $\phi \propto x^2$.*

The Boltzmann constant can be expressed as $k_B = \mathcal{R}/N_A$, with N_A Avogadro's number and $\mathcal{R}$ the gas constant. The average kinetic energy of a mole of particles is therefore $N_A k_B T = \mathcal{R}T$. In the previous chapter, we encountered the Boltzmann distribution in the Arrhenius expression (1.21). The reaction rate is thus proportional to the chance that particles have a thermal energy per mole $\mathcal{R}T$ that exceeds the activation energy $\mathcal{E}_a$. In Eq. (1.3) we introduced the potential energy $\mathcal{U} = q\phi$ of a charged particle in a electric potential field ϕ. We can write the charge q of a particle as a multiple, the charge number z, of the elementary charge (of a proton) $e = 1.602176634 \cdot 10^{-19}$ C as

$$q = ze. \tag{2.16}$$

In thermodynamic equilibrium, the concentration c of charged particles will be given by the Boltzmann distribution as

$$\boxed{c \propto \mathrm{e}^{-\frac{\mathcal{U}}{k_B T}} = \mathrm{e}^{-\frac{q\phi}{k_B T}} = \mathrm{e}^{-z\bar{\phi}}.} \tag{2.17}$$

In the second expression, we inserted Eq. (1.3) and in the third, we introduced the dimensionless electrostatic potential

$$\bar{\phi} = \frac{e\phi}{k_B T} = \frac{F\phi}{\mathcal{R}T}. \tag{2.18}$$

Figure 2.3 schematically illustrates the Boltzmann distribution of Eq. (2.17) for positively charged particles in thermal equilibrium distributed around a minimum in the electrostatic potential.

which is normalised such that the probability of finding a particle at all $\int_0^1 f(E)dE = 1$. The average energy $\int_0^\infty E f(E)dE$, is the thermal energy $k_B T$. This exponential relation is the only function for which $f(E_1)f(E_2)$ is a function of $E_1 + E_2$. This should hold since the probability of finding two particles with energy E_1 and E_2 can only depend on the sum of their energies.

Symbol	Value	Unit	Description
$\mathcal{R}T/F = k_\mathrm{B}T/e$	≈ 0.025	V	Thermal potential
z	..-2,-1,0,1,2,...	-	Charge number, q/e
$\mathcal{R}$	8.314	J/mol/K	Ideal gas constant
e	$1.602 \cdot 10^{-19}$	C	Elementary charge
k_B	$1.38 \cdot 10^{-23}$	J/K	Boltzmann constant
F	96485.332	C/mol	Faraday constant

Table 2.1: *Constants and notation used throughout the book. The dimensionless ionic potential $\bar{\phi} = F\phi/\mathcal{R}T$ is obtained by dividing the ionic potential by the thermal potential, whose numerical value is provided for room temperature.*

Another example of the Boltzmann distribution can be found in how molecules of an ideal gas distribute themselves in the presence of gravity in an isothermal atmosphere, as discussed in Appendix 2.E.

2.3.2 Einstein relation

As discussed in the previous chapter, charged particles will experience an electric force given by Eqs. (1.1), (1.2), and (2.16) as

$$F = -z e \nabla \phi. \tag{2.19}$$

This force will cause a drift velocity given by Eq. (2.15) as $u_\mathrm{d} = -z e \mathcal{M} \nabla \phi$. For a dilute concentration c, so that the particle drift does not influence the flow velocity, we can simply add this drift velocity to the flow velocity in Eq. (2.2) to give

$$N = \left(u - z e \mathcal{M} \nabla \phi \right) c - D \nabla c. \tag{2.20}$$

In thermodynamic equilibrium, without any flux and fluid flow, the concentration c will satisfy the Boltzmann distribution Eq. (2.17). Differentiating Eq. (2.17) using the chain rule gives $\nabla c = -z c \nabla \bar{\phi}$, which upon insertion into Eq. (2.20) with $N = u = 0$ gives 🏃

$$\mathcal{M} = \frac{D}{k_\mathrm{B}T}. \tag{2.21}$$

This proportionality between the mobility and the diffusivity is called the Einstein-Smoluchowski equation.[6] Because the mobility and diffusion coefficient are determined by the same collision rate, this linear relation may also be appreciated intuitively.

---

[6]Although Smoluchowski and Sutherland derived the same relation independently around the same time, Albert Einstein published it in 1905. We derived it here for the case of an electrical force, but there are more *Einstein relations*. With Eq. (2.C.72), the Stokes-Einstein relation $D = \frac{k_\mathrm{B}T}{3\pi\mu d}$ results, which was used by Einstein to support the molecule hypothesis using observation of the diffusive Brownian motion of tiny dust particles. The mobility $\mathcal{M}$ is the ratio between drift velocity and force, while sometimes the *electrical mobility* $\mathcal{M}_q = u_\mathrm{d}/E = q\mathcal{M}$ is used so that the Einstein-Smoluchowski relation reads $D = k_\mathrm{B}T\mathcal{M}_q/q$.

2.3.3 Nernst-Planck flux

Inserting the Einstein relation (2.21) into Eq. (2.20) gives, using Eq. (2.18) ⚡

$$\boldsymbol{N} = c\boldsymbol{u} - D\left(\nabla c + \varkappa c \nabla \bar{\phi}\right). \tag{2.22}$$

This expression for the flux of charged particles is referred to as the Nernst-Planck flux. For neutral particles with $z = 0$, or in the absence of an electric field $\boldsymbol{E} = -\nabla\phi$, Eq. (2.22) reduces to Eq. (2.2). In the absence of flow and concentration gradients the flux

$$\boldsymbol{N}^{\mathrm{mig}} = \frac{\varkappa F D c}{\mathcal{R}T} \boldsymbol{E}, \tag{2.23}$$

is solely due to the drift of charged particles constantly accelerating and colliding, a process sometimes referred to also as *migration* or *conduction*. We will sometimes use a superscript "mig" or "diff" to denote those parts of the flux that can be attributed to migration or diffusion, respectively. In this case, the concentration gradients and flow are negligible and a flux of charged particles leads to a current density that is proportional to the electric field. The proportionality constant, the conductivity κ, follows as ⚡

$$\boldsymbol{i} = \varkappa F \boldsymbol{N}^{\mathrm{mig}} = \kappa \boldsymbol{E} \quad \text{where} \quad \kappa = \frac{\varkappa^2 F^2 D c}{\mathcal{R}T}. \tag{2.24}$$

So we see that Ohm's law Eq. (1.5) also holds for charged particles in a well-mixed but otherwise stationary fluid.

We note that the Einstein relation, Eq. (2.21), with constant diffusivity, only holds for **dilute** mixtures, typically for concentrations well below 1 M. However, taking into account the concentration-dependence of the diffusivity D, the Nernst-Planck equation (2.22) can often be used as a reasonable approximation also at higher concentrations.

2.3.4 Multicomponent transport equations

As discussed in section 2.1.1, the charge density of an electrolyte can usually be considered to vanish, a condition referred to as electroneutrality or quasi-neutrality. Therefore, there have to be at least two charged species with opposite charges. We will label the different species[7] by an index i, not to be confused with the magnitude of the ionic current density, so that the Nernst-Planck flux of Eq. (2.22) becomes

$$\boxed{\boldsymbol{N}_i = c_i \boldsymbol{u} - D_i \left(\nabla c_i + \varkappa_i c_i \nabla \bar{\phi}\right).} \tag{2.25}$$

Each species diffuses with its own diffusivity D_i and migrates with its own mobility $D_i/k_{\mathrm{B}}T$ but all share the same advection velocity $\boldsymbol{u}$ and potential ϕ. Each species individually satisfies a conservation equation Eq. (2.1)

---

[7]An example is the commonly used electrolyte sulphuric acid $\mathrm{H}_2^+\mathrm{SO}_4^{2-}$ dissolved in water. There will be a concentration c_1 with charge number $\varkappa_1 = 1$ of H^+ and a concentration c_2 with charge number $\varkappa_2 = -2$ of SO_4^{2-}. The charge density $\rho_q = \varkappa_1 c_1 + \varkappa_2 c_2 = 0$ so that $c_1 = 2c_2$, so there are twice as many H^+ compared to SO_4^{2-}.

$$\frac{\partial c_i}{\partial t} = -\nabla \cdot \boldsymbol{N}_i + S_i. \tag{2.26}$$

Eqs. (2.25) and (2.26) together are called the Nernst-Planck equation or equations.[8]

The charge flux, or species current density, associated with $\boldsymbol{N}_i$ is $z_i F \boldsymbol{N}_i$ so that the total current density reads

$$\boldsymbol{i} = \sum z_i F \boldsymbol{N}_i, \tag{2.28}$$

where the summations here and below are understood to be over the index i. Inserting Eq. (2.25) into Eq. (2.28) gives

$$\boldsymbol{i} = \rho_q \boldsymbol{u} - F \sum z_i D_i \nabla c_i + \kappa \boldsymbol{E}, \tag{2.29}$$

where the charge density can be usually assumed to be zero in accordance with Eq. (2.8):

$$\rho_q = F \sum z_i c_i = 0, \tag{2.30}$$

and the ionic conductivity follows as

$$\kappa = \frac{F^2}{\mathcal{R}T} \sum z_i^2 D_i c_i. \tag{2.31}$$

Note from Eqs. (2.29) and Eq. (2.30) that the fluid velocity $\boldsymbol{u}$ does not influence the current of a quasi-neutral electrolyte, since anions and cations are advected equally. The linear dependence of conductivity on electrolyte concentration in Eq. (2.31) only holds for dilute electrolytes. Often, there is a maximum conductivity so that at higher concentrations, the electrolyte conductivity again decreases with increasing electrolyte concentrations.

In the **absence of concentration gradients**, Eq. (2.29) gives Ohm's law $\boldsymbol{i} = \kappa \boldsymbol{E}$, introduced in Eq. (1.5). Equation (2.31) generalises Eq. (2.24) to include the effect of several ions. The relative contribution of each species to the conductivity is expressed by the ion transport number or **transference number**

$$t_i = \left. \frac{z_i F N_i}{i} \right|_{\substack{u=0 \\ \nabla c=0}} = \frac{z_i^2 D_i c_i}{\sum z_i^2 D_i c_i}. \tag{2.32}$$

---

[8]Inserting (2.25) and assuming incompressible flow Eq. (2.A.61) and a divergence-free electric field by Eq. (2.6) and constant D_i gives

$$\frac{\partial c_i}{\partial t} + \left(\boldsymbol{u} + \boldsymbol{u}_{\mathrm{d},i}\right) \cdot \nabla c_i = D_i \nabla^2 c_i + S_i, \tag{2.27}$$

an advection-diffusion-reaction equation like Eq. (2.A.62) but with an additional drift velocity $\boldsymbol{u}_{\mathrm{d},i} = -D_i z_i \nabla \tilde{\phi}$.

In the absence of concentration gradients $\nabla c = 0$ this number expresses the fraction of the flux that is carried by a species.[9] By construction, they add up to unity $\sum t_i = 1$.

2.4 Binary electrolytes

2.4.1 General binary electrolytes

An important class of electrolytes is the binary electrolyte, which contains only two ions, one anion A and one cation C. Strong acids and bases show complete dissociation of their salts upon dissolving in water

$$AC \rightarrow \nu_- A^{z_-} + \nu_+ C^{z_+}. \tag{2.33}$$

Here z_- and z_+ represent the ion valencies and ν_- and ν_+ are the stoichiometric coefficients of the ions in the salt. For those in need of more practice with ion transport, appendix 2.F considers two examples of monovalent binary electrolytes, the acidic H^+Br^- used in redox flow batteries, and the alkaline K^+OH^- used in water electrolysis. Footnote 7 considers the divalent electrolyte H_2SO_4, which has $z_+ = 1$ and $z_- = -2$ and $\nu_+ = 2$ and $\nu_- = 1$ since it dissociates into two H^+ and one SO_4^{2-} ion. $CuSO_4$ on the other hand has $z_+ = -z_- = 2$ and $\nu_- = \nu_+ = 1$, because it dissociates into one Cu^{2+} and one SO_4^{2-} ion. In general, charge conservation requires

$$\nu_+ z_+ + \nu_- z_- = 0. \tag{2.34}$$

Therefore, we can define the salt concentration as

$$c \equiv \frac{c_+}{\nu_+} = \frac{c_-}{\nu_-}, \tag{2.35}$$

equal to the number of moles of dissolved salt AC per unit volume. Note that the salt concentration may not be equal to the ion concentration.

2.4.2 Monovalent binary electrolytes

Here we will outline the equations describing a monovalent binary electrolyte, $z_+ = -z_- = \nu_+ = \nu_- = 1$, reserving the general case of arbitrary valencies and stoichiometries for Appendix 2.G. We will assume that the ion diffusivities D_- and D_+ are constant. The electroneutrality condition (2.30) for a monovalent binary electrolyte gives $c_+ - c_- = 0$, which is automatically satisfied using a single salt concentration $c \equiv c_+ = c_-$. Equation (2.32) gives

---

[9]Sometimes in literature, this additional restriction of zero concentration gradient is not added. In this case, instead of a material parameter, the transference number becomes dependent on the particulars of the situation considered and which species reacts for example.

$$t_+ = \frac{D_+}{D_+ + D_-} \text{ and } t_- = \frac{D_-}{D_+ + D_-}, \tag{2.36}$$

satisfying $t_+ + t_- = 1$. Equation (2.25) gives

$$\boldsymbol{N}_+ = c\boldsymbol{u} - D_+ \left(\nabla c + c\nabla\bar{\phi} \right), \tag{2.37}$$
$$\boldsymbol{N}_- = c\boldsymbol{u} - D_- \left(\nabla c - c\nabla\bar{\phi} \right). \tag{2.38}$$

Equation (2.26) allows us to write

$$t_- \left(\frac{\partial c}{\partial t} + \nabla \cdot \boldsymbol{N}_+ - S_+ \right) + t_+ \left(\frac{\partial c}{\partial t} + \nabla \cdot \boldsymbol{N}_- - S_- \right) = 0, \tag{2.39}$$

because the expressions between brackets vanish individually.

Using $t_+ + t_- = 1$ 🏹

$$\frac{\partial c}{\partial t} + \nabla \cdot \boldsymbol{N} = S, \tag{2.40}$$

where $S \equiv t_- S_+ + t_+ S_-$ and the *salt flux*

$$\boldsymbol{N} \equiv t_- \boldsymbol{N}_+ + t_+ \boldsymbol{N}_- = c\boldsymbol{u} - D_a \nabla c. \tag{2.41}$$

The *ambipolar diffusivity* or *salt diffusivity* D_a is defined as

$$\boxed{D_a \equiv t_- D_+ + t_+ D_- = \frac{2D_+ D_-}{D_+ + D_-}.} \tag{2.42}$$

For an incompressible flow $\nabla \cdot \boldsymbol{u} = 0$ and Eq. (2.40) can be further simplified to 🏹

$$\boxed{\frac{Dc}{Dt} = D_a \nabla^2 c.} \tag{2.43}$$

Note that the potential has disappeared from Eqs. (2.40) and (2.43) because $t_- \boldsymbol{N}_+^{\text{mig}} + t_+ \boldsymbol{N}_-^{\text{mig}} = 0$ and. Remarkably, we have obtained an advection diffusion equation, similar to that of a neutral species. However, through the boundary conditions, the electric field may still affect the solution. The influence of the electric field may also be seen in the definition of the effective diffusion coefficient, Eq. (2.42). Due to electro-neutrality, there is an electrostatic connection between the ions, and together they can only move as fast as the slowest ion. The faster ions are held back by slower ions by electrostatic forces, and the slower ions are pulled along by the faster ones. If the ionic diffusivities are very different, D_a is about twice the lowest value.[10] The reason for this doubling is that the transport by migration is effectively included

---

[10]If $D_+ \gg D_-$ we have $D_a \approx 2D_-$ while if $D_- \gg D_+$ we have $D_a \approx 2D_+$

in the diffusivity. If the ion diffusivities are equal, there is no electrostatic tethering between ions and the ambipolar diffusivity becomes equal to the ion diffusivity.

The current density of Eq. (2.29) gives with $c_+ = c_- \equiv c$

$$i = F(D_- - D_+) \nabla c + \kappa E, \tag{2.44}$$

The first part gives the *diffusion current density*, proportional to the difference in ion diffusivities. In agreement with Eq. (2.31), the conductivity reads

$$\kappa = \frac{F^2}{\mathcal{R}T}(D_+ + D_-) c. \tag{2.45}$$

Note that, while the diffusion current is proportional to the difference in ion diffusivities, the conduction current is proportional to their sum. Using Eq. (2.45), Eq. (2.44) can alternatively be written as

$$i = -\kappa \left(\chi \frac{\nabla c}{c} + \nabla \phi \right), \tag{2.46}$$

where $\chi \equiv \frac{\mathcal{R}T}{F} \frac{D_+ - D_-}{D_+ + D_-}$. This characteristic diffusion potential is rarely much larger than around 10 mV, so that often, but not always, the diffusion current can be neglected. In this case, the current in a binary electrolyte can be approximately described by Ohm's law $i = -\kappa \nabla \phi$, where the conductivity depends on the ion concentration c through Eq. (2.45).

In case of a constant current boundary condition, we see from Eq. (2.44) that the electric field determines the concentration gradient boundary condition to Eq. (2.40) or (2.43).

2.4.3 Zero-flux ion

An often-encountered case in which we can analytically solve for the concentration profile is when only one of the ions in the binary electrolyte has a non-zero flux. The other ion has a zero flux.[11]

This happens, for example, when only one of the ions in a binary electrolyte participates in a steady-state reaction. In alkaline water electrolysis, for example, the cation K^+ does not react. It will have a net average zero flux in a steady state.

Let us consider the case of *a monovalent binary electrolyte with a zero-flux cation* for definiteness. The opposite case of a zero-flux anion is readily obtained by switching all $+$ and $-$ signs. We consider the case of a stagnant layer of thickness δ. This may be, for example, inside a microporous diaphragm with small enough pores to avoid fluid flow. It may also serve as a crude description of a hydrodynamic boundary layer.

---

[11]This happens, for example, near an ion exchange membrane, which only allows cations (PEM, proton exchange membrane) or anions (AEM, anion exchange membrane) to pass through. Such ions are 'blocked' while the term 'immobile' or 'fixed' ions is typically reserved for ions in a membrane.

$$N_+^{\mathrm{mig}} = -D_+ c\bar{\phi}'$$
$$N_+^{\mathrm{diff}} = -D_+ c'$$
$$N_-^{\mathrm{mig}} = D_- c\bar{\phi}'$$
$$N_-^{\mathrm{diff}} = -D_- c'$$
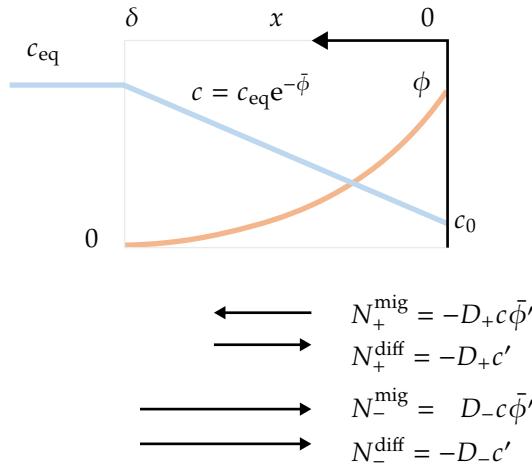
Figure 2.4: *The concentration and potential profiles in a stagnant layer between $x = \delta$, where the concentration is at its bulk value c_{eq} and $x = 0$, where the concentration c is lower. A zero-flux-cation's migration and diffusion fluxes cancel each other, which means they add for the anion. Note that the arrow sizes indicate that $D_- > D_+$.*

In the wall-normal direction, the assumption of a cation with zero flux in a stagnant layer allows us to write Eq. (2.37), for the cation flux, as

$$N_+ = -D_+ \left(c' + c\bar{\phi}' \right) = 0. \tag{2.47}$$

Here N_+ is used to denote the vector component of $\boldsymbol{N}_+$ in the x-direction, presently under consideration, so that it can also be negative. A prime indicates a derivative with respect to x, so $c' = \mathrm{d}c/\mathrm{d}x$.

Eq. (2.47) is solved by the Boltzmann distribution $c = c_{\mathrm{eq}}e^{-\bar{\phi}}$. This is expected, actually by construction, since the cations with zero flux are in thermodynamic equilibrium.[12] Here c_{eq} is the equilibrium bulk at $x = \delta$, where we take $\bar{\phi} = 0$, as illustrated in Figure 2.4.

Equation (2.38) gives the anionic flux in the x-direction as

$$N_- = -D_- \left(c' - c\bar{\phi}' \right). \tag{2.48}$$

This flux is now solely responsible for the ionic current density[13] $i = -FN_-$. Equation (2.47) gives $c' = -c\bar{\phi}'$, which inserted into Eq. (2.48) allows $i = D_- F \left(c'_- - c\bar{\phi}' \right)$ to be written as 🏃

---

[12]This is by construction, as this solution was actually used to derive the Einstein equation (2.21) used to formulate the Nernst-Planck equations.

[13]We will use i to denote the x-component of the ionic current density so i_x, dropping the sub-script x. This can, therefore, be positive or negative. Note that this contrasts with our use of j, which we use to denote the magnitude of the electronic current density, which is always positive.

$$i = -2D_- Fc\bar{\phi}' = 2D_- Fc'_-. \qquad (2.49)$$

The current can thus be described as a pure migration current, proportional to ϕ', or as a pure diffusion current density, proportional to c'. Or, of course, by the combination of both, which it really is. Both diffusion and migration will drive the current, but because these effects contribute in a fixed proportion, we can write the current density using either of the two terms. The reason for this fixed proportion is that the fluxes due to diffusion and migration have to be equal and opposite for the cation with zero flux, as described by Eq. (2.47). As a consequence, the diffusion and migration fluxes are equal and of the same sign for the other ion. This is schematically depicted by the arrows at the bottom of Fig. 2.4. In the case of a monovalent binary electrolyte, exactly half the current is transported by diffusion and the other half by migration. In Appendix 2.G.2 a general binary electrolyte is considered.

Note that we can reuse the analysis of section 2.2 concerning the concentration overpotential, where we also considered a Nernst boundary layer. Comparing Eq. (2.49) with Eq. (2.12), we see that we have to replace D with $2D_-$. The limiting current density of Eq. (2.13) then becomes

$$j_{\lim} \equiv nF \frac{2D_- c_{eq}}{\delta}. \qquad (2.50)$$

Here n denotes the number of electrons per reactant molecule. In the case of a redox reaction involving a monovalent binary electrolyte, generally $n = 1$. Using Eqs. (2.36) and (2.42)

$$2D_- = \frac{D_a}{1 - t_-}. \qquad (2.51)$$

The equations in this section are often found in the literature with the expression on the right-hand side instead of the left-hand side of Eq. (2.51).[14]

2.5 Supporting electrolyte

In the previous section we found that for a steady-state monovalent binary electrolyte without flow, half the current is carried by diffusion and half by migration. To reduce the ohmic losses associated with migration, sometimes a *supporting electrolyte* is added. This electrolyte is not involved in the reaction, but the additional ions do increase the conductivity through Eq. (2.31) and, therefore, reduce the potential gradient required for migration. It may seem somewhat strange at first that a species that does not contribute to the transport can do this, so the sceptical reader is referred

---

[14]One reason may be because of its natural generalisation to multi-component electrolytes. In case of a single ion i with a net flux we have $i = z_i F N_i = -z_i F D_i \left(\nabla c_i + z_i c_i \nabla \bar{\phi} \right) = -z_i F D_i \nabla c_i - t_i \kappa \nabla \phi$. When concentration gradients are small we can substitute the bulk relation $i = -\kappa \nabla \phi$ to give $i = z_i F N_i \approx -\frac{z_i F D_i}{1 - t_i} \nabla c_i$. This approximate relation looks similar to the exact Eq. (2.49) that can, with Eq. (2.51), be written as $i = -\frac{D_a z_- F}{1 - t_-} c'_-$.

to the derivation in Appendix 2.G.3. The main outcome of this analysis is that *when the supporting electrolyte concentration far exceeds the reactant concentration, the electric field and its effect through migration can be neglected.* Adding a supporting electrolyte essentially has the same effect as adding more of the reactant ion species. Equations (2.G.104) and (2.G.106) give, with the index i for the reacting ion and c_{supp} the concentration of the supporting electrolyte,

$$\frac{i}{z_i F} = 2 D_i c_{\text{supp}} \bar{\phi}' = -D_i c_i'. \tag{2.52}$$

As in the case of a binary electrolyte, Eq. (2.49), the current density can be written in terms of a pure diffusion current or a migration current, or a combination, because they are proportional. The first relation in Eq. (2.52) is similar to the first of Eq. (2.49) for a binary electrolyte. The difference is, however, that the concentration in Eq. (2.52) is not that of the reacting ion, but the concentration of the supporting electrolyte. Therefore, the supporting electrolyte concentration can be increased to reduce the potential gradient $\bar{\phi}'$. The second expression in Eq. (2.52) differs from that in Eq. (2.49) in that the additional factor two is missing.

The reason is that the potential gradient is strongly reduced due to the presence of the supporting electrolyte. Therefore, there can be little migration and the current is determined solely by diffusion. This reduces the limiting current density to

$$j_{\text{lim}} \equiv n F \frac{D_i c_{\text{eq}}}{\delta}, \tag{2.53}$$

so without the additional factor two of Eq. (2.50) due to migration. A small downside of adding a supporting electrolyte is thus a reduced limiting current density.

Note that the negligible electric field strength allows the reacting ion concentration to be described by an advection-diffusion equation. Equation (2.27) without the effect of migration becomes (2.3). The difference with the advection-diffusion equation derived for a binary electrolyte, Eq. (2.43), is the diffusion coefficient. Instead of the ambipolar diffusion coefficient, in the presence of a supporting electrolyte, it is the ion with a non-zero flux whose diffusivity appears. Also, the boundary conditions will be different. We summarise the differences between the case of a single ion with a non-zero flux in a binary electrolyte and a supporting electrolyte in Table 2.2.

2.6 Transient diffusion, constant current, Sand's analysis

We end this chapter by considering our first transient case. Shortly after a current is switched on, a growing boundary layer will arise in a stagnant electrolyte as illustrated in Figure 2.5. An analytical solution can be derived for a semi-infinite domain, as is outlined in Appendix 2.H. However, a more heuristic approach [4] is almost as accurate but arguably more insightful. Consider a neutral reactant or a reacting ion in a supporting electrolyte, with concentration c and diffusion coefficient

	Binary electrolyte	Supporting electrolyte
Diffusion coefficient	D_a	D_i
Conductivity $\|i\|/\|\nabla\phi\|$	$2D_i \frac{F^2}{\mathcal{R}T} c_i$	$2D_i z_i \frac{F^2}{\mathcal{R}T} c_{\text{supp}}$
Boundary condition for c_i'	$-i/2FD_i z_i$	$-i/F z_i D_i$
Limiting current density j_{lim}	$2nFD_i\|c_0'\|$	$nFD_i\|c_{i,0}'\|$

Table 2.2: *The differences between a monovalent binary electrolyte and a supporting electrolyte with concentration c_{supp} in which a single non-zero-flux-ion with charge number z_i and a concentration c_i carries the current. In the case of a binary electrolyte, generally, the number of electrons per reactant molecule $n = |z_i|$.*
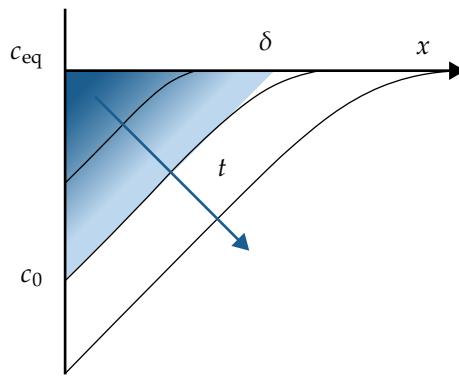
Figure 2.5: *Reactant concentration profiles $c(x,t)$ for various times t due to step change in current over time. The shaded blue triangle graphically depicts the linearisation approximation used Eq. (2.56).*

D. The reactant diffusive flux in the x-direction $N_x = -Dc' < 0$ so that the associated current is given by $j = nF|N_x|$. We consider the case in which the electrode potential is adjusted such that the current density becomes constant. Equation (2.52) gives the following boundary condition 🏃

$$c_0' = \frac{j}{nFD}. \tag{2.54}$$

Here a subscript 0 indicates the electrode surface at $x = 0$. Integrating Eq. (2.4) with respect to time t and dividing by the electrode area A gives the number of moles of reactant consumed per unit area as

$$\int \left(c_{\text{eq}} - c\right) \mathrm{d} = |N_x|t = \frac{jt}{nF}. \tag{2.55}$$
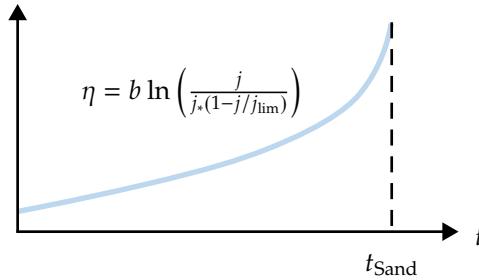
Figure 2.6: *The concentration overpotential increases with time and diverges as the surface concentration drops to zero at $t = t_{\mathrm{Sand}}$.*

The integral can be accurately approximated by the shaded area indicated in Figure 2.5. The area of this triangle is given by half the boundary layer thickness δ times $c_{\mathrm{eq}} - c_0 = c_0' \delta$, so

$$\frac{c_0' \delta^2}{2} \approx \frac{jt}{nF}. \tag{2.56}$$

This gives an expression for the boundary layer thickness $\delta \approx \sqrt{2Dt}$, which is close to the exact result derived in the appendix, Eq. (2.H.109):

$$\boxed{\delta \approx 2\sqrt{Dt/\pi}.} \tag{2.57}$$

The surface concentration $c_0 = c_{\mathrm{eq}} - \delta c_0'$ follows, using Eq. (2.54), as

$$c_0 = c_{\mathrm{eq}} \left(1 - \frac{j}{j_{\mathrm{lim}}} \right), \tag{2.58}$$

where

$$j_{\mathrm{lim}} = \frac{nFDc_{\mathrm{eq}}}{\delta} = \frac{nFDc_{\mathrm{eq}}}{2\sqrt{Dt/\pi}}. \tag{2.59}$$

The surface concentration c_0 decreases in time according to Eq. (2.58). This gives rise to a concentration overpotential that increases in time, as described by Eq. (2.14). When the concentration c_0 approaches zero, the overpotential diverges. This is schematically shown in Figure 2.6.

The requested constant current density can be maintained by increasing the overpotential. However, after some time the electrode concentration $c_0 = 0$ and the current density will have to decrease in time as the boundary layer thickness δ continues to increase while the concentration difference $c_{\mathrm{eq}} = c_0$ cannot be increased

further. These limiting current conditions are reached after a time called Sand's time given by solving $j = j_{lim}$, using Eq. (2.59) as 𓀀

$$t_{Sand} = \frac{\pi D}{4j^2}\left(nFc_{eq}\right)^2. \tag{2.60}$$

We note that when one of the ions of a binary electrolyte reacts, this same analysis holds using $D = 2D_i$, with D_i the diffusivity of the reacting ion. In this case, the ohmic drop will increase in time in addition to this overpotential activation since the ionic conductivity is proportional to the decreasing electrolyte concentration.

2.7 Summary

- The Nernst-Planck flux $\boldsymbol{N}_i = c_i\boldsymbol{u} - D_i\left(\nabla c_i + z_i c_i \frac{F}{\mathcal{R}T}\nabla\phi\right)$ (2.25) of a dilute ion concentration accounts for advection, diffusion, and migration, respectively. In the absence of flow and concentration gradients, the conductivity $\kappa = \boldsymbol{i}/\boldsymbol{E} = -\sum z_i F \boldsymbol{N}_i/\nabla\phi = \frac{F^2}{\mathcal{R}T}\sum_i z_i^2 D_i c_i$ (2.31). A zero-flux ion with $\boldsymbol{N}_i = 0$ in the absence of flow satisfies the Boltzmann distribution $c_i \propto e^{-\frac{z_i F}{\mathcal{R}T}\phi}$.

- The general conservation equations $\frac{\partial c_i}{\partial t} = -\nabla \cdot \boldsymbol{N}_i$ (2.26) for a *binary* electrolyte and incompressible flow reduce to an advection-diffusion equation $\frac{\partial c}{\partial t} + \boldsymbol{u} \cdot \nabla c = D_a \nabla^2 c$ (2.43) with the ambipolar diffusivity $D_a = \frac{2D_+ D_-}{D_+ + D_-}$. Without flow and for a monovalent cation with no flux, the anion flux $\boldsymbol{N}_- = 2D_- c\nabla\frac{F}{\mathcal{R}T}\phi = -2D_-\nabla c$ (2.49) equals twice the diffusion or migration flux since both are equal because $\boldsymbol{N}_+ = 0$. A supporting electrolyte strongly increases the conductivity, suppressing the electric field and associated migration, halving the limiting current density.

- The concentration overpotential $b\ln\left(\frac{c_{eq}}{c}\right)$ (2.10) diverges as c approaches zero. Without advection or migration, this happens at a limiting current density $j_{lim} = \frac{nFDc_{eq}}{\delta}$ (2.13). At constant current, the boundary layer thickness $\delta \approx 2\sqrt{Dt/\pi}$ is obtained after Sand's time $t_{Sand} = \frac{\pi D}{4j^2}\left(nFc_{eq}\right)^2$ (2.60).

2.8   Exercises

Exercise 2.1

Consider a fuel cell cathode in which oxygen, with a concentration c in air, reacts with protons to water.

a. What is the number n of electrons consumed per oxygen molecule in this reaction?
b. Give an expression for the limiting current density, assuming the oxygen molecules have to diffuse through an air layer of thickness L with a diffusivity D.
c. Now assume that this 'gas diffusion layer' consists of straight channels with a volume fraction ϵ in a solid. Give an expression for the limiting current density.

Exercise 2.2

Consider the porous separator inside a Li-ion battery, filled with the monovalent binary electrolyte $Li^+PF_6^-$. The electrolyte effective conductivity is $\kappa = 1.3$ S/m. The cathode where Li^+ is reduced is at $x = 0$ on the left, and the anode where it is oxidised is at $x = L$ on the right. Assume: 1D, steady-state, no flow, a temperature of 300 K, and a constant average electrolyte concentration $c = 800$ mol/m^3.

a. Derive an expression for the Li^+ diffusivity D_+ in terms of the ambipolar diffusivity D_a and the transfer coefficient $t_+ \equiv \frac{D_+}{D_+ + D_-}$.
b. Derive the electrolyte concentration profile for a given current density j.
c. Use the given conductivity $\kappa = 1.3$ S/m and cation transfer number $t_+ = 0.4$ to give a numerical value for the ambipolar diffusivity D_a.
d. Assuming $L = 200$ μm, what is the associated characteristic time-scale for diffusion $t \sim L^2/D_a$? Is the assumption of steady-state warranted? Give an expression for the magnitude of the limiting current density

Exercise 2.3

In electrolysers, a concern is hydrogen 'crossing over' through the membrane or separator to the anode, where at sufficiently high concentrations it could reach the 'lower explosion limit' of about 4 vol% hydrogen in oxygen.

a. If hydrogen is present at a concentration c_0 at the cathode and an approximately zero concentration at the anode, calculate the diffusive flux N_0 through a membrane with thickness L and effective diffusivity D
b. Now if there is a small pressure difference, perhaps because after start-up the pressure rises faster at the cathode due to the larger volume of gases produced, there may be a small flow velocity u through the separator from cathode to anode. The hydrogen flux in the x-direction from $x = 0$ at the cathode to $x = L$ at the anode is now given by $N = uc - D\frac{dc}{dx}$. Assuming a steady state, give the concentration profile through the membrane.

c. Give an expression for the flux N in terms of the Péclet number $\text{Pe} = uL/D$ and the flux N_0 without advection.

d. Considering a typical alkaline water electrolyser separator with an effective oxygen diffusion coefficient $D = 10^{-9}$ m^2/s and thickness $L = 0.5$ mm, at what velocity is diffusive flux doubled due to advection?

Exercises 2.4-2.19

Fill in the missing steps in the main text, indicated by the symbol ⋌.

Appendices *

2.A *Examples of conservation equations*

2.A.1 *Mass*

Eq. (2.1) is a general conservation equation that can describe various conserved quantities, such as mass. Instead of the molar concentration c we can use the density ρ [kg/m^3]. Without diffusion, the mass flux reads ρu so that without mass sources, $S = 0$, Eq. (2.1) gives $D\rho/Dt = -\rho\nabla\cdot u$. Moving along with the fluid flow, the density of most fluids stays approximately constant so that $D\rho/Dt = 0$. Even compressible fluids often approximately satisfy this criterion at flow velocities well below the speed of sound. Combining these two equations gives the equation describing *incompressible flow* as

$$\nabla\cdot u = 0. \tag{2.A.61}$$

In this book, generally, divergence-free flow is assumed to hold.

2.A.2 *Heat*

The thermal diffusivity is expressed as $\alpha = \lambda/\rho C_\mathrm{p}$ [m^2/s] with λ the thermal conductivity [W/m/K] and C_p [J/kg/K] the specific heat capacity. Replacing c by the volumetric thermal energy $\rho C_\mathrm{p} T$ [J/m^3] and D by α in Eq. (2.2) gives without flow, $u = 0$, and constant ρC_p

$$N = -\lambda\nabla T, \tag{2.A.62}$$

which is called Fourier's law. Eq. (2.3) becomes, again for constant ρC_p

$$\frac{DT}{Dt} = \alpha\nabla^2 T + \frac{S}{\rho C_\mathrm{p}}. \tag{2.A.63}$$

The heat source S [W/m^3] may include for example viscous heating or a source from an exothermic reaction.

2.A.3 *Momentum*

Equation (2.1) can also be used to describe the conservation of momentum, by replacing c in Equation (2.1) with the momentum density ρu. Because this is a vector, the flux N is replaced by a tensor τ, representing the momentum flux or force per unit area. For *Newtonian fluids* the viscous stress tensor, $\tau = \mu \left(\nabla u + \nabla u^{\mathrm{T}} \right)$, is proportional to the dynamic viscosity μ. An additional force in fluids is due to pressure p, which adds pI, with I the unit tensor. Finally adding the convective part ρuu gives

$$\frac{\partial \rho u}{\partial t} = -\nabla \cdot \left(\mu \left(\nabla u + \nabla u^{\mathrm{T}} \right) + pI + \rho uu \right) + S. \tag{2.A.64}$$

For a constant density and viscosity, assuming the flow is incompressible as described by Eq. (2.A.61), using some vector and tensor relations this can be simplified to the incompressible Navier-Stokes equation

$$\frac{Du}{Dt} = \nu \nabla^2 u - \frac{\nabla p}{\rho} + \frac{S}{\rho}, \tag{2.A.65}$$

where $\nu = \mu/\rho$ is the kinematic viscosity. The source term S/ρ represents any additional force per unit mass, for example, due to gravity $\frac{S}{\rho} = -g\hat{z}$ for a gravitational acceleration g [m/s^2] in the negative z-direction.

2.B *Stefan velocity*

The fickian diffusion flux in Eqs. (2.2) and (2.22) assumes that the concentration of the transported species c is much smaller than the total concentration C of the gas or liquid through which it is transported. If this were not the case, the concentration could influence the density, diffusivity, and other material parameters. Additionally, the flow velocity u cannot be seen as independent and is impacted by the moving species. To illustrate this, we consider the following example of a layer in which a species with a concentration c is transported from $x = 0$ to $x = L$ with constant flux, for example, because it is produced in a reaction and otherwise accumulates. Another species with concentration $\tilde{c}$ is assumed to have zero flux $\tilde{N}_x = u\tilde{c} - D\tilde{c}' = 0$, where D is the mutual diffusion coefficient. Especially in gases, to a good approximation, the total concentration $C = c + \tilde{c}$ is constant. This allows us to write

$$\tilde{N}_x = u\left(C - c \right) + D\tilde{c}' = 0, \tag{2.B.66}$$

so that the flux of the species with flux reads

$$N_x = uc - Dc' = uC. \tag{2.B.67}$$

We can solve the differential equation (2.B.66) to give

$$c(x) = C - \left(C - c(0) \right) e^{ux/D}. \tag{2.B.68}$$
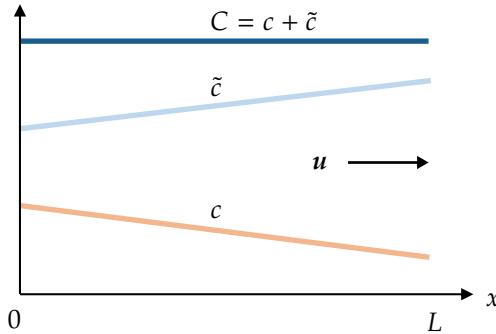
Figure 2.7: *The concentrations c and č of a species, with and without flux, respectively, adding up to a constant concentration C. The mass transport of the finite-flux species to the right introduces a Stefan flow velocity **u** that counteracts the diffusion flux of the zero-flux species.*

So we see that to maintain a zero flux of one species a velocity is induced, which makes the concentration of the reacting species vary exponentially with x. This velocity arises due to the transport of the mobile species and is called the Stefan velocity. As the concentration $c(x)$ decreases in the x-direction, the concentration $\tilde{c}$ has to increase. The Stefan velocity counteracts the diffusion flux that would otherwise force the zero-flux species to $x = 0$. Solving Eq. (2.B.68) for u and inserting in Eq. (2.B.67) gives, evaluated at $x = L$

$$N_x = \frac{DC}{L} \ln\left(\frac{C - c(L)}{C - c(0)}\right). \tag{2.B.69}$$

For low concentrations $c \ll C$ we can linearise this to give Fick's law $N_x = \frac{D}{L}(c(0) - c(L))$ and Eq. (2.B.68) to give the linear profile $c(x) = c(0) - u\frac{C-c(0)}{D}x$.

2.C *Mobility of a macroscopic particle*

For a mass moving with a velocity u relative to a fluid in rest, in response to a force F, we can write Newton's second law as follows:

$$m\frac{d\boldsymbol{u}}{dt} = \boldsymbol{F} + \boldsymbol{F}_{\mathrm{d}}. \tag{2.C.70}$$

Here $\boldsymbol{F}_{\mathrm{d}}$ is a frictional force or a drag force. Larger objects will experience a drag force approximately proportional to their velocity squared, due to inertial forces. For smaller particles viscous forces dominate. For small spherical particles, their velocity magnitude u relative to the fluid velocity and diameter d may be small enough that their particle Reynolds number $\mathrm{Re}_{\mathrm{p}} = \frac{\rho u d}{\mu} \ll 1$. In this case, the flow around them,
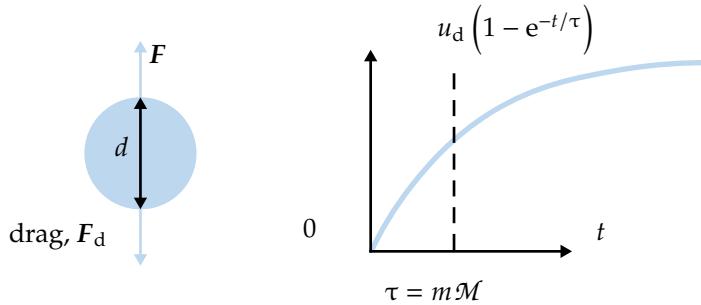
Figure 2.8: *An example particle with diameter d moving upwards due to a force **F**. A drag force **F**$_\mathrm{d}$ = −**u**$_\mathrm{d}$/$\mathcal{M}$ acts to decelerate the particle, resulting in the shown velocity profile.*

called Stokes flow, can be solved analytically neglecting fluid inertia. The resulting Stokes drag force is given by

$$\boldsymbol{F}_\mathrm{d} = -3\pi\mu d\boldsymbol{u}. \tag{2.C.71}$$

This drag force is opposite and proportional to the particle velocity $\boldsymbol{u}$ relative to the fluid, which we assume here to have a vanishing or at least constant velocity. In steady state $d\boldsymbol{u}/dt = 0$ and Eq. (2.C.70) gives $\boldsymbol{F} = -\boldsymbol{F}_\mathrm{d} = 3\pi\mu d\boldsymbol{u}_\mathrm{d}$ where $\boldsymbol{u}_\mathrm{d}$ is the steady-state velocity. The subscript d here stands for drag, or for drift considered in the next section. Comparing with Eq. (2.15) we see that

$$\mathcal{M} = \frac{1}{3\pi\mu d}. \tag{2.C.72}$$

So the mobility of a small spherical particle is inversely proportional to its size and the liquid viscosity.

Solving Eq. (2.C.70) with initial condition $\boldsymbol{u} = 0$ at $t = 0$ gives

$$\boldsymbol{u}\,(t) = \boldsymbol{u}_d \left(1 - \mathrm{e}^{-\frac{t}{\tau}}\right), \tag{2.C.73}$$

where $\boldsymbol{u}_\mathrm{d} = \mathcal{M}\boldsymbol{F}$ is the final steady-state velocity and the relaxation time $\tau = m\mathcal{M}$ is proportional to both the object's mass and mobility. With $m = \rho_\mathrm{p}\pi d^3/6$ the product of the particle density ρ_p and its volume, and Eq. (2.C.72) we obtain $\tau = \frac{\rho_\mathrm{p} d^2}{18\mu}$. With a typical $\mu/\rho_\mathrm{p} = 10^{-6}$ m^2/s a particle with a diameter of $d = 1$ µm gives $\tau \approx 6 \cdot 10^{-8}$ s and a particle with a diameter of $d = 1$ mm has a relaxation time of $\tau \approx 0.06$ s. Therefore, for small enough particles, the acceleration phase is only very short and assuming a steady-state force equilibrium with a constant particle velocity is a good approximation under many circumstances.

2.D *Simple conductance model*

We consider a constant charge density ρ_c *of charge carriers*, for example, electrons in a wire or transported ions in an electrolyte. An equal and opposite charge density of counterions will usually ensure a zero charge density. From the analysis of a macroscopic particle in the previous section 2.C, we found that the mobility $\mathcal{M} = \tau/m$ is proportional to the force equilibration time τ and inversely proportional to the particle mass. This will also hold for electrons or ions if we re-interpret τ as the characteristic time between collisions. By Eq. (2.C.71), a particle experiencing an electric force $F = qE$, Eq. (1.1), gives a drift velocity $u_{\mathrm{d}} = \mathcal{M}F = \frac{q\tau}{m}E$. The charge flux or the current density reads $i = \rho_c u_d$ in agreement with the general Eq. (2.2). We thus naturally recover Ohm's law $i = \kappa E$ which states a proportionality between current density and electric field. The conductivity

$$\kappa = \frac{\rho_c q \tau}{m}. \tag{2.D.74}$$

In this model, a simplification of the model proposed in 1900 by Paul Drude, the conductivity is proportional to the density of charge carriers and their charge squared, since also ρ_c is proportional to the carrier charge. This is in agreement with the result of Eq. (2.31), derived from the Nernst-Planck equation.

2.E *Boltzmann atmosphere*
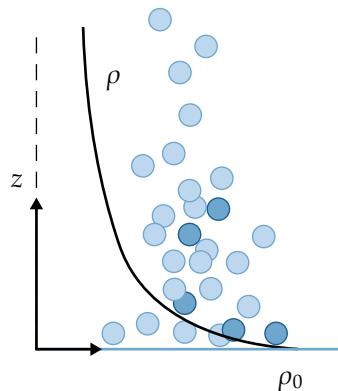
Figure 2.9: *Density distribution $\rho(z)$ as a function of the height of an ideal isothermal atmosphere satisfying the Boltzmann distribution.*

For those readers seeking to get more familiar with the Boltzmann distribution, we consider here the example of an isothermal atmosphere satisfying the ideal gas law. The electric force $F = -q\nabla\phi$ has a strong resemblance to the gravitational force, which is also a conservative force. The gravitational force is also proportional to the

gradient of a scalar, the gravitational potential. An obvious difference is of course that mass, unlike charge, can only be positive.

First, we obtain the hydrostatic force balance assuming zero flow velocity $u = 0$ in the Navier-Stokes Equation (2.A.65) and considering only the direction of gravity, the z-direction:

$$\frac{dp}{dz} = -\rho g. \tag{2.E.75}$$

The ideal gas law can be written as:

$$p = \frac{\mathcal{R}T}{\mathcal{V}_m} = \frac{\rho \mathcal{R}T}{M}, \tag{2.E.76}$$

where $\mathcal{V}_m = M/\rho$ [m^3/mol] is the molar volume, with M [kg/mol] the molarity.

Inserting Eq. (2.E.76) in Eq. (2.E.75) gives

$$\frac{d\rho}{dz} = -\frac{\rho}{H} \rightarrow \rho = \rho_0 e^{-\frac{z}{H}} \quad \text{with } H = \frac{\mathcal{R}T}{gM}. \tag{2.E.77}$$

The density in an isothermal atmosphere thus satisfies the Boltzmann distribution and decreases exponentially with height z from its value ρ_0 at ground level, $z = 0$. The characteristic atmosphere "height" $H \approx 9$ km, using the molarity of air and $T \approx 300$ K. Although our atmosphere is far from isothermal, most mass is roughly within twice this distance.

The argument of the exponent can be written as $-\frac{z}{H} = -\frac{\mathcal{E}_a}{\mathcal{R}T} = -\frac{\mathcal{U}}{k_B T}$ with $\mathcal{E}_a = gMz$ and $\mathcal{U} = gmz$ the average gravitational potential energy per mole or particle, respectively. Therefore, an isothermal ideal gas under the influence of a conservative force satisfies the Boltzmann distribution. The premise of section 2.3.1 is that ions in an electric field will equally satisfy this distribution.

2.F Balance sheets

2.F.1 Example: hydrogen-bromine redox flow battery

Consider a membrane-less cell with two electrodes far apart and the liquid electrolyte in between well-mixed. In this case, the electrolyte concentration is fairly constant in the centre, while concentration gradients can arise in thin boundary layers near the electrode, see Figure 2.10. Often only one of the ions in an electrolyte participates in a reaction. As an example, we consider the charging reaction of a hydrogen-bromine (H_2Br_2) redox flow battery:[15]

$$2Br_- \rightarrow 2e^- + Br_2, \tag{2.F.78}$$

$$2e^- + 2H^+ \rightarrow H_2. \tag{2.F.79}$$

---

[15]Note that in Fig. 2.10 we draw the oxidation reaction on the left and the reduction reaction on the right. In batteries, the electrode at which the oxidation reaction occurs is called the anode during discharging, but the cathode during charging. So, as an exception, we here have the cathode on the left.
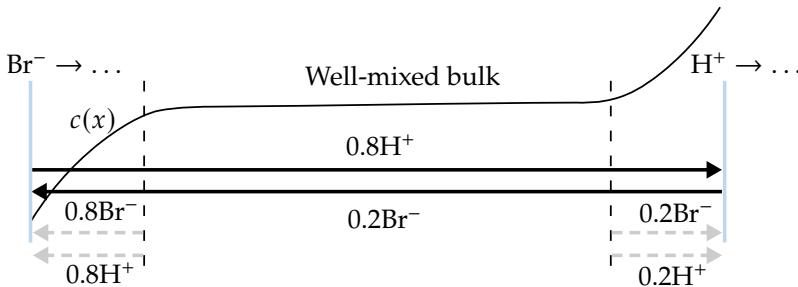
Figure 2.10: *The charging of a H_2-Br_2 flow battery, schematically split into a bulk region with only migration and a boundary layer region with also diffusion. The solid black arrows denote migration fluxes while the grey dashed arrows indicate diffusion fluxes. The difference in transference numbers $t_+ = 0.8$ and $t_- = 0.2$ is compensated by diffusion in the boundary layers near the electrodes.*

Because of its smaller size, the diffusivity of H^+ is substantially higher than that of Br^- so that the H^+ ions (protons) have an approximate transference number of $t_+ \approx 0.8$. In the well-mixed bulk, the electrolyte concentration is approximately constant, and diffusion does not play a role. As shown in Eq. (2.32), transference numbers can be used to indicate the fraction of the current carried by a particular ion in the absence of concentration gradients. Therefore, migration transports about four times as much H^+ in the direction of the electric field, to the right in Figure 2.10, as it transports Br^- in the opposite direction. However, by the reactions of Eqs. (2.F.78) and (2.F.79), equal amounts of H^+ and Br^- are consumed, so how can this be?

At the electrodes, there will be no fluid flow possible so the well-mixed condition cannot extend all the way to the electrode and there will be a diffusion boundary layer close to the electrodes. Here, diffusion will have to make up for the difference in transference number. Near the left Br^--consuming electrode a concentration gradient will arise that will aid the transport of Br^- but oppose the transport of H^+, cancelling the migration flux of H^+. Similarly, at the right H^+-consuming electrode, this concentration gradient will be much smaller since a smaller migration flux of Br^- has to be cancelled.

Note that in these reactions the electrolyte is consumed so that, to obtain a steady charging reaction, fresh electrolyte has to be supplied by advection. A flow velocity parallel to the electrodes will add additional fluxes, but since these will not contribute to the current, they do not impact the general picture of Fig. 2.10.

2.F.2 *Example: alkaline water electrolysis*

A typical electrolyte used in alkaline water electrolysis is potassium hydroxide, which dissociates into K^+ ions and OH^- ions. The diffusivity of K^+ ions is about three times smaller than that of OH^- so that $t_+ \approx 0.25$ and $t_- \approx 0.75$. In the reactions given by Eqs. (1.14) and (1.15), the potassium ion does not participate, so in steady-state and

$$4\,OH^- \longrightarrow 4\,e^- + O_2 + 2\,H_2O$$

$$K^+$$

$$c$$

$$t$$

$$OH^-$$

$$2\,H_2O + 2\,e^- \longrightarrow H_2 + 2\,OH^-$$
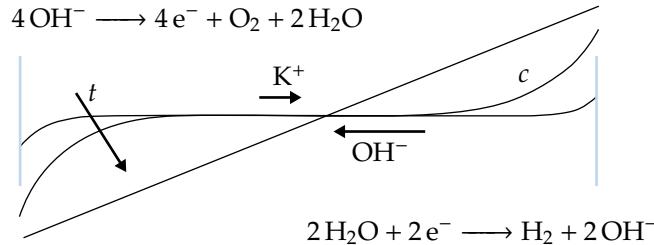
Figure 2.11: *The evolution from an initial concentration profile c to a steady state in alkaline water electrolysis. Initially, the situation is similar to that in Fig. 2.10: in the bulk, there are no concentration gradients and there is only migration. The transported K^+ does not participate in the reaction but moves from the anode on the left, where OH^- is consumed, to the cathode on the right where it is produced, to maintain charge neutrality. In the boundary layers, a concentration gradient arises in which diffusion and migration cancel for K^+, but add for OH^-. In the final steady state, this holds throughout the electrolyte.*

in the absence of flow, it has zero flux. Therefore, a concentration gradient arises that assists the transport of OH^- and completely cancels that of K^+. Figure 2.11 schematically shows the evolution of the concentration profile over time in an un-stirred electrolyte, inside a porous diaphragm for example. Initially, diffusion will only play a role in very thin boundary layers near the electrodes. Eventually, the concentration profile will be fully developed and the concentration gradient will be constant. In this steady state, the diffusion flux exactly cancels the migration flux of K^+ so that the net flux is zero. For the OH^- ion, the diffusion and migration fluxes add, as is considered in more detail in section 2.4.3.

2.G General binary electrolytes

2.G.1 General equations

Here we consider the case of a general binary electrolyte

$$AC \rightarrow \nu_- A^{z_-} + \nu_+ C^{z_+}, \tag{2.G.80}$$
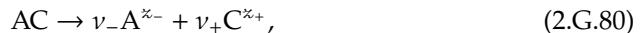
with arbitrary ion charge numbers z_+ and z_- and stoichiometries ν_+ and ν_-. Charge conservation requires

$$\nu_+ z_+ + \nu_- z_- = 0. \tag{2.G.81}$$

We can define the salt concentration as

$$c \equiv \frac{c_+}{\nu_+} = \frac{c_-}{\nu_-}. \tag{2.G.82}$$

Electroneutrality requires $\rho_q = F \sum z_i c_i$ or with $i = +, -$

$$\varkappa_+ c_+ + \varkappa_- c_- = 0. \tag{2.G.83}$$

Using this in in Eq. (2.32) gives

$$t_\pm = \frac{\varkappa_\pm^2 D_\pm c_\pm}{\varkappa_+^2 D_+ c_+ + \varkappa_-^2 D_- c_-} = \frac{|z_\pm| D_\pm}{\varkappa_+ D_+ - \varkappa_- D_-}. \tag{2.G.84}$$

The conservation equations for the cations and anions read, respectively:

$$\frac{\partial c_+}{\partial t} + \nabla \cdot \mathbf{N}_+ - S_+ = \frac{\partial c_-}{\partial t} + \nabla \cdot \mathbf{N}_- - S_- = 0, \tag{2.G.85}$$

where, from Eq. (2.25)

$$\mathbf{N_+} = c_+ \mathbf{u} - D_+ \left(\nabla c_+ + \varkappa_+ c_+ \nabla \bar{\phi} \right), \tag{2.G.86}$$

$$\mathbf{N_-} = c_- \mathbf{u} - D_- \left(\nabla c_- + \varkappa_- c_- \nabla \bar{\phi} \right). \tag{2.G.87}$$

Therefore,

$$\frac{t_-}{\nu_+} \left(\frac{\partial c_+}{\partial t} + \nabla \cdot \mathbf{N}_+ - S_+ \right) + \frac{t_+}{\nu_-} \left(\frac{\partial c_-}{\partial t} + \nabla \cdot \mathbf{N}_- - S_- \right) = 0. \tag{2.G.88}$$

With $t_+ + t_- = 1$ and some vector algebra this gives

$$\frac{\partial c}{\partial t} + \nabla \cdot \mathbf{N} + \mathbf{i} \cdot \frac{\nabla t_+}{F} = S, \tag{2.G.89}$$

where $S \equiv \frac{t_- S_+}{\nu_-} + \frac{t_+ S_-}{\nu_+}$ and

$$\mathbf{N} \equiv \frac{t_- \mathbf{N}_+}{\nu_+} + \frac{t_+ \mathbf{N}_-}{\nu_-} = c\mathbf{u} - D_a \nabla c, \tag{2.G.90}$$

and the ambipolar diffusivity D_a is defined as:

$$D_a \equiv t_- D_+ + t_+ D_- = \frac{(\varkappa_+ - \varkappa_-) D_+ D_-}{\varkappa_+ D_+ - \varkappa_- D_-}. \tag{2.G.91}$$

The current density of Eq. (2.29) gives, with $c_- = \varkappa_+ c_+ / \varkappa_-$ from Eq. (2.34),

$$\mathbf{i} = F (D_- - D_+) \varkappa_+ \nabla c_+ + \kappa \mathbf{E}, \tag{2.G.92}$$

where, from Eq. (2.31), the conductivity reads

$$\kappa = \frac{F^2}{\mathcal{R}T} (\varkappa_+ D_+ - \varkappa_- D_-) \varkappa_+ c_+. \tag{2.G.93}$$
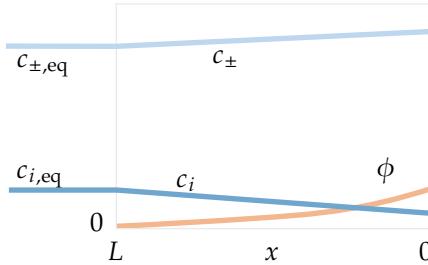
Figure 2.12: *The nernstian layer configuration we consider for the description of a ternary electrolyte. An ion i reacts at $x = 0$, while the supporting electrolyte with concentration $c_\pm$ has zero flux.*

2.G.2 Nernstian boundary layer with a cation with zero flux

Without flow, Eq. (2.G.86) for a zero-flux cation gives

$$\frac{N_+}{v_+} = -D_+ \left(c' + \varkappa_+ c \bar{\phi}' \right) = 0. \tag{2.G.94}$$

The solution is a Boltzmann distribution $c = c_{\text{eq}} e^{-\varkappa_+ \bar{\phi}}$, with c_{eq} the concentration at $x = \delta$, where we take $\bar{\phi} = 0$, as illustrated in Figure 2.4. The anionic flux

$$\frac{N_-}{v_-} = -D_- \left(c' + \varkappa_- c \bar{\phi}' \right), \tag{2.G.95}$$

determines $i = \varkappa_- F N_-$. The Boltzmann distribution gives $c' = -\varkappa_+ c \bar{\phi}'$ so

$$-\frac{i}{D_- z_- v_- F} = c' + \varkappa_- c \bar{\phi}' = c' \left(1 - \frac{\varkappa_-}{\varkappa_+} \right) = (\varkappa_- - \varkappa_+) c \bar{\phi}', \tag{2.G.96}$$

or

$$i = -D_- \varkappa_- F (\varkappa_- - \varkappa_+) c_- \bar{\phi}' = -D_- \left(1 - \frac{\varkappa_-}{\varkappa_+} \right) \varkappa_- F c'_-. \tag{2.G.97}$$

The additional factor $1 - \varkappa_- / \varkappa_+$ represents the additional transport due to migration. This becomes the factor two used for a monovalent binary electrolyte as obtained in Eq. (2.49). The limiting current of Eq. (2.13) is thus also proportionally larger

$$j_{\text{lim}} \equiv nF \frac{\left(1 - \frac{\varkappa_-}{\varkappa_+} \right) D_- c_{\text{eq}}}{L}. \tag{2.G.98}$$

2.G.3 *Ternary electrolyte*

We now consider what happens if we add a third species. In this *ternary electrolyte*, we assume that only one species, with concentration c_i, is transported; for example, because it reacts at $x = 0$. The remaining binary electrolyte with concentrations c_+ and c_- is assumed to satisfy $N_+ = N_- = 0$. This gives a Boltzmann distribution for the zero-flux cations

$$c_+ = c_{+0}e^{-z_+\bar{\phi}}, \tag{2.G.99}$$

and the zero-flux anions

$$c_- = c_{-0}e^{-z_+\bar{\phi}}. \tag{2.G.100}$$

According to electroneutrality

$$c_i = -\frac{z_+c_+ + z_-c_-}{z_i}. \tag{2.G.101}$$

Since the i-th species is the only one contributing to the current, we have $j = z_i F N_i$. The Nernst-Planck equation (2.25) in the absence of advection ($u = 0$) gives $N_i = -D_i\left(c_i' + z_i c_i \bar{\phi}'\right)$ so that

$$\frac{i}{-z_i F D_i} = c_i' + c_i z_i \bar{\phi}' = \left(\frac{\mathrm{d}c_i}{\mathrm{d}\bar{\phi}} + c_i z_i\right)\bar{\phi}' \tag{2.G.102}$$

$$= \left(z_+c_+\left(\frac{z_+}{z_i} - 1\right) + z_-c_-\left(\frac{z_-}{z_i} - 1\right)\right)\bar{\phi}'. \tag{2.G.103}$$

In the second step, we used that c_i through Eqs. (2.G.99), (2.G.100), and (2.G.101) is a function of $\bar{\phi}$ so we can use the chain rule to write $\frac{\mathrm{d}c_i}{\mathrm{d}x} = \frac{\mathrm{d}c_i}{\mathrm{d}\bar{\phi}}\frac{\mathrm{d}\bar{\phi}}{\mathrm{d}x}$. In the final step we used Eqs. (2.G.99) and (2.G.100), which give $\frac{\mathrm{d}c_+}{\mathrm{d}\bar{\phi}} = -z_+c_+$ and $\frac{\mathrm{d}c_-}{\mathrm{d}\bar{\phi}} = -z_-c_-$, respectively.

For example, in case of a monovalent electrolyte with a reacting anion we have $z_i = z_- = -z_+ = -1$ so that $z_-/z_i = 1$, and $z_+/z_i = -1$. In this case Eq. (2.G.103) simplifies to

$$i = -2FD_ic_+\bar{\phi}'. \tag{2.G.104}$$

The current is proportional to the ion diffusivity D_i as expected. However, interestingly and importantly, the current is proportional to the supporting binary electrolyte concentration $c_+ = c_-$ rather than the concentration c_i. Equation (2.G.103) gives

$$\frac{i}{FD_i} = c_i' - c_i\bar{\phi}' = c_i'\left(1 + \frac{c_i}{2c_+ - c_i}\right), \tag{2.G.105}$$

where, in the second step we compared with Eq. (2.G.104) to give $c_i' = (c_i - 2c_+)\, \bar{\phi}'$ or $\bar{\phi}' = \frac{c_i'}{c_i - 2c_+}$. Sometimes a large surplus of binary electrolyte, a supporting electrolyte, is added to a reacting species. In this case $\frac{c_i}{2c_+ - c_i} \approx \frac{c_i}{2c_+} \ll 1$, and Eq. (2.G.105) can be further simplified into:

$$i = FD_i c_i'. \tag{2.G.106}$$

As in the case of a binary electrolyte, we can again write the current density in terms of only diffusion, now with only the properties of the reacting ion playing a role. We have $\bar{\phi}' = \frac{c_i'}{c_i - 2c_+} \approx \frac{c_i'}{-2c_+}$ so that with $c_+ \gg c_i$ the variation in $\bar{\phi}$ is much small smaller than one and the potential variations are small compared to the thermal potential $\frac{RT}{F} \sim 25$ mV. The large conductivity introduced by the supporting electrolyte ensures the electric field is small, even though the supporting electrolyte ions do not move. The small electric field makes that migration can be neglected with respect to diffusion, resulting in Eq. (2.G.106).

2.H   *Transient diffusion: Sand's solution*

The one-dimensional diffusion equation (2.3) in the absence of flow, $u = 0$, and sources $S = 0$ reads

$$\frac{\partial c}{\partial t} = D \frac{\partial^2 c}{\partial x^2}. \tag{2.H.107}$$

The analytical solution with boundary condition (2.54) and $c(x \to \infty) = c_{\text{eq}}$ reads

$$c(x,t) = c_{\text{eq}} - c_0' \left\{ \frac{\Delta x}{\sqrt{\pi}} e^{-\left(\frac{x}{\Delta x}\right)^2} - x \left[1 - \text{erf}\left(\frac{\Delta x}{x}\right) \right] \right\}, \tag{2.H.108}$$

where $\Delta x = 2\sqrt{Dt}$. For $x \to 0$ this gives

$$c_0 = c_{\text{eq}} - \frac{c_0' \Delta x}{\sqrt{\pi}}. \tag{2.H.109}$$

Chapter 3

Porous electrodes

Using porous electrodes, the area available for redox reactions can be increased by many orders of magnitude, strongly reducing the activation overpotentials. However, a porous electrode that is too thick will reduce the "electrode effectiveness factor". This concept will be very useful in describing electrolysers, fuel cells and batteries in the subsequent chapters.

3.1 Porous structure

Porous electrodes are characterised by a large number of voids or *pores* inside the electrode volume. As a result, the total *internal* surface area can be much higher than its *external* surface area. Electrolyte ions, reactants, and products can diffuse or sometimes flow through the pores of the electrode. Figure 3.1 illustrates flow streamlines through a polydisperse spherical arrangement. Electrons can flow through the *matrix*, or the solid part, of the material.

When the porous material is not sufficiently reactive, a thin layer of small (nano-)particles can be used as a coating to create a large number of active sites. In this case, the porous material is just a support or substrate for the catalyst and additionally provides conductivity for electrons. Sometimes, binder materials or solid polymer electrolytes are also added to provide ionic conductivity.

3.1.1 Porosity

Most porous electrodes do not have a regular repeating structure, but their pore geometry is stochastic. Instead, these media are characterised by spatially averaged properties like porosity and tortuosity. The porosity can be defined by either volume fraction or area fraction:

$$\epsilon = \frac{\mathcal{V}_{\text{pore}}}{\mathcal{V}} = \frac{A_{\text{pore}}}{A},$$

(3.1)
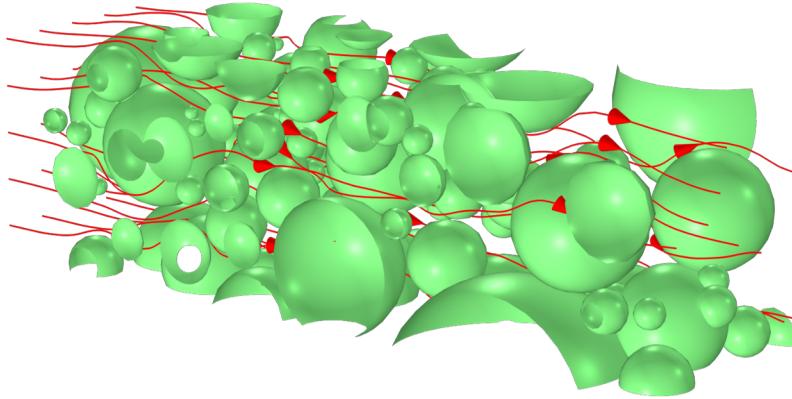
Figure 3.1: *A visualisation of the flow streamlines or ion trajectories inside a porous medium consisting of a polydisperse arrangement of spheres. Image made using the COMSOL Multiphysics® software; provided courtesy of COMSOL.*

$\mathcal{V}_{\text{pore}}$ is the void volume and A_{pore} is the average void area of the cross-section. In general, the volume and area ratios in Eq. (3.1) may be different and vary in space. However, these two definitions can be shown to give the same result for the random isotropic materials considered here.

3.1.2 Tortuosity

The English word tortuous is the antonym of straight: full of bends and twists. For a porous medium, we may define the tortuosity loosely as

$$\tau = \frac{l_{\parallel}}{l}. \tag{3.2}$$

In Figure 3.1, the streamlines travel a longer distance, $l_{\parallel}$, than the shortest path l, which is a straight line. By construction, the tortuosity τ is always equal to or larger than one. Since not all particles will traverse the same distance $l_{\parallel}$, this definition is mathematically not very rigorous. However, this should not bother us here. A high tortuosity is usually not desired because longer path lengths increase resistance and pressure drops and decrease diffusion rates.

3.1.3 Volumetric surface area

The *volumetric surface area*[1] is the combined total external surface area A_{s} per unit of total volume $\mathcal{V}$

---

[1]The quantity a is often referred to as *specific surface area*specific surface area, although this term should, strictly speaking, perhaps be reserved for the amount of surface area per unit mass.
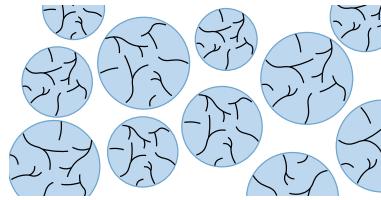
Figure 3.2: *A doubly porous medium with pores in between spherical particles which are themselves also porous.*

$$a \equiv \frac{A_\mathrm{s}}{\mathcal{V}}.$$
(3.3)

Often, porous electrodes consist of a collection of solid particles.[2] If these particles are all of similar size, we can write

$$\boxed{a = (1 - \epsilon)\, a_\mathrm{s},}$$
(3.4)

where $a_\mathrm{s} \equiv A_\mathrm{s}/\mathcal{V}_\mathrm{s}$ is the volumetric surface area of a single particle: the ratio of its area A_s and volume $\mathcal{V}_\mathrm{s}$. The subscript 's' here stands for surface, but for electrodes consisting of solid particles, it also stands for solid. For spherical particles of diameter d 🏃

$$a = \frac{6\,(1 - \epsilon)}{d}.$$
(3.5)

An inverse relationship between particle size and volumetric surface area generally holds for any shape. Rescaling all particles making up a porous electrode to half their geometrical size doubles the surface area without requiring any additional material. This is particularly important when the catalyst is very precious, for example, platinum or iridium. It explains why in fuel cells, for example, preferably Pt nanoparticles are used. These provide maximum surface area per unit weight.[3]
Note that in case the particles making up the porous medium themselves are also porous, as illustrated in Figure 3.2, Eq. (3.4) may still be used. In this case, a_s should include both internal and external particle surface area.

3.1.4   Superficial, interstitial, and local velocity

When a fluid flows through a porous medium, we can define its velocity in several ways. In this section, we will only consider velocity magnitudes, but in general, these

---

[2]Particles can be coalesced using heating or sintered so that they form a solid electrode. In pocket electrodes, fine particles are kept within a metallic perforated metal sock. With A_i and $\mathcal{V}_i$ the surface area and volume of the individual particles, $\sum_i \mathcal{V}_i$ gives the total particle volume and, since $1 - \epsilon$ is the fraction of particles, $V = \sum_i \mathcal{V}_i/(1 - \epsilon)$. With $A_\mathrm{s} = \sum_i A_i$, Eq. (3.3) gives $a = (1 - \epsilon)\, \frac{\sum_i A_i}{\sum_i \mathcal{V}_i}$.

[3]Below several nanometres, more subtle molecular quantum effects start to play a role, and fabricating even smaller particles is not necessarily worthwhile.
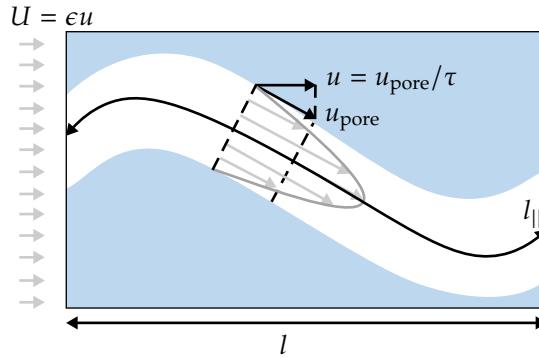
Figure 3.3: *An idealisation of a porous medium as a bundle of capillaries of which one is shown. The superficial velocity U that enters moves faster inside the pores where there is less space to give an interstitial velocity $u = U/\epsilon$. Because only part of the velocity is in the main flow direction, the average pore velocity $u_{\text{pore}} = u\tau$ is even faster. The peak velocities inside the pore can still be faster. Here the porosity and tortuosity $\epsilon = \mathcal{V}_{\text{pore}}/\mathcal{V}$ and $\tau = l_{\|}/l$.*

will be vectors which have a direction.

Pore velocity

The first, perhaps most obvious, velocity we can define is by looking inside a pore and measuring the velocity. This varies locally in magnitude and direction; for example, it becomes zero at the solid surface due to the no-slip condition. Therefore, we will average the velocity over the pore's cross-section to obtain the velocity magnitude, u_{pore}. An idealisation that is often made especially for hydraulic calculations is replacing the porous medium with a bundle of capillaries. Fig. 3.3 illustrates one such a capillary. This approach has many conceptual difficulties, but the didactic benefits arguably outweigh them. In this picture, the average pore velocity is an average over a single pore, which should then be representative of the entire porous medium.

Interstitial velocity

Because usually, the streamlines are not straight, there will be an average flow direction and magnitude that we will refer to as the *interstitial velocity u*. This is the volume-averaged velocity *in the main flow direction*. Volume-averaging the flow velocity magnitude gives the pore velocity, but averaging the velocity vectors and then taking the magnitude gives the interstitial velocity. In the latter procedure, any component not in the main flow direction averages out to zero.

The difference between pore velocity and interstitial velocity relates to the tortuosity. Consider Fig. 3.3 again. A fluid parcel moving with the average pore velocity u_{pore} takes a time $l_{\|}/u_{\text{pore}}$ to move from the entrance to the exit of the indicated region. With u as the average velocity in the main flow direction and l as the shortest

distance of the pore in this direction, this residence time can be equally written as l/u. Therefore, with the tortuosity $\tau = l_{||}/l$ of Eq. (3.2), we obtain

$$u = \frac{u_{\mathrm{pore}}}{\tau}. \tag{3.6}$$

The interstitial velocity is thus lower compared to the pore velocity by a factor given by the tortuosity.

Superficial velocity

A third velocity, the *superficial* velocity U can be defined as the fluid's velocity in the absence of the solid, assuming an equal volumetric flow rate. Alternatively, it is the bulk velocity of the fluid before entering the porous medium or after leaving it, when the total cross-sectional stays constant, see Fig. 3.3. Since the solid takes up part of the flow area, the interstitial flow velocity u inside the porous medium will be higher. Assuming incompressible flow, the flow rate AU equals $A_{\mathrm{pore}}u$. Using Eq. (3.1), we find

$$U = \epsilon u = \epsilon \frac{u_{\mathrm{pore}}}{\tau} \tag{3.7}$$

The superficial velocity U is lower than the average interstitial velocity u due to the reduced volume fraction ϵ available for the flow. In turn, the interstitial velocity is lower than the average pore velocity u_{pore} because it does not include all the deviations from the main flow direction introduced by the tortuosity.

3.1.5 Effective diffusivity in porous materials

When modelling the transport of species through a porous medium, computationally, we may resolve its full concentration in space and time. A two-dimensional example, for a neutral species, is depicted in Figure 3.1. Without a flow and no source, S, Eq. (2.3) becomes

$$\frac{\partial c}{\partial t} = D_{\mathrm{m}}\nabla^2 c. \tag{3.8}$$

Here, we added a subscript m for the *molecular* diffusivity D_{m} in an electrolyte, to distinguish it from the effective diffusion coefficient D that we will introduce in a moment.[4] The local flux inside a pore $N_{\mathrm{pore}} = -D_{\mathrm{m}}\nabla c$. However, often, we are not interested in the detailed concentration profile but rather in the average concentration and superficial flux in the direction of transport. Therefore, we average the partial differential equation (3.8) over all directions except the transport x-direction, to give an ordinary differential equation

---

[4]Most texts use a subscript "eff" to denote an effective diffusion coefficient D_{eff}. To keep the notation to a minimum, and since D_{m} is a special case of D without a porous medium, we only highlight the difference when otherwise confusion could arise.

$$\frac{\partial \epsilon c}{\partial t} = D \frac{\mathrm{d}^2 c}{\mathrm{d}x^2}. \tag{3.9}$$

We use the same symbol c in both equations but do realise that, while in Eq. (3.8) c depends on x, y, and z, in Eq. (3.9) it is averaged over y and z to become a function only of x. In Eq. (3.9), D is an effective diffusion coefficient that will be proportional to the molecular diffusivity D_{m} but will also depend on the structure of the porous electrode in a manner we will now investigate.

Consider a concentration difference Δc between two locations in Fig. 3.1 a distance l apart in the x-direction, amounting to a longer distance $l_\parallel$ inside the pores. Similar to Eq. (3.7) we can write the superficial molar flux $N = D\Delta c / l$ as

$$N = \epsilon \frac{N_{\mathrm{pore}}}{\tau}. \tag{3.10}$$

Since $N = D\Delta c / l$ and $N_{\mathrm{pore}} = D_{\mathrm{m}} \Delta c / l_\parallel$ we find

$$\boxed{D = \frac{\epsilon}{\tau^2} D_{\mathrm{m}}.} \tag{3.11}$$

Compared to Eq. (3.7) there is an additional factor τ, which has been missed by several authors before [11]. It derives from the factor that the local concentration gradients are inversely proportional to $l_\parallel$ instead of l, giving an additional factor $\tau = l_\parallel / l$.[5]

The exact same effects of porosity and tortuosity also play a role for conduction of ions through a porous medium.[6] The local version of Ohm's law reads $i_{\mathrm{pore}} = \kappa_{\mathrm{m}} E_{\mathrm{pore}}$ in terms of the molecular electrolyte conductivity κ_{m} and local electric field E_{pore}. This becomes in terms of the superficial current density $i = \kappa_{\mathrm{m}} E$ in terms of an effective conductivity κ and global electric field E. Therefore, analogous to Eq. (3.11) we will write for the effective conductivity

$$\boxed{\kappa = \frac{\epsilon}{\tau^2} \kappa_{\mathrm{m}}.} \tag{3.12}$$

3.1.6 Bruggeman approximation

In the case of a random configuration of particles of various sizes, you can perhaps imagine that the lower the porosity ϵ, the higher the tortuosity $\tau = l_\parallel / l$ will be. Transport is unimpeded for very high porosity and can proceed along straight paths

---

[5]Here, the squared tortuosity τ^2 is sometimes referred to as the *tortuosity factor* but is often erroneously referred to as the tortuosity and is even sometimes given the symbol τ. The combination $\tau^2 / \epsilon > 1$ is called the Macmullin number and is often used to characterise porous media. Note that the reasoning used to derive Eq. (3.11) only assumes a flux proportional to the gradient of a concentration. Therefore, it will equally hold for the transport of heat (Fourier's law), current (Ohm's law) or pressure-driven viscous flow (Darcy's law).

[6]And laminar pressure-driven flow, something we will consider in section 5.3.3.
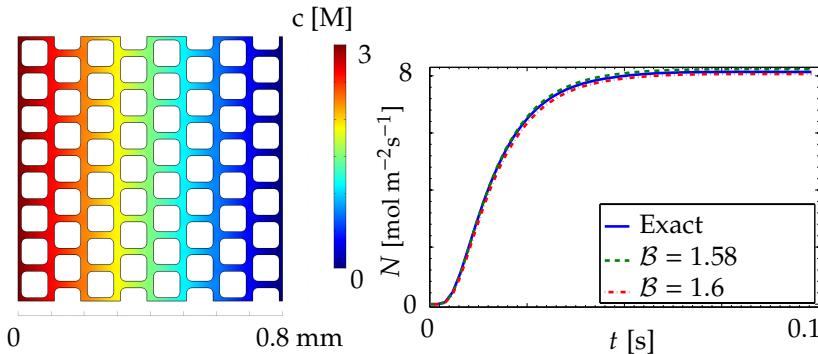
Figure 3.4: *The solution of the transient diffusion equation* (3.8) *in an artificial two-dimensional porous structure 0.1 seconds after a concentration of 3 M is set at the left boundary in a domain with initially zero concentration [9]. The graph on the right shows the evolution of the concentration at the right boundary and compares this with the 1D numerical solution to* $\frac{\partial \epsilon c}{\partial t} = D_m \epsilon^{1+\mathcal{B}} \frac{d^2 c}{dx^2}$ *[22]. The images were made using the COMSOL Multiphysics® software and are provided courtesy of COMSOL and Dr. Gregory L. Plett. See his open-access course ECE5710, Modeling, Simulation, and Identification of Battery Dynamics, lecture 11.*

with negligible tortuosity. For a very low porosity, the space is filled with particles, and even the space between particles is filled with smaller particles. In this case, the relative transport path lengths $l_\parallel / l$ becomes very large. It can be derived, see for example Ref. [28], that for a random polydisperse packing of spheres in 3D ($\mathcal{B} = 1/2$) or normal to a bundle of parallel cylinders in 2D ($\mathcal{B} = 1$)

$$\tau^2 \approx \epsilon^{-\mathcal{B}}. \tag{3.13}$$

This formula implies a relationship between porosity and tortuosity: the lower the porosity, the higher the tortuosity, following intuition. Inserting this approximation into Eq. (3.11) gives

$$D \approx \epsilon^{1+\mathcal{B}} D_m. \tag{3.14}$$

where D is the effective medium diffusion coefficient and D_m is the molecular diffusivity. With $\mathcal{B} = 1/2$ this gives $D \approx \epsilon^{1.5} D_m$, which is often a reasonable approximation for various random porous media, usually referred to as the Bruggeman approximation or correlation[7]

3.2   Macro-homogeneous porous electrode approach

---

[7]As pointed out in Ref. [28] these simple special cases do not appear in the original German work of Bruggeman from 1935. See, for example, Ref. [30] for application to batteries.
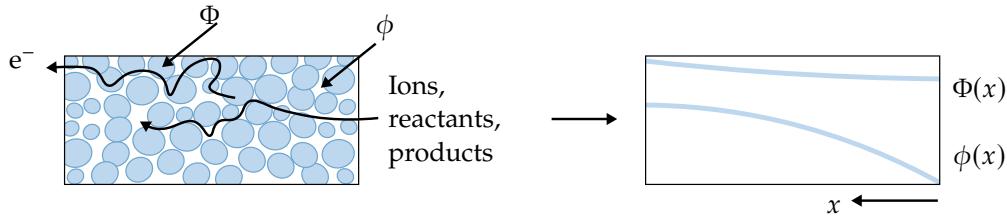
Figure 3.5: *Illustration of the averaging procedure of a porous electrode's ionic and electronic potentials. The electronic potential Φ is relatively flat due to a high metal conductivity, while the electrolyte potential varies more significantly due to ohmic resistance. The inter-electrode gap or membrane is at $x = 0$.*

3.2.1 Macro-homogeneous approach

A porous electrode, by definition, contains more than one phase.[8] The macro-homogeneous approach that we will outline here consists of treating some of these phases as *intertwined* continua—for example, a solid electrode and liquid electrolyte transport electrons and ions throughout the electrode. Even though, in reality, at each location, there will be either solid or liquid present, by mathematically averaging over space, these two phases will co-exist at the same location in the macro-homogeneous approach.

This averaging procedure is schematically depicted in Figure 3.5. On the left, at each location, there is either a solid with a potential Φ or a liquid with a potential ϕ. On the right, these potentials have been averaged over the y- and z-directions to give potentials $\Phi(x)$ and $\phi(x)$ that co-exist for each x. The potential difference $\Phi - \phi$ represents the jump in the potential that exists over the electric double layer in the electrolyte close to the solid.[9]

3.2.2 General porous electrode equations

The volume-average conservation law for a species in the pores of a porous electrode reads *per total unit volume*:

$$\boxed{\frac{\partial \epsilon c}{\partial t} = -\nabla \cdot \mathbf{N} + a N_\perp.}$$

(3.15)

Compared to the general conservation equation Eq. (2.1) the concentration c [mol/m$^3_{\text{pore}}$], which is on a per unit fluid basis, is multiplied with the porosity to

---

[8]For example, in a *flooded electrode*, there are two phases, a solid and a liquid phase. When one of the reactants or products is gaseous, as is often the case in fuel cells or electrolysers, there is an additional gas phase. In a polymer electrolyte fuel cell, there may even be an additional solid phase to transport the ions.

[9]Relative to its equilibrium value $\eta = \Phi - \phi - (\Phi - \phi)_{\text{eq}}$ is the local activation overpotential. Compared to Eq. (1.26), we allowed here for an electrode potential Φ that varies in space. In case the electrode has a non-negligible resistance, the solid phase potential Φ may vary, and a constant electrode potential E, as assumed in chapter 1, does not suffice.
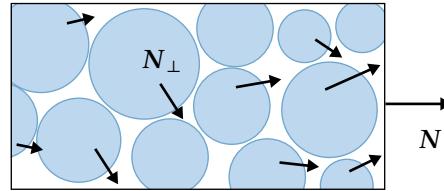
Figure 3.6: *The averaging domain used in Eq.* (3.17), *showing how the local surface fluxes* $N_\perp$ *add up to a superficial flux* N.

give ϵc [mol/m$^3_{\text{tot}}$], the number of moles per total unit volume, including both the pores and the solid. The Nernst-Planck equation Eq. (3.16) for the superficial flux N [mol s^{-1}m$^{-2}_{\text{tot}}$] becomes

$$N = Uc - D\left(\nabla c + zc\nabla\bar{\phi}\right). \tag{3.16}$$

Here U is the *superficial* velocity of Eq. (3.7) and D is the *effective* diffusivity, given by Eq. (3.11).

The source term $aN_\perp$ in Eq. (3.15) derives from the general local conservation considering Eq. (2.1) in steady-state $S = \nabla \cdot N_{\text{pore}}$ and volume-averaging so that

$$\frac{1}{\mathcal{V}}\int \nabla \cdot N_{\text{pore}}\mathrm{d}\mathcal{V} = \int N_{\perp,\text{pore}} \cdot \frac{\mathrm{d}A_{\text{s}}}{V} = aN_\perp, \tag{3.17}$$

where in the second step we used the divergence theorem to relate a divergence in the local pore flux N_{pore} to a local surface flux $N_{\perp,\text{pore}}$ through the solid-fluid interface.

The averaged local surface flux $N_\perp$ is related to the local current density by Faraday's law as

$$N_\perp = \pm\frac{j_\perp}{nF}. \tag{3.18}$$

As discussed in section 1.4.1, the number of transferred electrons $n > 0$ and normal fluxes $N_\perp$ and $j_\perp$ is positive when entering from the solid into the fluid. Therefore, depending on whether our species is a reaction product ($N_\perp > 0$) or a reactant ($N_\perp < 0$) and we are considering an anode ($j_\perp > 0$) or a cathode ($j_\perp < 0$), there is a plus or minus sign in Eq. (3.18).

The charge conservation equation (2.9), after volume-averaging similar to in Eqs. (3.15) and (3.17), reads

$$0 = -\nabla \cdot i + aj_\perp. \tag{3.19}$$

Now, i is a superficial current density per total unit area, even though the ionic current density is confined to the pores. Similarly, we can write a volume-averaged conservation equation for the superficial electronic current density j

$$0 = -\nabla \cdot j - aj_\perp. \tag{3.20}$$

Here, the negative sign in the final term arises because we defined $j_\perp$ to be positive when charge enters from the solid into the fluid, which is then a sink for electronic charge.

Adding Eqs. (3.20) and (3.19) gives

$$\nabla \cdot (\boldsymbol{i} + \boldsymbol{j}) = 0. \tag{3.21}$$

The sum of ionic and electronic current densities adds up to a constant current density $\boldsymbol{i} + \boldsymbol{j}$. By charge conservation, any reduction in ionic current density thus has to lead to an increase in electronic current density, and vice versa.

3.2.3 Ohm's law in porous electrodes

Ohm's law often holds to a reasonable degree of accuracy. This holds, for example, in metal electrodes, in solid electrolytes, for binary electrolytes at current densities well below the limiting current density, see section 2.4.3, and in the presence of a supporting electrolyte, see section 2.5. Therefore, to simplify the analysis we will assume Ohm's law to hold and write

$$\boldsymbol{i} = -\kappa \nabla \phi, \tag{3.22}$$
$$\boldsymbol{j} = -\sigma \nabla \Phi, \tag{3.23}$$
$$\nabla \cdot \boldsymbol{i} = -\nabla \cdot \boldsymbol{j} = a j_\perp. \tag{3.24}$$

where the final equations are Eq. (3.19) and Eq. (3.20). Here κ and σ are effective ionic and electronic conductivities, respectively, see Eq. (3.12). In the case of a particulate electrode, we may assume the Bruggeman relation (3.11) to hold and write

$$\kappa = \kappa_\mathrm{m} \epsilon^{1.5}, \tag{3.25}$$
$$\sigma = \sigma_\mathrm{m} (1 - \epsilon)^{1.5} \tag{3.26}$$

where κ_m and σ_m are the material conductivities. The electrode volume fraction is one minus the electrolyte volume fraction so $1 - \epsilon$ is used in Eq. (3.26).

To further simplify, we will neglect convection and also the final migration term in Eq. (3.16) and write $\boldsymbol{N} = -D\nabla c$. In the absence of flow, this would, of course, hold for neutral species, but also for a minority species in a supporting electrolyte. In the case of a binary electrolyte, D is replaced by the effective medium ambipolar diffusivity D_a.

With these assumptions Eq. (3.15) can, with Eqs. (3.18) and (3.24), be written as 🏃

$$\frac{\partial \epsilon c}{\partial t} = \nabla \cdot (D\nabla c) - \frac{\nabla \cdot \boldsymbol{i}}{nF}. \tag{3.27}$$
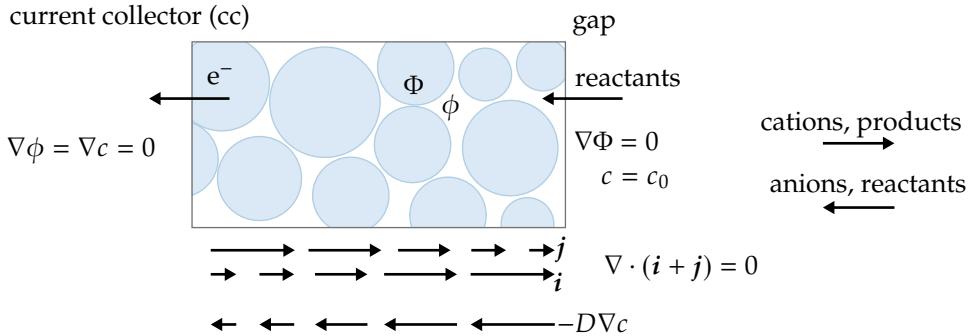
Figure 3.7: A schematic of a porous anode where electrons and reactants enter from opposite sides so ionic current $\boldsymbol{i}$ is converted into electronic current $\boldsymbol{j}$ as the reactant flux $-D\nabla c$ decreases. The boundary conditions for ionic potential ϕ, electronic potential Φ and reactant concentration c are indicated.

Here the minus sign in the final term describes a reactant in an anode, for which $N_\perp < 0$ and $\nabla \cdot \boldsymbol{i} = aj_\perp > 0$.[10]

As a boundary condition at a surface that allows no ions to pass through, Eq. (3.22) gives $\nabla\phi = 0$. Similarly, when no electronic current can enter Eq. (3.23) gives $\nabla\Phi = 0$. Finally, we have as a boundary condition $\nabla c = 0$ in case no molecules of the species under consideration can pass. These boundary conditions are illustrated in Fig. 3.7.

3.3 Simplified 1D porous electrode equations

We will further simplify the equations of the previous section, assuming:

- a *reactant* with a volume-averaged concentration $c(x)$ that varies only in a single spatial direction (x) inside an *anode*[10]

- an infinitely high electronic conductivity σ so that the electronic potential $\Phi = E$ is constant throughout.

- steady-state

- constant D

These assumptions simplify the above Eqs. (3.22)- (3.24) and (3.27) to

---

[10]Alternatively, it equally holds for a product in a cathode for which $N_\perp > 0$ and $\nabla \cdot \boldsymbol{i} = aj_\perp < 0$. For a reactant in a cathode or a product in an anode, the minus sign before the final term in Eqs. (3.27) and (3.30) has to be replaced with a plus sign.

$$i = -\kappa\phi', \tag{3.28}$$

$$i' = aj_\perp, \tag{3.29}$$

$$0 = Dc'' - \frac{i'}{nF}. \tag{3.30}$$

where $i = i_x$ is the x-component of the ionic current density. We use a prime to denote a derivative with respect to the x-coordinate so, for example, $i' = \mathrm{d}i/\mathrm{d}x$.

As shown in Figure 3.8, the x-coordinate inside a porous electrode is chosen to run from the inside of the cell outwards, from the gap or separator to the current collector assumed to be at $x = L$. For the anode on the left of Figure 3.8 that is from right to left. so the ionic current density from left to right gives $i < 0$. For the cathode, the x-coordinate would run from left to right. We take the current collector at $x = L$ to be impenetrable for both ions and reactants. The boundary conditions can, therefore, be written as

$$i = -j \quad \text{(at the separator, } x = 0\text{)}, \tag{3.31}$$

$$i = 0 \quad \text{(at the current collector, } x = L\text{)}. \tag{3.32}$$

Finally, the boundary condition for concentration gives[11]

$$c'(x = L) = 0. \tag{3.33}$$

With these boundary conditions, we can integrate Eq. (3.30) over the spatial coordinate x to give

$$\boxed{0 = Dc' - \frac{i}{nF}.} \tag{3.34}$$

3.3.1 The area multiplier aL

The derivative $i' = \mathrm{d}i/\mathrm{d}x$ is a measure of the local reaction rate since it describes how much ionic current is generated per meter. If it is a constant, we can integrate Eq. (3.29) to give the total current as $j = aLj_\perp$. Here

$$aL = \frac{A_s}{\mathcal{V}}\frac{\mathcal{V}}{A} = \frac{A_s}{A}, \tag{3.35}$$

---

[11]When a neutral reactant is supplied by flow channels engraved into the current collector (*flow field*) from $x = L$ and a membrane avoids these reactants to be transported beyond $x = 0$, Eq. (3.33) may be replaced $c'(x = 0) = 0$. When c describes the concentration of an ionic species supplied or removed through the separator or gap, the boundary condition $c'(x = L) = 0$ will, in case there is also a flow field, only hold exactly where there are no flow channels (*land area*). In the present 1D approximation, however, it will be a reasonable assumption to apply as an averaged condition.
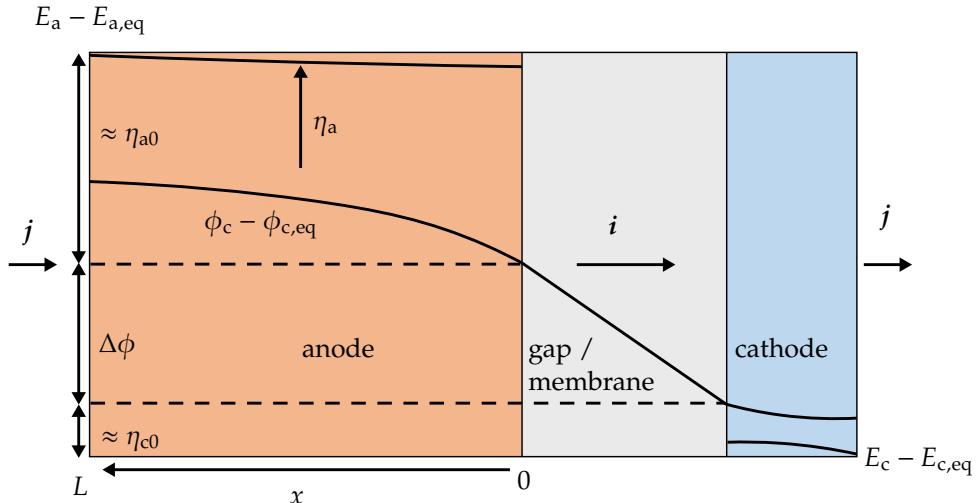
Figure 3.8: *The ionic and electronic potentials ϕ and Φ throughout a cell consisting of, from left to right, a porous anode where electronic current $\boldsymbol{j}$ is converted to ionic current $\boldsymbol{i}$, a gap or separator, and a cathode where the re-conversion to electronic current takes place. When the electronic conductivity σ is much larger than the ionic conductivity κ, the electronic potential drops are much smaller than the ionic potential drop; adding the vertical arrows on the left shows that $E_{cell} = E_c - E_a \approx E_{eq,c} - E_{eq,a} - (\eta_{a0} - \eta_{c0} + \Delta\phi)$.*

is the total electrode surface area A_s as a fraction of the cross-sectional electrode surface area A. It thus describes how much area is inside a porous electrode relative to its outside frontal area. The area multiplier $\frac{j}{j_\perp} = aL$ can be very large[12], and the current j entering or leaving the electrode can be several orders of magnitude larger than the ionic current $j_\perp$ locally entering or leaving the particles (or fibres) making up the porous medium. The much lower local current density $j_\perp$ gives rise to much-reduced activation overpotentials, which is the primary reason why porous electrodes are used.

3.3.2 Activation overpotential

For a reaction that is first order in the concentration c, the concentration-dependent Tafel equation (1.28) can be written as[13]

$$j_\perp = j_* \frac{c}{c_{eq}} e^{\eta/b}. \tag{3.36}$$

---

[12]Non-smooth electrode surfaces can have several times more actual reaction area than geometrical area. A similar multiplier is in this case sometimes referred to as the roughness factor.

[13]For a cathode we would write $j_\perp = -j_* \frac{c}{c_{eq}} e^{-\eta/b}$.

Replacing E with the local value Φ the definition of activation overpotential, Eq. (1.26), reads

$$\eta = \Phi - \phi - \left(E_{eq} - \phi_{eq}\right) \tag{3.37}$$

visualized in Figure 3.8. Since we assume an large electronic conductivity σ so that $\Phi' \approx 0$, we obtain $\eta' \approx -\phi'$. Inserting Ohm's law, Eq. (3.28), gives

$$\boxed{\eta' = \frac{i}{\kappa}} \tag{3.38}$$

As illustrated in Figure 3.8 the x-coordinate runs from left to right in a cathode, but from right to left in the anode. Therefore, this coordinate always starts at the electrode 'front', as seen from the gap or membrane, or 'entrance' for reactants.

The overpotential η is largest at $x = 0$ where the ionic current enters or leaves. Deeper into the electrode the overpotential decreases due to ohmic losses, leading to lower local current density. Mathematically, in the anode $i < 0$ and $\eta > 0$ so Eq. (3.38) gives $\eta' < 0$ and the overpotential decreases away from $x = 0$. In the cathode $i > 0$ and $\eta < 0$, so Eq. (3.38) gives $\eta' > 0$, and the overpotential becomes less negative the further away from $x = 0$. In either case, the driving force for the reaction, the magnitude of the activation overpotential, is highest where the ions enter and leave the electrode. Since in the Tafel regime the reaction rate is proportional to $e^{|\eta|/b}$, the highest reactivity is at the electrode entrance at $x = 0$. If the current is high and the ionic conductivity is low, it may be that there is very little reactivity near $x = L$.

When we neglect electronic resistance, the voltage losses in the simple cell of Figure 3.8 consists of an ohmic drop over the space between the electrodes and an anodic and cathodic activation overpotential, so

$$V_{cell} \equiv E_c - E_a = V_{eq} - (\eta_{a0} - \eta_{c0} + \Delta\phi). \tag{3.39}$$

where the activation overpotentials $\eta_0 = \eta(x = 0)$ and are evaluated at the front of the electrode at $x = 0$. This is the main difference with Eq. (1.35), derived previously, in which a planar electrode with a single overpotential was assumed.

From Eq. (3.39) it seems that the potential drops over the electrolyte inside the porous electrodes do not play a role. They do however play an implicit role[14] in determining the activation overpotential η_0 as we will show below. As a result of high electrolyte resistivity, the overpotential can strongly decrease away from $x = 0$, leading to a narrow reaction zone near $x = 0$. This decreases the available reaction area and thereby increases η_0. Due to this implicit influence of ohmic losses, η_0 cannot be seen purely as an activation overpotential. Activation losses and ohmic losses are intrinsically coupled and cannot always be clearly separated. This is because ions arriving at $x = 0$ have the choice to either all react directly, or travel a bit further to where there are fewer ions. The further the ions travel into the electrode, the more the magnitude of the overpotential decreases due to ohmic losses. The current

---

[14]Alternatively we can write $V_{cell} = E_c - E_a \approx V_{eq} - (\eta_{a,x=L} - \eta_{c,x=L} + \Delta\phi + \Delta\phi_a + \Delta\phi_c)$ so the electrolyte potential drops $\Delta\phi_a$ and $\Delta\phi_c$ appear explicitly.
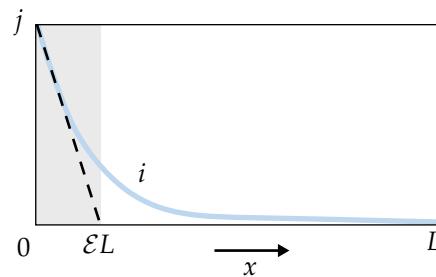
Figure 3.9: *The inhomogeneous ionic current distribution resulting from significant ohmic (or mass transport) resistance.*

distribution resulting from this balance is conveniently described by an effectiveness factor, which we will now introduce.

3.3.3   Electrode effectiveness factor

Inserting $i' = aj_\perp$ from Eq. (3.29) into Eq. (3.36) gives, with $c_0 = c(x = 0)$

$$i' = aj_* \frac{c}{c_0} e^{\eta/b}. \tag{3.40}$$

Here aj_* [A/m^3] is the volumetric exchange current density, which is a measure of how easily the reaction proceeds.[15] The reaction rate i' is here expressed in Coulombs generated or consumed per unit volume and time. Dividing by the number nF of Coulombs per mole of reactant gives the reaction rate in mol/m^3/s.

We define an *electrode effectiveness factor* as the average reaction rate relative to the maximum reaction rate[16], which is at $x = 0$ 🦅

$$\mathcal{E} = \frac{\text{average reaction rate}}{\text{maximum reaction rate}} = \frac{\frac{1}{L}\int_0^L i'\,\mathrm{d}x}{i'_0} = \frac{-i_0}{Li'_0} = \frac{j}{aLj_* e^{\eta_0/b}}, \tag{3.41}$$

where the current density magnitude $j = |i_0|$ in terms of $i_0 = i(x = 0)$. Equation (3.41) gives $\mathcal{E}L = -i/i'|_0$. As illustrated in Fig. 3.9, the *penetration depth* $\mathcal{E}L$ gives the position where the linearized current density profile $i \approx i_0 + i'_0 x$ vanishes. It follows that when $\mathcal{E} \ll 1$, the effectiveness factor roughly represents the fraction of the electrode that is effectively used. Beyond a fraction $\mathcal{E}$ of the total electrode thickness, the ionic current density has become negligible and this electrode area is ineffectively used.

---

[15]The combination $i'/nFc = aj_* e^{\eta/b}/nFc_0$ [s^{-1}] is a volumetric reaction rate coefficient, similar to ka_s used in Appendix 3.A.

[16]Using the boundary condition $i_L = 0$ of Eq. (3.32) and using the fundamental theorem of calculus to integrate a derivative, the average value of i' reads $\frac{1}{L}\int_0^L i'\,\mathrm{d}x = -i_0/L$. In the anode on the left of Figure 3.8 the ionic current is to the right, or in the negative x-direction so that $i_0 < 0$.

Equation (3.41) immediately allows us to write

$$\eta_0 = b\ln\left(\frac{j}{J_*\mathcal{E}}\right).$$

(3.42)

Equation (3.42) is very similar to Tafel's equation $\eta = b\ln\left(\frac{j}{j_*}\right)$ for a planar electrode, with two important differences.

Firstly, instead of j_*, what appears is the *superficial exchange current density*

$$J_* \equiv aLj_*.$$

(3.43)

As discussed in section 3.3.1, the multiplier aL indicates how much more area is inside the porous electrode relative to its frontal geometrical area. The quantity J_* is, therefore, a measure of the total or superficial exchange current density enhanced by the additional porous electrode surface area.

Secondly, the effectiveness factor $\mathcal{E}$ appears, since, in general, not the entire reactive area is used effectively. Note that $J_*\mathcal{E} = aL\mathcal{E}j_*$, where $L\mathcal{E}$ is the penetration thickness so that only that part of the electrode that is effectively used is counted towards the superficial exchange current density.

Our next goal will be to find out how $\mathcal{E}$ depends on the current density j and transport limitations due to a finite ionic conductivity κ or reactant diffusivity D.

3.3.4 Summary and characteristic dimensionless numbers.

We will consider an anode. Therefore $\eta > 0$ and $i < 0$, and Eqs. (3.34), (3.38), and (3.40) become 🏃

$$c' = i/nFD.$$

(3.44)

$$\eta' = i/\kappa.$$

(3.45)

$$i' = aj_*\frac{c}{c_0}e^{\eta/b}.$$

(3.46)

Note that $c', \eta' < 0$ and the reactivity $i' > 0$.[17] These are three coupled first-order ordinary differential equations for the concentration c, overpotential η, and i. The boundary conditions at the current collector at $x = L$, from Eqs. (3.33) and (3.48), read 🏃

$c'(x = L) = 0$		$c(x = 0) = c_0,$	(3.47)
$i(x = L) = 0$	or	$i(x = 0) = -j,$	(3.48)
$\eta'(x = L) = 0$		$\eta'(x = 0) = -j/\kappa.$	(3.49)

---

[17]For a cathode, where $\eta < 0$, and $i > 0$, the right-hand side of Eqs. (3.44) and (3.46) acquires a minus sign and the argument of the exponent in Eq. (3.46) reads $-\eta/b$. In this case $c', i' < 0$ and $\eta' > 0$. This is equivalent to changing the signs of η and i.

All three of the differential equations (3.44)-(3.46) contain either i or i'. Therefore, associated with these three equations are three characteristic current densities. The first one, J_*, associated with the last equation, Eq. (3.45), we already encountered in Eq. (3.43). The other two are obtained from the first two equations, Eq. (3.44) and (3.45), by inserting the characteristic gradients $\eta' \to -b/L$ and $c' \to -c_0/L$ and solving for $-i$ to give

$$J_D = \frac{nFDc_0}{L} \tag{3.50}$$

$$J_\kappa = \frac{b\kappa}{L} \tag{3.51}$$

$$J_* = aLj_* \tag{3.52}$$

Since the reaction rate in Eq. (3.46) is proportional to $i' \propto ce^{\eta/b}$, the characteristic gradients $\eta' \to -b/L$ and $c' \to -c_0/L$ will give a significant effect on i'. It follows that if the current density is much smaller (larger) than these characteristic values, J_D and J_κ, the gradients will also be much smaller (larger).

- The characteristic diffusional current density J_D is the limiting current density that could be sustained in case the reaction takes place only at $x = L$.

  - If $j \ll J_D$, diffusion limitations can be neglected and *the concentration c is approximately constant*.

- The characteristic ohmic current density J_κ is that which would give an ohmic drop equal to the Tafel slope b over the electrode thickness L.

  - If $j \ll J_\kappa$, ohmic limitations can be neglected and *the overpotential η is approximately spatially constant*.

- The superficial exchange current density J_* is the effective exchange current density that the porous electrode would have in case the electrode is used fully effectively.

  - If $j \ll J_*$, we can assume linear kinetics, while for $j \gg J_*$ the Tafel approximation will be valid.

We note that $J_\kappa/j = b\kappa/jL$ is sometimes referred to as the *Wagner number*. In the following section, we will continue with the example of an anode. It is worth noting that the case of a cathode can be easily obtained by changing the sign of both η and i.

3.4 Transport losses in porous electrodes

3.4.1 No transport limitations, $\mathcal{E} = 1$

We will first consider what happens inside a porous electrode in the absence of transport limitations. When $j \ll J_D$, there are no diffusion limitations and the
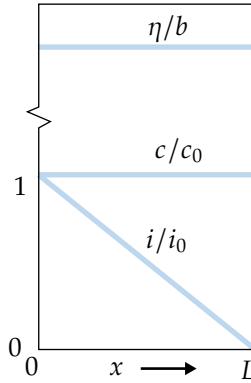
Figure 3.10: *Dimensionless ionic current density i/i_0, concentration c/c_0 and overpotential η/b in the porous electrode for no transport limitation. Note that the Tafel regime requires η/b to be well above 1.*

concentration $c \approx c_0$ throughout. When additionally $j \ll J_\kappa$ there are no ohmic limitations and the overpotential $\eta \approx \eta_0$ throughout.

Solving Eq. (3.46) with $c = c_0$ and $\eta = \eta_0$ and the boundary conditions of Eqs. (3.47)-(3.49) gives the simple linear profile

$$i = J_* e^{\eta_0/b} \left(\frac{x}{L} - 1 \right). \tag{3.53}$$

This situation is illustrated in Figure 3.10. At $x = 0$ we have $i = -j$ so that

$$\eta_0 = b \ln \left(\frac{j}{J_*} \right) = b \ln \left(\frac{j}{j_*} \right) - b \ln (aL). \tag{3.54}$$

This is Tafel's equation with j_* replaced by $J_* = aLj_*$. The larger effective exchange current density J_* is the result of the porous electrode area being a factor aL times larger than that for a planar surface.

In the Tafel regime, the larger area of a porous electrode lowers the overpotential by the second term in Eq. (3.54), $-b \ln (aL)$, compared to the overpotential $b \ln \left(\frac{j}{j_*} \right)$ of a non-porous electrode. This is because the local current density, and thereby the activation overpotential, decreases as the current spreads out over the larger porous electrode area.

3.4.2 Diffusion limitations

Figure 3.11 shows an example where there are diffusion limitations ($j \gg J_D$) but no ohmic limitations ($j \ll J_\kappa$). Without ohmic limitations, the overpotential η will be constant. Due to the finite diffusivity, the concentration decreases inside the
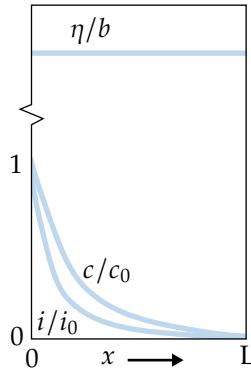
Figure 3.11: *The ionic current distribution i sharply decreases due to the depletion of reactants associated with the diffusion limitations that are a consequence of the high current density $j \gg J_D$. The ionic conductivity is large so that $j \ll J_\kappa$ and the overpotential η is constant.*

porous electrode, causing the reaction rate i' to drop proportionally. These conditions typically arise, for example, in the catalyst layers of fuel cells or CO_2-electrolysers, when they are *flooded* with water. These catalyst layers are usually thin enough to avoid significant ohmic drops, but due to the low solubility and diffusivity in water, the transport of gaseous reactants can be hindered by slow diffusion.

Taking the derivative of Eq. (3.44) and inserting Eq. (3.46), with $\eta = \eta_0$ constant, gives 🪁

$$\frac{d^2 c}{d\,(x/L)^2} = M^2 c, \tag{3.55}$$

where the *Thiele modulus* squared reads

$$M^2 = \frac{J_*}{J_D} e^{\eta_0/b} = \frac{J_* e^{\eta_0/b}}{nFDc_0/L}. \tag{3.56}$$

This dimensionless number represents the ratio between the integral reaction rate $J_* e^{\eta_0/b}$ and the characteristic diffusion rate Dc_0/L.

The limiting solution in case of high or low M reads 🪁

$$c = c_0 e^{-Mx/L} \quad (M \gg 1 \text{ or } M \ll 1) \tag{3.57}$$

In case $M \gg 1$ or $M \ll 1$ this gives $c(x = L) \approx 0$ or $c(x = L) \approx c_0$, respectively[18]. From Eq. (3.46), the reactivity i' is proportional to c so that the effectiveness factor of

---

[18]In these cases the solution satisfies the boundary condition $c'(x = L) = 0$. For intermediate values, we need to retain also the positive exponent solution $e^{Mx/L}$ and make a linear combination that satisfies the boundary condition, as is done in the appendix 3.A.3 to derive the full exact solution Eq. (3.A.85).

Eq. (3.41) reads[19] 🏃

$$\mathcal{E} = \frac{1}{L} \int_0^L \frac{c}{c_0} dx \approx \begin{cases} 1 & M \ll 1 \\ 1/M & M \gg 1. \end{cases} \tag{3.58}$$

In the latter case of strong diffusion limitations ($M \gg 1$), with Eqs. (3.41) and (3.56), this gives[20] 🏃

$$\boxed{\mathcal{E} = \frac{j}{J_* e^{\eta_0/b}} = \frac{1}{M} = \frac{j/J_D}{M^2} = \frac{J_D}{j} \ll 1.} \tag{3.59}$$

We thus find that in the presence of strong diffusion limitations the electrode effectiveness factor is given by the ratio of the characteristic current density J_D and the current density j. The lower the diffusion current density J_D, or the higher the current density, the lower the effectiveness factor. This is a simple but very useful result of the above analysis.

Inserting $\mathcal{E} = J_D/j$ in Eq. (3.42), using Eqs. (3.50) and (3.52), gives 🏃

$$\boxed{\eta_0 = b\ln\left(\frac{j^2}{aj_* nFDc_0}\right) = 2b\ln\left(\frac{j}{\sqrt{aj_* nFDc_0}}\right).} \tag{3.60}$$

In the second equation, we see Tafel's equation, but with a doubled Tafel slope $2b$ and a modified effective exchange current density

$$\sqrt{J_* J_D} = \sqrt{aj_* nFDc_0}. \tag{3.61}$$

This effective exchange current density is the geometrical mean of the original $J_* = aLj_*$ and the characteristic diffusion current density $J_D = nFDc_0/L$. A doubling in Tafel slope is bad news, as it means that reaching higher current densities comes at an increasingly large cell voltage. It arises because the higher the current density, the smaller the area inside the electrode that can be effectively used: the penetration thickness $\mathcal{E}L$ becomes inversely proportional to j. Note that the overpotential of Eq. (3.60) is independent of the electrode thickness L. This happens because in the considered case of strong diffusion limitations, the porous electrode is used very ineffectively. Because in the part beyond the penetration depth, virtually no reaction takes place, the electrode thickness does not matter.

3.4.3 Ohmic limitations

Next, we assume a sufficiently high diffusivity and reactant concentration, so $J_D \gg j$. In this case, no diffusion limitations arise and the concentration c is approximately

---

[19]Evaluating gives $\int_0^1 e^{-Mx/L} d\left(\frac{x}{L}\right) = \frac{1-e^{-M}}{M}$ which evaluates to $1/M$ for $M \gg 1$. For $M \ll 1$ a series expansion $e^{-M} \approx 1 - M$ gives that $\mathcal{E} \approx 1$.

[20]Using the exact solution $\mathcal{E} = \frac{\tanh M}{M}$ of Eq. (3.A.87) we see that to find M in terms of j requires solving $j/J_D = M \tanh(M)$, which has no general analytical solution for M.
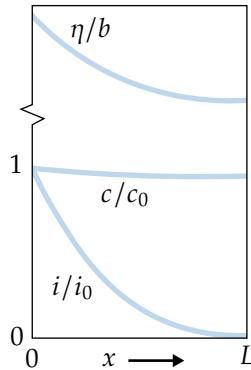
Figure 3.12: *The ionic current distribution i decreasing due to a decrease in activation overpotential associated with $j \gg J_\kappa$. The diffusivity is sufficiently large that $J_D \gg j$ and concentration profile c is approximately flat.*

constant. Nonetheless, when $j \gg J_\kappa = b\kappa/L$, a localised reaction zone appears near $x = 0$ due to ohmic limitations. Because the characteristic ohmic potential drop jL/κ is much larger than the Tafel slope b the reaction rate, proportional to $e^{\eta/b}$, is strongly impacted by ionic resistance. Deeper into the porous electrode, the overpotential η, and therefore the reaction rate, strongly decreases.

Combining Eqs. (3.45) and (3.46) with $c = c_0$ gives

$$e^{\eta/b} = \frac{\kappa}{a j_*} \eta''. \tag{3.62}$$

Using the chain rule $\frac{\mathrm{d}}{\mathrm{d}x} = \frac{\mathrm{d}\eta}{\mathrm{d}x} \frac{\mathrm{d}}{\mathrm{d}\eta}$, so

$$\eta'' = \eta' \frac{\mathrm{d}\eta'}{\mathrm{d}\eta} = \frac{1}{2} \frac{\mathrm{d}\eta'^2}{\mathrm{d}\eta}. \tag{3.63}$$

Inserting in Eq. (3.62) gives upon integration from η_0 at $x = 0$ to η_L at $x = L$

$$e^{\eta_L/b} - e^{\eta_0/b} = \frac{\kappa}{2 a j_* b} \left(\eta_L'^2 - \eta_0'^2 \right). \tag{3.64}$$

Inserting the boundary conditions of Eqs.(3.47)-(3.49) and assuming strong ohmic limitations $j \gg J_\kappa$ so that $e^{\eta_0/b} \gg e^{\eta_L/b}$ we obtain $e^{\eta_0/b} = j^2/2a j_* \kappa b$ or

$$\eta_0 = 2b\ln\left(\frac{j}{\sqrt{2 a j_* \kappa b}} \right). \tag{3.65}$$

The associated effectiveness factor $\mathcal{E} \equiv j/J_* e^{\eta_0/b}$ reads

$$\mathcal{E} = \frac{2J_\kappa}{j} \ll 1. \tag{3.66}$$

This simple expression is very similar to the result $\mathcal{E} = J_D/j$ of Eq. (3.59). Analogously, the ohmic Thiele modulus $M_\kappa = 1/\mathcal{E}_{\to 0} = j/2J_\kappa$ in this case. Again, the effectiveness factor is given by the ratio of a characteristic current density $2J_\kappa$ and the current density j. The lower J_κ, or thheb e higher the current density, the lower the effectiveness factor. Similar to Eq. (3.60), the overpotential of Eq. (3.65) does not depend on the electrode thickness L. Also in the case of strong ohmic limitations, the reaction is limited to a region near $x = 0$. Beyond a penetration depth $\mathcal{E}L$ the electrode volume is ineffectively used and does not help to further reduce the overpotential.

3.4.4 Combined ohmic and diffusion limitations - approximation

In the case of simultaneous diffusion and ohmic limitations, we can approximately add the Thiele moduli and obtain $\frac{1}{\mathcal{E}} \approx M + M_\kappa = \frac{j}{J_D} + \frac{j}{2J_\kappa} \gg 1$.[21] In the absence of transport limitations $\mathcal{E} \approx 1$ when $M + M_\kappa \ll 1$. An approximate expression that tends to both limits is 🏃

$$\mathcal{E} \approx \frac{1}{1 + j/J_D + j/2J_\kappa}. \tag{3.67}$$

This result will be accurate in case the combined Thiele modulus $M + M_\kappa$ is either much smaller or much larger than 1. It can only be expected to give a rough approximation for intermediate values. When $M + M_\kappa$ is large, the effectiveness factor is small. To make good use of the entire volume of the porous electrode, this regime should be avoided. Since the Thiele moduli $M = \frac{jL}{nFDc_0}$ and $M_\kappa = \frac{jL}{2\kappa b}$ are both proportional to the current density and the electrode thickness L, this implies that operation at high current density will require relatively thin electrodes. This will be the case, for example, in fuel cells or advanced electrolysers, where catalyst layers of sometimes only a few micrometres thick are used. Conversely, operating at low current densities allows for thicker electrodes. This will be the case, for example, in some batteries, that can have electrodes of several millimetre thick. These arguments thus go some way to explain the differences in electrode designs between various applications.

Having an electrode effectiveness factor value close to 1 sounds ideal, but it means that a thicker electrode could have been used to increase the reaction area. A very small effectiveness factor, on the other hand, means that most of the electrode area is unused and makes ineffective use of materials. Therefore, an optimal electrode effectiveness factor $\mathcal{E}_{\text{opt}}$ exists. In terms of this parameter, we find the optimal electrode

---

[21]In Appendix 3.C we derive the exact result and show that this simple addition gives a maximum relative error in the effectiveness factor of 12 %, making it a fairly accurate approximation.

thickness from Eq. (3.67) as 🏃

$$L_{\text{opt}} = \frac{1 - \mathcal{E}_{\text{opt}}}{\mathcal{E}_{\text{opt}}} \frac{nFDc_0 + 2\kappa b}{j}. \tag{3.68}$$

An often reasonable value [13] is $\mathcal{E}_{\text{opt}} \approx 1/3$, so that the pre-factor in Eq. (3.68) becomes $\frac{1 - \mathcal{E}_{\text{opt}}}{\mathcal{E}_{\text{opt}}} \approx 2$.

Inserting Eq. (3.67) in $\eta_0 = b\ln(j/J_*\mathcal{E})$ gives, when $\mathcal{E} \ll 1$:

$$\eta_0 \approx 2b\ln\left(\frac{j}{\sqrt{\frac{aj_*}{\frac{1}{2\kappa b} + \frac{1}{nFDc_0}}}} \right). \tag{3.69}$$

Compared to Eq. (3.54) the inverse electrode thickness $1/L$ is replaced by a sum of the inverse penetration depths $2\kappa b/j$ and $nFDc_0/j$. The shortest of the penetration depths thus dominates. This is to be expected since beyond the shortest of the two penetration depths, the reactivity decreases strongly, and the rest of the electrode helps very little in decreasing the overpotentials.

3.5 Summary

- The effective diffusivity, similar to other transport parameters like conductivity, can be described by $D = \frac{\epsilon}{\tau^2}D_{\text{m}}$ (3.11) with tortuosity squared $\tau^2 \approx \epsilon^{-\mathcal{B}}$. Factor $\mathcal{B} = 1/2$ for a porous medium consisting of spheres and $\mathcal{B} = 1$ for long cylinders.

- Per total unit volume, the conservation equation for a reactant $\frac{\partial \epsilon c}{\partial t} = \nabla \cdot (D\nabla c) - \frac{\nabla \cdot i}{nF}$ (3.27) becomes in 1D, steady-state, and assuming first-order Tafel kinetics:

$$i' = nFDc'' = aj_* \frac{c}{c_0} e^{\eta/b} \tag{3.70}$$

  viz. Eqs. (3.44) and (3.46). For negligible electrode resistance, the overpotential satisfies $\eta' = i/\kappa$ when $\sigma \gg \kappa$ (3.45).

- The occurrence of diffusion limitations $j \gg J_D = nFDc_0/L$ and/or ohmic limitations $j \gg J_\kappa = b\kappa/L$ can be described by the electrode effectiveness factor $\mathcal{E} \sim \frac{1}{L}\frac{\int i' dx}{i_0'} \approx \frac{1}{1+M} = \frac{1}{1+j/J_D+j/2J_\kappa}$. When only the electrode region within the penetration depth $\mathcal{E}L \ll L$ is effectively used, the activation overpotential $\eta_0 = b\ln\left(\frac{j}{J_*\mathcal{E}}\right) = 2b\ln\left(\frac{j}{\sqrt{aj_*}}\sqrt{\frac{1}{2\kappa b} + \frac{1}{nFDc_0}}\right)$, (3.42) and (3.69), attains a doubled Tafel slope.

Exercise 3.1

As an engineer at an electrode manufacturer, you performed several tests on a new porous electrode material consisting of sintered spherical particles.

a. You find the effective diffusivity to be one-fourth of the molecular diffusivity. Give an approximation for the porosity ϵ.

b. Estimate the diameter of the spherical particles in case you measure the specific interfacial surface area to be $a = 3.6 \cdot 10^5 \text{ m}^{-1}$.

Exercise 3.2

In an air-fed PEM fuel cell cathode, oxygen has to diffuse from the flow channel to the catalyst layer through a diffusion layer of 0.5 mm thick. This layer has an apparent density of 1260 kg/m^3 and is made from a solid material with an intrinsic density of 2100 kg/m^3. The bulk diffusivity of oxygen is $D_{O_2} = 20 \text{ mm}^2/\text{s}$ and the concentration at the flow channel interface is $5 \cdot 10^{-3}$ M. Calculate the limiting current density associated with this diffusion layer.

Exercise 3.3

Consider a cathodic reaction in a porous electrode. Assume concentration-independent Butler-Volmer kinetics

$$i' = a j_* \left(e^{\alpha \frac{F\eta}{\mathcal{R}T}} - e^{-(1-\alpha)\frac{F\eta}{\mathcal{R}T}} \right), \tag{3.71}$$

and Ohm's law $\Phi' = -i/\kappa$.

a. Under what conditions can we write $i' \approx \frac{\eta}{ARL}$?

b. Write an expression for area-specific resistance AR in terms of exchange current density j_*, volumetric interfacial surface area a, and thickness of electrode L.

c. Under the condition derived at a., find the expression for current density i using boundary condition $i(0) = j$ and $i(L) = 0$ in terms of $\nu \equiv L\sqrt{\frac{a j_* F}{\mathcal{R}T\kappa}}$.

d. Derive an expression for the linear electrode effectiveness factor $\mathcal{E}_{\text{lin}} \equiv \frac{j/L}{-i'(0)}$.

Exercise 3.4

The exchange current density and charge transfer coefficient of an electrochemical reaction at a planar cathode are $j_{*c} = 0.01 \text{ mA/cm}^2$ and $\alpha_R = 0.65$, respectively. We coat the cathode with a 1 μm thick, catalytically active layer with a volumetric surface area of 10^8 m^{-1}. By approximately how much will the cathode activation overpotential be reduced? Assume an electrode effectiveness factor $\mathcal{E} = 1$ and $T = 300$ K.

Exercises 3.5-3.25

Fill in the missing steps in the main text, indicated by the symbol 🏃.

Appendices *

3.A   *Pore versus effective medium*

There are two distinct ways to model a porous electrode: by using an effective medium approach as in the main text, or by studying a single pore. There has been somewhat of a divide in the literature on porous electrodes with, for example, de Levie studying single pores and Newman using effective medium equations. These approaches can give equivalent information when tortuosity and porosity are included properly. The pore perspective may be more intuitive for some, so we work out the simultaneous diffusion and reaction in a single pore.

Consider the idealised cylindrical pore in Figure 3.13. We will only consider transport in the axial direction, so the general steady-state conservation law in 1D reads

$$0 = -\frac{\mathrm{d}N}{\mathrm{d}x} + S, \tag{3.A.72}$$

where $N = -D\frac{\mathrm{d}c}{\mathrm{d}x}$. The reaction takes place only at the pore surface, not at the inlet on the left, nor at the end of the pore on the right. For a first-order reaction in the concentration c, with reaction rate constant k, the surface flux $N_\perp$ reads

$$N_\perp = -kc. \tag{3.A.73}$$

Since we are considering reactants, not products, this radial flux is in the direction from fluid to solid, hence the negative sign.
In a small axial segment with volume $\mathcal{V}_s$ and surface area A_s the surface reaction subtracts $N_\perp A_s$ moles of reactant per unit time. This gives a sink $S = N_\perp A_s / \mathcal{V}_s = a_s N_\perp$ per unit volume.[22] We can, therefore, write $S = -ka_s c$. The volumetric rate constant ka_s allows us to make an effective one-dimensional description of a two-dimensional pore.

---

[22]The volumetric surface area for a cylinder with diameter d without its two ends is $a_s = \frac{A_s}{\mathcal{V}_s} = \frac{\pi d}{\pi d^2/4} = \frac{4}{d}$, but we keep it as a general parameter to allow for arbitrary cross-sectional shapes.
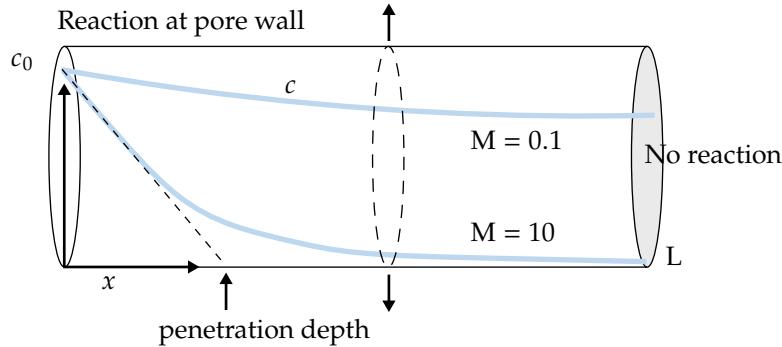
Figure 3.13: *Schematic representation of possible concentration profiles for different Thiele moduli* M *in a single pore, in which a reaction takes place at the pore wall and reactants diffuse inwards from* $x = 0$.

3.A.1 Effectiveness factor

The reaction at the pore wall will lead to an axial concentration gradient, bringing in new reactants by diffusion. For higher reaction rates, strong concentration gradients arise, and most of the pore volume can be deprived of reactants, as diffusion is not fast enough to meet the demand for reactants in the reaction.

To quantify this, we define the effectiveness factor as follows:

$$\mathcal{E} = \frac{\text{average reaction rate}}{\text{maximum reaction rate}} = \frac{\frac{1}{\mathcal{V}} \int k a_{\text{s}} c \, d\mathcal{V}}{k a_{\text{s}} c_0} = \frac{\langle c \rangle}{c_0}, \qquad (3.\text{A}.74)$$

where we assumed a reaction rate $S = -k a_{\text{s}} c$ with constant $k a_{\text{s}}$. The notation $\langle c \rangle = \frac{1}{\mathcal{V}} \int c \, d\mathcal{V}$ denotes a volume average. In the one-dimensional approximation we are after, c becomes only a function of x, and $\langle c \rangle = \frac{1}{L} \int_0^L c \, dx$. For a first-order reaction, the effectiveness factor is thus simply the average concentration relative to the entrance concentration. Next, we set out to find an expression for $\mathcal{E}$ as a function of the pore geometry, diffusion coefficient, and reaction rate.

3.A.2 Thiele modulus

Equation (3.A.72) becomes:

$$0 = D \frac{d^2 c}{dx^2} - k a_{\text{s}} c. \qquad (3.\text{A}.75)$$

To solve this second-order differential equation for the concentration profile, two boundary conditions are required as follows:

$$c(x = 0) = c_0, \tag{3.A.76}$$
$$c'(x = L) = 0. \tag{3.A.77}$$

Introducing the following dimensionless variables

$$\bar{x} = \frac{x}{L}, \quad \bar{c} = \frac{c}{c_0}, \tag{3.A.78}$$

Eqs. (3.A.75), (3.A.76) and (3.A.77) can be written in dimensionless form as

$$\bar{c}'' = M^2 \bar{c} \tag{3.A.79}$$
$$\bar{c}(\bar{x} = 0) = 1 \tag{3.A.80}$$
$$\bar{c}'(\bar{x} = 1) = 0 \tag{3.A.81}$$

Note that we use prime to denote a derivative with respect to $\bar{x}$ when considering $\bar{c}$, but a derivative with respect to x when considering c. The Thiele modulus squared is defined as:

$$M^2 = \frac{k a_s L^2}{D}. \tag{3.A.82}$$

Writing $M^2 = \frac{k a_s c_0 L}{D c_0 / L}$ we clearly see that it is a characteristic dimensionless number representing the ratio between reaction rate and diffusion rate.

3.A.3 *Analytical solution*

The general solution to Eq. (3.A.79) reads

$$\bar{c} = A e^{M\bar{x}} + B e^{-M\bar{x}}. \tag{3.A.83}$$

The boundary conditions, Eq. (3.A.76) and Eq. (3.A.77) give

$$A = \frac{e^{-M}}{e^M + e^{-M}}, \quad B = \frac{e^M}{e^M + e^{-M}}, \tag{3.A.84}$$

so

$$\bar{c}(\bar{x}) = \frac{e^{M(1-\bar{x})} + e^{-M(1-\bar{x})}}{e^M + e^{-M}} = \frac{\cosh(M(1-\bar{x}))}{\cosh(M)}. \tag{3.A.85}$$

The hyperbolic cosine is defined as $\cosh(x) = \frac{1}{2}(e^x + e^{-x})$.

We can now obtain $\langle \bar{c} \rangle = \int_0^1 \bar{c} \, d\bar{x}$ by directly averaging Eq. (3.A.85). Instead, we integrate Eq. (3.A.79) from $x = 0$ to $x = L$ and divide by L to give

$$-\bar{c}_0' = M^2 \langle \bar{c} \rangle, \tag{3.A.86}$$

where we used the boundary condition Eq. (3.A.81). This allows the effectiveness factor to be written as

$$\mathcal{E} = \langle \bar{c} \rangle = -\frac{\bar{c}_0'}{M^2} = \frac{\tanh(M)}{M}. \tag{3.A.87}$$

The final result can be obtained either by integration or differentiation of Eq. (3.A.85).

Performing a series expansion around $M = 0$ we have $\tanh(M) \approx M$ for small values $M \lesssim 0.4$ of the Thiele modulus. So when the reaction rate is low compared to the maximum diffusion rate, inserting this result into Eq. (3.A.87), the effectiveness factor is close to one:

$$\mathcal{E} \approx 1 \qquad (M \lesssim 0.4). \tag{3.A.88}$$

In this case, the concentration is approximately constant and equal to the inlet concentration throughout the pore, and the reaction rate is high throughout. See the $M = 0.1$ curve of Figure 3.13 for an illustration.

For roughly $M \gtrsim 4$ we have $\tanh(M) \approx 1$, so that

$$\mathcal{E} \approx \frac{1}{M} \qquad (M \gtrsim 4). \tag{3.A.89}$$

In this case, the maximum diffusion flux is insufficient to supply material to the end of the pore. This is illustrated by the curve in Figure 3.13, corresponding to $M = 10$. As the reactivity increases, less volume in the pore can be reached by diffusion, resulting in a smaller fraction of the pore length being used, hence a lower effectiveness factor. The inverse dependence on the Thiele modulus in Eq. (3.A.89) can be understood as follows. Doubling the reaction rate in this regime doubles the required diffusive flux at the entrance. This results in a concentration gradient that is twice as steep so that a near-zero concentration is reached at half the distance from the pore entrance, resulting in a halving of the effectiveness factor.

To quantify this, we define a penetration depth by linearising the concentration profile near $x = 0$ and seeing at which pore depth this linearised concentration profile reaches zero. The result is a distance $-\frac{c}{c'}\big|_{x=0}$. In dimensionless notation, dividing by L, the associated active fraction of the total pore is

$$-\frac{1}{\bar{c}_0'} \approx \frac{1}{M\tanh(M)} \xrightarrow{M \gg 1} \frac{1}{M}, \tag{3.A.90}$$

where we used Eq. (3.A.87). So for large M, similar to the effectiveness factor, the penetration depth also becomes inversely proportional to M. As is illustrated in Figure 3.13 the reaction rate does not immediately vanish beyond the penetration depth. It does give a rough idea of the length of the pore over which the reaction rate is significant.

3.B   *Dimensionless porous electrode equations*

The governing equations, Eqs. (3.44), (3.45) and (3.46), the boundary conditions, Eqs. (3.31) and (3.32), and Eq. (3.33) are made dimensionless using the following definitions:

$$\bar{x} = \frac{x}{L}, \; \bar{c} = \frac{c}{c_0}, \; \bar{\eta} = \frac{|\eta|}{b}, \; \bar{\imath} = \frac{i}{i_0}, \; \bar{\jmath} = \frac{j_x}{j_{xL}}. \tag{3.B.91}$$

The dimensionless coordinate $\bar{x}$ and concentration $\bar{c}$ we have used already in section 3.A.3. We will again use a prime to denote a derivative with respect to $\bar{x}$, not x as in the case of dimensional quantities. Note that the non-dimensionalization of the overpotential $\bar{\eta}$ deviates from our previous use of the dimensionless potential $\bar{\phi} = F\phi/\mathcal{R}T$ since $b = \mathcal{R}T/\alpha F$, with α the charge transfer coefficient, is used as the reference potential instead of the thermal potential $\mathcal{R}T/F$.

Finally, i and j_x are the x-components of the ionic and electronic current density. We introduced dimensionless ionic and electronic current densities $\bar{\imath}$ and $\bar{\jmath}$ by dividing their extremal value $j_{xL} = i_0$, equal in magnitude to the current density of the cell j. Charge conservation $i + j_x = j_{xL}$ then becomes

$$\bar{\imath} + \bar{\jmath} = 1. \tag{3.B.92}$$

Note that, by dividing with a quantity with the same sign, $\bar{\imath}$ and $\bar{\jmath}$ both vary between 0 and 1. At the electrode front $x = 0$ there is only ionic current, so $\bar{\imath} = 1$ and $\bar{\jmath} = 0$. At the back of the electrode $x = L$ all current is converted to electronic current so that $\bar{\jmath} = 1$ and $\bar{\imath} = 0$. Additionally, at $\bar{x} = 1$ reactants cannot leave or enter so that concentration gradients vanish, resulting in the following boundary conditions:

$$\bar{\jmath} = 0 \text{ or } \bar{\imath} = 1 \qquad\qquad\qquad (x = 0), \tag{3.B.93}$$
$$\bar{\jmath} = 1 \text{ or } \bar{\imath} = 0 \text{ and } \bar{c}' = 0 \qquad\qquad (x = L). \tag{3.B.94}$$

In dimensionless notation, Ohm's law (3.45), the diffusion equation (3.44), and Tafel's equation (3.46) become, respectively

$$\bar{\eta}' = -\bar{\jmath}_\kappa \bar{\imath} \tag{3.B.95}$$
$$\bar{c}' = -\bar{\jmath}_D \bar{\imath} \tag{3.B.96}$$
$$\bar{\jmath}_* \bar{\imath}' = -\bar{c} e^{\bar{\eta}} \tag{3.B.97}$$

where we introduced the following dimensionless current density magnitudes

$$\bar{j}_\kappa = \frac{j}{J_\kappa} \tag{3.B.98}$$

$$\bar{j}_D = \frac{j}{J_D} \tag{3.B.99}$$

$$\bar{j}_* = \frac{j}{J_*}. \tag{3.B.100}$$

Compared to the dimensional Eqs. (3.44)-(3.46) the right-hand side of each of these equations has a minus sign and holds not only for the anode but also for the cathode.

Instead of a dimensionless current density, we can also interpret $\bar{j}_\kappa$ as the ratio between the characteristic ohmic voltage drop jL/κ and the Tafel slope b. The inverse is sometimes referred to as the Wagner number $\mathrm{Wa} = 1/\bar{j}_\kappa = \kappa b/jL$. The number $\bar{j}_D$ divides the current density j with the current $J_D = \frac{nFDc_0}{L}$ that could be sustained by diffusion alone over a distance L.

The boundary conditions of Eq. (3.B.93) and Eq. (3.B.94), applied to Eq. (3.B.95), can equivalently be written as

$$\bar{\eta}_0' = -\bar{j}_\kappa, \tag{3.B.101}$$
$$\bar{\eta}_1' = 0. \tag{3.B.102}$$

Here, we again use a subscript 0 or 1 to denote the position $x = 0$ or 1. In the next few sections, we will consider various cases in which a simple analytical solution to this set of equations can be found. The goal will be to use these to find the relation between current density and potential losses.

In dimensionless notation Eq. (3.41) becomes

$$\mathcal{E} = \frac{1}{\bar{i}_0'} = \frac{\bar{j}_*}{e^{\bar{\eta}_0}}, \tag{3.B.103}$$

so that

$$\bar{\eta}_0 = \ln\left(\frac{\bar{j}_*}{\mathcal{E}}\right). \tag{3.B.104}$$

3.C *Combined ohmic and diffusion limitations - exact*

We will here define $\chi \equiv \frac{\bar{j}_\kappa}{\bar{j}_D} = \frac{J_D}{J_\kappa} = \frac{nFDc_0}{b\kappa}$, which is a characteristic ratio of ohmic and diffusive effects, and is independent of current density. In case $\chi \gg 1$, ohmic limitations are much stronger than diffusive limitations. When $\chi \ll 1$, ohmic effects

can be neglected relative to diffusive effects. This number only says something about the ratio of the two effects, not their magnitudes, which are given by $\bar{j}_\kappa$ and $\bar{j}_D$, respectively.

We can combine equations (3.B.95) and (3.B.96) to give $\eta' = \chi \bar{c}'$. Integrating, using $\bar{c}_0 = 1$ gives

$$\bar{c} = 1 + \frac{\bar{\eta} - \bar{\eta}_0}{\chi}. \tag{3.C.105}$$

Differentiating Eq. (3.B.95) and eliminating $\bar{\imath}'$ using Eq. (3.B.97), we get

$$\frac{\bar{j}_*}{\bar{j}_\kappa} \bar{\eta}'' = \bar{c} e^{\bar{\eta}}. \tag{3.C.106}$$

Using $\bar{\eta}'' = \frac{1}{2} \frac{d\bar{\eta}'^2}{d\bar{\eta}}$ from Eq. (3.63), we can integrate Eq. (3.C.107) over $\bar{\eta}$ from $\bar{\eta}_0$ to $\bar{\eta}_1$ to give

$$\frac{\bar{j}_*}{2\bar{j}_\kappa} \left(\bar{\eta}_1'^2 - \bar{\eta}_0'^2 \right) = \left(1 + \frac{\bar{\eta} - \bar{\eta}_0 - 1}{\chi} \right) e^{\bar{\eta}} \Big|_{\bar{\eta}_0}^{\bar{\eta}_1} \rightarrow \left(\frac{-1}{\chi} \right) e^{\bar{\eta}_1} - \left(1 - \frac{1}{\chi} \right) e^{\bar{\eta}_0}. \tag{3.C.107}$$

In the final expression, we assumed that $\bar{c}_1 = 1 + \frac{\bar{\eta}_1 - \bar{\eta}_0}{\chi} \approx 0$. This gives $\bar{\eta}_0 - \bar{\eta}_1 \approx \chi$, which we use to write the right-hand side of Eq. (3.C.107) as $\left(-\frac{1}{\chi} e^{-\chi} + \left(1 - \frac{1}{\chi} \right) \right) e^{\bar{\eta}_0} = \frac{\chi - 1 - e^{-\chi}}{\chi} e^{\bar{\eta}_0}$. Finally, we use the boundary conditions (3.B.101) to write the left-hand side as $\frac{\bar{j}_* \bar{j}_\kappa}{2}$ to give

$$e^{\bar{\eta}_0} = \frac{\chi \bar{j}_\kappa \bar{j}_* / 2}{\chi - 1 - e^{-\chi}} \approx \begin{cases} \frac{\bar{j}_\kappa \bar{j}_*}{2} = \frac{j^2}{2 a j_* \kappa b} & (\chi \gg 1) \\ \bar{j}_D \bar{j}_* = \frac{j^2}{a j_* n F D c_0} & (\chi \ll 1). \end{cases} \tag{3.C.108}$$

The final expression in Eq. (3.C.108) is obtained by making a Taylor expansion $e^{-\chi} \approx 1 - \chi + \chi^2/2$ to second order in $\chi \ll 1$. This result was first obtained in Ref. [2].

The physical interpretation of these results is that a proportionally smaller part of the electrode is used as the current increases. In case of diffusion limitations, the reactants will be depleted within a fraction of the electrode thickness. In the case of ohmic limitations, the ionic resistance decreases the overpotential so much that the reaction rate strongly decreases. The electrode thickness that is effectively used, therefore, shrinks. Thinner electrodes have a smaller total area and thus a smaller exchange current density ($J_* = aLj_*$). So when the current density is increased, not only does the numerator in the logarithm of Eq. (3.54) increase, but the denominator decreases as well. This gives rise to twice the normal activation losses or a doubled Tafel slope.

Inserting the polarisation relation of Eq. (3.C.108) we obtain, when $\mathcal{E} \ll 1$:

$$\mathcal{E} = 2\frac{\chi - 1 + e^{-\chi}}{\chi \bar{j}_\kappa} \approx \begin{cases} 2/\bar{j}_\kappa & (\chi \gg 1) \\ 1/\bar{j}_D & (\chi \ll 1) \end{cases}. \tag{3.C.109}$$

In case $\chi \ll 1$, ohmic limitations can be neglected, and only diffusion limitations are considered. One of the assumptions behind Eq. (3.C.108) was that $\bar{c}_1 \ll 1$, so that Eq. (3.C.109) is valid only in case of severe diffusion limitations.

The approximation of simply adding Thiele moduli to give $1/\mathcal{E} \sim \bar{j}_D + \bar{j}_\kappa/2$, as done in section 3.4.4, is quite accurate. The relative error in the effectiveness factor compared to the exact result of Eq. (3.C.109) is only 12 % and occurs when $\chi \approx 2.7$.

Chapter 4

Batteries

This chapter introduces several fully analytical battery models. At high charge or discharge rates, the reaction zone model considers a steep reaction front that slowly moves through the battery electrode. At low discharge rates, slow diffusion into the solid active material can allow using a single particle model. We briefly consider the general structure of modern battery models, which contain both the reaction zone and single particle model as its limits. Finally, we consider a solution to the porous electrode equations for a binary electrolyte.

4.1 Introduction

For short-term storage of electricity, for example in electronics and electric vehicles, batteries are a popular choice. With the advent of renewable energy, they may also play a role in mitigating the problem of intermittency of renewable sources, which requires highly efficient storage of electricity over the scale of hours or shorter.

4.1.1 *Types of batteries **

Historically, the word battery refers to a series of at least a few electrochemical cells, typically put in series to obtain large voltages. While some batteries still contain several cells, the word presently can also refer to a single electrochemical cell. For example, common 1.5 V batteries usually consist of a single cell, while a nine-volt *block battery* consists of six such batteries in series.

1. **Primary batteries**: These batteries are for one-time use. They are not rechargeable. In other words, the electrochemical reactions involved are not reversible. An example is the ubiquitous AA *alkaline battery*.

2. **Secondary batteries:** These are rechargeable and can be used for many cycles. An example is the *lithium-ion battery*, commonly used in mobile phones and laptops.

Starting from the voltaic pile explored by Alessandro Volta around 1800, continuous improvements in batteries led to the use of rechargeable *Nickel Cadmium alkaline batteries* developed in the 1960s and modern-day *Nickel-metal hydride (NiMH)* and *lithium-ion batteries* in the 1990s. Figure 4.1 shows the energy density of various types of batteries. Note that batteries typically have an energy density that is at least one to two orders of magnitude smaller than that of liquid fuels like gasoline (13000 Wh/kg, 9500 Wh/l).
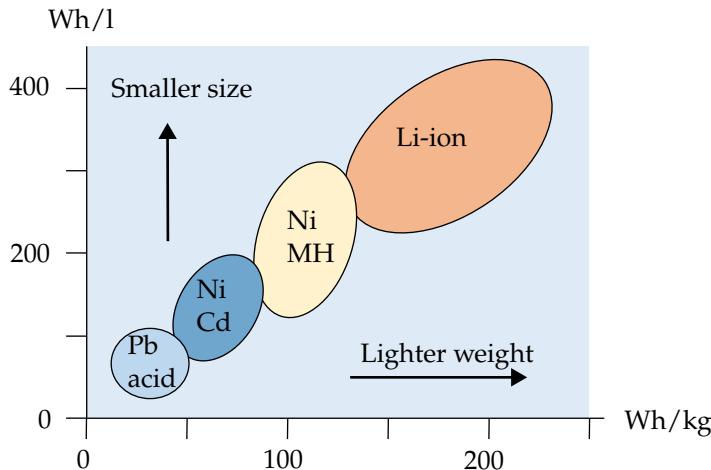
Figure 4.1: Specific energy density [Wh/kg] as a function of volumetric energy density [Wh/l]. Along the horizontal axis, a higher energy density indicates lighter batteries; along the vertical axis, a higher energy density indicates that batteries can be made smaller.

Often, liquid binary electrolytes are used in batteries, including:

- Potassium hydroxide (K^+OH^-) in alkaline (Zn/MnO_2), Ni-Cd, and Ag-Zn batteries

- Sulphuric acid ((H^+)$_2SO_4^{2-}$) in lead-acid batteries, and

- Lithium hexafluorophosphate ($Li^+PF_6^-$) in Li-ion batteries

State-of-the-art lithium-ion batteries use an electrolyte like $LiPF_6$ in an organic solvent, a $LiCoO_2$ cathode, and a carbon graphite anode with reactions that can be represented during discharging as, at the anode[1]

---

[1]Note that during discharging, oxidation takes place at the anode and reduction at the cathode, as in any other electrochemical cell. However, in batteries, the anode and cathode during discharging remain the anode and cathode during charging. Therefore, only during the charging of batteries can oxidation take place at the cathode and reduction at the anode.
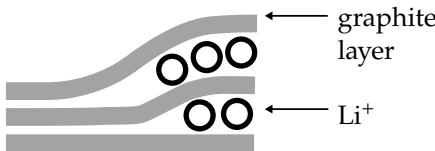
Figure 4.2: *The intercalation of Lithium ions between graphene layers inside an electrode. The intercalation process is alternated with de-intercalation, in which the Lithium ions move out again, which gives Li-ion batteries their nickname 'rocking-chair batteries'.*

$$C_6Li_x \xrightleftharpoons[\text{charge}]{\text{disch.}} xLi^+ + C_6 + xe^-, \qquad \text{(anode)} \qquad (4.1)$$

$$Li_{1-x}CoO_2 + xLi^+ + xe^- \xrightleftharpoons[\text{charge}]{\text{disch.}} LiCoO_2. \qquad \text{(cathode)} \qquad (4.2)$$
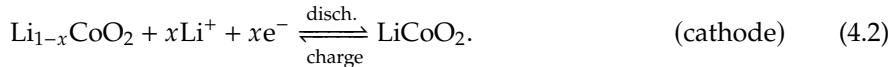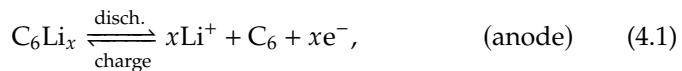
The fractional reaction stoichiometry x indicates the number of Lithium ions per carbon atom that is integrated into the layered graphite structure through a process called *intercalation* or *insertion*, see Fig. 4.2.

In an alkaline battery, the following redox reaction takes place

$$Zn + 2OH^- \xrightleftharpoons[\text{charge}]{\text{disch.}} ZnO + H_2O + 2e^- \qquad \text{(anode)} \qquad (4.3)$$

$$2MnO_2 + 2H_2O(l) + 2e^- \xrightleftharpoons[\text{charge}]{\text{disch.}} 2MnO(OH) + 2OH^-. \qquad \text{(cathode)} \qquad (4.4)$$
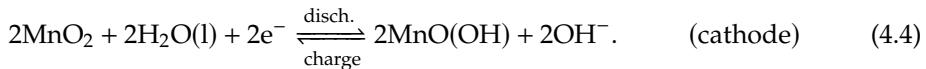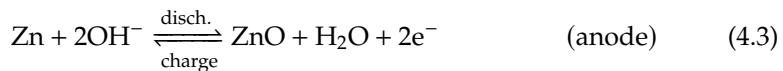
4.1.2   Battery terminology

Battery researchers have their own terminology and conventions, sometimes somewhat different from other parts of electrochemistry and electrochemical engineering fields. Here, we list some of the definitions and terms we will use later on.

1. **Cut-off voltage** (V_d): the voltage below which the battery is considered empty or discharged; hence the subscript d. Below this voltage, the battery can no longer be used satisfactorily for the intended application; further discharging may even damage the battery.

2. **Theoretical capacity** (Q_{max}): The maximum "charge" the battery can hold. The battery is electrically neutral, but this indicates the amount of charge that can be maximally converted through redox reactions. Often units of Ampere-hours are used (1 Ah = 3600 A s = 3600 C) instead of C, the Coulomb.

3. **Volumetric theoretical capacity** (q_{max}): Maximum charge per unit volume. Considering only a single porous electrode volume, we can write $q_{max} = \frac{Q_{max}}{AL}$, with A the separator area and L the electrode thickness.

4. **Discharge time** (t_d): The time required for a full discharge, until the cut-off voltage is reached.

5. **Discharge rate (C/#)**: A measure of how long it takes to discharge a battery from its maximum theoretical capacity. This is often expressed as a C rate. For example, a rate of C/3 means the battery is discharged in 3 hours and 3C means a full discharge in 20 minutes. Using a similar notation, the charging rate is sometimes expressed as an E rate.

6. **Current density** (j): Rarely used when describing batteries; its average value can be related to the 'actual' battery capacity $Q \leq Q_{max}$ and the discharge time through 🏃

$$j = \frac{Q}{At_d} = \frac{qL}{t_d} = \frac{q_{max}L}{3600N}. \tag{4.5}$$

7. **State of charge** (SOC): Represents the amount of charge stored, as a fraction of the theoretical capacity Q_{max}. We will use the symbol S_{oC}, where,

$$S_{oC}(t) = 1 - A\frac{\int_0^t j\,dt}{Q_{max}} = 1 - \frac{1}{L}\frac{\int_0^t j\,dt}{q_{max}}. \tag{4.6}$$

8. **Terminal voltage** (V_{cell}): This is the voltage between the positive and negative terminals of a battery. For a single electrochemical cell or cells in parallel, this is equal to the cell voltage, so we will use the same notation as before. It is a multiple of the cell voltage for batteries consisting of several cells in series. The terminal voltage is not to be confused with the cut-off voltage.

9. **Energy density**: The maximum available energy per unit volume or unit mass of the battery. Often units of Wh = 1 W·3600s = 3600 J are used instead of Joules. Hence, common units for energy density are Wh/l or Wh/kg, for *volumetric* and *gravimetric* energy density (*specific energy*), respectively.
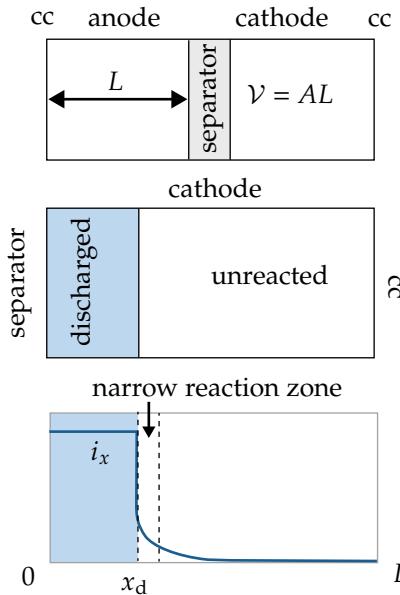
Figure 4.3: *The typical battery layout considered (top), an electrode separated in distinct discharged and unreacted parts in the reaction zone model (middle), and the distribution of ionic current i_x in an example cathode assuming $j \gg J_\kappa$. The fraction of reacted material is equal to the dimensionless position of the reaction zone x_d/L.*

4.2 Moving reaction zone model

4.2.1 Assumptions

We consider a porous battery electrode with negligible electrode resistivity but significant ohmic limitations in the electrolyte. We assume a constant electrolyte conductivity κ.[2] In the terminology of Chapter 3, we consider the case $j \gg J_\kappa = b\kappa/L$ so, by Eq. (3.66), the effectiveness factor $\mathcal{E} \ll 1$. This implies that the reaction takes place primarily over a reaction zone with a thickness equal to the penetration depth $\mathcal{E}L \ll L$. This allows us to split the discharging battery electrode into three zones, with the thin reaction zone demarcating discharged and not yet discharged zones as shown in Figure 4.3.[3] A *moving reaction zone model* based on this idealisation was developed in Ref. [27].

---

[2]Commonly in batteries, the metal electrodes allow a high conductivity for electrons. At the same time, there are large research efforts to develop electrolytes with sufficiently high ionic conductivity. *Solid-state batteries* use solid electrolytes, which may approximately satisfy Ohm's law, as considered here.

[3]We will in this chapter generally talk about discharging, while the descriptions equally apply to charging. We will also only consider a single electrode at a time to keep the notation minimal. It will usually be straightforward to add the second electrode in the same manner.
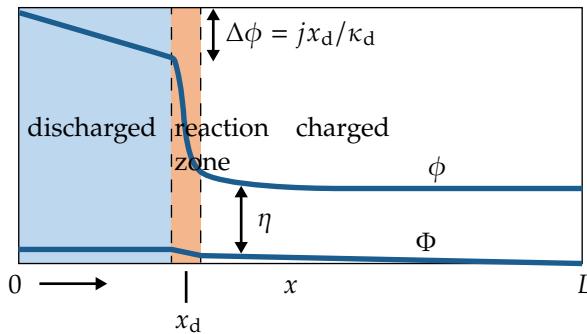
Figure 4.4: *Distribution of ionic and electronic potential ϕ and Φ respectively, with the voltage drop $\Delta\phi$ due to ohmic resistance over the discharged region and the strong drop in activation overpotential in the reaction zone.*

4.2.2 The terminal voltage

We will write the cell voltage using Eqs. (3.39) and (1.35) as

$$V_{\text{cell}} = V_{\text{eq}} - \Delta V - \Delta\phi, \tag{4.7}$$

where[4]

$$\Delta V = \eta_{\text{a0}} - \eta_{\text{a0}} + ARj. \tag{4.8}$$

Figure 4.4 shows the distributions of potentials inside a porous battery electrode with a sharp, moving reaction zone front. There is no reaction over the discharged region so, by Ohm's law in the form of Eq. (1.8), the ionic potential drop up to the reaction zone reads:

$$\Delta\phi = \frac{jx_{\text{d}}}{\kappa_{\text{d}}}, \tag{4.9}$$

where x_{d} is the thickness of the discharged layer and κ_{d} is the effective ionic conductivity of the discharged material.[5]

Figure 4.5 shows the cell voltage as a function of the discharged layer thickness x_{d}. When x_{d} approaches the electrode thickness L and little reactive material is left, the activation losses will increase, causing the strong decrease in terminal voltage depicted in Fig. 4.5. At a cut-off voltage V_{d}, the battery is considered discharged for practical purposes. The final state of charge will typically be non-zero because some capacity remains left, which can be used at a lower current.

---

[4]In Eq. (1.35), we reserved ΔV for just electronic losses in the electrodes, cables, etcetera. Here, in ΔV, we also include the activation losses and ionic ohmic losses in the membrane. Since we assume $j \gg J_\kappa$, Eq. (3.65) can be used to give the overpotential at the beginning of the reaction zone. Strictly speaking, this will cease to hold when the reaction zone comes very close to the right boundary, requiring $S_{\text{oC}} \geq 2J_\kappa/j$.

[5]Note that since the reaction in a battery involves the solid electrode material, the porosity may change due to the reaction, changing the ionic conductivity compared to that in the unreacted electrode material.

$$V_{\text{cell}} = V_{\text{eq}} - \Delta V - j x_{\text{d}} / \kappa_{\text{d}}$$
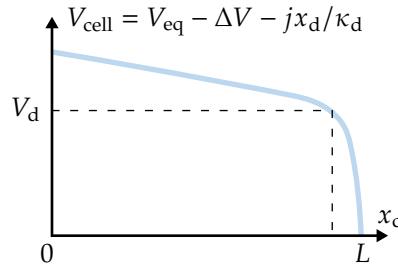
Figure 4.5: *The terminal voltage V_{cell} as a function of the position x_{d} of the reaction zone. Ideally, the cut-off voltage (V_{d}) is reached when x_{d} approaches L at the end of the porous electrode. In reality, the activation losses start to increase when x_{d} approaches L resulting in the terminal voltage dropping below the cut-off voltage.*

4.2.3 Optimal battery electrode thickness

Combining Eqs. (4.7) and (4.9) gives the position of the reaction front at the end of the discharge when the terminal voltage V_{cell} equals the cut-off voltage V_{d} 🏃

$$x_{\text{r}} = \kappa_{\text{d}} \frac{V_{\text{eq}} - V_{\text{d}} - \Delta V}{j} = L_{\text{opt}}. \tag{4.10}$$

Here $V_{\text{eq}} - V_{\text{d}}$ is the maximum allowable voltage drop of the battery over its discharge. Subtracting other losses ΔV, the numerator $V_{\text{eq}} - V_{\text{d}} - \Delta V$ gives the voltage that 'remains' for ohmic losses in the electrolyte of the porous electrode.

Ideally, the final state of charge is small, and the reaction zone has approximately reached the end of the battery electrode, so little unreacted electrode material remains. Therefore, Eq. (4.10) directly gives the optimal porous electrode thickness L_{opt} for this current density j. Similar to what we found in Eq. (3.68), higher current densities and lower conductivities dictate the use of thinner electrodes.

Often, we want to discharge a battery in a certain given time t_{d} rather than at a given current density. In this case using Eq. (4.5), $j = \frac{qL}{t_{\text{d}}}$, in Eq. (4.10) and neglecting the current density dependence of ΔV, gives a quadratic equation for L that is solved

by[6] 🏋

$$L_{\text{opt}} = \sqrt{\kappa_{\text{d}} \frac{V_{\text{eq}} - V_{\text{d}} - \Delta V}{q} t_{\text{d}}}. \tag{4.12}$$

For example, with $t_{\text{d}} = 10$ h, $\kappa_{\text{d}} = 1$ S/m, $V_{\text{eq}} - V_{\text{d}} = 0.1$ V, and $q_{\text{max}} \approx 1$ kAh/l, we obtain $L \approx 1$ mm. The effective conductivity in batteries is usually relatively low compared to that in fuel cells, electrolysers, and flow batteries. Unlike in these other applications, the electrodes themselves are the reactants. Therefore, battery electrodes are relatively thick, which is necessary to achieve a high capacity. Through Eqs. (4.10) and (4.12), this implies that batteries have relatively low current densities or long discharge times.

4.3   Single particle models

4.3.1   Solid diffusion

The moving reaction zone model we just considered is expected to be a good approximation for high discharge rates when ohmic limitations in the electrolyte are limiting. However, the slow penetration of reactants and products inside solids is often the limiting process. The model we follow here is inspired by a common approach to battery modelling discussed in more detail in section 4.3.6. We assume that redox reactions take place at the battery particle surface after which the products diffuse towards the bulk of the particle. [7] The diffusion coefficient in gases and liquids are typically of the order of 10^{-5} and 10^{-9} m^2/s, respectively, whereas in solids it can be still many orders of magnitude lower than in liquids. See Tbl. 4.1 for typical diffusion coefficients in various Lithium compounds.

We will denote the radius of a spherical particle with R, trusting that it will not lead to confusion with the resistance for which we used same symbol before. The

---

[6]Neglecting the current-density dependence of $\eta_{\text{a0}} - \eta_{\text{a0}}$ but including the final term ARj in Eq. (4.8) gives a quadratic equation for L that can be solved by

$$L = \frac{AR\kappa_{\text{d}}}{2} \left(\sqrt{1 + \frac{4}{AR\kappa_{\text{d}}} \frac{t_{\text{d}}}{q} \frac{V_{\text{eq}} - \eta - V_{\text{d}}}{AR}} - 1 \right) \approx \begin{cases} \sqrt{\kappa_{\text{d}} \frac{V_{\text{eq}} - V_{\text{d}} - \Delta V}{q} t_{\text{d}}} & \text{if } AR \ll \frac{L}{\kappa_{\text{d}}} \\ \frac{t_{\text{d}}}{q} \frac{V_{\text{eq}} - \eta - V_{\text{d}}}{AR} & \text{if } AR \gg \frac{L}{\kappa_{\text{d}}}. \end{cases} \tag{4.11}$$

The bottom expression uses the expansion $\sqrt{1 + x} \approx 1 + \frac{x}{2}$ for $x \ll 1$. Typically, the separator will be much thinner and less resistive than the electrode so that $L/\kappa_{\text{d}} \gg AR$ and the top expression, or Eq. (4.12), will be more relevant.

[7]It may be argued [6] that the intercalation of e.g. Lithium in the *intercalation host* graphene show in Fig. 4.2 is not a purely faradaic process. This is a process in which electrons are transferred, and redox reactions occur. When the charged lithium cations move between the carbon sheets, they attract electrons in the carbon phase, creating a capacitance. Even in the absence of reactions, such a process could store electrical energy. Both processes may also occur simultaneously.

Material	D [m^2/s]
LiCoO$_2$	$10^{-14} - 10^{-12}$
LiMn$_2$O$_4$	$10^{-15} - 10^{-13}$
LiFePO$_4$	$10^{-19} - 10^{-18}$

Table 4.1: *Diffusivities of lithium ions in different electrode materials used in Li-ion batteries.*

characteristic time-scale for diffusion over a distance R is[8]

$$t_D \equiv \frac{R^2}{D}. \tag{4.13}$$

Discharging a porous battery electrode consisting of particles with radius R over a discharge time t_d thus requires $R \lesssim \sqrt{Dt_d}$. For a discharge time of $t_d \sim 1$ hour, Table 4.1 gives a radius of a few micrometres for LiCoO$_2$ and only a few tens of nanometres for LiFePO$_2$. Therefore, solid diffusion requires battery electrodes to consist of very small particles or highly porous materials in which the electrolyte is never far away from the electrode-electrolyte interface.

4.3.2   The single particle model

Reactants and products of the redox reactions in the electrolyte are transported by diffusion and, in the case of ions, migration. At low to moderate discharge rates, gradients in the concentration and overpotential can usually be neglected. In Chapter 3, this was quantified using $j \ll J_D, J_\kappa$. Under these conditions, the concentrations and overpotential in the electrolyte can be taken to be approximately constant, as schematically illustrated in the below Figure 4.6. We will allow a significant drop in concentration and potential over the separator but do consider homogeneous conditions throughout the electrodes. This means that all active particles that comprise the porous electrode experience the same conditions, so we can describe their charging and discharge by considering a single representative particle.

The reactant or product ion flux $N_\perp$ at the surface of each particle will be the same throughout the porous electrode. The constant associated local surface current density $j_\perp$ adds up for all particles, using Eqs. (3.18) and (3.21), to give a total current density magnitude 🚶

$$j = aL|j_\perp|, \; = aLnF|N_\perp|. \tag{4.14}$$

Here, Eq. (3.4) gives the total volumetric surface area $a = (1 - \epsilon)\, a_s$ [m^2_s/m^3] in terms of the volumetric surface area a_s of a single battery particle and the porosity ϵ. As

---

[8]Eq. (2.57), for example, gave for the one-dimensional diffusion boundary layer thickness in case of a constant flux $\delta \sim \sqrt{Dt}$.
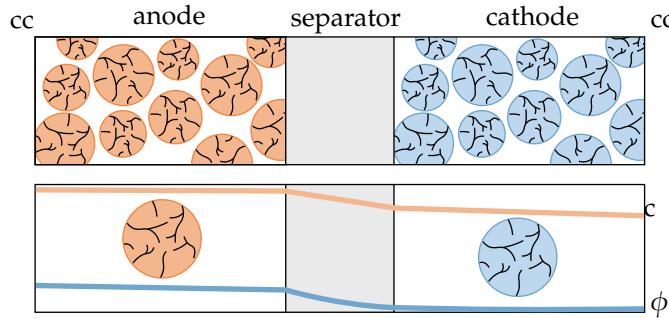
Figure 4.6: *A battery electrode consisting of many small particles in a 'single particle model' is represented by a single characteristic particle, assuming all particles in an electrode experience the same electrolyte potential ϕ and concentration.*

discussed in section 3.3.1, the multiplication factor aL is the conversion factor between the total internal and external electrode area.

4.3.3 Diffusion in a spherical particle

We will denote the concentration of solid reactant material, per total unit volume, with a capital C [mol/m^3], and reserve the lower case c for the concentration of a reactant in a fluid or the electrolyte concentration. As discussed above, we assume the redox reactions occur at the particle surface and assume that the transport of reactants from the interior of the battery material can be described by diffusion. We can thus describe the solid reactant concentration C by the general conservation equation, Eqs. (2.1) and (2.2) without flow and sources,

$$\frac{\partial C}{\partial t} = -\nabla \cdot \boldsymbol{N}, \text{ where } \boldsymbol{N} = -D\nabla C. \tag{4.15}$$

Consider the spherical particle shown in Figure 4.7. Its solid material with an initial concentration $C_{\max}$ reacts at the surface at a radial coordinate $r = R$, equal to the sphere radius R. The surface flux

$$N_\perp (t) = -D\frac{\partial C}{\partial r}\bigg|_R , \tag{4.16}$$

is positive for flux from the solid in the direction of the electrolyte, which is the case in Figure 4.7. The effective medium diffusivity D used here may differ from the material diffusivity in case the particle is porous. At the centre of the particle, by symmetry, there is zero flux, so $D\frac{\partial C}{\partial r}\big|_{r=0} = 0$. Using these boundary conditions while integrating Eq. (4.15) over the particle volume and dividing by the volume V_s gives, using the divergence theorem 🏃
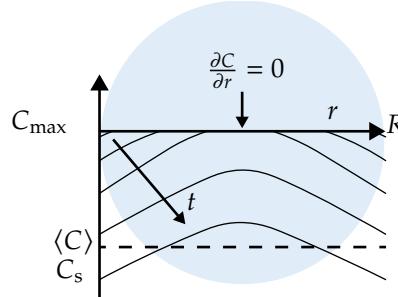
Figure 4.7: *The concentration profiles in a spherical particle at various times for a constant charge or discharge rate. Initially, the concentration profile forms a transient boundary layer near the surface, while all of the sphere's volume is affected for longer times.*

$$\frac{d\langle C\rangle}{dt} = -a_s N_\perp,\tag{4.17}$$

where $\langle C\rangle \equiv \frac{1}{\mathcal{V}_s}\int C d\mathcal{V}$ is the average concentration, and $a_s \equiv A_s/\mathcal{V}_s$ the particle volumetric surface area. Equation (4.17) holds for any particle shape, but for a sphere we have $a_s = \frac{4\pi R^2}{\frac{4}{3}\pi R^3} = \frac{3}{R}$.[9]

Equation (4.16) can be solved analytically, resulting in a somewhat complicated series solution for $C(r,t)$. Alternatively, in two limiting cases, we can solve Eq. (4.17) for the average concentration $\langle C\rangle$. We define the mass transfer coefficient by the ratio of the flux and the difference between the average and surface concentration:

$$k_m \equiv \frac{N_\perp}{\langle C\rangle - C_s},\tag{4.18}$$

where $C_s \equiv C(r = R)$ is the surface concentration. Simple expressions for this mass transfer coefficient exist in two distinct regimes, shown in Figure 4.7:

1. *Developing* ($t \ll t_D$): the concentration boundary layer is much thinner than the particle radius.

2. *Developed* ($t \gg t_D$): the concentration profile changes throughout the entire particle.

For short times $t \ll t_D$, the concentration varies only in a thin layer near the particle surface, so the exact particle shape does not matter, and we can use the solution of the one-dimensional diffusion equation. With $N_\perp = D\frac{\langle C\rangle - C_s}{\delta}$ we see from Eq. (4.18) that

---

[9]In case of spherical symmetry, $\nabla^2 C = \frac{1}{r^2}\frac{\partial}{\partial r}\left(r^2\frac{\partial C}{\partial r}\right)$. Multiplying Eq. (4.15) by $4\pi r^2$ and integrating from $r = 0$ to $r = R$ and dividing by the particle volume $V_s = 4\pi R^3/3$ gives with $\langle C\rangle = \frac{1}{V_s}\int_0^R C(r)4\pi r^2 dr$, again, Eq. (4.17). However, using the divergence theorem is arguably easier and more general.

$k_m = D/\delta$. For a constant flux $N_\perp$, Sand's analysis gives a boundary layer thickness described by Eq. (2.57) so the mass transfer coefficient k_{m0} at time $t = 0$ is given by

$$k_{m0} = \sqrt{\frac{\pi D}{4t}}. \tag{4.19}$$

While initially it is very high, the mass transfer coefficient decreases as time progresses and the boundary layer thickness increases. As the boundary layer approaches the order of the particle size, Eq. (4.19) becomes invalid. In Appendix 4.A, we show for a spherical particle that δ can be approximately replaced by $R/5$ in this case, so the mass transfer coefficient for times $t \gg t_D$ reads

$$k_{m\infty} \approx \frac{5D}{R}. \tag{4.20}$$

The smaller the particle, the larger the mass transfer coefficient. This is expected because of the larger concentration gradients that are associated with smaller length scales.

4.3.4 State of charge

Assuming a first-order reaction takes place at the particle surface, we can write

$$N_\perp = kC_s, \tag{4.21}$$

where k is the reaction rate coefficient. In general, this will depend on the overpotential and the electrolyte concentration. In a single particle battery model, these are assumed constant throughout the electrode, so we can treat k as a constant here.

Combining Eqs. (4.21) and (4.18), we can solve for $C_s = \frac{k_m}{k+k_m} \langle C \rangle$ to give

$$N_\perp = k_{tot} \langle C \rangle \,, \text{where} \frac{1}{k_{tot}} = \frac{1}{k} + \frac{1}{k_m}. \tag{4.22}$$

The total transfer resistance $1/k_{tot}$ is obtained as a reaction resistance $1/k$ and a mass transfer resistance $1/k_m$, acting in series. With this, Eq. (4.17) can be written as

$$\boxed{\frac{d \langle C \rangle}{dt} = -a_s k_{tot} \langle C \rangle.} \tag{4.23}$$

The state of charge is given by the average reactant concentration divided by the maximum. Integrating Eq. (4.23), with the initial condition $\langle C \rangle (t = 0) = C_{max}$, gives

$$S_{oC} = \frac{\langle C \rangle}{C_{max}} = e^{-\int \frac{dt}{\tau}}, \text{with } \tau = \frac{1}{a_s k_{tot}}. \tag{4.24}$$

For $t \ll t_D$, the boundary layer will be very thin, and the mass transfer resistance $1/k_m$ can be neglected. In case $k_{tot} \approx k$ is constant, the state of charge $S_{oC} = \frac{\langle C \rangle}{C_{max}} = e^{-ka_s t}$ decays exponentially with time.

For $t \gg t_D$, assuming $1/k_m \gg 1/k$, for a spherical particle Eq. (4.20) can be used to give for the characteristic time-scale of Eq. (4.24) 🏃

$$\tau_\infty \equiv \frac{1}{k_{m\infty}a_s} = \frac{R^2}{15D}.$$ (4.25)

In this regime of mass transfer-limited discharging, Eq. (4.25) shows that smaller particles can be discharged faster. However, for very small particles, the reaction may become limiting. As an example, for a solid diffusivity $D = 10^{-13}$ m²/s, to have $\tau_\infty \lesssim 1$ h requires a particle radius $R \lesssim 75$ μm.

In both of the above examples, the discharge rate decreases with time. However, often, batteries will be used with a more or less constant discharge rate. In this case, the state of charge will go down linearly as $S_{oC} = 1 - \frac{t}{\tau_0}$. Inserting this into Eq. (4.24) gives 🏃

$$\frac{1}{\tau} = a_s k_{tot} = \frac{1}{\tau_0 - t}.$$ (4.26)

So, as time increases, the total transfer coefficient has to decrease to compensate for the reduced reactant concentration. For redox reactions, this can be realised by increasing the overpotential. As t approaches $\tau_0 = \frac{1}{a_s k(t=0)}$, Eq. (4.26) shows that ever-larger overpotentials will be needed. This additional concentration overpotential will be quantified further in the next section.

4.3.5 Polarisation relation

Assuming first-order Tafel kinetics $j_\perp = j_* \frac{C_s}{C_{max}} e^{\eta/b}$ so, using Eq. (4.14), the overpotential is given by 🏃

$$\eta = b \ln \left(\frac{j C_{max}/J_*}{\langle C \rangle \left(1 - \frac{j}{j_{lim}}\right)} \right),$$ (4.27)

where the numerator represents the surface concentration C_s, Eq. (3.43) gives $J_* \equiv aLj_*$, and we introduced

$$j_{lim} = aLnFk_m\langle C \rangle.$$ (4.28)

Using Eq. (4.24), Eq. (4.27) can be written as 🏃

$$\frac{\eta}{b} = \ln\left(\frac{j}{J_*}\right) + \int \frac{dt}{\tau} + \ln\left(\frac{1}{1 - \frac{j}{j_{lim}}}\right).$$ (4.29)

where $j_{lim} = aLnFk_mC_{max}e^{-\int \frac{dt}{\tau}}$. Here, the first term represents the activation overpotential. The second term represents the concentration overpotential due to the decrease in the average concentration. The final term is the additional concentration

overpotential that arises because, as a result of internal mass transport limitations, the surface concentration C_s will always be below the average particle concentration. This term can diverge even for non-zero average concentration because the internal mass transfer coefficient is finite.

Unlike the other terms, the second term in Eq. (4.29) is not a logarithm. This is because the average concentration decreases exponentially, cancelling the logarithm. Because the solid concentration decreases exponentially, the overpotential increases linearly with time. It implies that for each decrease of the state of charge $S_{oC} = \langle C \rangle / C_{max}$ by a factor e, the overpotential η increases with a Tafel slope b. Or, every halving in the state of charge adds $b\ln2 \approx 0.7b$ to η. As j approaches j_{lim}, the increase will increase dramatically. While the physics is quite different, we thus find a similar behaviour as with the moving reaction zone model, as shown in Fig. 4.5. Initially, cell potential decreases linearly, followed by a large drop due to activation overpotential associated with reactant depletion until the cut-off voltage is reached.

4.3.6 Pseudo-2D Model *

Most battery models use some form of the *pseudo-two-dimensional* (or P2D) model developed by Doyle, Fuller, and Newman [10]. It effectively applies a single particle model to each point along a one-dimensional coordinate x through the battery electrode. Therefore, it allows for the inclusion of both the behaviour inside the battery particles and in the electrolyte. For the electrolyte, we may use the porous electrode binary electrolyte equations consisting of Eq. (3.15) and (3.18) combined with Eq. (2.41) without flow

$$\frac{\partial \epsilon c}{\partial t} - \nabla \cdot (D_a \nabla c) = a j_\perp, \tag{4.30}$$

where for the local current density the Butler-Volmer equation is used,

$$j_\perp = j_{*s} \left(e^{\alpha \frac{F\eta}{\mathcal{R}T}} - e^{-(1-\alpha)\frac{F\eta}{\mathcal{R}T}} \right). \tag{4.31}$$

Here j_{*s} may depend on the surface concentration of electrolyte c_s and solid reactant C_s, see Eq. (1.B.42). For a binary electrolyte with an anion with zero flux,[10] Eqs. (2.49) and (2.51) give for the flux

$$N(x = 0) = -\frac{D_a}{1 - t_+} \frac{dc}{dx}, \tag{4.32}$$

which forms the boundary condition to Eq. (4.30). This approach allows each particle to experience a different electrolyte concentration and overpotential and have a different time evolution. At each electrode position, we have a second coordinate r inside the particle. The solid concentration is obtained by solving Eq. (4.15) or, in radial coordinates,

---

[10]For example, in a Lithium-ion battery where lithium cations carry the charge. For a zero-flux cation, t_+ is replaced by t_- in Eq. (4.32).

$$\frac{\partial C}{\partial t} = \frac{D}{r^2}\frac{\partial}{\partial r}\left(r^2\frac{\partial C}{\partial r}\right). \tag{4.33}$$

Solving for the entire concentration profile as a function of r is not necessary since only its surface value $C_s = C(r = R)$ is needed. For example, solving Eqs. (4.23) and Eq. (4.20) can lead to a much faster one-dimensional model.

A concentrated-solution theory equation like $\boldsymbol{i} = -\kappa\nabla\phi - \kappa_d\nabla\ln c$ is typically used since the electrolyte concentration can be high. This closely resembles our dilute solution theory expression Eq. (2.46), with the difference that the conductivity κ and *diffusive conductivity* $\kappa_d = \chi\kappa$ will strongly depend on the local electrolyte concentration.

4.4   Binary electrolyte

In the moving reaction zone model of section 4.2 we assumed Ohm's law with a constant conductivity, which may be fine for e.g. solid-state batteries. However, battery electrolytes are often binary electrolytes, whose concentration can vary throughout the electrode. As in section 2.4, we consider the equations for a monovalent binary electrolyte with a reacting anion and a zero-flux cation.[11] Equation (2.49) gives the conductivity $\kappa = -i/\phi'$ as

$$\kappa = \kappa_0\bar{c}, \text{where}\quad \kappa_0 = \frac{2D_-F^2c_0}{\mathcal{R}T}. \tag{4.34}$$

Here, the dimensionless concentration $\bar{c} = c/c_0$ is obtained by dividing by the electrolyte concentration $c_0 = c(x = 0)$ at the entrance of the porous electrode. As derived in section 2.4.3, the factor two originates from diffusion, which contributes to the current in equal proportion to migration. Since the conductivity now depends on concentration, we have to modify the porous electrode equations (3.44)-(3.46) slightly, to 🏃

$$\bar{c}' = i/2FD_-c_0, \tag{4.35}$$
$$\eta' = i/\kappa_0\bar{c}, \tag{4.36}$$
$$i' = aj_*\bar{c}^r e^{\eta/b}, \tag{4.37}$$

where we used Eq. (2.49) to modify Eq. (3.44). For generality, we consider a general reaction order r.

Dividing Eq. (4.35) by (4.36), we get 🏃

---

[11]This is relevant, for example, for an alkaline battery with a K^+OH^- electrolyte. Equations (4.3)-(4.4) show that OH^- is a reactant at the anode during discharging and at the cathode during charging. Non-monovalent electrolytes like $H_2^+SO_4^{2-}$ can be described using small modifications considered in Appendix 2.G. The case of a reacting cation, to describe a Li-ion battery electrolyte, for example, is obtained by changing all pluses into minuses and minuses into pluses below.
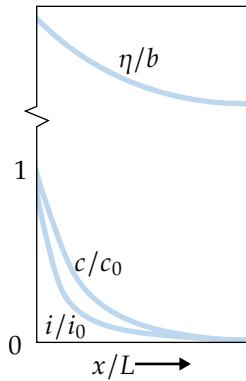
Figure 4.8: *A schematic illustration of the transport of ions of a binary electrolyte in a porous electrode where $x = 0$ represents the reaction front or the 'entrance' of the porous electrode at the start of a charge or discharge.*

$$\frac{d\bar{c}}{d\eta} = \frac{\bar{c}}{\mathcal{R}T/F} \rightarrow \bar{c} = e^{F\frac{\eta-\eta_0}{\mathcal{R}T}}. \tag{4.38}$$

As expected for a (cat)ion in thermal equilibrium, the electrolyte concentration is described by a Boltzmann distribution. As the current penetrates into the porous electrode, the overpotential and the reactant concentration decrease due to resistance and diffusion, respectively. Figure 4.8 shows the expected solution schematically. Here, $x = 0$ represents the 'entrance' of the porous electrode when the battery is fully charged or discharged. Alternatively, it represents the location of a moving reaction zone front. In this case, all battery material has reacted for $x < 0$ while for $x > 0$ the battery electrode has not yet reacted, and L becomes the length of this unreacted area.

Differentiating Eq. (4.35) with respect to x, inserting Eqs. (4.37) and (4.38) and using $b = \mathcal{R}T/\alpha F$ gives

$$\bar{c}'' = \frac{2M^2/L^2}{1+r+\alpha}\bar{c}^{r+\alpha}, \text{where } M^2 \equiv L^2\frac{1+r+\alpha}{2}\frac{aj_*e^{\eta_0/b}}{2FD_-c_0}. \tag{4.39}$$

This is equal to a reaction-diffusion equation with a reaction order not equal to r but $r + \alpha$. This is because the reaction coefficient, through its proportionality to $e^{\eta/b} = e^{\eta_0/b}\bar{c}^{\alpha}$, depends itself on concentration.

Eq. (4.39) can be solved analytically only for particular values of $r + \alpha$. However, for $M \gg 1$ we can deploy a similar approach as that followed in section 3.4.3. Similar to Eq. (3.63), we can write $\bar{c}'' = \frac{1}{2}\frac{d\bar{c}'^2}{d\bar{c}}$. Integrating Eq. (4.39) from $x = 0$ to the electrode end at $x = L$ gives

$$\frac{\bar{c}_L'^2 - \bar{c}_0'^2}{2} = \frac{2M^2/L^2}{(1+r+\alpha)^2}\left(\bar{c}_L^{1+r+\alpha} - \bar{c}_0^{1+r+\alpha}\right) \xrightarrow{\bar{c}_L' \ll 1} |\bar{c}_0'| = \frac{2M/L}{1+r+\alpha}. \tag{4.40}$$

The final expression holds in case of sufficiently large current densities, giving strong diffusion limitations. As illustrated in Fig. 4.8, the reactant concentration will then approximately vanish at the end of the electrode. Comparing this expression with Eq. (4.35), evaluated at $x = 0$, gives

$$M = \frac{1+r+\alpha}{2}\frac{jL}{2FD_-c_0}. \tag{4.41}$$

Comparing this expression with that of Eq. (4.39) gives, after some algebra

$$\eta_0 \approx 2b\ln\left(\frac{j}{\sqrt{\frac{4FD_-c_0}{1+r+\alpha}}aj_*}\right), \tag{4.42}$$

where we again find a doubled Tafel slope $2b$. Equation 4.42 may equally be written in the general form $\eta_0 = b\ln\left(\frac{j}{J_*\mathcal{E}}\right)$ of Eq. (3.42) with $J_* = aLj_*$ and an effectiveness factor $\mathcal{E} = 1/M$.[12] This explicit polarisation relationship is equal to Eq. (3.60), obtained in the case of only diffusion limitations, upon replacing $D \to \frac{2D_-}{(1+r+\alpha)/2}$. The only differences are the doubled diffusivity $D = 2D_-$ and the division by $(1+r+\alpha)/2$. For a reaction order $r = 1$ and $\alpha = 1/2$ this becomes $1.6D_-$. This result is also equal to Eq. (3.65), obtained for a constant conductivity, upon replacing $b \to \frac{\mathcal{R}T/F}{1+r+\alpha}$.

4.5 Summary

- When $j \gg J_\kappa$, the moving reaction zone model gives voltage losses in a battery electrode as $\eta + jx_d/\kappa_d$ where $x_d = S_{oC}L$ is the position of the reaction zone.

- When $j \ll J_\kappa$, the single-particle model describes the state of charge $S_{oC} = \frac{\langle C \rangle}{C_{max}} = e^{-\int \frac{a_s}{1/k+1/k_m}dt}$ (4.24) using a series resistance of the inverse of a reaction-rate coefficient $k = \frac{j_*}{nFC_{max}}e^{\eta/b}$ and the inverse of a mass-transfer coefficient k_m, the latter tending to $5D/R$ for long times.

- For a binary electrolyte, the diffusion and migration flux are equal, and we obtain for an r-th order reaction in case of strong transport limitations an effectiveness factor $\mathcal{E} \approx 1/M \ll$ with $M \approx \frac{1+r+\alpha}{2}\frac{j}{2FD_-c_0} \gg 1$.

---

[12]Therefore, we anticipate that, as discussed in section 3.4.4, using $\mathcal{E} \approx \frac{1}{1+M}$ will give a reasonable approximation for all current densities.

4.6 Exercises

Exercise 4.1

A present disadvantage of electric vehicles would disappear if their charging time could be reduced to a time not much longer than is required for refuelling a petrol car.

a. If we want to charge an electric vehicle in 5 minutes, for what E-rate should its battery be designed?

b. For a 50 kWh battery, to what power does this rate correspond?

Exercise 4.2

Consider a battery electrode operated at high current density ($j \gg J_\kappa$), so the moving reaction zone model can be used. The battery has a separator of thickness L_s and conductivity κ_s. You may neglect the activation overpotential.

a. Write an expression for the potential difference $\Delta\phi_s$ across the separator at a current density j.

b. Now, consider a single porous electrode with a volumetric capacity q. We switch on the current when the electrode is fully charged. Write an expression for the position x_d of the reaction zone at a certain time, t.

c. Assuming that the conductivity of the reacted electrode is κ_d, write an expression for the potential drop over the distance x_d of reacted electrode.

d. Assuming no appreciable voltage losses arise at the other electrode of the battery, and with an equilibrium voltage V_{eq}, write an expression for the voltage V_{cell} that can be drawn from the battery at time t.

e. The amount of useful energy or work $\mathcal{U}$ that can be obtained from the battery is given by the integral of terminal voltage over the charge transferred. Using the above formulation for the battery terminal voltage, write an expression for this total energy, per unit membrane area, obtained over a discharge time t.

f. Using the above formulation, write an expression for the optimal thickness L_{opt} of the electrode for maximal capacity. (Hint: this implies the whole electrode is utilised when the maximal capacity is used)

Exercise 4.3

Consider a laptop Li-ion battery consisting of many cells in parallel. Each cell has a cross-sectional area of $A = 5$ cm^2, and consists of an anode and a cathode of $L = 0.1$ mm thick and a volumetric capacity of $q = 10^6$ Ah/m^3 each.

a. When discharging at C/5, what current is drawn per cell?

b. Consider a discharge of this battery using a moving reaction zone model, assuming equal ohmic losses in the anode and cathode. The ohmic drop over one fully discharged electrode is ten times that over the separator, which is 0.1 V at the considered current density. If the equilibrium voltage is $V_{eq} = 3.6$ V, at what state of charge is the cut-off voltage $V_d = 3$ V reached?

Exercises 4.4-4.21

Fill in the missing steps in the main text, indicated by the symbol ⋏.

Appendices *

4.A Parabolic polynomial approximation

We postulate that the concentration profile can be written as

$$C(r,t) = \langle C \rangle(t) + \frac{N_\perp(t)R}{D}f(r). \tag{4.A.43}$$

To satisfy Eq. (4.16), we require $f(R) = -1/R$ and $\langle f \rangle = 0$ to ensure that $\langle C \rangle$ represents the average of C. In case of spherical symmetry $\nabla^2 C = \frac{1}{r^2}\frac{\mathrm{d}}{\mathrm{d}r}\left(r^2\frac{\mathrm{d}C}{\mathrm{d}r}\right)$ and Eq. (4.15) becomes

$$\frac{\partial C}{\partial t} = \frac{D}{r^2}\frac{\mathrm{d}}{\mathrm{d}r}\left(r^2\frac{\mathrm{d}C}{\mathrm{d}r}\right). \tag{4.A.44}$$

Inserting Eq. (4.A.43) gives $\frac{-3}{R^2} = \frac{1}{r^2}\frac{\mathrm{d}}{\mathrm{d}r}\left(r^2\frac{\mathrm{d}f}{\mathrm{d}r}\right)$. This is solved by $f(r) = \frac{3}{10} - \frac{r^2}{2R^2}$, which satisfies $\frac{\mathrm{d}f}{\mathrm{d}r}(r = R) = -1/R$ and $\langle f \rangle = \frac{1}{4\pi R^2}\int_0^R 4\pi r^2 f(r)\mathrm{d}r = 0$. This parabolic solution gives the name to this approximation method, which is popular in battery modelling. Inserting Eq. (4.A.43) in Eq. (4.18) gives

$$k_{m\infty} = -\frac{D}{Rf(R)} = \frac{5D}{R}. \tag{4.A.45}$$

4.B Dimensionless binary electrolyte porous electrode model

For a binary electrolyte with varying conductivity, given by Eq. (4.34), the porous electrode equations (4.35)-(4.37) become in the dimensionless notation of section 3.B (and for a general reaction order r):

$$\bar{c}' = -\bar{j}_D\bar{\iota}, \quad \bar{\eta}' = -\bar{j}_\kappa/\bar{c}\bar{\iota}, \quad \bar{j}_*\bar{\iota}' = -\bar{c}^r e^{\bar{\eta}}. \tag{4.B.46}$$

Here $\bar{j}_\kappa = j/J_\kappa$ and $\bar{j}_D = j/j_D$, with J_κ and J_D given by

$$J_\kappa = \frac{\kappa_0 b}{L}, \quad J_D = \frac{2FD_-c_0}{L}. \tag{4.B.47}$$

A factor two multiplies the anion diffusivity in J_D in accordance with Eq. (2.49). With these definitions and $b = \mathcal{R}T/\alpha F$ we have 🏃

$$\frac{J_D}{J_\kappa} = \alpha. \tag{4.B.48}$$

Therefore, for a binary electrolyte, there is no need for a separate J_κ and J_D since migration and diffusion are coupled.

By differentiating the first of Eqs. (4.B.46) and inserting the last we obtain, with $\bar{c} = e^{\frac{\bar{\eta} - \bar{\eta}_0}{\alpha}}$ from Eq. (4.38),

$$\bar{c}'' = \frac{\bar{j}_D \bar{c}^r}{\bar{j}_*} e^{\bar{\eta}} = \frac{2M^2}{1 + r + \alpha} \bar{c}^{r+\alpha}, \tag{4.B.49}$$

where

$$M^2 \equiv \frac{1 + r + \alpha}{2} \frac{\bar{j}_D e^{\bar{\eta}_0}}{\bar{j}_*} = \frac{1 + r + \alpha}{2} \bar{j}_D. \tag{4.B.50}$$

The final expression in Eq. (4.B.50) is the dimensionless form of Eq. (4.41). The dimensionless overpotential $\bar{\eta}_0 = \ln\left(\frac{\bar{j}_*}{\mathcal{E}}\right)$ with $\mathcal{E} \approx 1/M \ll 1$ becomes $\bar{\eta}_0 = \ln\left(\frac{1+r+\alpha}{2} \bar{j}_D \bar{j}_*\right)$.

Chapter 5

Fuel cells

This chapter concerns the modelling of fuel cells, with a particular focus on the effects of produced water in hydrogen fuel cells. First, the transport of water in the membrane and flow channels is briefly described, primarily empirically. A multiphase Darcy flow model is derived for water transport in the diffusion layer. Finally, a flooded agglomerate model *of the catalyst layer is presented that takes into account diffusion inside the water-filled catalyst particles.*

Fuel cells are galvanic cells that generate electricity, as illustrated in Figure 5.1. Where batteries have solid reactants, fuel cells have gaseous or sometimes liquid reactants. Similar to rechargeable batteries, the reaction in fuel cells can sometimes be reversed, allowing the gases or liquids to store energy. If these galvanic and electrolytic reactions occur within the same cell, the resulting system is called a flow battery. Therefore, many aspects of fuel cell modelling also apply to flow batteries. Conversely, most aspects treated in chapter 7 on redox flow batteries will also be relevant for fuel cells. While chapter 7 will focus on two-dimensional single-phase transport, we will consider aspects related to multiphase flow. In particular, we will focus on the case in which gaseous reactants produce liquid products. This occurs, for example, in a PEM[1] fuel cell. Hydrogen and oxygen are converted to water according to the following redox reactions

$$2H_2 \rightarrow 4H^+ + 4e^- \qquad \text{(anode)}, \qquad (5.1)$$
$$O_2 + 4H^+ + 4e^- \rightarrow 2H_2O. \qquad \text{(cathode)} \qquad (5.2)$$

5.1 *Types of fuel cells* *

A concise overview of the most important types of fuel cells is given in Table 5.1. The redox reactions given by Eqs. (5.1) and (5.2) assume acidic conditions, as occur in

---

[1]PEM can stand for either Polymer Electrolyte Membrane or Proton Exchange Membrane.
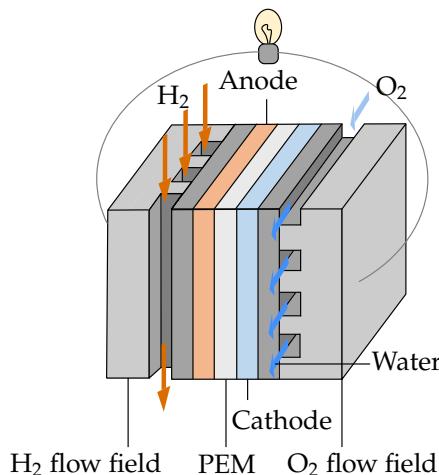
Figure 5.1: *The different types of fuel cells are usually named after their electrolyte and typically operate on hydrogen, oxygen, or air.*

e.g. polymer electrolyte fuel cells (PEMFCs) and phosphoric acid fuel cells (PAFCs).[2] An exception is the direct-methanol fuel cell (DMFC), which, as its name suggests, converts methanol instead of hydrogen. Unlike the other fuel cells, it is named after its reactant and not after its electrolyte or membrane.

Solid oxide fuel cells (SOFC) and molten carbonate fuel cells (MCFC) offer greater fuel versatility than traditional fuel cells, which are limited to only hydrogen. These types of fuel cells also allow various other input gasses, such as methane. Due to their high operating temperature, they can internally catalytically reform these gases into hydrogen. Their high temperature allows for cheaper catalysts but leads to a more complex design and higher material requirements.

Alkaline fuel cells were the first fuel cells commercially available, following their introduction during the 1960 Apollo space missions. However, catalyst poisoning due to CO and CO_2 from the atmosphere somewhat limited their success on Earth. Phosphoric acid fuel cells (PAFC) do not operate at the same high temperatures as SOFCs and MCFCs but still benefit from higher temperatures, which allow them to increase their electrolyte conductivity. However, these fuel cells are currently losing ground to polymer electrolyte fuel cells (PEMFC), which will be the primary focus of this chapter.

---

[2]In alkaline fuel cells, hydroxide ions (OH^-) are the charge carrier and $4OH^-$ should be added on both sides of both reactions. Subsequently $4OH^- + 4H^+$ may be replaced by $4H_2O$. In SOFCs, the oxygen ion (O^{2-}) is the charge carrier and $2O^{2-}$ should be added on both sides of both reactions. Subsequently $2O^{2-} + 4H^+$ may be replaced by $2H_2O$. Finally, MCFCs have CO_3^{2-} as the charge carrier and $2CO_3^{2-}$ should be added along with using $2CO_3^{2-} + 4H^+ \rightarrow 2H_2O + 2CO_2$.
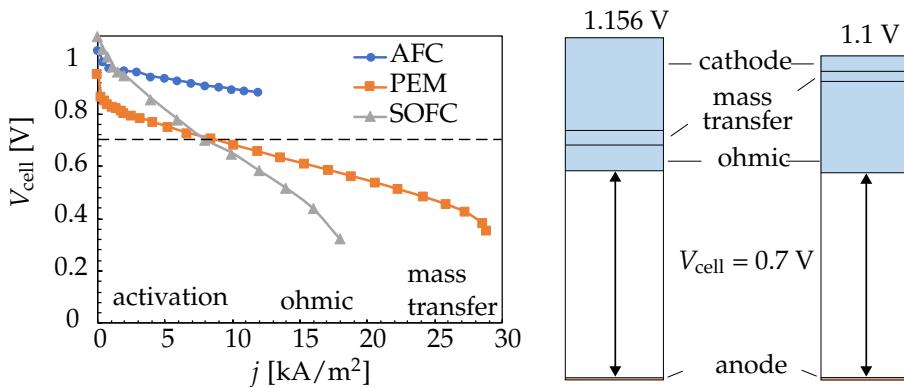
Figure 5.2: *A graph showing typical polarisation curves of an Alkaline Fuel Cell (AFC), Polymer Electrolyte Membrane (PEM), and Solid Oxide Fuel Cell (SOFC). The bar charts on the right show the approximate contributions of activation, mass transfer and ohmic losses to the overall cell voltage of the PEMFC and SOFC, operating at 0.7 V. It is evident, from the strong linear decrease, that the SOFC in this figure experiences substantial ohmic losses. However, the activation losses are considerably smaller, allowing it to outperform the PEMFC at low current densities. With kind permission from Thomas F. Fuller and John Harb for allowing re-use of their data [12]..*

	PEMFC	**AFC**	**PAFC**	**MCFC**	**SOFC**	**DMFC**
Electrolyte	Polymer	KOH	H_3PO_4	K_2CO_3	Ceramics	Polymer
Catalyst (a/c)	Pt/Ni	Fe,Ni/Ag	Pt	Ni	Cermet	Pt,Ru
Temp. (°C)	40-80	65-220	205	650	600-1000	25-90
Charge carrier	H^+	OH^-	H^+	CO_3^{--}	O^{--}	H^+

Table 5.1: *A short overview of the most important fuel cells: the polymer electrolyte/proton exchange membrane (PEMFC), alkaline (AFC), phosphoric acid (PAFC), solid oxide (SOFC), and direct methanol (DMFC) fuel cell. Only the most commonly used materials and operating temperatures are indicated. A cermet is a ceramics-metal mixture, typically Nickel with Yttria-Stabilised Zirconium (YSZ).*

Figure 5.2 shows typical polarisation curves of three different types of fuel cells, the AFC, PEM, and SOFC.

The splitting of hydrogen at the anode (Eq. (5.1)) is a simple reaction. In an acidic medium, platinum is an almost ideal catalyst, so the activation losses involved are often negligible. This is clear from the bottom part of Fig. 5.2, where the losses of a PEMFC and SOFC are split into their different components at a current density for which their voltage is similar. The anode polarisation, shown at the bottom, is very small. Clearly, the ohmic resistance of the reported SOFC is much higher than that of the shown PEMFC. This means that the latter clearly outperforms the former at high

current densities. However, at low current densities, the cell voltage of the SOFC is substantially higher than that of the PEMFC because of the higher equilibrium voltage associated with its higher temperature.

## 5.2 Water management

5.2.1 Catalyst layer
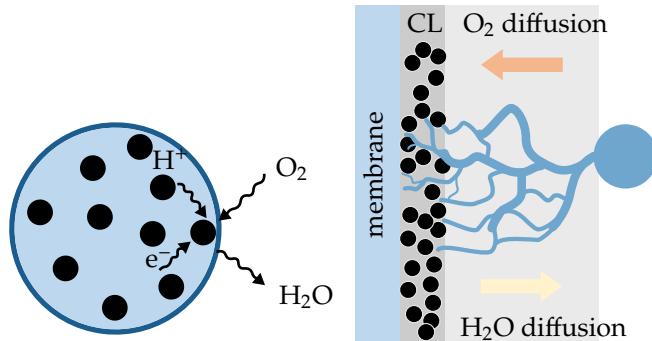
Figure 5.3: *Left: a schematic illustration of PEM fuel cell carbon-supported catalyst particle showing the black catalyst particles surrounded by a carbon/ionomer/binder mixture. Right: water that is produced at the cathode catalyst layer (CL) of a PEM fuel cell permeates as a liquid by capillary action or diffuses out as water vapour. The gas flow of oxygen or air can transport away droplets that form in the flow channel. [10]*

At the cathode of a PEMFC, oxygen reacts with electrons, and the protons are transported from the membrane to form water according to Eq. (5.2). The cathode catalyst layer, therefore, plays an important and intricate role, as it needs to facilitate the conduction of protons and electrons while also allowing gases to enter and liquid water to exit. These different demands are achieved by porous particles whose pores are wetted by the generated water. Oxygen can dissolve in this water and reach the active catalytic sites dispersed throughout the particles. These catalyst nanoparticles should be in good contact with the electrolyte, which is a solid polymer in a PEM fuel cell, and the electrode material, typically carbon. These two phases are mixed and held together by a binder material. See, for example, Figure 5.13. Additionally, the right-hand side of Fig. 5.3 provides a schematic representation of the path followed by liquid water and water vapour.

A gas diffusion layer (GDL) exists between the gas channel, which provides the reactant gases, and the thin catalyst layer, where the reactions take place. Because the catalyst layer is integrated into this layer, the combination is also sometimes called a gas-diffusion electrode (GDE). Section 5.3 will be fully dedicated to the mathematical description of this layer.

5.2.2 Flow channel
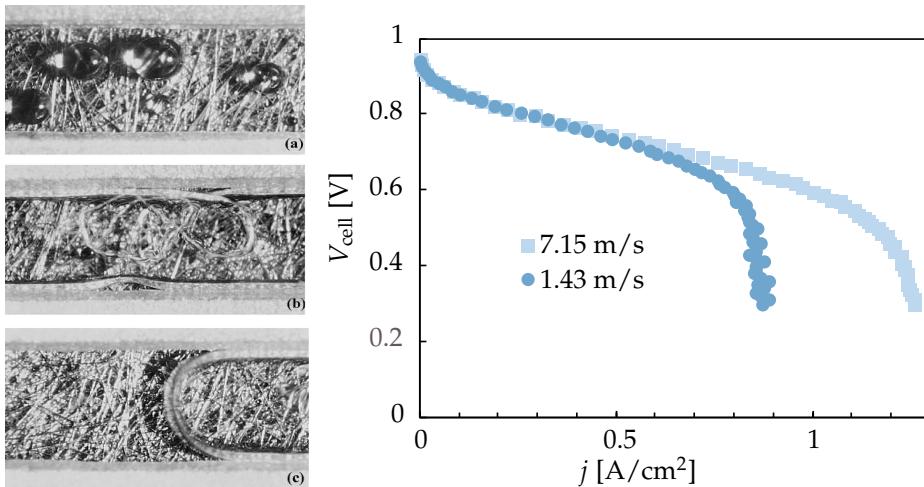
Figure 5.4: *Left: different flow regimes in a PEM fuel cell flow channel bordering a carbon paper GDL [31] with (a) droplets, (b) annular film (c) slug flow. Right: Cell voltage measurements at 80 °C show a strong dependence on average airflow velocity. [31] The transition from the droplet flow regime to the occurrence of films and slugs below roughly 4 m/s was assumed to be at least partly responsible. [31]*

Water making its way through the diffusion layer at the cathode side has to be transported out of the cell through the flow channel. The left-hand side of Fig. 5.4 shows different possible flow regimes. The droplet or spray regime may be the most favourable, as gas is in the continuous phase. In the film and slug flow regimes, the continuous liquid phase impedes the efficient transport of oxygen.

Through the resulting concentration overpotential, the flow channel can affect the cell performance. The right-hand side picture in Figure 5.4 shows the influence of the gas flow velocity on the cell voltage. The occurrence of liquid films and slugs in the flow channel was assumed to be at least partially responsible for the decrease in cell voltage at relatively low velocities and high current densities. [31]

5.2.3 Membrane

The presence of water is necessary for the polymer membrane to function well. The most commonly used polymer electrolyte membrane is Nafion.[3] The conductivity of this polymeric membrane material is crucially dependent on the water content, typically expressed in terms of a parameter λ_{H_2O} indicating the number of water

---

[3]This is a sulfonated tetrafluoroethylene. Ethylene (C_2H_4) in which the hydrogen atoms are replaced by fluorine and which is polymerised into chains that are terminated by a sulfonic acid (SO_3H) group.
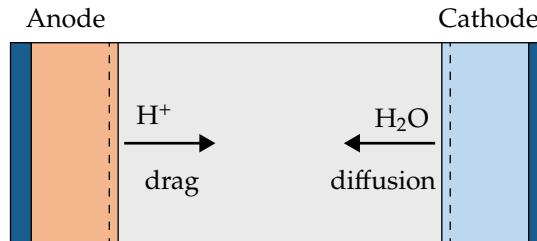
Figure 5.5: *A schematic of a PEM fuel cell, focused on the membrane in grey. Protons moving from anode to cathode bring along the water with them through electro-osmotic drag. On the other hand, water will also want to diffuse in the opposite direction, from cathode to anode.*

molecules per sulfonic acid group. The PEM membrane conductivity $\kappa \approx \kappa_0 + \lambda_{H_2O}\kappa'$ roughly increases linearly with the water content.

Protons can hop along the polymeric structures, but while doing so, they typically drag along several water molecules. This phenomenon is referred to as electro-osmotic drag. The electro-osmotic drag coefficient, ξ, denotes the average number of water molecules carried per proton. Consequently, an electro-osmotic molar flux $\xi j/F$ of water will follow the proton current from the anode to the cathode.

Because water is generated at the cathode, see Eq. (5.2), it tends to diffuse through the membrane to the anode. An accurate quantitative picture requires concentrated solution theory. However, as a rough approximation, we may write

$$\boldsymbol{N}_{H_2O} \approx \frac{\xi \boldsymbol{j}}{F} - D\nabla c_{H_2O}. \tag{5.3}$$

Note that in a membrane, water can be a minority species and can build up gradients. Fick's law of diffusion has been found to hold reasonably well for many polymer membranes. The balance between these opposing fluxes determines how well the membrane is hydrated and, therefore, its conductivity. In this way, water transport significantly impacts the overall cell resistance. Adding to this possible flooding of the catalyst layer, discussed in the next section, water management emerges as a complex but important aspect of obtaining good fuel cell performance.

5.3 Multiphase gas diffusion layer model

The gas diffusion layer typically consists of carbon microfibres made into felts, cloths, or papers. Coatings of PTFE (Teflon) or similar materials are used to make the fibres hydrophobic. This porous layer is placed in between the catalyst layer and the flow channel. It serves several purposes:

1. Providing mechanical strength and shielding the precious and fragile catalyst layer from the channel flow, reducing erosion and degradation.
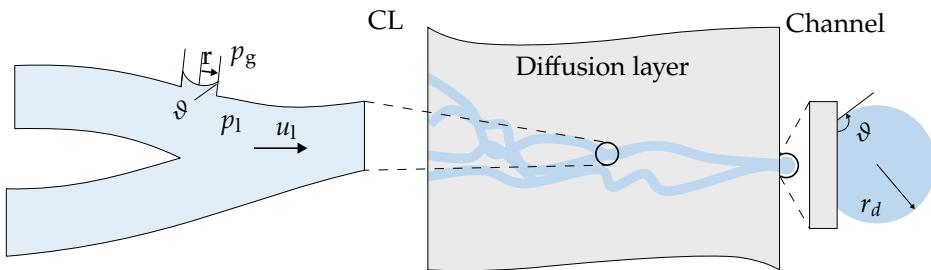
Figure 5.6: *This idealised schematic of a hydrophobic (contact angle $\vartheta > 90°$) cathode diffusion layer illustrates how liquid water, produced at the catalyst layer (CL) on the left, is transported towards the flow channel on the right, through 'channels' formed by the largest pores.*

2. Providing an electronic connection between the catalyst particles and the bipolar plate.

3. Removing water due to its hydrophobic nature, while allowing oxygen to enter.

This section will primarily focus on this last functionality. The gas phase will contain significant amounts of water vapour at temperatures approaching the boiling point. We will consider relatively low temperatures, so we may neglect water vapour transport. We will also neglect the frictional pressure drop due to gas flow, which will be a reasonable approximation at liquid fractions that are not too high. Therefore, the following model is not a substitute for more rigorous models but serves primarily to illustrate the important mechanism of capillary transport.

Figure 5.6 shows the cathode diffusion layer, where liquid water is generated at the catalyst layer (CL) on the left and transported by capillary action out to the right. The capillary force, or surface tension force, keeps the liquid together. It allows the formation of droplets on the surface of the diffusion layer, as shown on the left Fig. 5.4. Next, the gas flow shears and takes away these droplets.

The cathodic gas diffusion layer is porous and resembles paper or a sponge. But because it is made hydrophobic, it will soak up gas instead of water. A water droplet on the surface of a hydrophobic material will approximately have the shape of a capped sphere. As illustrated in Fig. 5.6, the contact angle ϑ is defined as the angle between the surface of the material and the surface of the droplet, *through the liquid phase*.[4] This angle will be larger than ninety degrees for a hydrophobic surface, creating droplets larger than hemispheres.

The approximately spherical shape of droplets arises because the attractive forces between water molecules are much larger than between gas molecules. This results in a minimisation of the droplet surface area. Although attractive forces exist between

---

[4]On a surface that is not flat but rough or irregular over the scale of the wetted area, like the porous materials we consider here, droplets will show an *apparent contact angle* that may differ from the contact angle on a flat surface of the same material, which can be described by the Cassie-Baxter equation.
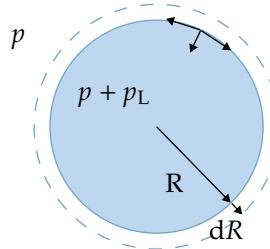
Figure 5.7: *The pressure inside a droplet or bubble is elevated compared to its surroundings by the Laplace pressure p_L. It is caused by the attractive forces in the liquid. Their tangentially oriented force at the gas-liquid surface results in a net inwards surface tension force, somewhat similar to the force exerted by the rubber surface of a balloon. Therefore, increasing the radius by an infinitesimal amount from R to R+dR results in work dW done by the Laplace pressure.*

the water and the solid surface, for a hydrophobic surface, these are weaker than those between water molecules, resulting in a limited *wetted area*.

The liquid is pushed away from where it is produced near the catalyst layer by pressure forces. The left part of Fig. 5.6 shows a magnification of a pore splitting into three smaller pores. Due to the hydrophobic nature of the pores, the liquid chooses to flow through the largest pores. Despite a positive pressure difference $p_l > p_g$ between the liquid and the gas, the liquid does not enter the small capillary. The liquid follows irregular paths through preferentially larger pores. The reason can be understood using the concept of capillary pressure.

5.3.1 Capillary pressure

Surface tension results from the attractive forces between molecules making up a liquid. In the bulk, these forces are in all directions, resulting in a net zero force. However, they do not exactly cancel each other out on a curved gas-liquid interface. As illustrated in Fig. 5.7, the direction of their net pulling force is tangential to the surface. Due to the curvature, this results in a net inward force. This restoring force is trying to make the surface as flat as possible. This can be described by the minimisation of a *surface energy* $U = \gamma A$ proportional to the surface area A times the surface tension γ [J/m^2]. Surface tension hardly depends on the type of gas and is a property primarily of liquids.[5]

For the spherical gas-liquid surface of Fig. 5.7, this additional inwards force results in a higher pressure inside the closed surface compared to its outside. This additional pressure is called the *Laplace pressure* and exists for both droplets and bubbles. We can derive its magnitude from an energy balance using the following reasoning.

---

[5]The more general term *interfacial tension* describes the energy of interfaces that can also be between two liquids, a liquid and a solid, or between a gas and a solid.
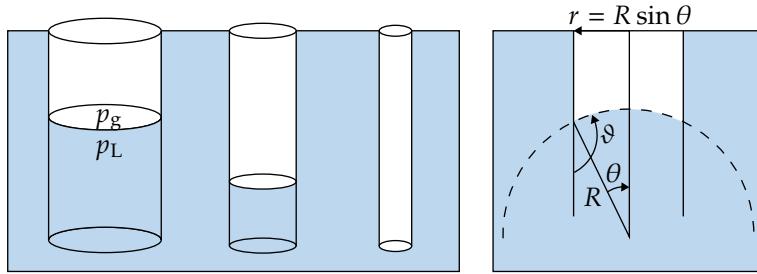
Figure 5.8: Three hydrophobic capillaries or 'straws' with different radii are immersed in water, illustrating how the height of the water column pushed down will be larger for thinner capillaries (left). The liquid surface will be approximately spherical with radius $R = r/\sin\theta = -r/\cos\vartheta$.

Because the pressure inside is higher than outside, the Laplace pressure p_L can be used to do work. An increase of the sphere radius R by an infinitesimal amount dR to $R + dR$ increases its volume $\mathcal{V} = \frac{4}{3}\pi R^3$ by $d\mathcal{V} = 4\pi R^2 dR$ and its surface area $A = 4\pi R^2$ by $dA = 8\pi R$. This exerts a work $dW = p_L d\mathcal{V}$ on the sphere's surroundings while changing its surface energy by $d\mathcal{U} = -\gamma dA$. Conservation of energy $pV + \mathcal{U}$ gives $dW = -\mathcal{U}$, so we find 🏃

$$p_L = \frac{2\gamma}{R}. \tag{5.4}$$

Because the Laplace pressure can become very high for small radii R, creating very small droplets or bubbles is exceedingly difficult.

Now consider Fig. 5.8, showing three hydrophobic straws or *capillaries* immersed in water. The straw area does not like to be wet, and the larger capillaries have a larger surface area, so why will the liquid level be lower in the thinner tubes? This is because of the smaller 'radius of curvature' that the liquid surface will have inside the capillaries.[6] The right-hand side of Fig. 5.8 shows a zoom of the convex surface associated with a hydrophobic contact angle $\vartheta \geq \pi/2$. The *radius of curvature R* is the radius of the approximately spherical surface. Using geometry and Eq. (5.4), the Laplace pressure is equal to[7] 🏃

$$\boxed{p_{cap} \equiv p_l - p_g = \frac{2\gamma|\cos\vartheta|}{r}.} \tag{5.5}$$

This pressure is usually referred to as the *capillary pressure* and Eq. (5.5) as the Young-Laplace equation. It shows that the smaller the radius r of the capillary, the higher

---

[6]The opposite happens in hydrophilic materials, where the water level creeps up more in smaller capillaries.

[7]An absolute value is taken as we defined the contact angle ϑ through the liquid phase so that hydrophobic materials have $\theta > \pi/2$ and $\cos\vartheta < 0$. However, the capillary pressure is defined by Eq. (5.5) as the pressure difference between the non-wetting phase and the wetting phase and is positive.
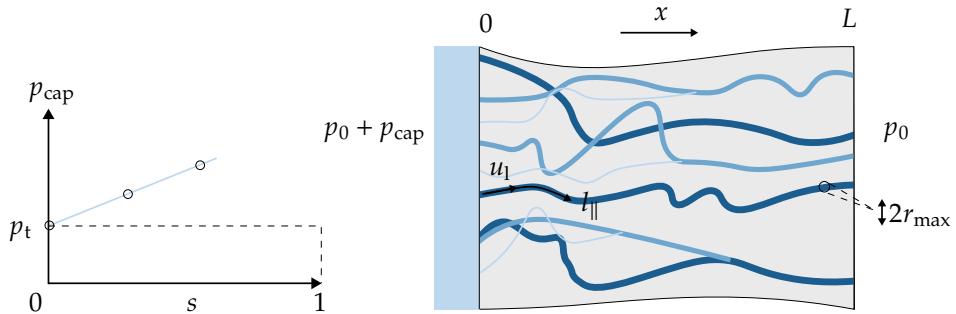
Figure 5.9: *By increasing the differential pressure p_{cap} between a water reservoir on the left of a gas-filled diffusion layer and recording the water saturation s, a capillary pressure-saturation curve can be generated. The largest pore (dark blue) with radius r_{max} forms a water channel first at the threshold p_{t}. At higher pressures p_{cap} the lighter-coloured pores follow, increasing s.*

the pressure difference between the liquid and the gas that can be sustained. In Fig. 5.8 this is hydrostatic pressure, while in Fig. 5.6 it is the frictional pressure drop required to push the water out. The capillary pressure thus explains why the fluid preferentially takes the path traced by the largest pores and does not enter the smaller pores. In the next section, we will consider how to quantify this behaviour.

5.3.2 Capillary pressure-saturation curve

Instead of the well-defined cylindrical capillaries used in the experiment of Fig. 5.8, diffusion layers typically do not consist of regular-sized capillaries, although making such structured diffusion media is an active research area. The carbon paper that is typically used consists of a random arrangement of approximately cylindrical fibres, with the space in between forming a wide pore-size distribution. This distribution can quantified using the procedure[8] illustrated in Fig. 5.9.

A gas-filled diffusion layer is bordered on one side by water, which is gradually increased in pressure. At the *threshold pressure*, or *breakthrough pressure*, p_{t}, the first liquid permeates through.[9] By Eq. (5.5) this pressure can be related to the *maximum pore radius r_{max}* as

$$p_{\text{t}} = \frac{2\gamma |\cos\vartheta|}{r_{\text{max}}}. \tag{5.6}$$

The *water saturation s* is defined as the volume fraction of the local pore volume that is occupied by water. Before the breakthrough pressure is reached, the saturation $s = 0$. With increasing liquid pressure, first, the largest pores and, eventually, the

---

[8]This is called the *porous diaphragm method*, or *restored capillary pressure method*. It is not often used because of its rather slow nature.

[9]For a hydrophilic material, the pressure at which gas first penetrates a water-filled porous medium is observable by the first bubble appearing on the liquid side and is therefore referred to as the bubble point.

smaller capillaries fill with liquid. With increasing liquid pressure, the liquid flow rate increases, and the saturation increases. The resulting curve that can be obtained between applied capillary pressure p_{cap} and water saturation s is shown on the left-hand side of Fig. 5.9. The slope $\partial p_{\text{cap}}/\partial s = p_{\text{t}}/\lambda$ can be characterised in terms of the *pore-size distribution index* λ, so[10]

$$p_{\text{cap}}(s) = p_{\text{t}}\left(1 + \frac{s}{\lambda}\right) \quad \text{for } s \approx 0. \tag{5.7}$$

Comparing with Eq. (5.5) we see that $\frac{r(s)}{r_{\text{max}}} = \frac{p_{\text{t}}}{p_{\text{cap}}} = \frac{1}{1+\frac{s}{\lambda}}$. This gives the smallest pore size r filled with liquid at a liquid saturation s. The average squared pore radius filled with water is given by

$$\left\langle\frac{r^2(s)}{r_{\text{max}}^2}\right\rangle = \frac{1}{s}\int_0^s \frac{p_{\text{t}}^2}{p_{\text{cap}}^2}ds = \int_0^s \frac{ds}{\left(1 + \frac{s}{\lambda}\right)^2} = \frac{\lambda}{s + \lambda}. \tag{5.8}$$

A high λ gives a relatively flat $p_{\text{cap}} - s$ curve that indicates a relatively homogeneous pore size distribution with fairly equal pore sizes. A small λ gives a relatively steep $p_{\text{cap}} - s$ curve, indicating a wide pore size distribution with many widely differing pore radii.

5.3.3 Darcy's law

A fluid flowing through a porous medium will incur a frictional pressure gradient similar to flow through a tube. For steady laminar flow through a cylindrical pore, the *Hagen-Poiseuille equation* gives:[11]

$$-\frac{\mathrm{d}p}{\mathrm{d}x_\parallel} = \frac{8\mu u_{\text{pore}}}{r^2}. \tag{5.9}$$

Here, $x_\parallel$ is a coordinate parallel to the flow. The pressure gradient is linear in the average velocity u_{pore} and scales inversely proportional to the square of the channel radius r.

As we have done in section 3.1, we may approximate a porous medium by a bundle of capillaries. Equation (3.7) gives the superficial velocity through a porous medium of porosity ϵ as $U = \epsilon \frac{u_{\text{pore}}}{\tau}$. Here, the tortuosity defined in Eq. (3.2) $\tau = \partial x_\parallel/\partial x$ gives the length of the pores compared to the shortest length.

---

[10]One of the simplest $p_{\text{cap}} - s$ models that approximately works well for many materials is the Brooks-Corey relation $p_{\text{cap}} = p_{\text{t}}(1-s)^{-1/\lambda}$. For $s \approx 0$ this can be linearised to give Eq. (5.7). Another popular relation, the Udell Leverett-J function $J(s) = p_{\text{cap}}/p_{\text{t}} = 1.417s - 2.21s^2 + 1.263s^3$, describes certain rock types. Linearising near $s = 0$ shows this corresponds to $\lambda = 1/1.417 = 0.706$.

[11]The steady incompressible Navier-Stokes equation $0 = \nu\nabla^2 u - \nabla p$ for a uni-axial flow velocity $u(r)$ in the x-direction as a function of the radial coordinate r becomes $0 = \frac{\mu}{r}\frac{\mathrm{d}}{\mathrm{d}r}\left(r\frac{\mathrm{d}u}{\mathrm{d}r}\right) - \frac{\mathrm{d}p}{\mathrm{d}x}$. With boundary condition $u(r) = 0$ this is solved by the parabolic profile $u(r) = 2\langle u\rangle\left(1 - (r/r)^2\right)$ with the average velocity $u_{\text{pore}} \equiv \frac{1}{\pi r^2}\int u(r)2\pi r\,\mathrm{d}r$ given by Eq. (5.9).

Therefore, *absolute permeability* or *single-phase permeability* of the porous medium reads ⟨

$$K \equiv \frac{\mu U}{\mathrm{d}p/\mathrm{d}x} = \frac{\lambda}{1 + \lambda} \frac{\epsilon}{8\tau^2} r_{\max}^2 \tag{5.10}$$

where we used Eq. (5.8) (with $s = 1$, for all pores filed with liquid) to replace r^2 with an average value. This will only give a rough numerical approximation,[12] but it does show the expected dependencies with pore size, porosity, and tortuosity.

The linear dependence of superficial velocity and pressure gradient, with a proportionality constant K/μ, is called *Darcy's law*.

5.3.4   Relative permeability

For a porous medium consisting of cylindrical channels, Eq. (3.13) gave $\tau^2 \approx \epsilon^{-1}$ so the permeability becomes proportional to ϵ^2. If a static gas phase is also present besides the flowing liquid phase, the available pore fraction for the liquid becomes ϵs. Furthermore, for $\lambda \gg 1$, another factor s is added to give ⟨

$$\boxed{-\frac{\mathrm{d}p_\mathrm{l}}{\mathrm{d}x} = \frac{\mu U_\mathrm{l}}{Kk},} \tag{5.11}$$

where *the relative permeability*

$$k = s^3. \tag{5.12}$$

The *total permeability Kk* is defined by Eq. (5.11).[13]

5.3.5   An equation for s

The water saturation s will be highest at the catalyst layer at $x = 0$, where water is produced, and lowest at the gas channel at $x = L$, where water is removed. Therefore, following Eq. (5.7), the capillary pressure will be highest near the catalyst layer. This pushes water towards the flow channel, in what is called *capillary action*. To reduce the exposure of the hydrophobic material to water, a flow is established to move the water out.

Taking the spatial derivative of Eq. (5.5), assuming $\mathrm{d}p_\mathrm{g}/\mathrm{d}x \ll \mathrm{d}p_\mathrm{l}/\mathrm{d}x$, and inserting Eqs. (5.7) and (5.11) gives the following differential equation for the water saturation ⟨

$$\boxed{\frac{\mathrm{d}s}{\mathrm{d}x} = -\frac{\lambda\mu}{p_\mathrm{t}K} \frac{U_\mathrm{l}}{s^3}.} \tag{5.13}$$

---

[12]For a porous medium consisting of spheres of diameter d_p, the often-used Cozeny-Karman relation $K = \frac{\mathrm{d}_\mathrm{p}^2 \epsilon^3}{180(1-\epsilon)^3}$ is obtained by inserting into Eq. (5.9) the hydraulic pore radius $r = \frac{\epsilon d_\mathrm{p}/2}{1-\epsilon}$ and $\tau = 180/32 \approx 5.6$.

[13]Several admittedly heuristic arguments have led to Eq. (5.12). Therefore, unsurprisingly, various other results can be found in the literature; for example, Eq. (5.12) but with the power 3 replaced with anywhere between 2 and 8 [17].

This shows how the liquid saturation s will decrease in the liquid flow direction. The decrease will be more rapid for larger flow velocities and higher liquid viscosity, particularly at low liquid saturations near $s = 0$. A larger permeability and threshold pressure decrease the variation in the saturation. As expected, the liquid saturation decreases in the x-direction, away from the catalyst layer.

Assuming that all the produced water leaves in liquid form through the diffusion layer, so neglecting water vapour and transport through the membrane, Faraday's law gives

$$U_l = \frac{j \mathcal{V}_m}{2F},$$
(5.14)

where, at ambient conditions, $\mathcal{V}_m \approx 1.8 \cdot 10^{-5}$ m^3/mol is the molar volume of liquid water and $n = 2$ electrons are consumed per water molecule produced, according to Eq. (5.2). Inserting into Eq. (5.13) gives

$$\frac{ds}{d(x/L)} = -\frac{j/J_c}{s^3}.$$
(5.15)

Here the characteristic capillary current density 🏃

$$J_c = \frac{p_t K}{\lambda \mu L} \frac{2F}{\mathcal{V}_m} \approx \frac{\gamma |\cos \vartheta|}{2\mu(1+\lambda)} \frac{\epsilon}{\tau^2} \frac{F}{\mathcal{V}_m} \frac{r_{max}}{L} \approx 3 \cdot 10^{10} \frac{r_{max}}{L} \text{ A/m}^2,$$
(5.16)

where in the second expression, we used Eqs. (5.6) and (5.10). In the final expression we used $\mathcal{V}_m = 1.8 \cdot 10^{-5}$ m^3/mol and $\mu = 4.7 \cdot 10^{-3}$ Pas for water at 60 °C and 1.2 bar, $\gamma |\cos \vartheta| = 0.05$ Pas, and $\frac{\epsilon}{(1+\lambda)\tau^2} \approx 0.1$. A typical diffusion layer pore size $r_{max} \approx 10$ µm and thickness $L \approx 300$ µm gives $L/r_{max} \approx 30$, so that along its width only a few dozen of the largest pore size fit into the diffusion layer. This makes $J_c \approx 10^9$ A/m^2 and at typical fuel cell current densities $j = (1-3) \cdot 10^4$ A/m^2 we see that $j \ll J_c$.

To determine a boundary condition for Eq. (5.15), we consider the water droplets illustrated in Fig. (5.8) on the surface of the diffusion layer. If these are sufficiently larger, their capillary pressure is small so that Eq. (5.7) gives at the channel-diffusion layer interface[14]

$$s(x = L) = 0.$$
(5.17)

5.3.6 A solution for s

Solving Eq (5.13) with boundary condition (5.17) gives 🏃

$$\boxed{s(x) = \left(\frac{4j}{J_c} \left(1 - \frac{x}{L} \right) \right)^{1/4}, \quad \text{for } j \ll J_c.}$$
(5.18)

---

[14]We assume the droplet radius $r_d \gg r_{max}$ so their Laplace pressure $p_{cap} = 2\gamma/r_d \ll p_t$ will be negligible. Neglecting any frictional or kinetic pressure drops between inside and outside, we can assume the same holds just inside the porous medium.
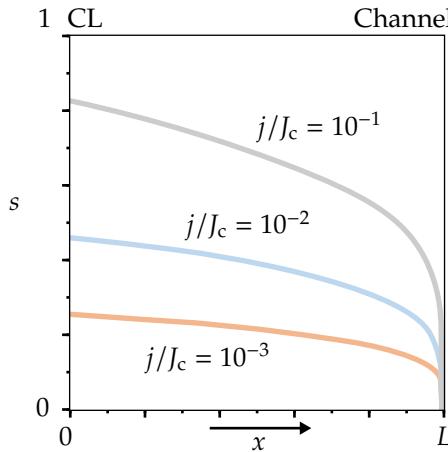
Figure 5.10: *The water saturation* $s(x) = \left(\frac{4j}{J_c} \left(1 - \frac{x}{L} \right) \right)^{1/4}$ *of Eq. (5.18) for various* j/J_c. *The boundary condition* $s(x = L) = 0$ *near the gas channel is associated with a large pressure drop due to the low permeability* $k = s^3$. *To maintain a low liquid saturation* $s < 0.25$ *everywhere requires* $j/J_c \lesssim 0.75$.

This solution is shown in Fig. 5.10 for various values of j/J_c. A large decrease in the water saturation can be seen close to the gas channel at $x = L$. The low water saturation leads to a lower permeability that induces a large frictional pressure drop. Therefore, the saturation strongly decreases towards the gas channel.

The main disadvantage of a high saturation is that oxygen transport will be hindered. Since the oxygen solubility and diffusivity are low in water, the sustainable diffusion flux of oxygen through water is orders of magnitude lower. In the next section, we will consider the effect of water on the diffusion of oxygen in the diffusion layer.

5.3.7 Effective oxygen diffusivity

Without water present, an oxygen diffusion flux $N = D(c_L - c_0)/L$ can be sustained for an oxygen concentration difference $c_L - c_0$ over the diffusion layer of thickness L. Here $D \approx \epsilon^{1+B} D_m$, as given by Eq. (3.14), is lower than the molecular diffusion coefficient D_m due to porosity ϵ and tortuosity τ. When the oxygen concentration vanishes in the catalyst layer, a limiting current density arises. Without any water present, it reads

$$j_{\text{lim}0} = \frac{4FDc_L}{L},\tag{5.19}$$

where Eq. (5.2) gives that $n = 4$ electrons are converted per oxygen molecule. With a typical oxygen concentration $c_L \approx 10 \text{ mol/m}^3$ in air at typical elevated temperature and pressure, $D \approx 10^{-5} \text{ m}^2/\text{s}$, and $L = 300 \text{ μm}$, this gives about 13 A/m^2, several

times higher than typical fuel cell current densities.

The increase in water saturation s further decreases the volume fraction $1 - s$ of the pores available for gas diffusion, and increases the tortuosity. We will model this with a modified diffusivity $D(1-s)^m$, similar to the Bruggeman correction of Eq. (3.14), with a power m depending on the geometry of the medium. This gives for the molar oxygen flux $N = D(1-s)^m \frac{dc}{dx}$. Integrating over the entire diffusion layer gives $j = 4FD_{\text{eff}} \frac{c_L - c_0}{L}$, where 🏃

$$\frac{D_{\text{eff}}}{D} = \frac{1}{L} \int_0^L (1-s)^{-m} \, dx. \tag{5.20}$$

Inserting Eq. (5.18) does not give simple expressions for D_{eff}. Instead, we provide the following approximation[15]

$$\frac{D_{\text{eff}}}{D} \approx \left(1 - (1.6j/J_c)^{1/4}\right)^{-m}. \tag{5.21}$$

We have $j_{\text{lim}} = \frac{D_{\text{eff}}}{D} j_{\text{lim}0}$ where D_{eff} by Eq. (5.21) depends on j_{lim}/J_c. Experiments show that m varies over a wide range between different materials. Taking $m = 4$ we can solve this to give 🏃

$$j_{\text{lim}} = \frac{j_{\text{lim}0}}{\left(1 + \left(\frac{1.6 j_{\text{lim}0}}{J_c}\right)^{1/4}\right)^4}. \tag{5.22}$$

This solution is plotted in Fig. 5.11.

As estimated at the beginning of this section, typical 'dry' limiting current densities $j_{\text{lim}0}$ are only several times higher the current densities normally used in fuel cells. Therefore, to avoid significant concentration overpotentials, the presence of water cannot lower the limiting current density by much.

To avoid the limiting current density dropping below, say, 50 % of its 'dry' value $j_{\text{lim}0} \sim 10^5$ A/m^2, according to Eq. (5.22) $J_c \gtrsim 10^3 j_{\text{lim}0} \sim 10^8$ A/m^2 is required. Equation (5.16) then gives $L/r_{\text{max}} \lesssim 300$. Therefore, avoiding a too-low limiting current density requires a diffusion layer that is less than a few hundred times its maximum pore radius. With typical values $r_{\text{max}} \sim 10$ μm and $L = 300$ μm, this is taken into consideration in the design of modern diffusion layers.

5.4 Flooded agglomerate model

5.4.1 Ohmic and diffusion limitations

Figure 5.13 shows an image of a catalyst particle in a PEM fuel cell cathode. It contains fine carbon particles to conduct electrons, ionomer to conduct ions, and plat-

---

[15]This is obtained by expanding Eq. (5.18) to first order in $(4j(1-x/L)/J_c)^{1/4}$ to write $(1-s)^{-m} \approx 1 + m(4j(1-x/L)/J_c)^{1/4}$ and integrating to give $\frac{D_{\text{eff}}}{D} \approx 1 + \frac{4m}{5}(4j/J_c)^{1/4}$. With $\frac{4}{5}4^{1/4} \approx 1.6^{1/4}$ this is the first-order approximation of Eq. (5.21).
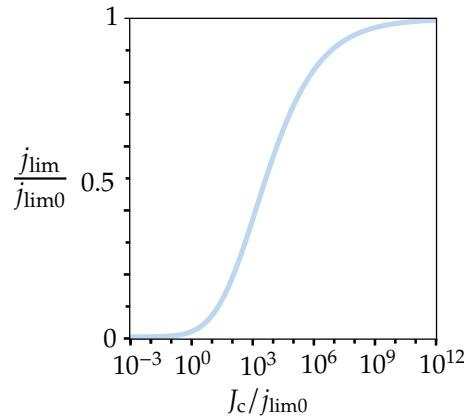
Figure 5.11: *The solution* $j_{\mathrm{lim}} = \dfrac{j_{\mathrm{lim}0}}{\left(1+\left(\frac{1.6 j_{\mathrm{lim}0}}{J_{\mathrm{c}}}\right)^4\right)^4}$ *of Eq. (5.22) plotted as a function of* $j_{\mathrm{lim}0}/J_{\mathrm{c}}$.
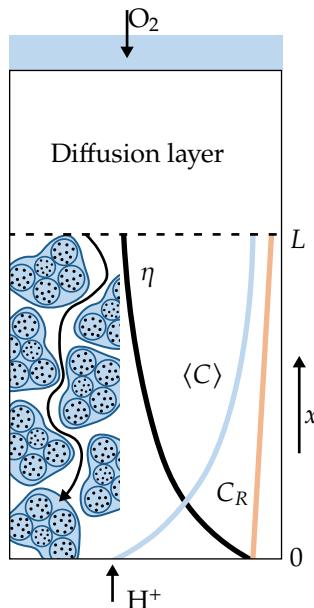

Figure 5.12: *A schematic of the cathode catalyst layer structure and profiles of the overpotential* η *and oxygen concentration C. Note: this is not to scale; the catalyst layer is typically much thinner than the diffusion layer. The flooded agglomerate model consists of agglomerates of several carbon-supported catalyst particles flooded by water from the reaction. The dissolved oxygen concentration at the agglomerate surface* C_R, *see Fig. 5.13, is in equilibrium with the approximately constant gas phase concentration. Near* $x = 0$, *the reaction is fastest because the overpotential* η *is highest.*
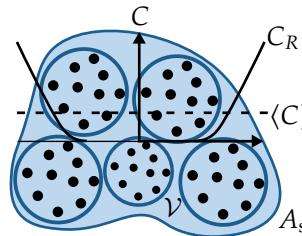
Figure 5.13: *A schematic illustration of an agglomerate of PEM fuel cell carbon-supported catalyst particles with volume $\mathcal{V}$ and surface area A_s. The black catalyst particles are surrounded by a carbon/ionomer/binder mixture. The dissolved oxygen concentration decreases from its value C_R at the particle surface towards the interior of the particle, due to the oxygen reduction reaction.*

inum nanometre-sized particles to increase the reactivity. These carbon-supported particles are typically a few to tens of nanometres in size, but they can agglomerate to agglomerates of a few or many particles in size extending to tens to hundreds of nanometres. The water produced in the reaction of Eq. (5.2) floods the pores of these carbon particles and often the inter-particle space within an agglomerate. The carbon particles will be flooded with the water produced in the reaction, hence the term *flooded agglomerate model*. As a consequence, for oxygen to reach the catalyst particles inside these agglomerates, it first has to dissolve and then diffuse inwards while reacting.

Both the concentration and the diffusivity of oxygen drop dramatically when dissolved in water. Therefore, the intra-agglomerate pores ideally remain dry to allow oxygen to diffuse towards the agglomerates in the gas phase. *Flooding* of the catalyst layer, when the inter-agglomerate space also fills with water, makes it impossible for the oxygen to reach much of the catalyst layer. On the other hand, flooding of the agglomerates themselves is hard to avoid and less of an issue because of their much smaller size. Due to the good hydration of the ionomer and their small size, ohmic limitations inside the agglomerates can be neglected. However, limitations of oxygen mass transfer may have to be considered inside the water-filled agglomerate.

On the other hand, ohmic limitations may arise over the catalyst layer's thickness. This leads to the profiles shown in Fig. 5.12 where we consider variation in the overpotential η and the average oxygen concentration $\langle C \rangle$ inside the agglomerates, but the concentration C_R at the surface is assumed to be constant throughout. The reason is that this surface is in equilibrium with the oxygen concentration in the gas phase, which will be constant throughout the catalyst layer.[16]

---

[16]By Henry's law, the oxygen concentration in the liquid phase at the interface with the gas is given by $C_R = H p_{O_2}$ with p_{O_2} the partial pressure of oxygen in the gas. Here H is Henry's constant.

5.4.2 Model equations

To describe the activation overpotential, we consider Tafel kinetics, first-order in the oxygen concentration. We start from the porous electrode equation Eq. (3.62), which we modify to:

$$e^{\eta/b} = \mathcal{E}_a \frac{\kappa}{a j_*} \eta''. \tag{5.23}$$

Here, $\mathcal{E}_a = \langle C \rangle / C_R$ is the agglomerate effectiveness factor. Similar to the approximation $\mathcal{E} = \frac{1}{1+M}$ introduced in section 3.4.4, in Appendix 5.A we show

$$\mathcal{E}_a \approx \frac{1}{\sqrt{1 + M_a^2}}, \tag{5.24}$$

in terms of the agglomerate Thiele modulus M_a. In Eq. (3.56) we obtained the porous-electrode expression $M^2 = \frac{J_*}{J_D} e^{\eta_0/b}$, where $J_D \equiv nFDc_0/L$. Analogously, we will use here

$$M_a^2 = \mathcal{M}^2 e^{\eta/b}, \text{where } \mathcal{M}^2 = \frac{j_*}{J_D}, \text{and } J_D \equiv nFDa_sC_0 \tag{5.25}$$

where the effective medium diffusivity D now refers to that inside the agglomerate particle instead of the porous electrode as a whole. Other differences with the porous electrode expressions that we obtained before are:

1. Instead of the overpotential η_0 at the 'entrance' of the electrode, at $x = 0$ near the membrane, we use the overpotential η at the 'entrance' of the agglomerate. Due to ohmic limitations, this overpotential can vary throughout the catalyst layer.

2. Instead of the total exchange current density $J_* = aLj_*$ of the entire electrode, the exchange current density j_* of a single agglomerate particle is used.[17]

3. Instead of the effective-medium electrode thickness L, we use as a length-scale $1/a_s$, where a_s is the volumetric surface area of a single agglomerate. This is shown to be a sensible replacement in Appendix 5.A.1. For a sphere of radius R this would replace L with $1/a_s = \frac{4}{3}\pi R^3 / 4\pi R^2 = R/3$.

Inserting Eqs. (5.24) and (5.25) into Eq. (5.23) gives

$$\eta'' \approx \frac{a j_*}{\kappa} \frac{e^{\eta/b}}{\sqrt{1 + \mathcal{M}^2 e^{\eta/b}}}. \tag{5.26}$$

---

[17]Here a is now the external area of the agglomerates per total unit volume of the catalyst layer. Considering an agglomerate to be porous, we may further write j_* in terms of the intrinsic exchange current density of a platinum particle times the ratio between the combined platinum surface area, divided by the agglomerate area.

5.4.3 Overpotential

Equation (5.26) can be solved approximately under the assumption $\mathcal{M}^2 e^{\eta_1/b} \ll 1$, so the agglomerate effectiveness factor $\mathcal{E}_a(x = L) \approx 1$. This will be the case at sufficiently strong ohmic limitations, such that the reaction rate at $x = L$ is negligible. We can use a similar solution method as in sections 3.4.3 and 4.4 to give:[18]

$$\eta_0 = b \ln\left(\frac{j^2}{2b\kappa a j_*}\left(1 + \frac{j^2}{8b\kappa a J_D}\right)\right) \approx \begin{cases} 2b \ln\left(\frac{j}{\sqrt{2b\kappa a j_*}}\right) & \left(\frac{j^2}{8b\kappa a J_D} \ll 1\right) \\ 4b \ln\left(\frac{j}{\sqrt{4b\kappa a \sqrt{j_* J_D}}}\right) & \left(\frac{j^2}{8b\kappa a J_D} \gg 1\right) \end{cases} \tag{5.27}$$

The agglomerate effectiveness factor at $x = 0$ reads

$$\mathcal{E}_{a0} = \frac{1}{\sqrt{1 + \mathcal{M}^2 e^{\eta_0/b}}} = \frac{1}{\sqrt{1 + \frac{j^2}{2b\kappa a J_D}\left(1 + \frac{j^2}{8b\kappa a J_D}\right)}}, \tag{5.28}$$

so that the top and bottom case correspond to $\mathcal{E}_{a0} \approx 1$ and $\mathcal{E}_{a0} \ll 1$, respectively.

In the top case, the agglomerates are used effectively ($\mathcal{E}_{a0} \approx 1$), and we obtain the same result as in section 3.4.3. In this case, ohmic limitations over the catalyst layer thickness lead to a doubling in the Tafel slope to $2b$ and an apparent exchange current density $\sqrt{2b\kappa a j_*}$.

In the bottom case, besides these ohmic limitations, additional internal diffusion limitations lead to a further doubling or quadrupling in the Tafel slope to $4b$. [21] The apparent exchange current density is replaced by a geometric average of a resistive current density $4b\kappa a$ and a geometrical average of a diffusive current density $J_D = \frac{a_s^2}{a} n F D C_R$ and j_*. Because of the very weak dependence on j_* catalyst improvements, they only very weakly improve performance in this undesirable regime. The predicted doubling and quadrupling of the Tafel slope is compared to experimental data in Figure 5.14.

The quadrupled Tafel slope regime is obviously not a desirable operational regime for a fuel cell. To avoid this, under all operating conditions, the Thiele moduli must remain small.

5.4.4 Example calculation

Using the following typical values for a PEM fuel cell [14]: a diffusivity $D = 5 \cdot 10^{-9}$ m^2/s and solubility $C_R = 7.6$ mol/m^3 of oxygen in water at elevated pressure, $b = 0.05$

---

[18]The chain rule gives $\frac{d}{dx} = \frac{d\eta}{dx}\frac{d}{d\eta}$ so that $\eta'' = \eta'\frac{d\eta'}{d\eta} = \frac{1}{2}\frac{d\eta'^2}{d\eta}$. The integral $\int \frac{e^{\eta/b}\,d\eta}{\sqrt{1+\mathcal{M}^2 e^{\eta/b}}} = \frac{2b\sqrt{1+\mathcal{M}^2 e^{\eta/b}}}{\mathcal{M}^2}$ so integrating from η_0 to η_1, assuming $\mathcal{M}^2 e^{\eta_1/b} \ll 1$, gives $\eta_0'^2 \approx \frac{4a j_* b}{\kappa}\frac{\sqrt{1+\mathcal{M}^2 e^{\eta_0/b}}-1}{\mathcal{M}^2}$. The boundary condition (3.B.101) gives $|\eta_0'| = jL/\kappa$, resulting in Eq. (5.27).
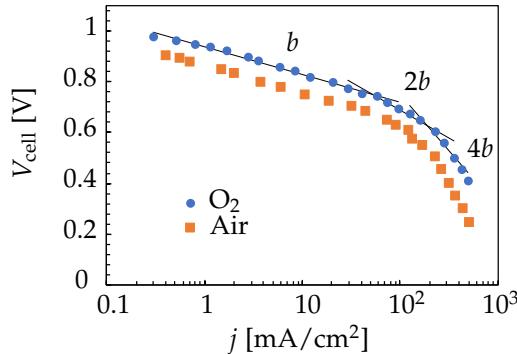
Figure 5.14: *Experimental data for a phosphoric acid fuel cell [18] with a catalyst loading of 0.63 mg Pt cm^{-2} and catalyst layer thickness of 200 μm on Vulcan XC-72R containing 50 wt% PTFE and in 105 wt% H$_3$PO$_4$. The potential as a function of current density seems to show a doubling and then a quadrupling in Tafel slope per decade, from 110 mV, to 220 mV, to 440 mV [21].*

V, $n = 4$, and $aj_* = 4 \cdot 10^4$ A/m^3, we find for an agglomerate radius of $R = 10^{-7}$ m that $\mathcal{M}^2 = \frac{aj_* R^2}{9nFDC_R} \sim 3 \cdot 10^{-10}$. To reach a Thiele modulus squared $M_a^2 = \mathcal{M}^2 e^{\eta/b}$ of the order unity requires in this case $\eta \approx 22b \approx 1$ V. Such high overpotentials will never be used, since there will be no useful potential left in this case. Therefore, modern catalyst layers in which agglomerates are of the order of 100 nm in radius or smaller should be free of diffusion limitations and should not show the Tafel slope quadrupling of Figure 5.14.

5.5   Summary

- The capillary pressure inside a porous medium is given by the Young-Laplace equation as $p_{cap} = p_l - p_g = \frac{2\gamma|\cos\vartheta|}{r} = \frac{2\gamma|\cos\vartheta|}{r_{max}}\left(1 + \frac{1-s}{\lambda}\right)$ (5.5). The second equation linearises its dependence on saturation $s \approx 1$. Combined with Darcy's equation $-\frac{dp_l}{dx} = \frac{\mu U_l}{Kk}$ (5.11) and a relative permeability $k = s^3$ this gives $\frac{ds}{dx} = -\frac{\lambda\mu}{p_t K}\frac{U_l}{s^3} = -\frac{j/j_c}{Ls^3}$ (5.13), which describes how s decreases away from the catalyst layer.

- If the increase in s decreases the local effective gas diffusivity from D to $D(1-s)^4$, the limiting current density is decreased from j_{lim0} to $\dfrac{j_{lim0}}{\left(1+\left(\frac{1.6j_{lim0}}{j_c}\right)^{1/4}\right)^4}$ (5.22).

- Assuming ohmic limitations over the thickness of the catalyst layer, where the gas phase ensures high reactant diffusivity, and potential diffusion lim-

itations inside the flooded agglomerates, which are small enough to avoid ohmic limitations, we obtained an analytical expression for the overpotential $\eta_0 = b\ln\left(\frac{j^2}{2b\kappa a j_*}\left(1 + \frac{j^2}{8b\kappa a J_D}\right)\right)$ (5.27). The Tafel slope doubled by the ohmic limitations gets doubled again in case of diffusion limitations inside the agglomerates.

Exercise 5.1

A limiting current arises in the cathode of a PEM fuel cell when the oxygen concentration reaches zero at the catalyst layer. Assume that the only significant transport resistance is in the diffusion layer of thickness L, where oxygen has to diffuse through air and water vapour with an effective diffusivity, D.

a. Give an expression for the limiting current associated with this diffusion layer in terms of the oxygen concentration c_L at the gas channel.

b. Give a numerical value for this current density when $D = 10^{-5}\,\text{m}^2/\text{s}$, $L = 0.3$ mm, and the oxygen concentration is that in air at ambient pressure, or $c_L = 10$ mM. (N.B. Regularly much lower limiting currents of the order of 1 A/cm^2 are found. This may be due to an unaccounted-for transfer resistance, like that associated with the dissolution of oxygen.)

c. In case of two resistances in series, with mass transfer coefficients k_1 and k_2 give an expression for the overall mass transfer coefficient (remember that the mass transfer coefficient is the flux divided by the driving concentration difference).

d. Assume that these mass transfer resistances combine to a single transfer coefficient given by $k = \frac{N}{c_L - c_0}$ with c_L the local concentration of oxygen at the catalyst layer-diffusion layer interface and c_0 the concentration at the catalyst surface where the reaction takes place. Give an expression for the limiting current, including this resistance and that of the diffusion layer.

Exercise 5.2

Equation (5.13) was derived neglecting the friction of the gas phase.

a. Modify Eq. (5.13) to include the effect of the gas pressure gradient.

b. The liquid pressure gradient will dominate for a very low liquid saturation $s \approx 0$, while the gas fraction will be largest for very low values of s. For what saturation s_* will the gas and liquid pressure gradients be equal? Give a formula and fill in the properties of water and air at 60 °C and 1.2 bar to give a numerical value.

Exercise 5.3

Consider a PEM fuel cell cathode catalyst layer with spherical platinum particles with a radius R at a volume fraction φ.

a. Give a formula the volumetric surface area of the catalyst.

b. If the intrinsic exchange current density of a platinum surface for the oxygen reduction reaction is known to be $j_* = 10^{-1}$ A/m^2, the nanoparticles have a radius of $R = 2.5$ nm and are used at a volume fraction of $\varphi = 10^{-3}$ give the effective exchange current density aj_* per unit of total catalyst layer volume.

c. If the catalyst layer has a thickness $L = 5$ μm and is used effectively, given a Tafel slope $b = 50$ mV, what are the expected cathodic activation losses at 1 A/cm^2?

d. What overpotential can be saved when the catalyst layer thickness is increased tenfold and remains fully effective? Give your answer in the form of a formula.

e. If the effective ionic conductivity is 1 S/m, what will be the approximate effectiveness factor when increasing the electrode thickness by a factor of 10?

Exercises 5.4-5.12

Fill in the missing steps in the main text, indicated by the symbol 𝕁.

*Appendices ***

5.A   *Generalised Thiele modulus*

5.A.1   *General particle shape*

The Thiele modulus squared $M^2 = \frac{L^2 k}{D}$ is expressed as the ratio of the *volumetric* reaction rate kC and a characteristic diffusion rate DC/L^2. And we found the effectiveness factor $\mathcal{E} = \frac{\tanh M}{M}$ for a planar configuration. In this section, we will generalise this result to apply approximately to any shape. Consider a general volume, V, as shown in Figure 5.13, which has a concentration C_R at the boundary of the volume.
The diffusion-reaction conservation equation inside the particle reads

$$0 = D\nabla^2 C - \hbar C. \tag{5.A.29}$$

The effectiveness factor is defined as the ratio of the average and maximum reaction rates:

$$\mathcal{E} \equiv \frac{\frac{1}{V}\int \hbar C \, d\mathcal{V}}{\hbar C_0} = \frac{D\int \nabla^2 C \, d\mathcal{V}}{\hbar C_0 \, \mathcal{V}} = \frac{D\int \nabla C \cdot dA}{\hbar C_0 \mathcal{V}} \approx \frac{D a_s}{\hbar} \left. \frac{|\nabla C|}{C}\right|_{\text{surface}}. \tag{5.A.30}$$

In the second equation, we inserted Eq. (5.A.29); in the third, we applied the divergence theorem, and in the final approximation, we assumed that ∇c is constant over the surface of the particle and aligned with the outwards directed dA. This allowed us to replace and introduce the volumetric surface area $a_s = A/V$.
Comparing Eq. (5.A.30) with the expression $\mathcal{E} = -\frac{L\,c'/c|_0}{M^2}$ for the 1D pore case, we see that we can maintain the definition $M^2 = \frac{L^2 \hbar}{D}$ if we replace L by $1/a_s$. For a pore of radius R and length L of which only the sides react, we have $a_s = \frac{\pi R^2}{\pi R^2 L} = 1/L$ as before.
With this replacement, we obtain the generalised Thiele modulus

$$M^2 = \frac{k}{a_s D}, \tag{5.A.31}$$
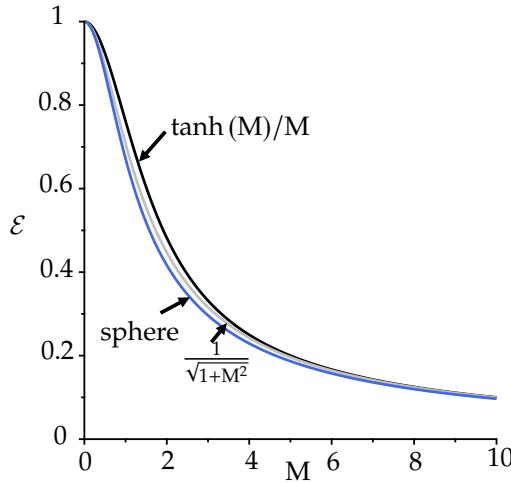
Figure 5.15: *The effectiveness factor $\mathcal{E} = \frac{\tanh(M)}{M}$ for a planar configuration (dark blue), $\frac{1}{M}\left(\frac{1}{\tanh(3M)} - \frac{1}{3M}\right)$ for a sphere and an approximation $\frac{1}{\sqrt{1+M^2}}$ showing only very small differences using the generalised Thiele modulus of Eq. (5.A.31).*

where we also inserted the reaction coefficient $k = \hbar/a_{\mathrm{s}}$ per unit external surface area.

For a spherical particle with radius R we have $a_{\mathrm{s}} = \frac{4\pi R^2}{\frac{4}{3}\pi R^3} = \frac{3}{R}$ so that with $L = R/3$ we have $M^2 = \frac{R^2 \hbar}{9D} = \frac{Rk}{3D}$.

5.A.2 *Effectiveness factor approximation*

Besides the planar case we considered previously, the reaction-diffusion equation can also be solved exactly in, for example, a sphere. The result is for this is shown in Figure 5.15. It can be seen that the curves are very similar. This allows us to use the planar result $\mathcal{E} = \frac{\tanh(M)}{M}$ with a reasonable degree of accuracy, also for the case of a sphere using the generalised Thiele modulus of Eq. (5.A.31).

Figure 5.15 also shows the approximation

$$\mathcal{E} \approx \frac{1}{\sqrt{1 + M^2}}. \tag{5.A.32}$$

This result also tends to the correct limits $\mathcal{E} \approx 1$ when $M \ll 1$ and $1/M$ when $M \gg 1$. It can be seen that this approximation is also quite close to both the spherical and planar results. Usually, this approximation is sufficiently accurate, especially since the exact particle shape is often not well known.

5.A.3 *Dimensionless flooded agglomerate model*

Eq. (5.23) in the dimensionless notation of Appendix 3.B reads

$$e^{\bar{\eta}} = \mathcal{E}_a \frac{\bar{j}_*}{\bar{j}_\kappa} \bar{\eta}'', \tag{5.A.33}$$

and Eq. (5.26) becomes

$$\bar{\eta}'' \approx \frac{\bar{j}_\kappa}{\bar{j}_*} \frac{e^{\bar{\eta}}}{\sqrt{1 + \mathcal{M}^2 e^{\bar{\eta}}}}. \tag{5.A.34}$$

The chain rule gives $\frac{\mathrm{d}}{\mathrm{d}\bar{x}} = \frac{\mathrm{d}\bar{\eta}}{\mathrm{d}\bar{x}} \frac{\mathrm{d}}{\mathrm{d}\bar{\eta}}$ so that $\bar{\eta}'' = \bar{\eta}' \frac{\mathrm{d}\bar{\eta}'}{\mathrm{d}\bar{\eta}} = \frac{1}{2} \frac{\mathrm{d}\bar{\eta}'^2}{\mathrm{d}\bar{\eta}}$. The integral $\int \frac{e^{\bar{\eta}} d\bar{\eta}}{\sqrt{1+\mathcal{M}^2 e^{\bar{\eta}}}} = \frac{2\sqrt{1+\mathcal{M}^2 e^{\bar{\eta}}}}{\mathcal{M}^2}$ so that integrating from $\bar{\eta}_0$ to $\bar{\eta}_1$ assuming $\mathcal{M}^2 e^{\bar{\eta}_1} \ll 1$ gives

$$\bar{\eta}_0'^2 \approx \frac{4\bar{j}_\kappa}{\bar{j}_*} \frac{\sqrt{1 + \mathcal{M}^2 e^{\bar{\eta}_0}} - 1}{\mathcal{M}^2}. \tag{5.A.35}$$

The boundary condition (3.B.101) gives $\bar{\eta}_0'^2 = \bar{j}_\kappa^2$ resulting in

$$\bar{\eta}_0 = \ln\left(\frac{\bar{j}_\kappa \bar{j}_*}{2}\left(1 + \frac{\bar{j}_\kappa \bar{j}_* \mathcal{M}^2}{8}\right)\right) \approx \begin{cases} \ln\left(\frac{\bar{j}_\kappa \bar{j}_*}{2}\right) & \left(\frac{\bar{j}_\kappa \bar{j}_* \mathcal{M}^2}{8} \ll 1\right), \\ 2\ln\left(\frac{\bar{j}_\kappa \bar{j}_* \mathcal{M}}{4}\right) & \left(\frac{\bar{j}_\kappa \bar{j}_* \mathcal{M}^2}{8} \gg 1\right). \end{cases} \tag{5.A.36}$$

Inserting dimensional quantities again gives Eq. (5.27).

Chapter 6

Electrolysers

In this chapter, we consider the modelling of electrolysers and, in particular, the effect that gas evolution has on the vertical current distribution and the electrolyte flow. We start with the rise of a single bubble, its relation to the gas fraction, and the impact of the gas fraction on conductivity. Next, we develop a model for the vertical gas distribution and its impact on the current density. Finally, we consider how gas bubbles can be used to drive a circulating electrolyte flow, which is useful for transporting heat and bubbles out of the cell.

6.1   Introduction

Throughout the twentieth century various alkaline water electrolysers have been used to generate hydrogen, in particular near hydropower plants. While steam methane reforming has taken over most hydrogen production, a clear comeback of water electrolysis seems imminent.[1]

The term electrolyser generally refers to an electrolytic cell in which current is used to drive a reaction. In this chapter, we will primarily focus on electrolysers that produce, or *evolve*, gases.[2] We will focus here on alkaline water electrolysers, for the production of hydrogen. However, the phenomena we will model also apply to various other types of gas-evolving electrochemical cells and devices. Figure 6.1 shows two types of electrolyser designs: the traditional one on the right is more and more replaced by a *zero-gap* configuration in which there is no space between

---

[1]Other processes are most cost-effective, or even only possible, using electrolysis. An example is the *chlor-alkali process*. Here, NaCl is converted in an electrochemical cell into chlorine gas, hydrogen, and NaOH. Sodium chlorate, potassium chlorate, and several other organic compounds are also produced through electrolysis. The electrolytic production of metals, or *electrometallurgy*, is perhaps most well-known for making aluminium from alumina Al_2O_3 in the *Hall-Héroult process*.

[2]In many industrially relevant electrolysers, gases are evolved, which can have deleterious effects on the process. In the production of aluminium, for example, in the *anode effect*, a bubble cloud covers the anode. This increases the ohmic losses due to their insulating nature and increases the activation losses by partially covering the electrode area.
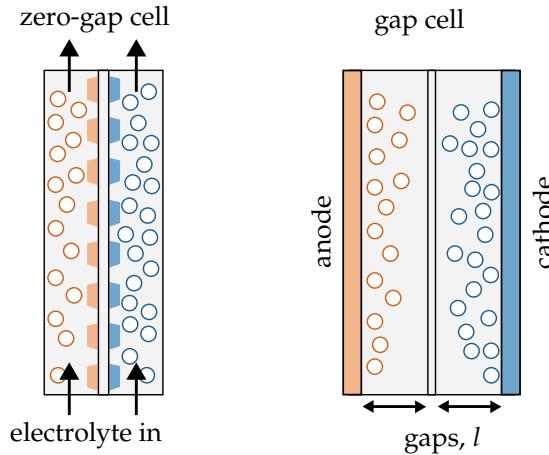
Figure 6.1: *The left-hand figure shows an electrolyser in a zero-gap configuration where perforated electrodes are positioned directly adjacent to the diaphragm to reduce ohmic losses. The right-hand figure shows the traditional configuration with gaps between planar electrodes and the diaphragm.*

the electrodes and the diaphragm to reduce ohmic overpotentials, as shown on the left-hand side of Fig. 6.1.

Often, a pump is used to drive a liquid flow through the cell. This is beneficial, first and foremost, in transporting away the heat generated in the reaction. Sometimes, the natural lift induced by the bubbles generates this liquid flow.[3] In section 6.5, we will consider how to model this. However, first, we will consider how to predict the average gas fraction in electrolysers, not through the use of computational fluid dynamics as in Figure 6.2, but through simplified one-dimensional analytical modelling.

6.2 A current distribution model

So far, we have only considered one-dimensional models with a spatial coordinate in the direction of the current. Here, we will consider variation in the direction normal to the current, to model the gas fraction as a function of height. In the next chapter on flow batteries, we will develop a quasi-two-dimensional model that allows for the description of variations in the direction parallel to the current *and* the flow.

---

[3]This is, for example, typically the case in chlor-alkali electrolysers where liquid flow is essential to improve mass transport. Also, a few alkaline water electrolysers that operate at near-atmospheric pressure make use of this principle.
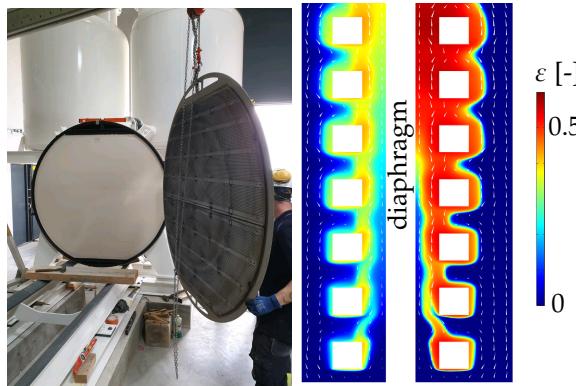
Figure 6.2: *A Nickel-plated perforated plate electrode of roughly 2 m² being lifted into a NEL alkaline water electrolyser stack (left, used with permission from Lhyfe). A 2-3 mm gap separates the diaphragm from the electrodes. There is a larger space behind the electrodes. About 230 cells are stacked in series to make up a roughly 10-metre-long electrolyser. A pump is used to flow liquid through the cell with a small velocity of $W_l \approx 0.3$ mm/s. This design is made for a relatively low current density of 750-2000 A/m². On the right is a 2D mixture-model simulation of the gas fraction at $j = 10^4$ A/cm² in the first few millimetres. The electrode, diaphragm, and gap thickness are all 0.5 mm. We used the COMSOL Multiphysics® software to perform the modelling [8]. Simulations by W.L. v.d. Does.*

6.2.1   Cell model

We write the cell model of Eq. (1.36), similar to Eq. (4.7) as

$$V_{\text{cell}} \approx V_{\text{eq}} - \left(\eta + \frac{jl}{\kappa} + \frac{jl_{\text{eff}}}{\kappa_{\text{m}}} \right), \tag{6.1}$$

where η is the sum of the combined anode and cathode activation overpotentials.[4] Here, l and κ are the thickness and effective conductivity of the bubble-filled gap under consideration. The final term in Eq. (6.1) gives additional ohmic losses, for example in the diaphragm or a gas-free electrolyte layer, in terms of an equivalent thickness l_{eff} of a layer with conductivity κ_{m}.[5]

We recall that electrolytic cells have $V_{\text{cell}} < 0$, so the various voltage losses increase the cell potential magnitude. This is different from the galvanic batteries and fuel cells considered in the previous sections.

We will use term jl/κ in Eq. (1.35) to describe the electrolyte ohmic drop over the 'gaps' between the electrode and diaphragm, or the space behind the electrodes in

---

[4]For planar electrodes $\eta = \eta_{\text{a}} - \eta_{\text{c}}$, where $\eta_{\text{a}} > 0$ and $\eta_{\text{c}} < 0$. Ohmic losses in cables or connections that only depend on the total current may also be added here.

[5]For example, using Eq. (3.12), a diaphragm with thickness l_{d}, porosity ϵ, and tortuosity τ gives an ohmic drop $jl_{\text{eff}}/\kappa_{\text{m}} = jl_{\text{d}}\tau^2/\epsilon\kappa_{\text{m}}$ so $l_{\text{eff}} = l_{\text{d}}\tau^2/\epsilon$.
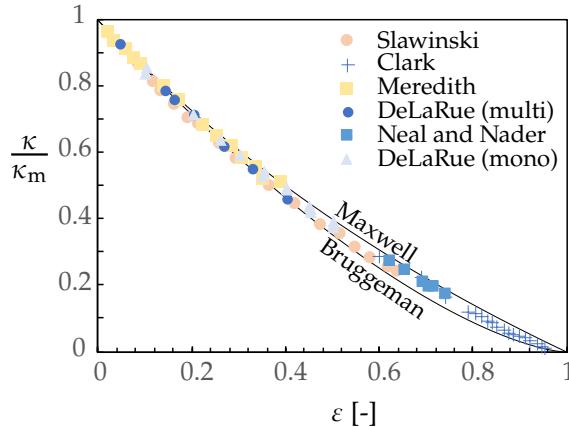
Figure 6.3: *Experimental data from various sources on the relative effective conductivity κ/κ_m of spherical packings of insulating spheres, emulsions (Meredith), and foams (Clark) [24]. A comparison is shown with the relations, Eq. (6.2), of Maxwell $\left(\frac{1-\varepsilon}{1+\varepsilon/2}\right)$ and Bruggeman $\left((1-\varepsilon)^{1+\mathcal{B}}\right)$ for $\mathcal{B} = 1/2$.*

a zero-gap configuration. See Fig. 6.2. The rest of the ohmic drop, including that in the diaphragm, is included in the final term jl_{eff}/κ_m.

The space we consider will horizontally be filled homogeneously with bubbles at a volumetric gas fraction ε. Similar to the solid material in a porous electrode, the presence of gas will reduce the effective conductivity from its molecular value κ_m. Analogous to Eq. (3.25), we write[6]

$$\frac{\kappa}{\kappa_m} = \begin{cases} (1-\varepsilon)^{1+\mathcal{B}} & \text{Bruggeman,} \\ \frac{1-\varepsilon}{1+\varepsilon/2}. & \text{Maxwell} \end{cases} \tag{6.2}$$

We have previously considered Bruggeman's relation to describe polydisperse spherical particles using $\mathcal{B} = 1/2$. The second expression[7] is often used to model the thermal conductivity of porous media. As shown in Fig. 6.3, both expressions give similar results[8] and compare reasonably well with experiments.

---

[6]Mind you that in a porous electrode, the porosity ϵ denotes the volume fraction available for the electrolyte, while in the presence of a gas fraction ε this is $1 - \varepsilon$.

[7]It is named after James Clerk Maxwell and derived for a dilute random distribution of spherical particles. It has analogues for the refractive index: the Lorentz-Lorenz equation named after Hendrik Antoon Lorentz and Ludvig Lorenz; and permittivity: the Clausius-Mossotti relation and the mixing formula derived by Maxwell Garnett, whose father named him after his friend J.C. Maxwell.

[8]At low gas fractions, their predictions overlap for $\mathcal{B} = 1/2$, as they have the same first-order Taylor expansion $1 - 3\varepsilon/2$. At high gas fractions nearing 1, both results tend to 0.

6.2.2   The bubble rise velocity

Bubbles coming from electrodes tend to be small, typically of the order of 0.1 mm.[9] Due to surface tension, such small bubbles are approximately spherical. Buoyancy will cause an upwards *slip* velocity w_s, defined as the difference between the gas bubble velocity w_g and the liquid velocity

$$w_s \equiv w_g - w_l. \tag{6.3}$$

We will use a w to denote velocity components in the vertical z-direction, in keeping with the fluid dynamics notation to write the velocity vector $\boldsymbol{u} = u\hat{\boldsymbol{x}} + v\hat{\boldsymbol{y}} + w\hat{\boldsymbol{z}}$. Superficial velocities will be denoted by capitals as before, so the vertical superficial gas velocity $W_g = w_g \varepsilon$ and the liquid superficial velocity $W_l = (1 - \varepsilon)w_l$.

For small enough bubbles, the Reynolds number $\text{Re} \equiv \frac{\rho w_s (2R)}{\mu} \lesssim 1$, and we can use the Stokes drag force expression of Eq. (2.C.71):[10]

$$F_D = 6\pi\mu R w_s, \tag{6.4}$$

for the drag force magnitude, with μ the dynamic viscosity of the liquid. The buoyancy force $\frac{4\pi R^3}{3}\rho g$ is proportional to the liquid density ρ. Neglecting the gravitational force on the bubbles, equating these forces, we find for the *Stokes rise velocity* 🏃

$$w_S = \frac{2gR^2}{9\nu}, \tag{6.5}$$

where $\nu = \mu/\rho$ is the liquid kinematic viscosity.

Inserting, for example, $2R = 0.1$ mm,[11] $\nu = 10^{-6}$ m²/s, and $g = 9.8$ m/s² gives a slip velocity of $w_S \approx 5$ mm/s. This corresponds to a Reynolds number of 0.5, for which the Stokes drag force expression of Eq. (6.4) can still be used to a reasonable approximation.

6.3   One-dimensional model

The general conservation equation (2.1) for the volume of gas becomes in steady-state $\nabla \cdot \boldsymbol{U}_g$ or in two dimensions

$$\frac{\partial U_g}{\partial x} + \frac{\partial W_g}{\partial z} = 0, \tag{6.6}$$

---

[9]This depends on the type of electrolyte, electrode, potential, etc. and is, of course, a distribution rather than a single size.

[10]This approximates bubbles as rigid particles, neglecting potential internal fluid circulation. In the presence of surfactants, this is usually a good approximation.

[11]A very rough idea of the bubble release diameter on a horizontal electrode can be obtained from a force balance between the attractive surface tension force and the buoyancy force away from the electrode, see Eq. (6.A.29). However, because this is usually a too strong oversimplification, we only include this analysis for the interested reader in appendix 6.A.
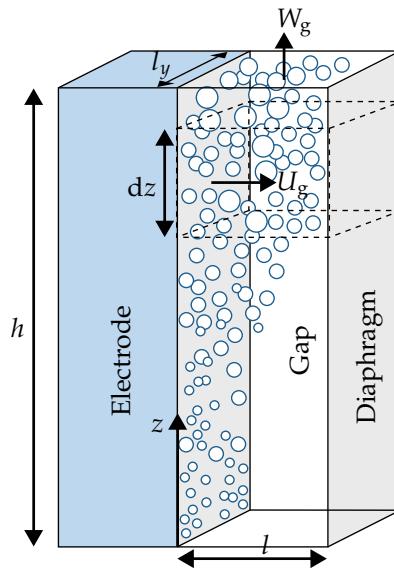
Figure 6.4: *The configuration, dimensions, and velocities used in the analysis of the present section. The gas fraction is averaged over the horizontal direction. The dashed box gives the control volume used in Eq. (6.8).*

where the volumetric gas flux, or superficial gas velocity components in the horizontal x and vertical z-directions, read $U_g = \varepsilon u_g$ and $W_g = \varepsilon w_g$.

As illustrated in Fig. 6.4, for a small enough distance between the electrode and the diaphragm and above a certain height, the gas fraction variation in the horizontal direction may become negligible compared to that in the vertical direction. Here, we will develop a one-dimensional model that can describe the gas fraction as a function of height.

We integrate Eq. (6.6) over the dashed box in Fig. 6.4 from $x = 0$ at the electrode to $x = l$ at the diaphragm and divide by l to give the x-averaged equation[12] 🏃

$$\frac{dW_g}{dz} = \frac{j\mathcal{V}_m}{nFl}. \tag{6.7}$$

Here, we re-use the symbol $W_g(z) = \frac{1}{l}\int_0^{-l} W_g(x,z)dx$ for the x-averaged superficial vertical gas velocity, which hopefully does not lead to confusion. The right-hand side gives the volumetric gas flow rate, U_g, at which the gas enters the domain, divided by l. Here $\mathcal{V}_m$ is the molar volume of the gas. For an ideal gas $\mathcal{V}_m = \mathcal{R}T/p$ is equal to 30 l/mol at 85 °C and 1 bar.

---

[12]In case an additional space of thickness l_b exists behind the electrode, for example in case of a zero-gap or almost zero-gap configuration, we may replace here l with $l + l_b$. In case the bubbles distribute homogeneously horizontally, the analysis will remain the same otherwise.

Assuming $w_s \equiv w_g - w_l = \frac{w_S}{1-\varepsilon}$,[13] we have

$$W_g = \left(W_g + W_l + w_S\right) \varepsilon, \tag{6.8}$$

where $W_l = w_l \left(1 - \varepsilon\right)$ is the volumetric liquid flux or superficial liquid velocity, so

$$\varepsilon = \frac{W_g}{w_S + W_l + W_g/\varepsilon_{max}}. \tag{6.9}$$

Here $\varepsilon_{max} = 1$, but we will allow different values to be able to describe a maximum gas fraction as $W_g \to \infty$.[14]

Equation (6.9) can be solved for W_g to give

$$W_g = \frac{\varepsilon}{1 - \varepsilon/\varepsilon_{max}} \left(W_l + w_S\right) \tag{6.10}$$

Taking the derivative with respect to z, neglecting the dependence[15] of w_S on z gives, with Eq. (6.7):

$$\frac{\mathrm{d}}{\mathrm{d}z} \left(\frac{\varepsilon}{1 - \varepsilon/\varepsilon_{max}}\right) = \frac{\mathrm{d}W_g/\mathrm{d}z}{W_l + w_S}. \tag{6.11}$$

If we know the current distribution j as a function of height or gas fraction, we can solve this equation for the gas fraction. This will be the goal of the next section.

6.4   Vertical gas fraction and current distributions

6.4.1   Constant current density

we take $z = 0$ to be at the bottom of the electrode, and we assume that no gas exists below the electrode. If the current density is constant and we use $W_g(z = 0) = 0$, Eq. (6.7) gives $W_g = \frac{\mathrm{d}W_g}{\mathrm{d}z} z$ with $\frac{\mathrm{d}W_g}{\mathrm{d}z}$ given by Eq. (6.7). Inserting this into Eq. (6.9) gives

$$\frac{\varepsilon}{\varepsilon_{max}} = \frac{z}{z_c + z}, \tag{6.12}$$

where, with $j_0 \equiv j(z = 0)$:

$$z_c = \varepsilon_{max} \frac{w_S + W_l}{\mathrm{d}W_g/\mathrm{d}z\big|_{z=0}} = \varepsilon_{max} l \frac{w_S + W_l}{j_0 \mathcal{V}_m/nF}. \tag{6.13}$$

---

[13]The lower effective mixture density and 'hindrance' between bubbles reduce the single-bubble rise velocity at higher gas fractions. However, measurements with rising bubbles show that with increasing gas fraction, they mostly speed up due to clustering effects. We model this very crudely by dividing the Stokes rise velocity by $1 - \varepsilon$.

[14]The experiments reported in Ref. [7] are described well with $w_S = 0$ and $\varepsilon_{max} = 0.7$, close to the maximum packing fraction of spheres.

[15]By conservation of liquid volume, the superficial liquid velocity W_l does not depend on z.
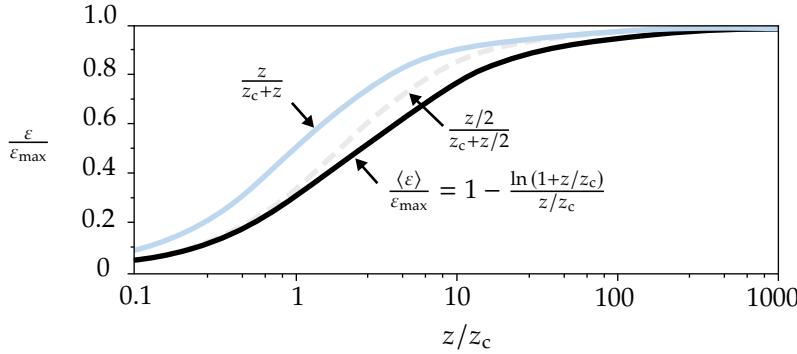
Figure 6.5: *The gas fraction* $\frac{\varepsilon}{\varepsilon_{\max}} = \frac{z}{z_c + z}$ *as a function of the dimensionless height* z/z_c *as given by Eq. (6.12) (solid blue line) and its running average* $\langle \varepsilon \rangle = \frac{1}{z} \int \varepsilon \mathrm{d}z$ *(solid black line) and its approximation as given by Eq. (6.14).*

To derive Eq. (6.12) we considered a constant current density. However, anticipating a variable current density in the next section, we defined z_c in this more general way.

For $z \ll z_c$, Eq. (6.12) gives $\frac{\varepsilon}{\varepsilon_{\max}} \approx \frac{z}{z_c}$, from which we see that z_c is a characteristic length-scale associated with the initial increase of the gas fraction with height. In the case of a constant current density, Eq. (6.12) shows that z_c gives the height at which the gas fraction has increased to half its maximum value. A higher current density or lower gap width l increases the volumetric gas flux and thus decreases z_c. The higher the superficial liquid velocity W_l or the bubble slip velocity w_s, the more gas can be transported away, the lower the gas fraction, and the larger z_c will be. When z/z_c is no longer small, the gas fraction will increase sub-linearly and will asymptotically approach its maximum value, see Fig. 6.5.

We are also interested in the average gas fraction $\langle \varepsilon \rangle = \frac{1}{h} \int_0^h \varepsilon \mathrm{d}z$, which gives 🏃

$$\frac{\langle \varepsilon \rangle}{\varepsilon_{\max}} = 1 - \frac{\ln(1 + h/z_c)}{h/z_c} \approx \frac{h/2z_c}{1 + h/2z_c}. \tag{6.14}$$

In Fig. 6.5, the approximation on the right-hand side is compared with the exact result, showing that this is a reasonably good approximation.[16]

6.4.2 Variable current density

In the traditional cell configuration, on the right of Figure 6.1, and to a much lesser extent also in the zero-gap configuration on the left, bubbles increase the ohmic drop

---

[16]For $h/z_c \ll 1$, Eq. (6.12) gives $\frac{\varepsilon}{\varepsilon_{\max}} = \frac{z}{z_c}$. Taking the first order approximation gives $\langle \varepsilon \rangle = \frac{1}{h} \int_0^h \frac{z}{z_c} dz = h/2z_c$, which is equal to the first order approximation of Eq. (6.14). At higher gas fractions, diving by a higher value than 2, e.g. $\frac{h/3z_c}{1+h/3z_c}$ would give a lower error, but the error would be unacceptably large at lower gas fractions. The relative error compared to the approximation in Eq. (6.14) with the exact result over the entire range of gas fractions is acceptable at less than 12%.
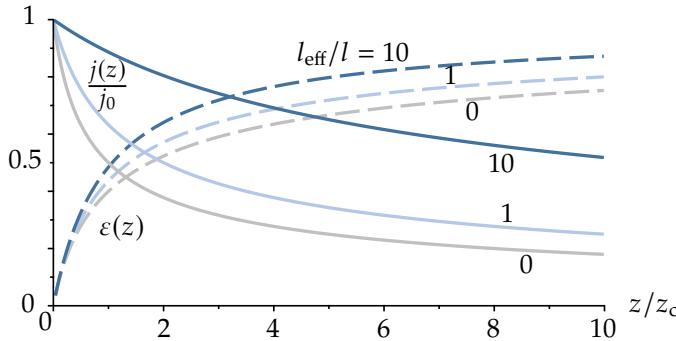
Figure 6.6: *Profiles of the normalized current density j/j_0 (solid) and the gas fraction (dashed) as a function of height z. Various ratios l_{eff}/l, between the non-gap-related cell areal resistance l_{eff}/κ_m, and the bubble-free areal resistance l/κ_m of the gap, are plotted. The higher this ratio, the larger the height over which the current distribution decreases.*

in the electrolyte potential. As bubbles accumulate with height, the impact on the current density will become larger. Here we will try to quantify this effect.

In the original analysis of Charles W. Tobias [29], the gas velocity w_g was taken to be constant, no maximum gas fraction was considered, and no other voltage losses than the ohmic losses in the gap were considered. Here, we make this analysis more realistic by including these additional effects.

From Eq. (6.1) we find the current density to be given by

$$j(z) = \frac{V_{eq} - V_{cell} - \eta}{l/\kappa(z) + l_{eff}/\kappa_m}.$$ (6.15)

The presence of bubbles decreases the gap conductivity κ, which decreases the current density. Inserting Eq. (6.15) into Eq. (6.11), using Eq. (6.7), gives

$$\frac{d}{d(z/z_c)}\left(\frac{\varepsilon/\varepsilon_{max}}{1 - \varepsilon/\varepsilon_{max}}\right) = \frac{j(z)}{j_0}.$$ (6.16)

We expect this dimensionless current distribution to decrease with height z as the bubble resistance decreases the current. Equation (6.15) gives $\frac{j}{j_0} = \frac{1 + l/l_{eff}}{1 + l\kappa_m/l_{eff}\kappa}$. Inserting the Maxwell relation Eq. (6.2) we can solve this for ε to give

$$\frac{\varepsilon}{1 - \varepsilon} = \frac{2}{3}\frac{j_0 - j}{j}\left(1 + \frac{l_{eff}}{l}\right)$$ (6.17)

For $\varepsilon_{max} = 1$ we can insert this into Eq. (6.16) to obtain a separate first-order ordinary differential equation for $j(z)$. Solving it, with as a boundary condition a fixed j_0,

gives 🚶

$$\frac{j}{j_0} = \frac{1}{\sqrt{1 + \frac{3z/z_c}{1+l_{\text{eff}}/l}}}.$$ (6.18)

This relationship gives that the current $j(z) = j_0/2$, so it is halved compared to the current at $z = 0$, for a height given by $z_c \left(1 + \frac{l_{\text{eff}}}{l}\right)$, which reduces to z_c in the case of negligible resistance $l_{\text{eff}} \ll l$. For a constant current density, this is also the height at which the gas fraction reaches half its maximum. Any additional resistance in the diaphragm will cause the current density to halve at a larger height. This is also clearly visible from the graphical depiction in Fig. 6.6.

Inserting Eq. (6.18) into Eq. (6.17) gives the gas fraction profile as a function of height.[17] This exact solution is shown as the dashed lines in Fig. 6.6 and gives a result very similar to $\frac{z}{z+z_c}$ of Eq. (6.12), with a maximum relative error below 22 %. Therefore, at least for $\varepsilon_{\max}$, this simpler relation can be used to obtain a rough indication of the gas fraction profile.[18]

6.5 Natural liquid circulation

High gas fractions can lead to dry zones, called *hot-spots*, that can become dangerously hot. To avoid this, Eq. (6.12) shows that z_c should be sufficiently high compared to the electrolyser height. According to Eq. (6.13) this characteristic height increases with increasing l. Therefore, scaling up the electrolyser height also requires more horizontal space for the gas. Alternatively, Eq. (6.13) shows that z_c also increases with increasing superficial liquid velocity W_l. Using electrolyte convection can, therefore, help to remove the gas more effectively and allow for more compact electrolysers. Additionally, liquid flow also helps transport heat out of the cells.

The use of a pump adds additional costs for power use and maintenance. Therefore, some atmospheric pressure electrolysers use the buoyancy of the rising bubbles to set the electrolyte into motion. Fig. 6.7 illustrates the operational principle behind a natural recirculation electrolyser. The rising bubbles drag liquid flow upwards in what we will call the '*riser*'. This is the bubble-filled space between the diaphragm and the electrode or behind the electrode in case of a zero-gap electrolyser. After the bubbles are removed in a *gas-liquid separator*, the bubble-free electrolyte flows downwards through a '*downcomer*' and re-enters the bottom of the electrolyser.

Due to the presence of the bubbles, the liquid column near the electrode will be lighter than that of the bubble-free downcomer. The hydrostatic pressure in the

---

[17]Alternatively, in Appendix 6.B we solve Eqs. (6.16) and (6.15) directly for the gas fraction. The result is the same and provided in Eq. (6.B.33).

[18]We note from Eq. (6.18) that the highest height-average current density is obtained when $l = 0$. Therefore, to maximise the total current, the gap l should be made as small as practically possible. This is indeed what most of the data of Ref. [19] shows. However, for some of the higher current densities, an optimum gap l is observed that is not predicted by our model. This may indicate, for example, the transition to a slug flow regime or some other effect not incorporated here.
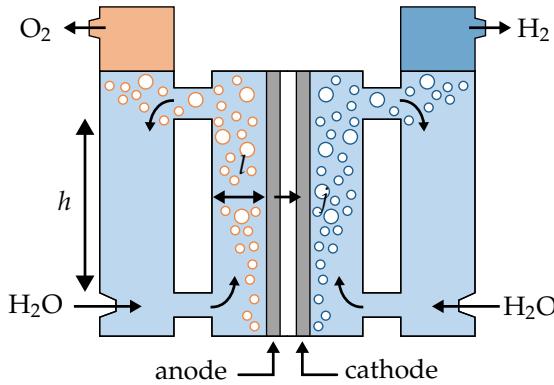
Figure 6.7: *An illustration of the natural liquid recirculation that will arise due to the buoyancy of the gas evolving from the electrodes. When there is a closed loop where liquid can recirculate in a* downcomer, *the difference in weight of the liquid with and without bubbles will drive a natural circulation pattern.*

downcomer is $\rho_l g h$, while that in the riser is $\rho_l \left(1 - \langle \varepsilon \rangle\right) g h$, where $\rho_l \left(1 - \langle \varepsilon \rangle\right)$ is the average mixture density in the riser. The pressure difference $\rho_l g h \langle \varepsilon \rangle$ between the riser and downcomer will create an upward flow in the riser, which will induce a frictional pressure drop Δp_f. In a steady-state, the resulting pressure balance reads 🏃

$$\rho_l g h \langle \varepsilon \rangle = \Delta p_f. \tag{6.19}$$

We will write this frictional pressure drop as

$$\Delta p_f \approx \frac{1}{2} \rho W_l^2 K, \tag{6.20}$$

where we can add $K = \sum_i K_i$ the contributions of various *irreversible loss coefficients* due to bends ($K \approx 1$) and contractions ($K \approx 1.5$) to the frictional contribution of the riser[19]

$$K_{\text{riser}} = f \frac{h}{l}. \tag{6.21}$$

For turbulent single-phase flow the coefficients K and the *friction factor*[20] f depend only weakly on the liquid velocity W_l. Using these same values for multi-phase flow will only be a crude approximation. In general, they will also depend on the gas fraction and/or the gas velocity W_g.

---

[19]In case the flow area A_i of segment i differs from the flow area $A_\perp$ of the riser, we may write $K = \sum_i \left(\frac{A_\perp}{A_i}\right)^2 \left(K_i + f_i \frac{h_i}{d_i}\right)$. The hydraulic diameter $d_i = 4A_i/P_i$ with P_i the perimeter and area of segment i. For a circular cross-section, this is the diameter, while for two parallel plates, it is the distance l_i between them. The prefactor $\left(\frac{A_i}{A_\perp}\right)^2$ corrects the local velocity to $W_i = \left(\frac{A_\perp}{A_i}\right)^2 W_l$.

[20]This is the Darcy friction factor, which is four times the Fanning fraction factor. Inserting Eq. (6.21) into Eq. (6.20) gives the Darcy-Weisbach equation.

The maximum liquid velocity $W_{l,max}$ arises when the average gas fraction in the riser is equal to the maximum $\langle \varepsilon \rangle = \varepsilon_{max}$. In this case, Eqs. (6.19) and (6.21) combine to give

$$W_{l,max} = \sqrt{\frac{2gh\varepsilon_{max}}{K}}. \tag{6.22}$$

Note that $\sqrt{2gh}$ is the maximum velocity that a free-falling object[21] attains when dropped from a height h.

To make further analytical progress, assume a constant current density and use the approximation in Eq. (6.14). Together with Eq. (6.13), this reads

$$\frac{\langle \varepsilon \rangle}{\varepsilon_{max}} \approx \frac{W_g/2\varepsilon_{max}}{w_S + W_l + W_g/2\varepsilon_{max}} \tag{6.23}$$

where

$$W_g = \frac{h}{l}\frac{j\mathcal{V}_m}{nF}, \tag{6.24}$$

is the superficial gas flux at the top of the electrolyser at $z = h$.[22]

From Eqs. (6.19) and (6.20) the superficial liquid velocity squared, W_l^2, is proportional to the average gas fraction $\langle \varepsilon \rangle$. Therefore, Eq. (6.23) gives

$$W_l^2 \approx \frac{2gh\varepsilon_{max}/K}{1 + 2\varepsilon_{max}\frac{w_S+W_l}{W_g}}. \tag{6.25}$$

Here the numerator is the squared maximum superficial liquid velocity of Eq. (6.22), which is obtained in case the superficial gas velocity W_g far exceeds $w_S + W_l$. The denominator brings down this maximum velocity when the average fraction in the riser is not equal to the maximum. This depends on the ratio between the sum of the upwards velocities $w_S + W_l$ and the superficial gas velocity W_g.

For K independent of W_l, Eq. (6.25) is a cubic equation for W_l that can be solved analytically. However, this gives a somewhat lengthy expression and a good approximation is provided in Eq. (6.C.37). Here, we consider only its limits. Neglecting the Stokes slip velocity[23], the limits of relatively high and low superficial gas velocity

---

[21]This is called Toricelli's law. Equation (6.22) reminds us of the terminal velocity of an object in the presence of a drag force, with K appearing instead of a drag coefficient. The ratio $\mathrm{Fr} \equiv W_l/\sqrt{2gh}$ is referred to as the Froude number, which according to Eq. (6.22) will satisfy $\mathrm{Fr} \leq \sqrt{\varepsilon_{max}/K}$.

[22]Obtained by integrating Eq. (6.7) from $z = 0$ to $z = h$.

[23]The cases of dominant superficial gas velocity and liquid velocity are shown in Eq. (6.26). Assuming the opposite limit of dominant slip velocity $w_S \gg \left(W_{l,max}^2 \frac{W_g}{2\varepsilon_{max}}\right)^{1/3}$, $\frac{W_g}{2\varepsilon_{max}}$ gives $W_l \approx \sqrt{\frac{W_{l,max}^2}{w_S}\frac{W_g}{2\varepsilon_{max}}} = \sqrt{\frac{W_g}{w_S}\frac{gh}{K}}$. Depending on the relative magnitude of W_g, $W_{l,max}$ and w_S, the liquid velocity can scale with the square root of the current density, the cubic root, or not at all.

read, respectively 🏃

$$W_l \approx \begin{cases} W_{l,max} & \text{for } W_{l,max} \ll \frac{W_g}{2\varepsilon_{max}}, \\ \left(W_g \frac{gh}{K}\right)^{1/3} & \text{for } W_{l,max} \gg \frac{W_g}{2\varepsilon_{max}}. \end{cases} \tag{6.26}$$

The top limit in Eq. (6.26) is obtained for relatively high superficial gas fluxes W_g, so the maximum gas fraction is obtained. The lower limit in Eq. (6.26) is obtained for relatively low superficial gas fluxes W_g,[24] requiring, according to Eq. (6.24), relatively low current densities j, heights h, and/or relatively large gaps l. In this regime, the superficial liquid velocity increases proportional to $\left(jh^2/Kl\right)^{1/3}$.

For a typical atmospheric pressure electrolyser we take $\mathcal{V}_m = 0.06$ m^3/mol,[25], a height $h = 1$ m, a gap of $l = 1$ cm, and $j = 1$ A/cm^2. Inserting into Eq. (6.24) gives $W_g \approx 0.3$ m/s for the hydrogen side ($n = 2$). Usually, the inlets and outlets of cells have areas that are much smaller than the riser flow area,[26] which can lead to very large values of K, see footnote 19. For example, a reduction in flow area by a factor 10^2 gives $K \approx 10^4$, for which the top limit of Eq. (6.26) gives $W_l \approx 4$ cm/s. This is more than sufficient to remove the heat and gas from the cell. However, in larger stacks or at higher pressure, the limited recirculation velocity may require the use of a pump.

6.6 Summary

- For a maximum gas fraction $\varepsilon_{max} = 1$, the gas fraction inside the electrolyser $\varepsilon = \frac{W_g}{w_S + W_l + W_g} = \frac{z}{z_c + z}$ (6.9), (6.12) increases to 1/2 at a height $z_c = l \frac{w_S + W_l}{j_0 \mathcal{V}_m/nF}$ (6.13). A relatively high superficial liquid velocity W_l or Stokes rise velocity w_S can increase this height, while a higher current density and a smaller gap thickness l decrease it.

- In a traditional electrolyser design where the bubbles rise in the inter-electrode spacing, the current will decrease with height according to $\frac{j}{j_0} = \frac{1}{\sqrt{1 + \frac{3z/z_c}{1 + l_{eff}/l}}}$. For higher areal resistance l_{eff}/κ_m relative to that of the gap l/κ_m, the height at which the current density halves, increases.

- In a natural recirculation electrolyser the pressure difference between riser and downcomer is compensated by friction: $\langle\varepsilon\rangle\rho_l g h = \Delta p_f$. Considering only turbulent friction $\Delta p_f \approx \frac{1}{2}\rho W_l^2 K$ (6.20) gives $W_{l,max} = \sqrt{\frac{2gh\varepsilon_{max}}{K}}$ (6.22) in case the maximum gas fraction is reached in the riser.

---

[24]The friction in the downcomer circuit, as quantified by K, should also be small enough to allow the slip velocity to be neglected with respect to the superficial liquid velocity.

[25]With $T = 80°$ C and $p = 10^5$ Pa, the ideal gas law gives $\mathcal{V}_m \approx 0.03$ m^3/mol, but at such temperatures the gas bubbles will also contain significant amounts of water vapour, easily doubling the gas volume.

[26]In a bipolar stack this is required to avoid 'shunt currents' that arise when ions skip a number of cells by travelling out of their cell.

Exercise 6.1

a. High gas fractions can give rise to hot spots. When problems arise near the cathode of a water electrolyser when $\varepsilon = \varepsilon_c < \varepsilon_{max}$, give an expression for the maximum electrolyser height to stay below this gas fraction You may assume a constant current density and a half-cell width l.

b. With $j = 1 \, \text{A/cm}^2$, $\varepsilon_{max} = 0.9$, $\varepsilon_{max} = 1$, $l = 1 \, \text{cm}$, and $w_S + W_l = 1 \, \text{cm/s}$, give a numerical value for this maximum electrolyser height at ambient conditions.

Exercise 6.2

Consider a half-cell of a traditional electrolyser configuration with a gap of thickness l, an electrolyte conductivity κ_m and an approximately constant current density j.

a. Assuming the tortuosity squared (τ^2) of the ion path around the bubbles with a gas fraction ε is given by $\frac{1}{1-\varepsilon}$, give an expression for the local ohmic voltage drop over the gap.

b. When $\varepsilon \approx z/z_c \ll 1$, give an expression for the height-averaged ohmic drop at a height h to first order in $h/z_c \ll 1$.

c. Give an expression for only the *additional* dissipated ohmic power [J/s] as a consequence of the presence of bubbles for an electrode of area A.

d. Assuming $\varepsilon_{max} = 1$ and neglecting w_S, Eq. (6.13) gives $z_c = \frac{lW_l}{j\mathcal{V}_m/nF}$. Increasing the liquid velocity W_l thus increases z_c and decreases the bubble-associated ohmic dissipation. However, this goes at the expense of additional pumping power $Q\Delta p$, with $Q = W_l Al/h$ the volumetric flow rate. Assume that the Hagen-Poiseuille equation $\Delta p = 12\mu W_l/l^2$ holds and that Stokes slip is negligible. Give an expression for the optimal superficial liquid velocity W_l that minimises the total dissipation.

e. With $j = 0.3 \, \text{A/cm}^2$, $h = 1 \, \text{m}$, $l = 1 \, \text{cm}$, $\kappa_m = 100 \, \text{S/m}$, and $\mu = 1 \, \text{mPas}$, give this optimal velocity for the hydrogen side at ambient conditions.

Exercise 6.3

In the main text, we assumed that the gas fraction depends only on height z, while it may also depend on a horizontal coordinate x across the cell. Here we consider the simplest way to model this for a zero-gap electrolyser.

a. If the (constant) current is j, the number of electrons per gas molecule n, the gas molar volume $\mathcal{V}_m$, and Faraday's constant F, what is the superficial gas velocity emanating from the electrode in the x-direction?

We assume that :

- at $z = 0$ there is no gas,
- the average interstitial gas velocity is a constant w_g,
- the gas fraction is a constant ε between the electrode at $x = 0$ and $x = \delta$,
- the gas fraction is zero between $x = \delta$ and the back wall at $x = l$.

b. Using conservation of gas volume, give an expression for the bubble plume thickness δ.

c. Assuming $w_g = 0.3$ m/s, $\varepsilon = 0.2$, $j = 0.2$ A/cm^2, $\mathcal{V}_m = 25$ l/mol, and $n = 2$, what will be the plume thickness at a height of $z = 1$ m?

Exercise 6.4

A perforated plate electrode used in gas-evolving electrolysers may be treated as a porous medium with a tortuosity equal to 1. Its front and back areas do not participate in the reaction; only the electrode area inside the perforations does.

a. If the holes make up a fraction ϵ of the electrode area, and these holes contain a gas fraction ε, what is the ohmic drop if a current density j, as always per total unit area, traverses the full thickness L of the electrodes when the electrolyte conductivity is κ?

b. With b the Tafel slope of the electrode, what is the Thiele modulus M associated with this ohmic limitation?

c. If M $\gg$ 1, by what number is the effectiveness factor multiplied when the gas fraction increases from 0.3 to 0.6?

d. Give a formula for the overpotential that can be attributed to the presence of bubbles.

Exercises 6.5-6.17

Fill in the missing steps in the main text, indicated by the symbol ⚒.

Appendices *

6.A *Bubble release diameter*

As we saw in section 6.3, the gas fraction ε is determined by how much gas is produced and how fast it can be removed. This can occur through the flow of electrolytes but also due to the velocity of the bubbles relative to the liquid. To determine this buoyant rise velocity, as discussed in section 6.2.2, we have to know their size. The size distribution of bubbles is very hard to model due to the complex interactions between bubbles, the bubbles and the electrode, and the electrolyte flow. In the context of describing boiling, some limited success has been obtained by considering the force balance. Such types of analysis are complicated because the exact shape of the bubble at the point of its release must be known to evaluate all the forces accurately. This can be solved exactly in the special case of single bubbles in a quiescent liquid on a horizontal surface. Since this can give us an idea of typical bubble sizes, we will consider this force balance here.
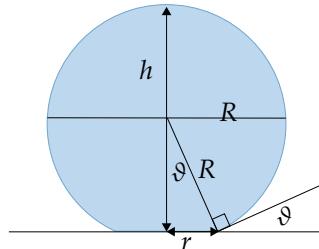
Figure 6.8: *A spherical cap bubble on a horizontal surface, showing the contact angle ϑ.*

Consider the approximately *spherical cap* bubble of Fig. 6.8. The surface tension force keeping the bubble attached to the surface despite its buoyancy is given by γ times sin ϑ, times the perimeter of the contact line.[27] By solving for the exact shape of the bubble, it can be shown that at the point of release 3/4 of this force will

---

[27]The surface tension potential energy reads $\mathcal{U} = \gamma \pi r^2$ so that the principle of virtual work gives the force associated with a change in the bubble radius as $\partial \mathcal{U} / \partial R = \sin \vartheta \partial \mathcal{U} / \partial r = 2\pi r \sin \vartheta \gamma$.

be cancelled by the additional Laplace pressure inside the bubble[28] so that the net attractive force reads

$$F_\downarrow = \frac{\pi R}{2} \gamma \sin^2 \vartheta. \tag{6.A.27}$$

The main force away from the surface, $F_\uparrow$, is that due to buoyancy. We will consider the contact angle to be small, $\vartheta \ll \pi/2$, and approximate the volume of the bubble by that of a sphere so that, neglecting the gas density,

$$F_\uparrow = \frac{4\rho g}{3} \pi R^3. \tag{6.A.28}$$

Equating these forces gives for the bubble release radius R

$$R = \vartheta \sqrt{\frac{3\gamma}{8\rho g}}. \tag{6.A.29}$$

This is called the Fritz equation, where we note that ϑ is in radians and is assumed to be small compared to $\pi/2$.[29] Using $\gamma = 73$ mN/m and $\rho = 10^3$, typical for aqueous electrolytes, and $\vartheta = 20° \frac{\pi}{180}$, typical for smooth pure metal surfaces, this gives a release diameter $2R = 120$ μm. Interactions with other bubbles and flow will usually tend to decrease this release radius further. Especially hydrogen bubbles in alkaline electrolytes can be much smaller still.

6.B *Dimensionless current distribution*

We introduce the dimensionless current density profile $\bar{j} = j/j_0$, where $j_0 = \frac{V_{eq} - V_{cell} - \eta}{l/\kappa + l_{eff}/\kappa_m}$. In dimensionless notation, Eq. (6.15) can be written as

$$\bar{j} = \frac{1 + \bar{R}}{1/\bar{\kappa} + \bar{R}}, \tag{6.B.30}$$

where $\bar{R} = l_{eff}/l$ is the diaphragm resistance relative to the bubble-free gap resistance. Inserting Eq. (6.B.30) in Eq. (6.11) gives, assuming $\varepsilon_{max} = 1$,

$$\frac{\mathrm{d}}{\mathrm{d}\bar{z}} \left(\frac{\varepsilon}{1 - \varepsilon} \right) = \frac{1 + \bar{R}}{1/\bar{\kappa}(\varepsilon) + \bar{R}}. \tag{6.B.31}$$

---

[28]The Laplace pressure is given by Eq. (5.4) as $p_1 = 2\gamma/R$ so that multiplying with the contact area $\pi r^2 = \pi R^2 \sin^2 \vartheta$ gives a repulsive force $2\pi\gamma R \sin^2 \vartheta$, equal and opposite to the surface tension force. However, buoyancy will slightly lift the bubble, changing its shape, so one can show that the cancellation is incomplete.

[29]For small contact angles we have $\sin \vartheta \approx \vartheta$. Using degrees instead of radians sometimes $2R = 0.021\vartheta\sqrt{\frac{\gamma}{8\rho}}$ can also be found in the literature [25].

where $\bar{z} \equiv z/z_c$. We can solve Eq. (6.B.31) using the Maxwell relation (6.2),[30] to give

$$\varepsilon\left(\bar{z}\right) = \frac{1}{1 + \frac{3}{2\left(1+\bar{R}\right)\left(\sqrt{1+\frac{3\bar{z}}{1+\bar{R}}}-1\right)}} \approx \begin{cases} \frac{\sqrt{1+3\bar{z}}-1}{\sqrt{1+3\bar{z}}+\frac{1}{2}} & \bar{R} = 0, \\ \frac{\bar{z}}{1+\bar{z}} & \bar{R} \to \infty. \end{cases} \tag{6.B.32}$$

For $\bar{z} \ll 1$ the solution approximates to $\varepsilon \approx \bar{z} \ll 1$, independent of $\bar{R}$. This is equal to the previous result of Eq. (6.12) for constant current density. In dimensional notation, Eq. (6.B.32) reads

$$\varepsilon\left(z/z_c\right) = \frac{1}{1 + \frac{3}{2(1+l_{\text{eff}}/l)\left(\sqrt{1+\frac{3z/z_c}{1+l_{\text{eff}}/l}}-1\right)}} \approx \begin{cases} \frac{\sqrt{1+3z/z_c}-1}{\sqrt{1+3z/z_c}+\frac{1}{2}} & l_{\text{eff}} = 0, \\ \frac{z}{z_c+z} & l_{\text{eff}} \to \infty. \end{cases} \tag{6.B.33}$$

In the limit $l_{\text{eff}} \to \infty$, the resistance of the gap can be neglected so the current density will be independent of the gas fraction in the gap, and we retain the previous result of Eq. (6.12) for constant current density.

Inserting the solution of Eq. (6.B.33) into Eq. (6.B.30) gives Eq. (6.18), or in dimensionless form

$$\bar{j} = \frac{1}{\sqrt{1 + \frac{3\bar{z}}{1+\bar{R}}}}. \tag{6.B.34}$$

In the limit $\bar{z} \gg 1 + \bar{R}$, this tends to zero.

6.C   *An expression for the liquid recirculation velocity*

In terms of $W_{l,\text{max}}$ defined in Eq. (6.22) we can approximate the solution to Eq. (6.25) by

$$W_l \approx \frac{\left(W_g W_{l,\text{max}}^2/2\varepsilon_{\text{max}}\right)^{1/3}}{\left(1 + \left(\frac{w_S + W_g/2\varepsilon_{\text{max}}}{\left(W_g W_{l,\text{max}}^2/2\varepsilon_{\text{max}}\right)^{1/3}}\right)^{p/2}\right)^{1/p}} \approx \begin{cases} \frac{W_{l,\text{max}}}{\sqrt{1+2\varepsilon_{\text{max}}w_S/W_g}} & \ll w_S \text{ or } \frac{W_g}{2\varepsilon_{\text{max}}}, \\ \left(\frac{W_g W_{l,\text{max}}^2}{2\varepsilon_{\text{max}}}\right)^{1/3} & \gg w_S \text{ and } \frac{W_g}{2\varepsilon_{\text{max}}}. \end{cases} \tag{6.C.35}$$

This is nearly identical to the exact result using $p \approx 2.6$. For $p = 3$ and inserting Eqs. (6.24) and (6.22):

---

[30]The resulting differential equation $\frac{1}{1+\bar{R}}\left(\frac{1+\varepsilon/2}{1-\varepsilon} + \bar{R}\right)\frac{\mathrm{d}}{\mathrm{d}\bar{z}}\left(\frac{\varepsilon}{1-\varepsilon}\right) = 1$, with the substitutions $\tilde{\varepsilon} = \frac{\varepsilon}{1-\varepsilon}$ and $\frac{1}{\bar{\kappa}} = \frac{1+\varepsilon/2}{1-\varepsilon} = 1 + \frac{3}{2}\tilde{\varepsilon}$, reads $\frac{1+3\tilde{\varepsilon}/2+\bar{R}}{1+\bar{R}}\frac{\mathrm{d}\tilde{\varepsilon}}{\mathrm{d}\bar{z}} = 1$, so that, with the boundary condition $\varepsilon(0) = 0$, we find $\int_0^{\tilde{\varepsilon}}\left[1 + \frac{3\tilde{\varepsilon}}{2(1+\bar{R})}\right]d\tilde{\varepsilon} = \tilde{\varepsilon} + \frac{3\tilde{\varepsilon}^2}{4(1+\bar{R})} = \bar{z}$. This quadratic equation is solved by $\tilde{\varepsilon} = \frac{2(1+\bar{R})}{3}\left(\sqrt{1+\frac{3\bar{z}}{1+\bar{R}}}-1\right)$ or $\varepsilon = \frac{\tilde{\varepsilon}}{1+\tilde{\varepsilon}}$ given by Eq. (6.B.32).

$$W_l \approx \frac{(gh/K)^{\frac{1}{3}}}{\left(\frac{1}{W_g} + \left(\frac{w_S/W_g + 1/2\varepsilon_{max}}{(gh/K)^{\frac{1}{3}}}\right)^{\frac{3}{2}}\right)^{\frac{1}{3}}} \approx \begin{cases} \sqrt{\frac{2gh\varepsilon_{max}/K}{1+\frac{2\varepsilon_{max}w_S l}{h}\frac{nF}{j\mathcal{V}_m}}} & \ll w_S \text{ or } \frac{W_g}{2\varepsilon_{max}}, \\ \left(\frac{j\mathcal{V}_m}{nF}\frac{gh^2}{Kl}\right)^{1/3} & \gg w_S \text{ and } \frac{W_g}{2\varepsilon_{max}}. \end{cases} \tag{6.C.36}$$

The limits of high gas velocity, high slip velocity, and high liquid velocity can be written, respectively as:

$$W_l \approx \begin{cases} W_{l,max} & W_{l,max}, w_S \ll \frac{W_g}{2\varepsilon_{max}}, \\ \sqrt{\frac{W_{l,max}^2}{w_S}\frac{W_g}{2\varepsilon_{max}}} & \left(W_{l,max}^2\frac{W_g}{2\varepsilon_{max}}\right)^{1/3}, \frac{W_g}{2\varepsilon_{max}} \ll w_S, \\ \left(W_{l,max}^2\frac{W_g}{2\varepsilon_{max}}\right)^{1/3} & \frac{w_S^3}{W_{l,max}^2} \ll \frac{W_g}{2\varepsilon_{max}} \ll \frac{W_{l,max}}{2\varepsilon_{max}}. \end{cases} \tag{6.C.37}$$

Chapter 7

Redox Flow Batteries

Redox flow batteries are reversible fuel cells or integrated fuel cell-electrolyser combinations. They typically use liquid electrolyte flow, normal to the current density. Properly describing the mass transport parallel to the current, coupled to the current distribution parallel to the flow, inherently requires two-dimensional models. We will take a decoupled approach where we consider these directions independently. The resulting models will also be useful for describing fuel cells.
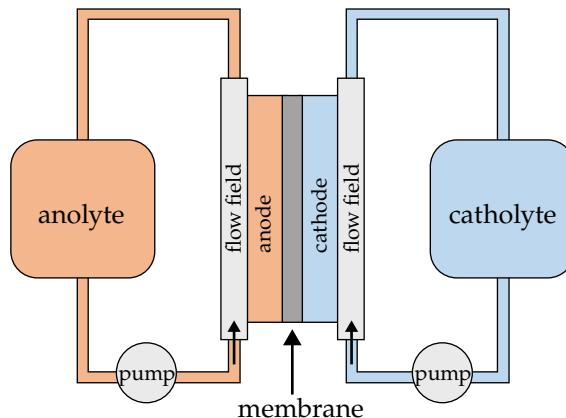
Figure 7.1: *A schematic of a generic redox flow battery where the reactants, oxidant and reductant, are stored in separate tanks and pumped into the cell that can be operated both galvanically and electrolytically.*

7.1 Introduction

Redox flow batteries are essentially fuel cells and electrolysers made into one device. They use redox couples that are reversible enough so that, with low activation overpotentials, they can be both oxidised and reduced. The most commonly used reaction is with Vanadium due to its stability, relatively low toxicity, and ability to be used to both anode and cathode, minimising problems with crossover. However, its high cost, low energy, and power density leave room for the development of different types of flow batteries.

The two redox couples, with or without additional supporting electrolytes, are usually stored in two separate tanks, see Fig. 7.1. A pump supplies them to the cell at the desired rate. Most often, redox flow batteries work with aqueous solutions, although sometimes non-aqueous solvents, gases, or even suspended solid particles are used. See section 7.2 for a classification of the various types of flow batteries.
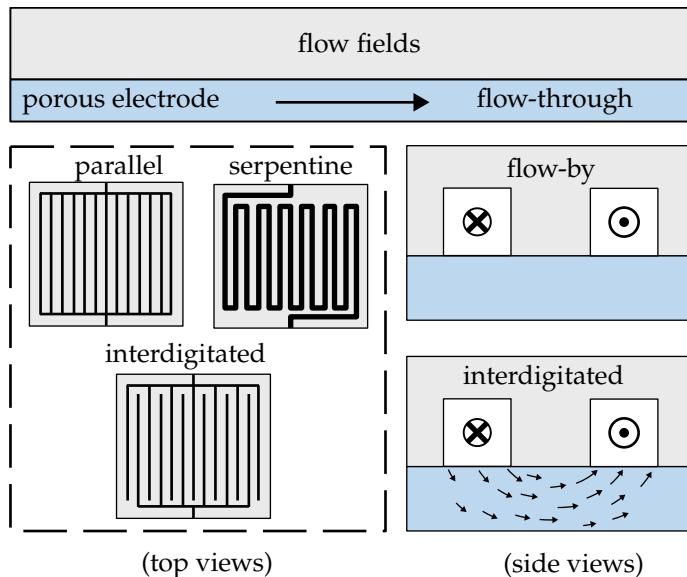
Figure 7.2: *The three main flow modes of redox flow batteries are flow-through (top), flow-by (middle), and interdigitated (bottom). In flow-through cells, there is no flow field, and the electrolyte flows through the porous electrode. In a flow-by configuration, there is little to no flow inside the electrodes, and reactants diffuse in. A serpentine flow field may be used to increase the flow path length. Interdigitated designs combine the advantages of both flow-through and flow-by properties.*

A potential advantage compared to batteries is that the reactants in flow batteries can flow and, therefore, can be conveniently stored in a tank outside of the electrochemical cell. This decoupling of the power, determined by the cell design, and the storage capacity, determined by the external tanks, gives additional design

freedom. It makes redox flow batteries suitable for storing energy for the day-night cycle variations in electricity supply and demand.

Inside the cell, the reactants are sometimes pumped directly through a porous electrode, in what is called a *flow-through* configuration, shown in Fig. 7.2.[1] The small pores in the carbon paper, mesh, or cloth electrode can cause large pressure drops. Therefore, the middle row of Fig. 7.2 shows the *flow-by* alternative, in which the flow passes by the electrode through channels engraved in the current collector/bipolar plate. In this case, the flow inside the electrode will be very small, and reactants primarily diffuse towards their reaction sites. If additional channel length is desired, for example, to ensure that a large fraction of the reactants is converted, a *serpentine flow field* forms a suitable alternative to a *parallel flow field*.

A third option, shown at the bottom of Fig. 7.2, is an interdigitated configuration. Here, the inlet and outlet channels are not connected, so the electrolyte has to flow through the electrode to reach the outlet. This gives the same advantage of advective mass transport as in a flow-through configuration but with much smaller pressure drops since the distance over which the fluid travels is much smaller.

7.2   *Types of redox flow batteries* *

While most commercial systems are based on Vanadium, research on many other chemistries and cell designs exists. While there may be overlap and combinations possible, we can distinguish the following broad classification of flow battery types.

- Traditional: this comprises the most common Vanadium-based redox flow batteries, such as the all-Vanadium type, see Tbl. 7.1, but also, for example, the Vanadium-Bromine alternative. Vanadium-Oxygen redox flow batteries have the advantage that air can be used, which does not have to be stored. Also in this category is the unitised regenerative fuel cell, a H_2/O_2 fuel cell and water electrolyser combined in the same device. When one of the reactants is gaseous, for example in the H_2/Br_2 flow battery, a gas-breathing electrode is used.

- Hybrid: sometimes, a flow battery half-cell is combined with a normal battery half-cell. Most commonly, Zinc is used for the battery electrode. Halogens like Bromine or Iodine are often used for the flow battery electrode. The energy density of a Zinc-air battery could potentially be similar to that of Li-ion batteries. Making this type of battery rechargeable has proven to be challenging.

- Organic: potentially more eco-friendly and versatile, organic redox couples are intensively researched. Most types depend on quinones, which have a benzene ring with an even number of C-H-bonds changed to C=O double bonds.

---

[1]In this case, the flow is normal to the current density. Traditionally, the term flow-through electrode was also used to describe a flow parallel to the current. Contrary to modern flow-battery parlance, which we will follow here, the term flow-by was sometimes used to refer to flow through a porous electrode normal to the current density, which is now called flow-through.

- Semi-solid: To combine battery chemistries with the scalability and storage advantages of flow batteries, solid battery particles may be put into suspension. This allows pumping the battery particles in a suspension-based flow battery.

- Membraneless/microfluidic: Since liquids have relatively low diffusion coefficients, their laminar concentration boundary layers are relatively thin. In case of two reactants, by placing the one with the highest density below the one with a lower density a stably stratified laminar flow can be created. In case the reactants are miscible in each other, a diffusion boundary layer arises that can be kept thin with sufficient flow, as schematically illustrated at the top of Fig. 7.3. The bottom part of this figure shows a case of effective product separation. Membraneless cells H_2/Br_2 cells have shown high power densities, nearing $1\,W/cm^2$.[26].

Name	Anode	Cathode
all-Vanadium	$VO^{2+} + H_2O \longleftrightarrow VO_2{}^+ + 2\,H^+ + e^-$	$V^{2+} + e^- \longleftrightarrow V^{2+}$
Zinc/Bromine hybrid	$2\,Br^- \longleftrightarrow Br_2 + 2\,e^-$	$Zn^{2+} + 2\,e^- \longleftrightarrow Zn$
Iron/Chromium	$Fe^{2+} \longleftrightarrow Fe^{3+} + e^-$	$Cr^{3+} + e^- \longleftrightarrow Cr^{2+}$
Hydrogen/Bromine	$2\,Br^- \longleftrightarrow Br_2 + 2\,e^-$	$2\,H^+ + 2\,e^- \longleftrightarrow H_2$

Table 7.1: *An arbitrary selection of some of the more commonly investigated chemistries for redox flow batteries.*

7.3   Flow-through electrodes

As shown in Fig. 7.2, in the flow-through electrode configuration, there is no separate flow channel, and the flow goes entirely through the electrodes. This is typically used to improve the rate of mass transfer. The length scale over which reactants have to diffuse is reduced to a fraction of a pore size so that the limiting current density can be relatively high.

As discussed in the introduction and shown in Fig. 7.2, an alternative with lower pressure drops is the interdigitated design. The analysis given below will approximately hold in this case when the channel length h is replaced by some characteristic distance relevant for the flow, of the order of the distance between interdigitated channels [5].

As argued in section 7.5.1, diffusive transport in the flow direction can usually be neglected relative to advective transport. For a superficial velocity W in the z-direction, Eqs. (3.15), (3.16) and (3.18) in steady-state combine to give

$$W\frac{dc}{dz} = \frac{a j_\perp}{nF}.$$

(7.1)

Here, we assume that the concentration $c(z)$ will only be a function of the flow direction z.[2] For an anode, inserting the concentration-dependent Tafel equation (1.28) $j_\perp = j_* \frac{c}{c_{in}} e^{\eta/b}$, Eq. (7.1) gives

$$W \frac{dc}{dz} = -kac \quad \text{where } k = \frac{j_* e^{\eta/b}}{nFc_{in}}. \tag{7.2}$$

For a constant reaction rate coefficient $k = j_\perp/nFc$, the solution of Eq. (7.2) with boundary condition $c(0) = c_{in}$ reads

$$\boxed{c(z) = c_{in} e^{-\frac{ka}{W} z}.} \tag{7.3}$$

So, the reactant concentration decreases exponentially in the flow, as is expected from a reaction rate that is proportional to the concentration.[3]

Integrating Eq. (7.1) over x over the electrode thickness L gives

$$WL \frac{dc}{dz} = \frac{j}{nF} \tag{7.4}$$

where $j = aLj_\perp$, using the conversion factor aL introduced in Eq. (3.35). It is solved by

$$c(z) = c_{in} - \frac{\int_0^z j dz}{nFWL}. \tag{7.5}$$

For a constant current density j, this gives the linearly decreasing profile $c(z) = c_{in} - \frac{j}{nFWL} z$. In general, the concentration will lie somewhere in between this linearly decreasing profile and the exponential decrease of Eq. (7.5).

We define the (degree of) conversion as the fraction of inlet concentration that is converted at the exit:

$$X \equiv \frac{c_{in} - c_m^{out}}{c_{in}} = 1 - e^{-\frac{ka}{W} h}, \tag{7.6}$$

where we evaluated Eq. (7.22) at the outlet using $\langle S \rangle_{out} = \langle S \rangle (z = h)$. The longer the channel length h, or the lower the flow velocity $\langle w \rangle$, the more material converts. Also, the lower the average overall dimensionless transfer resistance $1/\langle S \rangle_{out}$ the higher the conversion. This will require the channel and diffusion layers to be sufficiently thin and the reaction to be sufficiently fast.

Equation 7.6 may be used to determine a suitable channel length h associated with a desired conversion X to give

$$h_{opt} = \frac{W}{ka} \ln \left(\frac{1}{1 - X} \right). \tag{7.7}$$

---

[2]In case there are no ohmic limitations, the electrode effectiveness factor is close to 1, and the reaction rate will be approximately constant in the transverse x-direction.

[3]Note also the similarity with Eq. (7.18), the concentration profile in a flow-by configuration under limiting current conditions when replacing k_m with k. The reason is that both mass transfer and the considered first-order reaction are linear in the concentration.

A high conversion may be preferable to reduce separation costs of the outlet stream and avoid having to recirculate. However, it is not always desirable. For example, for an air-fed fuel cell or CO_2 electrolyser cathode, a high velocity with a low conversion may be preferable to maximise the reactant concentration in the channel. A high reactant concentration minimises the concentration overpotential and undesirable side reactions. Flowing faster will require a higher compressor duty or pumping power, which can also be a consideration.

7.4   Optimal electrolyte channel width
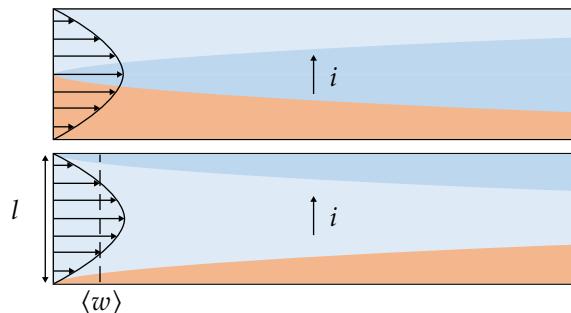
Figure 7.3: In a membraneless flow battery, laminar electrolyte flow keeps the mixing region between two reactants (top, in this co-laminar configuration a light blue and heavier orange reactant mix in the centre) or the developing product boundary layers (bottom) away from the opposing electrodes. Note that the boundary layers are drawn in an idealised fashion and will be more spread out in reality.

Usually, the flow channel, as seen from the membrane, is on the other side of the electrode. In this 'back-fed' configuration, the resistance is lower as ions do not have to traverse the flow channel. A front-fed configuration, in which the flow channel is on the other side, is also sometimes used. An example are *membraneless* or *micro-fluidic* redox flow batteries. When the flow is fast but still laminar, the products of the reaction can be transported out with the flow before they diffuse to the other side of the channel. The laminar boundary layers ensure separation, so that a membrane is not needed, see Fig. 7.3. Using a thin channel with a high-conductivity electrolyte, such a configuration can have a similar or lower ohmic drop compared to a configuration with a membrane without the cost, degradation and other limitations of membranes. In CO_2 electrolysers, a fluid channel between the cathode and a membrane is often used to supply water and minimise cross-over.

A thinner channel reduces the ohmic losses but increases the pumping losses. Therefore, there will be a channel width l for which the combined losses will be minimal. Here, we set out to find a relation for this optimal channel width.

For a cell thickness l_y in the direction normal to the flow and current, the electrode

area is $A = hl_y$, and the flow channel cross-sectional area reads ll_y. The power P_{res} dissipated by resistance is approximately given by the product of current $\langle j \rangle A$ and average potential drop $\langle j \rangle l/\kappa$, so[4]

$$\frac{P_{\text{res}}}{A} \approx \frac{\langle j \rangle^2 l}{\kappa}. \tag{7.8}$$

The laminar pressure drop is given by the Hagen-Poiseuille equation as[5]

$$\Delta p = 12\mu \frac{\langle w \rangle}{l^2} h. \tag{7.9}$$

The power dissipated by friction P_{fr} in the channel is given by the product of the volumetric flow-rate $ll_y \langle w \rangle$ and so ⟨

$$\frac{P_{\text{fr}}}{A} = \frac{12\mu \langle w \rangle^2}{l} = \frac{12\mu \langle j \rangle^2}{(nFXc_{\text{in}})^2 l^3}, \tag{7.10}$$

where we used Eqs. (7.15) and (7.6) to write $\langle w \rangle = \frac{\langle j \rangle}{nFlXc_{\text{in}}}$.

The optimal gap thickness l is that for which the combined power losses $P_{\text{fr}} + P_{\text{res}}$ are minimal. Solving $\frac{\partial}{\partial l}\left(\frac{P_{\text{fr}}}{A} + \frac{P_{\text{res}}}{A}\right) = 0$ for l, for constant X, gives ⟨

$$\boxed{l_{\text{opt}} = (36\mu\kappa)^{(1/4)} \sqrt{\frac{l}{nFXc_{\text{in}}}}.} \tag{7.11}$$

Using typical numbers $\mu = 1$ mPas and $\kappa = 1$ S/cm gives $l_{\text{opt}} = 140$ μm$\sqrt{\frac{l[\text{m}]}{nc_{\text{in}}[\text{M}]X}}$ so that for $l = 1$ m and $Xc_{\text{in}} = 1$ M, the optimal gap is 140 μm wide.

7.5 Flow-by

7.5.1 Quasi-2D model

Figure 7.4 introduces a coordinate system with z along the flow and x in the perpendicular direction, from the flow channel to the catalyst layer or porous electrode. Sometimes, in the case of gaseous reactants, between the two a diffusion layer exists, as considered in chapter 5. In the case of liquid reactants, there is often no such layer.[6]

---

[4]We should actually average the product of the current and potential drop, instead of multiplying their averages. For not-too-large variations in $j(z)$, the difference between $\langle j^2 \rangle$ and $\langle j \rangle^2$ may be acceptably small to allow usage of this approximation.

[5]The derivation of this result proceeds similarly to the cylindrical case treated in footnote 11 of chapter 5. Using the planar Laplacian d^2/dx^2 gives a prefactor 12 instead of 8.

[6]In the case of a flow-by configuration, the porous electrode is sometimes referred to as a liquid-diffusion layer. However, on the pore surface the redox reactions take place, contrary to in a gas diffusion layer (GDL).
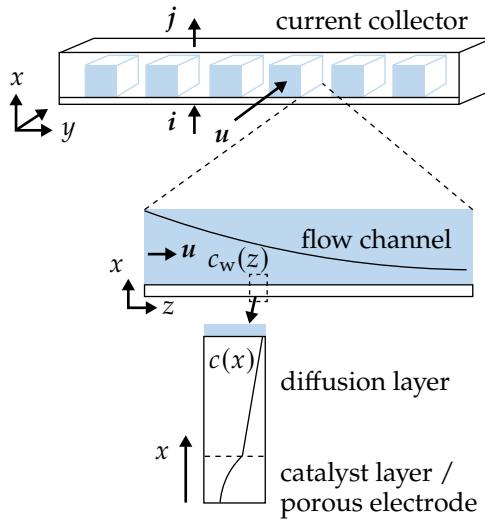
Figure 7.4: *A schematic of the metal current collector with carved-out flow channels (blue) in which the reactant concentration decreases along the flow direction (z) as well as in the direction inside the gas diffusion layer (x), towards the catalyst layer. The first and second close-ups represent the domains for the channel problem and the membrane-electrode-assembly (MEA) problem, respectively.*

The flow channels can be straight or form, for example, a serpentine *flow field* going back and forth many times, as shown in Figure 7.2. A first simplification is that we do not consider any variation in the *y*-direction, which is normal to both the current and the flow. There will obviously be differences in the concentration profiles directly below a flow channel or the *land area* where the current is collected; see Figure 7.4. Therefore, our model will be some sort of average over this *y*-direction.

The distance the fluid travels in the flow direction is typically of the order of $h \sim 0.1\text{-}10$ m. However, the flow channels ($l \sim 1$ mm) and porous electrodes (or diffusion layer with catalyst layer) (~ 100 μm) are generally much thinner in the *x*-direction. Therefore, typical diffusive fluxes $N_z \sim \frac{Dc}{h}$ due to the same concentration difference c in the *z*-direction are several orders of magnitude smaller than those $N_x \sim \frac{Dc}{l}$ in the *x*-direction: $\frac{N_z}{N_x} \sim \frac{l}{h} \ll 1$. So we can usually safely neglect diffusion parallel to the flow (N_z) and take the flux in this direction to be solely due to advection. In the *x*-direction, on the other hand, we will neglect any advection.

Considering advection only in the *z*-direction and diffusion only in the *x*-direction allows making separate models for each direction and coupling them afterwards. Respectively, these two decoupled problems are sometimes referred to [15] as

1. The *Channel problem* or *along-the-channel problem*, and

2. The membrane-electrode-assembly or *MEA problem*.

In the former we solve for the mean concentration $c_m(z)$, or the wall concentration $c_w(z)$, inside the flow channel as a function of the streamwise coordinate z. In the latter problem, we take these profiles as a given and calculate for each z the concentration profile $c(x)$ throughout the electrode (or diffusion and catalyst layers) and possibly the membrane. In the following sections, we will subsequently consider how to model these two problems analytically.

7.5.2 Channel problem

Figure 7.5 introduces again the x, z coordinate system, the channel dimensions (a streamwise 'height' h and channel thickness l) and flow channel velocity profile ($w(x)$, with average velocity $\langle w \rangle$). Neglecting the diffusion term ($D \frac{\partial^2 c}{\partial z^2}$) in the z-direction, as discussed in the previous section, the two-dimensional steady-state advection-diffusion equation (2.3) reads

$$ 0 = -w\frac{\partial c}{\partial z} + D\frac{\partial^2 c}{\partial x^2} . \tag{7.12}$$

The boundary conditions are: zero flux at the top wall, representing the current collector at $x = l$; and a prescribed but yet unknown flux $\frac{j}{nF} = D\frac{dc_w}{dx}$ at the flow channel-diffusion layer interface at $x = 0$. The channel problem consists of finding the concentration $c_w = c(x = 0)$. This concentration will provide the connection with or input to the MEA model.

Integrating Eq. (7.12) from $x = 0$ to $x = l$ gives for the wall flux[7] 🏃

$$ \frac{j(z)}{nF} = -\frac{d}{dz}\int_0^l wc\,dx = -\langle w \rangle l \frac{dc_m}{dz}, \tag{7.13}$$

where the integral $\int_0^l D\frac{\partial^2 c}{\partial x^2}dx = D\frac{\partial c}{\partial x}\big|_l - D\frac{\partial c}{\partial x}\big|_0$ is evaluated using the boundary conditions shown in Figure 7.5. We defined the *cup-mixing concentration* as

$$ c_m(z) \equiv \frac{1}{\langle w \rangle l}\int_0^l wc\,dx. \tag{7.14}$$

This represents the average concentration that is obtained when letting liquid at a position x flow into a cup. It weights the concentration with the local velocity since faster-flowing liquid contributes more to what is collected.

Integrating Eq. (7.13) once more, but now in the z-direction, gives for the average current density $\langle j \rangle = \frac{1}{h}\int_0^h j\,dz$ 🏃

$$ \boxed{\frac{\langle j \rangle h}{nF} = \langle w \rangle l \,(c_{in} - c_{out}).} \tag{7.15}$$

---

[7]Here, n is the positive number of electrons consumed or generated per molecule of reactant.
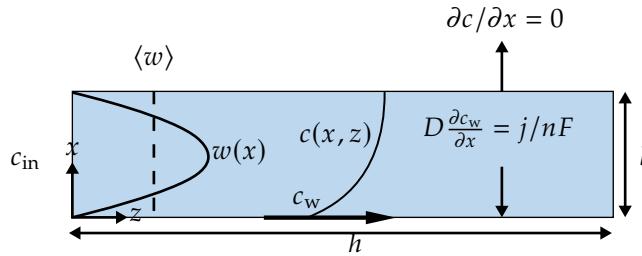
Figure 7.5: A schematic drawing, introducing the (Neumann) boundary conditions at the two walls and the (Dirichlet) boundary condition c_{in} at the entrance of the flow channel, its dimensions (h and velocity profile (w(x), with average velocity $\langle w \rangle$) in the flow channel. The channel problem consists of determining the 'wall' concentration c_w at the flow channel-diffusion layer interface at $x = 0$.

Here, c_{in} and c_{out} are the cup mixing concentrations, at the inlet at $z = 0$ and at the outlet $z = h$.[8]

Using the definition in Eq. (7.17) gives for the molar flux

$$\boxed{\frac{j}{nF} = -l\langle w \rangle \frac{dc_m}{dz} = \text{Sh} \frac{D(c_m - c_w)}{l}.}$$

(7.16)

Here, we introduced the *Sherwood number* Sh, representing the ratio between the flux $N = j/nF$ and a characteristic diffusion flux $D\frac{c_m - c_w}{l}$ so that

$$\text{Sh} \equiv \frac{Nl/D}{c_m - c_w}.$$

(7.17)

This is a dimensionless number, analogous to the *Nusselt number* for heat transport. In terms of the mass transfer coefficient $k_m = N/\Delta c$ used in chapter 4, we have $\text{Sh} = k_m l/D$. Near the entrance, the concentration profile is developing so that Sh will be very large.[9]

When $c_w = 0$, the flux cannot be further increased so that a limiting current arises. In this case, Eq. (7.16) is solved by 🧗

$$c_m = c_{in} e^{-\frac{\langle \text{Sh} \rangle D}{\langle w \rangle l^2} z}.$$

(7.18)

Here, $\frac{\langle \text{Sh} \rangle D}{\langle w \rangle l^2} z = \frac{\langle k_m \rangle}{\langle w \rangle l} z$ and the running-average Sherwood number $\langle \text{Sh} \rangle (z) = \frac{1}{z} \int_0^z \text{Sh} \, dz$. If the Sherwood number is constant, the cup-mixing average concentration c_m decreases exponentially over a length scale $\frac{\langle w \rangle l^2}{\text{Sh} D}$, independent of h. Because the rate

---

[8]With l_y the width in the y-direction, the number of moles $l l_y \langle w \rangle (c_{in} - c_m)$ that leave the channel equate to $\langle j \rangle h l_y / nF$, giving Eq. (7.15).

[9]For a constant velocity $\langle w \rangle$ this is similar to the Sands solution $\text{Sh} = l/\delta = \sqrt{\pi l^2/4tD}$ but with $z/\langle w \rangle$ instead of t. Further down the channel, as the concentration profile fully develops, Exercise 7.3 shows that Sh becomes $35/13 \approx 2.7$.

at which concentration is removed by diffusion is proportional to the concentration, an exponential decrease results. Therefore, removing the last bit of reactant concentration from the flow channel becomes increasingly difficult.

To find a general solution to Eq. (7.16), also valid under non-limiting current conditions, requires an expression for c_w. We know it will be lower than c_m to provide the required diffusion flux towards $x = 0$, see Figures 7.5 and 7.6. Finding an expression for c_w will be the goal of the MEA problem, which we will consider in the next section.
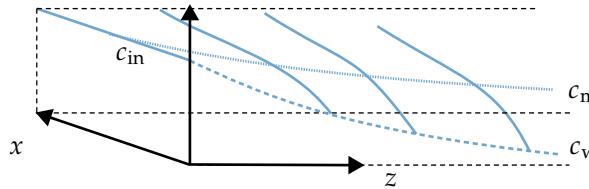
Figure 7.6: An example concentration profile showing that the cup-mixing average concentration c_m and wall concentration c_w decreases in the streamwise z-direction. The concentration profile also decreases towards $x = 0$, where reactants enter the porous electrode or gas diffusion layer. The wall concentration c_w is always lower than c_m providing the necessary diffusion flux.

7.5.3 MEA problem

Here, we focus on modelling the porous electrode, or the diffusion and catalyst layer, in the case of gaseous reactants. Figure 7.7 depicts these layers as resistances in series, sandwiched between the flow channel and the membrane. As nothing reacts in the diffusion layer, the reactant flux from the flow channel can be equated to that over the diffusion layer and to that entering the catalyst layer. Equation (7.16) is then extended to 🧑

$$\frac{j}{nF} = -l\langle w\rangle\frac{dc_m}{dz} = \text{Sh}\frac{D\,(c_m - c_w)}{l} = \text{Sh}_d\frac{D\,(c_w - c_r)}{l} = \hbar c_r = \text{S}\frac{Dc_m}{l}. \qquad (7.19)$$

Applying Fick's law $\frac{j}{nF} = D_d\frac{c_w - c_r}{l_d}$ over the diffusion layer gives

$$\text{Sh}_d = \frac{D_d}{D}\frac{l}{l_d}. \qquad (7.20)$$

In the third equation of Eq. (7.19), we assumed a reaction that is first order in the concentration c_r, with an integral reaction rate coefficient $\hbar$ (see Fig. 7.7).[10] As no reactants enter the membrane, the flux can be equated to this reaction flux.

---

[10]We introduce a new different symbol $\hbar = j/nFc_r$ here, because this rate-constant is an integral value for an entire reactive layer. Unlike the previously used local rate coefficient $k = N_\perp/c$, it does not multiply
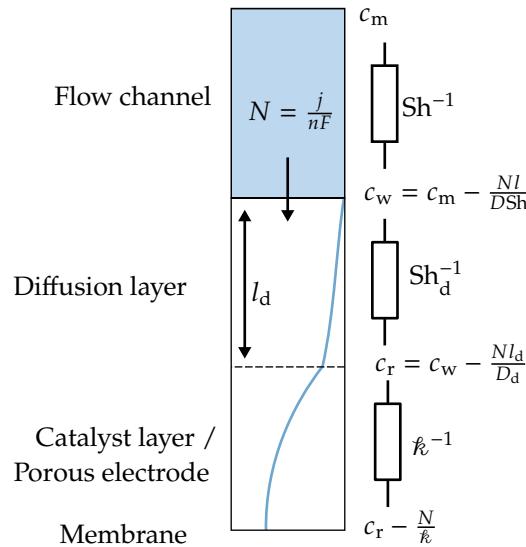
Figure 7.7: *A membrane electrode assembly (MEA) consists of from top to bottom: (sometimes) a diffusion layer in which reactants enter from the flow channel (in blue) with a concentration c_w and leave after a distance l_d to the porous electrode or catalyst layer (below the dotted line which is entered with a concentration c_r. The membrane is not shown and would be below this figure.*

The final expression of Eq. (7.19) is actually a definition of the *overall dimensionless transfer coefficient* S. Since the preceding equations constitute three linear equations for the three unknowns c_w, c_r, and c_m, these may be solved for c_m to give 🏃

$$\frac{1}{\text{S}} = \frac{1}{\text{Sh}} + \frac{1}{\text{Sh}_d} + \frac{D}{\Bbbk l}. \tag{7.21}$$

The molar flux and concentration differences in Eq. (7.19) are analogous to the current density and potential differences in Ohm's law, Eq. 1.8, respectively. The dimensionless *mass transfer resistances* 1/Sh and 1/Sh$_d$ and the reaction resistance $D/\Bbbk l$ then form a series circuit as shown in Figure 7.8. The combined resistance $\frac{1}{\text{Sh}} + \frac{1}{\text{Sh}_d}$ is the overall resistance to mass transfer. When it is much smaller than $\Bbbk l/D$, mass transfer is 'limiting' and provides the dominant resistance. When, on the other hand, it is much smaller than $\Bbbk l/D$, the process is said to be *reaction-limited*.

Eq. (7.19) is solved by 🏃

$$\boxed{c_m = c_{in} e^{-\frac{\langle S \rangle D}{\langle w \rangle l^2} z},} \tag{7.22}$$

the local concentration c but a boundary value c_r and is defined relative to the electrode area rather than the solid-electrolyte interfacial area.

where the running-average value $\langle S \rangle (z) = \frac{1}{z} \int_0^z S\,\mathrm{d}z$. The only difference with Eq. (7.18) is that the dimensionless mass transfer coefficient for the channel, Sh, is replaced by the overall transfer coefficient S, which also includes the transfer resistance of the diffusion layer, if present, and that of the reaction.[11]

The current density will decrease as the concentration c_m depletes along the channel. Using Eq. (7.22), Eq. (7.19) gives the local current density as

$$j = nFS\frac{Dc_\mathrm{in}}{l}\mathrm{e}^{-\frac{\langle S \rangle D}{\langle w \rangle l^2}z}. \tag{7.23}$$

Upon integrating this, or Eq. (7.19), the channel average flux $\langle j \rangle \equiv \frac{1}{h}\int_0^h j\,\mathrm{d}z$ gives again Eq. (7.15):

$$\langle j \rangle = nF\langle w \rangle l\left(c_\mathrm{in} - c_\mathrm{m}\right) = nF\langle w \rangle l c_\mathrm{in}\left(1 - \mathrm{e}^{-\frac{\langle S \rangle D}{\langle w \rangle l^2}z}\right), \tag{7.24}$$

where in the second expression, we inserted Eq. (7.22).

7.5.4 Cell model
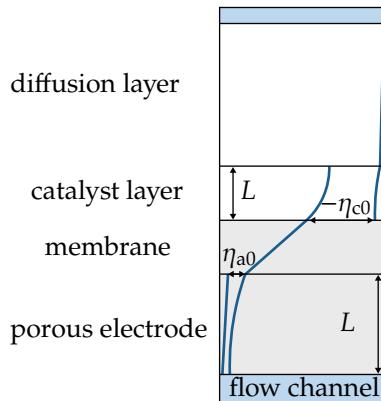
Figure 7.8: The potential profiles throughout a cell at a given streamwise coordinate z. Reactants diffuse from the cathode flow channel (in blue) through a diffusion layer into the catalyst layer. In this example, the anode consists of a porous electrode.

Besides its effect on conversion, reactant depletion in the streamwise direction also impacts the current distribution and energy efficiency, which we will investigate here. In the case of first-order Tafel kinetics, Eq. (3.B.104) gives

---

[11]In the absence of mass-transfer limitations, $S = \mathcal{k}l/D$ and, with $\mathcal{k} = aLk$, Eq. (7.3) is retained upon replacing l with L. Similar to Eq. (7.7), Eq. (7.22) gives an optimal channel length $h_\mathrm{opt} = \frac{\langle w \rangle l^2}{\langle S \rangle_\mathrm{out} D}\ln\left(\frac{1}{1-X}\right)$.

$$j = \mathcal{E} \frac{c_r}{c_{in}} J_* e^{\eta_0/b}. \tag{7.25}$$

Here $\eta_0 = \eta_{a0} > 0$, or $-\eta_{c0} > 0$ is the activation overpotential of the electrode under consideration at the membrane-electrode interface at $x = 0$, see Fig. 7.8.

Adding the second and third expression in Fig. 7.7, and using Eq. (7.21), gives 🏹

$$c_r = c_m \left(1 - \frac{j}{j_{lim}} \right) \quad \text{where } j_{lim} = nF \frac{1}{\frac{1}{Sh} + \frac{1}{Sh_d}} \frac{D c_m}{l}. \tag{7.26}$$

Equations (7.25) and (7.26) combine to give

$$\eta_0 = b \ln \left(\frac{j/\mathcal{E} J_*}{\frac{c_m}{c_{in}} \left(1 - \frac{j}{j_{lim}} \right)} \right). \tag{7.27}$$

This relation is similar to Eq. (4.27), which we derived for a battery particle. Also in that case, diffusion and reaction resistances acted in series.

In chapter 3 on porous electrodes, we derived approximate expressions for the effectiveness factor $\mathcal{E}$ in the presence of diffusion limitations or ohmic limitations that we can insert here.[12]

In case of no ohmic limitations but strong diffusion limitations, Eq. (3.59) gives for the effectiveness factor $\mathcal{E} = \frac{nFDc_r}{jL}$. Inserting in Eq. (7.27) and using Eq. (7.26), gives 🏹

$$\eta_0 \approx 2b \ln \left(\frac{j/\sqrt{J_D J_*}}{1 - \frac{j}{j_{lim}}} \right), \tag{7.28}$$

where $j_D = nFDc_m/L$ is based on the channel cup-mixing concentration. Note that the entire activation overpotential, including the concentration overpotential $b \ln \left(\frac{1}{1 - \frac{j}{j_{lim}}} \right)$, is doubled.

A schematic overview of the potential and overpotential profiles is shown in Figure 7.8. The flow channel-electrode or flow channel-diffusion layer interface can be assumed to have a spatially constant electrostatic potential, because it is connected to a well-conducting current collector, see Fig. 7.4. The constant cell voltage can thus be taken as the difference between the potentials in the two current collectors. From Eq. (3.39), we can write the overpotential at the electrode-membrane interface as[13]

$$\eta_{a0} - \eta_{c0} = V_{eq} - V_{cell} - jAR. \tag{7.29}$$

---

[12]Equation (3.67), for combined ohmic and diffusion limitations will not be applicable in case of the 'back-fed' electrode considered here, where reactants and ions come from opposite sides because it was derived for the case that reactants and ions come from the side. In the case of strong ohmic limitations, a low effectiveness factor gives a narrow reaction zone on the membrane side of the electrode. This will add approximately the electrode thickness L to l to determine the limiting current.

[13]This is always positive, noting that $\eta_c < 0$. Under galvanic conditions $V_{eq} > V_{cell} > 0$ and under electrolytic conditions $V_{cell} < V_{eq} < 0$.

We will consider a single porous electrode and neglect the activation overpotential of the other electrode.[14] The overpotential may vary throughout the electrode/catalyst layer. Therefore, as discussed in the porous electrode chapter 3, the overpotential value at the interface with the membrane, where the ionic current comes from, should be used.

Note that since AR, V_{cell} and V_{eq} are constant, Eq. (7.29) implies that, while the reactant concentration goes down and the concentration potential goes up in the stream-wise z-direction, $\eta + jAR$ remains constant. This forces the current density $j(z)$ to go down with increasing z.

Using Eqs. (7.27) and (7.22) in Eq. (7.29) gives

$$V_{cell} \approx V_{eq} - \left(ARj + b \ln \left(\frac{j/J_*\mathcal{E}}{1 - j/j_{lim}} \right) + \frac{\langle S \rangle D}{\langle w \rangle l^2} z \right), \tag{7.30}$$

where Eqs. (7.25) and (7.21) combine to give for the reaction rate coefficient $k = j/nFc_r$

$$S = \left(\frac{1}{Sh} + \frac{1}{Sh_d} + \frac{nFDc_{in}/l}{\mathcal{E}J_* e^{(V_{eq} - V_{cell} - jAR)/b}} \right)^{-1}. \tag{7.31}$$

The quasi-two-dimensional cell model of Eq. (7.30) succinctly summarises many of the concepts we considered in this book. The equilibrium potential V_{eq} and ohmic losses ARj, considered in chapter 1. The concentration overpotential $b \ln (c_m/c_r) = -b \ln (1 - j/j_{lim})$ studied in chapter 2 is extended in this chapter to include both the flow channel and diffusion layer, using the series expression of Eq. (7.26). The porous electrode activation losses $b \ln (j/J_*\mathcal{E})$ were discussed in chapter 3. The final term represents a second part of the concentration overpotential $b \ln (c_{in}/c_m)$ and is due to the decrease in the cup-mixing average concentration c_m with increasing z. The approximately exponential decrease in concentration results in a linearly increasing overpotential.[15]

Providing you with an understanding of this and similar equations has been a major aim of this book. In general, this equation has to be solved numerically for $j(z)$. Section 7.3 considers the simplest case, in which there are concentration variations only in the z-direction.

7.6 Summary

- Due to the large aspect ratio of most flow channels, streamwise diffusion can be neglected, so that a 1D+1D modelling approach allows solving the *along the*

---

[14]Or assume it can be linearised and included in AR. Alternatively, in case the anode and cathode happen to have the same thickness and exchange current density, their Tafel slopes may be added in b so Eq. (7.27) represents the combined activation losses.

[15]This is similar to the second term in Eq. (4.29), which we derived for a battery particle. Here, a concentration that linearly decreases in time led to a linearly increasing activation overpotential.

channel and MEA problems independently. Along the channel, the reactant cup-mixing concentration decreases, viz. $\frac{dc_m}{dz} = -\text{Sh}\frac{D(c_m - c_w)}{l^2 \langle w \rangle}$ (7.16) so that $c_m = c_{in}e^{-\frac{\langle S \rangle D}{\langle w \rangle l^2} z}$, (7.22), where the dimensionless transfer resistance $\frac{1}{S} = \frac{1}{\text{Sh}} + \frac{1}{\text{Sh}_d} + \frac{D}{kl}$ (7.21) consists of the sum of those in the channel, diffusion layer, and due to the reaction, respectively.

- Inserting this exponentially decreasing solution into the expression for the electrode activation overpotential gives, see Eqs. (7.27) and (7.30):

$$\eta_0 = b \ln \left(\frac{j/\mathcal{E}J_*}{\frac{c_m}{c_{in}} \left(1 - \frac{j}{j_{lim}}\right)} \right) = b \ln \left(\frac{j/J_*\mathcal{E}}{1 - \frac{j}{j_{lim}}} \right) + \frac{\langle S \rangle D}{\langle w \rangle l^2}z, \qquad (7.32)$$

gives a concentration polarisation that linearly increases along the channel.

- For a flow channel in between the electrode and membrane, a larger width increases the ohmic drop, while a smaller width increases the power dissipated in pumping. At constant conversion, an optimal gap width $l_{opt} = (36\mu\kappa)^{(1/4)}\sqrt{\frac{l}{nFc_{in}X}}$ (7.11) is obtained.

- In a flow-through electrode, neglecting streamwise diffusion, the porous electrode advection-reaction equation $W\frac{dc}{dz} = \frac{aj_\perp}{nF}$ gives an exponentially decreasing concentration $c(z) = c_{in}e^{-\frac{ka}{W}z}$ in case of constant first-order reaction rate coefficient k.

Exercise 7.1

Often in electrolysers and flow batteries it will be beneficial to have a high conversion, in order to avoid the process of separating the products from the reactants, or reach a low state of charge in a single pass, respectively.

a. Assuming a constant overall transfer coefficient S = 0.5, what value for the dimensionless (Graetz) number $\frac{\langle w \rangle l^2}{hD}$ gives a conversion of 99 %?

b. What is the ratio between the average current density and the current density near the inlet in this case?

c. If a flow field is used of length $h = 0.1$ m and channel thickness l=1 mm, and the diffusivity $D = 2 \cdot 10^{-5}$ m^2/s. What flow velocity is required to reach this desired conversion?

d. What is the conversion that can be reached if a serpentine flow field is used instead, with n turns so that the total channel length becomes nh. Give your answer in the form of a formula containing only n as a free parameter

Exercise 7.2

Consider a unitised regenerative fuel cell running on hydrogen and air ($f = 21$ % oxygen by volume, assume ideal gas behaviour) at 80 °C and atmospheric pressure. The electrode dimensions h and w are both 10 cm, giving an area $A = hw = 100$ cm^2. A current $I = 100$ A is used so that the current density $j = I/A = 1$ A/cm^2. For a $l = 1$ mm wide single cathode flow channel without a flow field, what average inlet air velocity $\langle w \rangle$ is minimally required to supply enough oxygen?

Exercise 7.3

a. Assuming $\frac{\partial c}{\partial z}$ is constant, give the solution $c(x)$ of Eq. (7.12) for $c(x)$ for a parabolic laminar flow profile $w(x) = 6\langle w \rangle \frac{x}{l}\left(1 - \frac{x}{l}\right)$ using the boundary conditions $\frac{\partial c}{\partial x} = 0$ at $x = l$ and $c = c_w$ at $x = 0$.

b. Calculate the cup-mixing concentration $c_m \equiv \frac{1}{\langle w \rangle l}\int_0^l wc\,\mathrm{d}x$ in terms of c_w and $\frac{\partial c}{\partial z}$.

c. Assuming $\frac{\partial c}{\partial z} = \frac{\partial c_m}{\partial z}$, calculate the Sherwood number from Eq. (7.16).

Exercises 7.4-7.15

Fill in the missing steps in the main text, indicated by the symbol ⚐.

Appendices *

7.A *Dimensionless transport equations*

The Sherwood number of Eq. (7.A.33) can also be defined as the ratio between dimensionless flux and dimensionless concentration difference as

$$\text{Sh} \equiv \frac{\bar{\bar{j}}_l}{\bar{c}_m - \bar{c}_w}, \tag{7.A.33}$$

where $\bar{c} = c/c_{\text{in}}$ and

$$\bar{\bar{j}}_l = \frac{j}{J_l} \quad \text{where } J_l = nF\frac{Dc_{\text{in}}}{l}, \tag{7.A.34}$$

is relative to the characteristic diffusion driven flux $nFDc_{\text{in}}/l$. Note that J_l is similar to J_D used in porous electrode modelling, except that the length scale used is that of the flow channel, l, rather than that of the catalyst layer, L. Introducing also a non-dimensional axial coordinate $\bar{z} = z/h$, running from zero at the inlet to 1 at the outlet, we can write Eq. (7.16) as

$$\text{Gz}\frac{d\bar{c}_m}{d\bar{z}} = -\bar{\bar{j}}_l = -\text{Sh}\left(\bar{c}_m - \bar{c}_w\right), \tag{7.A.35}$$

where the *Graetz* number

$$\text{Gz} \equiv \frac{\langle w \rangle l^2}{hD}, \tag{7.A.36}$$

is similar to the *Péclet* number[16] $\text{Pe} = \frac{\langle w \rangle l}{D}$, but with a different length scale l^2/h rather than l. From Eq. (7.12), the characteristic magnitude of the advection and diffusion terms are $\langle w \rangle c/h$ and Dc/l^2 respectively. The Graetz number provides the ratio of these two characteristic values. If $\text{Gz} \gg 1$, advection dominates. If $\text{Gz} \ll 1$, transverse diffusion dominates.

Non-dimensionalising all concentrations with c_{in}, Eq. (7.19) becomes

$$\bar{\bar{j}}_l = \text{Sh}\left(\bar{c}_m - \bar{c}_w\right) = \text{Sh}_d\left(\bar{c}_w - \bar{c}_r\right) = \bar{k}\bar{c}_r \equiv S\bar{c}_m, \tag{7.A.37}$$

---

[16]This is in turn similar to the *Reynolds number* $\text{Re} = \frac{\langle w \rangle l}{\nu}$, but with the diffusivity D instead of the kinematic viscosity $\nu = \mu/\rho$.

where the dimensionless reaction rate constant is

$$\bar{k} = \frac{k}{D/l}.$$

(7.A.38)

Using Eq. (7.A.37) in Eq. (7.A.35) gives the dimensionless form of Eq. (7.A.39) as

$$\text{Gz}\frac{d\bar{c}_m}{d\bar{z}} = -\bar{j}_l = -S\bar{c}_m.$$

(7.A.39)

This is solved by

$$\bar{c}_m = e^{-\frac{\langle S \rangle}{\text{Gz}}\bar{z}}.$$

(7.A.40)

Eqs. (7.A.40) and (7.A.39) give the flux at $\bar{z}$ as

$$j = j_l S e^{-\frac{\langle S \rangle}{\text{Gz}}\bar{z}}.$$

(7.A.41)

Upon integration, the channel average flux $\langle \bar{j}_l \rangle \equiv \int_0^1 \bar{j}_l d\bar{z}$ reads

$$\langle \bar{j}_l \rangle = \text{Gz}\left(1 - \bar{c}_m^{out}\right) = \text{Gz}\left(1 - e^{-\frac{\langle S \rangle_{out}}{\text{Gz}}}\right).$$

(7.A.42)

This is the dimensionless version of Eq. (7.24). Finally, the conversion in dimensionless notation reads

$$X \equiv 1 - \bar{c}_m^{out} = 1 - e^{-\frac{\langle S \rangle_{out}}{\text{Gz}}}.$$

(7.A.43)

7.B *Dimensionless cell model*

With $j/nF = kc_r$ and Eq. (7.A.38), Eq. (7.25) gives with $\bar{\eta}_0 = |\eta_0|/b$:

$$\bar{k} = \frac{\mathcal{E}J_* e^{\bar{\eta}_0}}{J_l}.$$

(7.B.44)

Non-dimensionalising Eq. (7.29) gives, neglecting as in the main text one of the overpotentials

$$\bar{\eta}_0 = \Delta\bar{V} - \bar{j}_l\bar{R},$$

(7.B.45)

where $\bar{R} = \frac{ARj_l}{b}$ and $\Delta\bar{V} \equiv \frac{|V_{eq} - V_{cell}|}{b}$. With Eqs. (7.A.38) and (7.B.44), Eq. (7.21) becomes

$$\frac{1}{S} = \frac{1}{\text{Sh}_{tot}} + \frac{1}{\frac{J_*}{J_l}e^{\Delta\bar{V} - \bar{j}_l\bar{R}}},$$

(7.B.46)

where we define $\frac{1}{\text{Sh}_{tot}} \equiv \frac{1}{\text{Sh}} + \frac{1}{\text{Sh}_d}$. This can then be used in Eq. (7.A.39) to give

$$\text{Gz}\frac{d\left(\bar{j}_l/S\right)}{d\bar{z}} = -\bar{j}_l.$$

(7.B.47)

In general, this ordinary differential equation has to be solved numerically.

Chapter 8

Additional exercises

Exercise 8.1 constitutes an exercise encompassing knowledge from various chapters. Exercises 8.2-8.8 constitute a 3-hour closed-book practice exam of 40 points in total. You may use only the formula sheet. The answers are provided from page 203 onwards. A pass requires a minimum of 22 points.

Exercise 8.1

In this additional exercise we will build up an analytical cell model, including much of the theory discussed in the various chapters. For definiteness, let's consider a water electrolyser, for making hydrogen. Try initially to answer the questions without referring to the text. Towards the end of the questions, you may have to look up a few things.

a. Give an expression for the cell voltage as a function of current density j, considering only the equilibrium potential V_{eq} and the area-specific resistance AR.

b. When the resistance is purely due to the finite conductivity κ of a liquid electrolyte in a microporous separator with thickness l and porosity ϵ, give an expression for AR, assuming Bruggeman's relation.

c. What term has to be added to the cell voltage model when we include the activation overpotential of a smooth planar anode (neglecting that of the cathode) satisfying Tafel kinetics with Tafel slope b and exchange current density j_*?

d. If the same anode material is turned into a porous electrode with volumetric surface area a and thickness L, what is the effective total exchange current density?

e. If the effectiveness factor of the electrode is $\mathcal{E}$, give an expression for the activation overpotential.

f. Give an expression for the effectiveness factor $\mathcal{E} \ll 1$ in terms of the Thiele modulus M.

g. If the effective electrode conductivity is κ, give an expression for the Thiele modulus in case of ohmic limitations inside the electrode.

h. In alkaline water electrolysis, per electron, one hydroxide ion (OH^-) is produced at the cathode and consumed at the anode. Consider two electrodes with a gap of thickness d in between them, in the presence of a large surplus of supporting electrolyte that does not contain OH^-. Give an expression for the limiting current density due to the finite concentration c and diffusivity D of OH^-.

i. Also give an expression for the limiting current density in the absence of a supporting electrolyte.

j. The oxygen evolution reaction at the anode is first-order in the OH^- concentration. Assuming Tafel kinetics on a planar electrode, provide an expression for the concentration overpotential in terms of the limiting current density j_{lim}.

k. Due to the supporting electrolyte, ohmic limitations inside the electrode have disappeared, while diffusion limitations due to OH^- exist. Assuming the concentration at the 'entrance' of the porous electrode is c, give an expression for $\mathcal{E} \ll 1$.

l. Give also the expression for $\mathcal{E} \ll 1$ in the absence of a supporting electrolyte when the charge transfer coefficient of the oxidation reaction is α.

m. Assume that the anode consists of porous particles with small nanopores that cause the hydroxide diffusivity to decrease to a value D. If the current is switched on at $t = 0$ and we approximate the resulting concentration profile with a region of constant concentration gradient, give an expression for the limiting current density.

n. In a conventional 'gap electrolyser' configuration, a flow parallel to the electrodes in the gap of thickness d between anode and cathode is added to remove the heat of the reaction. When the flowing electrolyte contains a contaminant that reacts very rapidly at the anode surface, and the Sherwood number can be approximated by a constant Sh, after what distance is its concentration reduced by a factor $1/e = 0.368$?

o. If the majority of the losses are due to ohmic resistance in the cathodic gap, at what height do hydrogen bubbles decrease the current density by 1% compared to that at the bottom? Assume that Bruggeman's relation holds and that the liquid velocity can be neglected.

Exercise 8.2

Air with $f = 21$ vol% oxygen at ambient conditions enters a PEM fuel cell cathode flow channel of thickness $l = 1$ mm and length $h = 0.1$ m, sufficiently long to approximate the channel Sherwood number with a constant value Sh = 2.7. The hydrophobic diffusion layer between the flow channel and the catalyst layer has a thickness $l_d = 0.6$ mm, porosity $\epsilon_d = 0.8$, and squared tortuosity $\tau^2 = 1.7$, and can be assumed to be devoid of water. The molecular diffusion coefficient of oxygen in air $D_m = 2 \cdot 10^{-5}$ m^2/s. The catalyst layer consists of wet agglomerates of approximately equal and spherical shape, with radius $R = 10^{-6}$ m, and an effective oxygen diffusion coefficient $D_{agg} = 10^{-9}$ m^2/s. The dissolved oxygen concentration will be $c = 1$ mol/m^3 at the agglomerate surface. The fuel cell is operated at 1 A/cm^2.

a. (3) Neglecting all other transport losses, give a rough approximate value for the effectiveness factor $\mathcal{E}_a$ inside an agglomerate near the diffusion layer.

b. (3) What average airflow velocity $\langle w \rangle$ in the flow channel will be minimally required to supply enough oxygen to sustain the cathodic reaction?

c. (5) Assuming $\langle w \rangle$ is much larger than the value calculated in the previous question, give an estimate of the limiting current density j_{lim}.
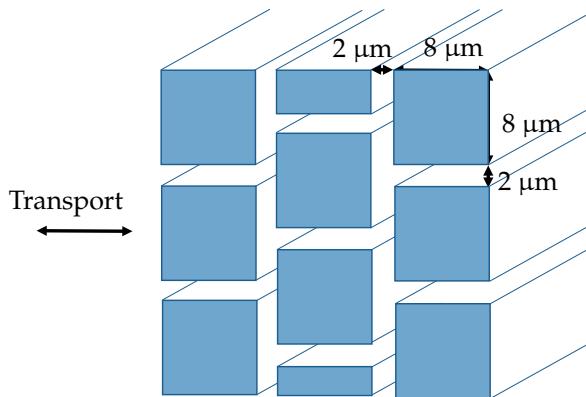
Exercise 8.3

Consider the medium schematically depicted above. The indicated pattern extends into *all three* directions x, y, and z indefinitely. The transport takes place in the horizontal direction as indicated by the arrow.

a. (1) Use its definition to estimate the tortuosity of this porous medium in the indicated transport direction.

b. (1) Calculate the porosity of this material.

c. (1) Using your values at a) and b), does this medium satisfy Bruggeman's relation numerically? Why (not)?

d. (1) In case of transport normal to the indicated transport direction, into the paper, parallel to the beam-like structure, can a higher, lower, or equal diffusion flux be obtained with equal concentration gradient and why?

e. (1) Calculate the volumetric surface area a of this material.

Exercise 8.4

A special type of membraneless alkaline water electrolyser consists of two parallel plates, a very small distance $l = 0.01$ mm apart, so that it can operate with low ohmic losses even at low electrolyte concentrations. Assume an electrolyte with concentration $c = 0.1$ M, consisting of potassium cations K^+ with diffusion coefficient $D_+ = 2 \cdot 10^{-9}$ m^2/s and hydroxide anions OH^- with diffusion coefficient $D_- = 5 \cdot 10^{-9}$ m^2/s. The effects of electrode end-effects, water consumption, flow, and bubbles can be neglected, so you can consider a one-dimensional concentration profile between $x = 0$ at the anode and $x = l$ at the cathode. Assume ambient conditions.

a. (5) Give the steady-state electrolyte potential drop $\Delta\phi$ between the electrodes when operating at a current density j, equal to 80 % of the limiting current density j_{lim}. *Hint: the total amount of electrolyte will remain constant after switching on the current. Consider what will be the relation between cation concentration and potential.*

b. (4) A monovalent supporting electrolyte, with anion and cation diffusivities both equal to 10^{-9} m^2/s, is added to give a supporting electrolyte concentration of 1 M. What will be the approximate electrolyte potential drop $\Delta\phi$ over the gap between the electrodes at a current density equal to 80 % of the *new* limiting current density?

Exercise 8.5

a. (2) Explain under what assumptions the moving reaction zone model and the single particle model for porous battery electrodes can be used, respectively. Illustrate your explanation with quantitative criteria in the form of formulas.

Exercise 8.6

Consider a planar anode for a redox reaction, satisfying concentration-independent Butler-Volmer kinetics with an exchange current density j_* and charge transfer coefficient α.

a. (1) Under what condition(s) does the activation overpotential η increase linearly with increasing current density? Provide criteria in the form of a formula, or formulas.

b. (2) Derive an expression for the equivalent area-specific resistance AR in this case.

Exercise 8.7

Consider a high-pressure zero-gap electrolyser with electrolyte flowing up near the electrodes due to natural convection of bubbles produced in the reaction, and back through a downcomer after removal of these bubbles. The laminar flow in between the electrodes of height h and their respective current collectors at a distance l can be assumed to be laminar and described by the planar Hagen-Poiseuille equation.

a. (4) At very low gas fractions, neglecting bubble slip, and friction in the down-comer, the superficial liquid recirculation velocity W_l near the electrodes increases proportional to the square root of the current density j. Why? Use formulas to explain your answer.

b. (2) Will viscous friction in the downcomer increase or decrease the gas fraction near the electrodes? Why?

Exercise 8.8

a. (4) Consider a porous anode of volumetric surface area a and thickness L whose pores are filled with a supporting electrolyte, giving an effective ionic conductivity κ. The oxidation reaction under consideration satisfies concentration-independent Tafel kinetics with a Tafel slope b and exchange current density j_*. Give an approximate equation for the activation overpotential η_0 at the location where the ionic current leaves the electrode, as a function of current density j, including the effect of ohmic limitations. Use it to derive that for high current densities the effective Tafel slope $\frac{\partial \eta_0}{\partial \ln j} = j \frac{\partial \eta_0}{\partial j}$ equals $2b$. Also, explain, in words, the reason for this Tafel slope doubling.

Answers to exercises

CHAPTER 1

1.1: -0.3 V

1.2: $\frac{V_{eq}-\eta}{2AR}$

1.3:

  a. $b_a + b_c$

  b. $\frac{1}{1/\alpha_a + 1/\alpha_c} = \frac{\alpha_a \alpha_c}{\alpha_a + \alpha_c}$

  c. $j_{*a}^{b_a/b} j_{*c}^{b_c/b} = j_{*a}^{\alpha/\alpha_a} j_{*c}^{\alpha/\alpha_c}$

1.4:

  a. $7.2 \cdot 10^3 \ \mathrm{m}^2$

  b. 63 %

CHAPTER 2

2.1:

  a. 4

  b. $4F\frac{Dc}{L}$

  c. $4F\frac{Dc}{L}\epsilon$

2.2:

  a. $\frac{D_a}{2(1-t_+)}$

  b. $\frac{j(1-t_+)}{FD}\left(\frac{L}{2} - x\right) + c$

  c. $2.1 \times 10^{-10} \ \mathrm{m}^2$

d. Minutes, yes, $\frac{2FDc/L}{1-t_+}$

2.3:

a. Dc/L
b. $c_0\frac{e^{ux/D}-e^{uL/D}}{1-e^{uL/D}}$
c. $N = N_0\frac{\text{Pe }e^{\text{Pe}}}{e^{\text{Pe}}-1}$
d. $3.2 \cdot 10^{-6}$ m/s

CHAPTER 3

3.1:

a. 0.4
b. 10 μm

3.2: 1.93 A/cm^2

3.3:

a. $|\eta| \ll \mathcal{R}T/F$
b. $\frac{\mathcal{R}T/F}{aLj_*}$
c. $j\frac{\sinh(\nu(1-x/L))}{\sinh(\nu)}$
d. $\frac{\tanh(\nu)}{\nu}$

3.4: 0.18 V

CHAPTER 4

4.1:

a. 12E
b. 600 kW

4.2:

a. $\frac{jL}{\kappa_s}$
b. $x_d = \frac{jt}{q}$
c. $\Delta\phi_d = \frac{jx_d}{\kappa_d} = \frac{j^2t}{q\kappa_d}$
d. $V_{eq} - \frac{jL_s}{\kappa_s} - \frac{j^2t}{q\kappa_d}$

e. $jV_{eq}t - \frac{j^2 L_s}{\kappa_s}t - \frac{j^3}{2q\kappa_d}t^2$

f. $\frac{V_{eq}\kappa_d}{j} - L_s\frac{\kappa_d}{\kappa_s}$

4.3:

a. 0.01 A

b. 75%

CHAPTER 5

5.1:

a. $\frac{4FDc_L}{L}$

b. 13 A/cm^2

c. $\frac{k_1 k_2}{k_1 + k_2}$

d. $\frac{nFc_L}{1/k + L/D}$

5.2:

a. $\frac{ds}{dx} = -\frac{\lambda}{p_t K}\left(\frac{\mu_g U_g}{(1-s)^3} + \frac{\mu U_l}{s^3}\right)$

b. $\frac{1}{1 + (\mu_g \mathcal{V}_{m,g}/2\mu \mathcal{V}_{m,l})^{1/3}} \approx 0.36$

5.3:

a. $3\varphi/R$

b. 0.12 A/cm^3

c. 0.49 V

d. $b\ln(10)$

e. 0.2

CHAPTER 6

6.1:

a. $\frac{nFl}{j\mathcal{V}_m}\frac{\varepsilon_c}{1 - \varepsilon_c/\varepsilon_{max}}(w_S + W_l)$

b. 0.7 m

6.2:

a. $\frac{jl}{\kappa_m(1-\varepsilon)^2}$

b. $\frac{jl}{\kappa_m}\left(1 + \frac{h}{z_c}\right)$

c. $\frac{j^2 l}{\kappa_m} \frac{h}{z_c} A$

d. $j \left(\frac{lh^2}{24\mu\kappa_m} \frac{V_m}{nF} \right)^{1/3}$

e. 2.4 m/s

6.3:

a. jV_m/nF

b. $jV_m z/nF\varepsilon w_g$

c. 4.3 mm

6.4:

a. $jL/\kappa\epsilon(1-\varepsilon)$

b. $jL/2b\kappa\epsilon(1-\varepsilon)$

c. 0.57

d. $b \ln\left(\frac{1}{1-\varepsilon}\right)$

CHAPTER 7

7.1:

a. 0.11

b. 0.215

c. 0.22 m/s

d. $1 - 0.01^N$

7.2: 7.6 cm/s

7.3:

a. $c_w + \frac{\langle w \rangle l^2}{hD} \left(\left(\frac{x}{l}\right)^2 \left(1 - \frac{x}{2l}\right) - 1 \right) \frac{\partial c}{\partial z} \frac{x}{l}$

b. $35/13 \approx 2.7$

CHAPTER 8

8.2:

a. To a rough approximation we can use $\mathcal{E}_a \sim \frac{1}{1+j/J_D}$, where $J_D = nFD_{agg}c/R$. With $n = 4$ electrons per oxygen molecule $j/J_D = 26$ so $\mathcal{E}_a \sim 0.04$.

b. Conservation of oxygen volume gives $\langle w \rangle = jh/nFlc_{in}$. Using the ideal gas law gives $c_{in} = fp/\mathcal{R}T = 8.6$ mol/m^3 so $\langle w \rangle = 0.3$ m/s.

c. The assumed high velocity makes the channel concentration approximately constant and equal to c_{in}. Adding the mass transfer resistances of the channel and diffusion layers in series gives $j_{lim} = \frac{nFc_{in}}{l_d/D_d + l/ShD_m}$. Using the effective diffusion layer diffusivity $D_d = D_m \epsilon_d / \tau^2 \approx 9.4 \cdot 10^{-6}$ m^2/s gives $j_{lim} = 4 \cdot 10^4$ A/m^2.

8.3:

a. Follow a path through the 'channels' in between the solid from left to right until the pattern repeats. This gives a horizontal distance $l = 20$ μm and a vertical translation of 5 μm up and 5 μm down so that the total distance covered is $l_{\parallel} = 30$ μm and $\tau = l_{\parallel}/l = 1.5$.

b. Considering a repetitive unit cell of cross-sectional area $A = 100$ μm^2 around one solid 'beam' of depth 1 m, the cross-sectional pore area $A_{pore} = 8$ μm $\times 4$ μm $= 32$ μm^2 + 4×1 μm^2 = 36 μm^2, so that $\epsilon = A_{pore}/A = 0.36$.

c. Bruggeman's approximation asserts that $\tau^2 \approx \epsilon^{-\mathcal{B}}$ with $\mathcal{B} = 1/2$ for a random arrangement of polydisperse spheres or $\mathcal{B} = 1$ for cylinders. Neither of these results describes our answers at (a) and (b), which is also not expected. We find $\mathcal{B} \approx 0.8$, somewhere in between the result for spheres and cylinders.

d. In the direction parallel to the beam-like structure, the tortuosity $\tau = 1$ is lower, giving a higher effective diffusion coefficient, which is proportional to ε/τ^2. Therefore, a higher diffusion flux can be obtained with equal concentration gradient.

e. The unit cell considered at (b) has a surface area $A_s = 4 \times 8$ μm $\times 1$ m $= 32 \cdot 10^{-6}$ m^2 and a volume $V = A \times 1$ m $= 1 \cdot 10^{-10}$ m^3 so $a = A_s/V = 3.2 \cdot 10^5$ m^{-1}.

8.4:

a. The immobile cation satisfies $N_+ = -D_+ \left(\frac{dc}{dx} + c \frac{F}{\mathcal{R}T} \frac{d\phi}{dx} \right) = 0$, where ϕ is the electrolyte potential. The concentration thus satisfies a Boltzmann distribution $c \propto e^{\frac{F}{\mathcal{R}T}\phi}$. Therefore, the potential drop $\Delta\phi = \frac{\mathcal{R}T}{F}\Delta \ln c = \frac{\mathcal{R}T}{F} \ln \frac{c_c}{c_a}$, with c_a and c_c the electrolyte concentration at the anode and cathode, respectively. Since there is no reaction between the electrodes, the concentration profile varies linearly in space. At the limiting current density $c_a = 0$ at the anode, where the OH$^-$ is consumed. At the cathode, where OH$^-$ is produced, $c_c = 0.2$ M in order to give the average $c = 0.1$ M. At 80 % of the limiting current density, the concentration gradient will be 80 % of that at the limiting current density so $c_a = 0.02$ M and $c_c = 0.18$ M and $\Delta\phi = 0.02$ V.

b. Due to the high supporting electrolyte concentration we use Ohm's law to write $\Delta\phi = \frac{j_{lim}l}{\kappa}$. The limiting current density reads $j_{lim} = \frac{nFD_-\Delta c}{l}$. With $n = 1$ electrons per OH$^-$ and $\Delta c = 0.2$ M this gives $j_{lim} = 7.7 \cdot 10^3$ A/m^2. The conductivity $\kappa = \frac{F^2}{\mathcal{R}T} \sum z_i^2 D_i c_i \approx 7.6$ S/m, using $z_i^2 = 1$ and $D_i = 10^{-9}$ m^2/s of the supporting electrolyte. This gives $\Delta\phi \approx 10^{-2}$ V.

8.5:

The assumption of a thin reaction layer in the moving reaction zone model requires an effectiveness factor $\mathcal{E} \ll 1$. Assuming Tafel kinetics, this requires a high current density $j \gg J_\kappa = \kappa b/L$, where κ is the effective electrode conductivity, b the Tafel slope, and L the electrode thickness.

The single particle model assumes a constant overpotential and reactant concentration throughout the electrode, so $\mathcal{E} \approx 1$. A constant overpotential requires $j \ll J_\kappa$. A constant reactant concentration requires $j \ll j_D = nFDc_0/L$, where n is the number of electrons per reactant molecule, D the effective reactant diffusivity, and c_0 the reactant concentration at the 'entrance' of the electrode. For a reacting binary electrolyte these two criteria are related.

8.6:

a. The exponentials in the concentration-independent Butler-Volmer equation $j_\perp = j_* \left(e^{\frac{\alpha F \eta}{\mathcal{R}T}} - e^{-\frac{(1-\alpha)F\eta}{\mathcal{R}T}} \right)$ can be linearized if their arguments $\frac{\alpha F \eta}{\mathcal{R}T}, \frac{(1-\alpha)F\eta}{\mathcal{R}T} \ll 1$. In this case $j_\perp$ becomes proportional to η.

b. Using the leading-order series expansion $e^x \approx 1 + x$ for $x \ll 1$ gives $j_\perp \approx \eta/AR$ with $AR = \frac{\mathcal{R}T}{j_* F}$.

8.7:

a. Neglecting friction in the downcomer, the hydrostatic pressure difference between top and bottom $\rho_l g h$ equals that between the top and bottom of the riser $\rho_l (1 - \langle\varepsilon\rangle) g h + 12\mu \frac{W_l}{l^2}$ so that $W_l = \rho_l \langle\varepsilon\rangle g h l^2/12$. Neglecting slip, at very low gas fractions $\varepsilon = \frac{W_g}{w_s + W_l + W_g/\varepsilon_m} \approx \frac{W_g}{W_l}$. We thus find that $W_l \propto \langle\varepsilon\rangle \propto W_g/W_l$ so $W_l \propto \sqrt{W_g} \propto \sqrt{j}$. Because the bubbles escape faster with increasing liquid velocity, the driving force for natural recirculation is reduced with increasing liquid flow.

b. Viscous friction in the downcomer decreases W_l. Since $\varepsilon \approx W_g/W_l$, this will increase the gas fraction. A lower liquid velocity will transport less gas, increasing the gas fraction near the electrodes.

8.8:

For concentration-independent Tafel kinetics $\eta_0 = b \ln \left(\frac{j}{\mathcal{E}J_*} \right)$ where $J_* = alj_*$ and, allowing for ohmic limitations, the effectiveness factor $\mathcal{E} \sim \frac{1}{1+2j/J_\kappa}$, with $J_\kappa = \kappa b/L$. Therefore,

$$\eta_0 \approx \begin{cases} b \ln \left(\frac{j}{J_*} \right) & j \ll J_\kappa \\ b \ln \left(\frac{j^2}{2J_* L\kappa b} \right) = 2b \ln \left(\frac{j}{\sqrt{2J_* L\kappa b}} \right) & j \gg J_\kappa \end{cases} \tag{8.1}$$

From these limits we see that the Tafel slope $\frac{\partial \eta_0}{\partial \ln j}$ doubles from b when $j \ll J_\kappa$ to $2b$ when $j \gg J_\kappa$.

At high current densities, the effectiveness factor $\mathcal{E} \approx 2\kappa b/jL$ becomes inversely proportional to j since ohmic resistance makes the activation overpotential η decrease over a penetration-depth inversely proportional to j. Therefore, the effectively available reactive surface area, or $J_* \mathcal{E}$, decreases inversely proportional to j, causing the doubling in the Tafel slope.

Chapter 9

Formula sheet

Constants

Faraday's constant $F = 96485$ C/mol, Elementary charge $e = 1.60217662 \cdot 10^{-19}$ C, Gas constant $\mathcal{R} = 8.314$ J/mol/K.

Formulas

$$j_\perp = nFN_\perp \qquad \text{Faraday's law} \qquad (1.19)$$

$$j_\perp = j_* \left(\frac{c_R}{c_{R,eq}} e^{\frac{\alpha_O F \eta}{\mathcal{R}T}} - \frac{c_O}{c_{O,eq}} e^{-\frac{\alpha_R F \eta}{\mathcal{R}T}} \right) \qquad \text{Butler-Volmer equation} \qquad (1.27)$$

$$V_{cell} = V_{eq} + \eta_c - \eta_a - \Delta\phi - \Delta V \qquad \text{Cell voltage} \qquad (1.35)$$

$$\boldsymbol{N}_i = c_i \boldsymbol{u} - D_i \left(\nabla c_i + z_i c_i \frac{F}{\mathcal{R}T} \nabla\phi \right) \qquad \text{Nernst-Planck} \qquad (2.25)$$

$$\kappa = \frac{F^2}{\mathcal{R}T} \sum z_i^2 D_i c_i \qquad \text{Ionic conductivity} \qquad (2.31)$$

$$D_a \equiv t_- D_+ + t_+ D_- = \frac{2D_+ D_-}{D_+ + D_-} \qquad \text{Ambipolar diffusivity} \qquad (2.42)$$

$$k_{m0} = \sqrt{\frac{\pi D}{4t}}, \quad k_{m\infty} = \frac{5D}{R} \qquad \text{Sand's / developed spherical} \qquad (2.57)$$

$$\frac{\partial \epsilon c}{\partial t} = -\nabla \cdot \boldsymbol{N} + aN_\perp \qquad \text{Conservation equation} \qquad (3.15)$$

$$\mathcal{E} \approx \frac{1}{1 + j/J_D + j/2J_\kappa} \qquad \text{Effectiveness factor} \qquad (3.67)$$

$$\frac{\langle C \rangle}{C_{\max}} = e^{-\int \frac{a_s}{1/k + 1/k_m} dt} \qquad \text{SOC single battery particle} \qquad (4.24)$$

$$p_c = p_l - p_g = \frac{2\gamma \cos \vartheta}{r} \qquad \text{Laplace} \qquad (5.5)$$

$$-\frac{dp_l}{dx} = \frac{\mu U_l}{Kk} \qquad \text{Darcy} \qquad (5.11)$$

$$\frac{ds}{dx} = -\frac{\lambda \mu}{p_t K} \frac{U_l}{s^3}, \qquad \text{Water saturation neglecting } p_g' \qquad (5.13)$$

$$F_D = 3\pi \mu d \left(w_g - w_l \right) \qquad \text{Stokes drag force} \qquad (6.4)$$

$$\varepsilon = \frac{W_g}{w_S + W_l + W_g/\varepsilon_m} \qquad \text{Bubble gas fraction} \qquad (6.9)$$

$$\Delta p_f = \frac{12\mu W_l}{l^2} h \qquad \text{Planar Hagen-Poiseuille} \qquad (7.9)$$

$$\eta_0 = b \ln \left(\frac{j/\mathcal{E} J_*}{\frac{c_m}{c_{in}} (1 - j/j_{\lim})} \right) \qquad \text{Activation overpotential} \qquad (7.27)$$

The porous electrode equations, associated with the characteristic current densities $J_D = nFDc_0/L$, $J_\kappa = b\kappa/L$, and $J_* = aLj_*$, respectively

$$c' = i/nFD \qquad (3.44)$$

$$\eta' = i/\kappa \qquad (3.45)$$

$$i' = aj_* \frac{c}{c_0} e^{\eta/b} \qquad (3.46)$$

Not in the formula sheet

The above equations represent a selection of what may be considered the most important formulas of this book. However, there are many relevant equations not given here, either because they are assumed to be widely known, should be learned by heart, or can be derived from the above. Here, we will consider these categories in some detail.

Assumed background knowledge

This category includes, for example, the area (πd^2) and volume ($\pi d^3/6$) of a sphere of diameter d, the ideal gas law ($p\mathcal{V}_\mathrm{m} = \mathcal{R}T$), Ohm's law ($\boldsymbol{i} = \kappa \boldsymbol{E}$), the buoyancy force ($F_\mathrm{b} = \rho g \mathcal{V}$) on a volume $\mathcal{V}$, a general conservation equation ($\frac{\partial c}{\partial t} = -\nabla \cdot \boldsymbol{N} + S$), an advection-diffusion equation ($\frac{\partial c}{\partial t} + \boldsymbol{u} \cdot \nabla c = D\nabla^2 c$), and the hydrostatic pressure $p_\mathrm{h} \approx (1-\epsilon)\rho g h$.

Memorise from this course

Things that should be memorised include the conventions and definitions discussed at the end of the Nomenclature section, or in section 4.1.2, the definition of an activation overpotential ($\eta = (E - \phi) - (E - \phi)_\mathrm{eq}$), Bruggeman's relation $\tau^2 \approx \epsilon^{-1/2}$ for spheres and $\tau^2 \approx \epsilon^{-1}$ for cylinders, some relations like $\alpha_O + \alpha_R = 1$, the definition of energy/voltage efficiency $\varphi_\mathrm{e} = V_\mathrm{cell}/V_\mathrm{eq}$ for Galvanic or $\varphi_\mathrm{e} = V_\mathrm{eq}/V_\mathrm{cell}$ for electrolytic cells, and:

$$\boldsymbol{i} = \sum z_i F \boldsymbol{N}_i \qquad \text{Ionic current density} \qquad (2.28)$$

$$\eta_0 = b\ln\left(\frac{j}{J_* \mathcal{E}}\right), \qquad \text{Overpotential entrance porous electrode} \qquad (3.42)$$

$$\mathcal{E} \approx \frac{1}{1 + j/J_D + j/2J_\kappa} \qquad \text{Effectiveness factor} \qquad (3.67)$$

$$N_\perp = kc^r \qquad \text{Reaction of order } r \qquad (1.20)$$

$$D = \frac{\epsilon}{\tau^2} D_\mathrm{m} \qquad \text{Effective transport coefficients} \qquad (3.11)$$

$$a = (1-\epsilon)\,a_\mathrm{s} \qquad \text{volumetric surface area} \qquad (3.4)$$

$$0 = -\nabla \cdot \boldsymbol{i} - aj_\perp \qquad \text{Charge conservation} \qquad (3.19)$$

Inserting Eq. (3.67) in Eq. (3.42) gives 🤾

$$\eta_0 \approx 2b\ln\left(\frac{j}{\sqrt{\frac{aj_*}{\frac{1}{2\kappa b} + \frac{1}{nFDc_0}}}}\right). \qquad (3.69)$$

The expression for the effectiveness factor can also be derived from the formulas in the formula sheet,[1] but it may be easier to memorise these. In the next paragraph we will consider a few relations that can be derived from the formula sheet, so do not necessarily have to be memorised.

Derive from the formula sheet 🖐

- From the Nernst-Planck equation (2.25), you can derive the advection-diffusion flux for neutral particles $N = uc - D\nabla c$, Ohm's law $i = -\kappa\nabla\phi$, the ionic conductivity $\kappa = \frac{F^2}{\mathcal{R}T}\sum_i z_i^2 D_i c_i$, and the Boltzmann distribution ($c \propto e^{-z_i F\phi/\mathcal{R}T}$ for a zero-flux ion i).

- From Faraday's and Fick's law $N_\perp = D\Delta c/\delta$, the limiting current density $j_{\lim} = D\Delta c/nF\delta$ follows. From Sand's equation (2.57) we find the mass transfer coefficient of a growing boundary layer as $k_m \equiv N_\perp/\Delta c = D/\delta = \sqrt{\pi D/4t}$, which is Eq. (4.19).

- The Stokes rise velocity $w_S = \rho g d^2/18\mu$ follows from equating $F_b = \rho g\pi d^3/6$ to the Stokes drag force, which is valid for $\rho w_S d/\mu \lesssim 1$.

- The state-of-charge of a battery particle $S_{oC} = \frac{\langle C\rangle}{C_{\max}}$ is provided, including $k_m = N_\perp/(C_{\max} - \langle C\rangle)$ for small and large values of time. The first-order reaction rate coefficient k can be obtained as $k = N_\perp/c = j_* e^{\eta/b}/nF$ for concentration-dependent Tafel kinetics.

- From the Butler-Volmer equation (1.27) you can derive the equations for concentration-independent Butler-Volmer kinetics $j_\perp = j_*\left(e^{\frac{\alpha_O F\eta}{\mathcal{R}T}} - e^{-\frac{\alpha_R F\eta}{\mathcal{R}T}}\right)$, symmetric kinetics $\eta = b\,\mathrm{asinh}\left(\frac{j_\perp}{2j_*}\right)$, Tafel kinetics $j_\perp = j_*\frac{c}{c_0}e^{\eta/b}$, and concentration-independent linear kinetics $j_\perp = j_* F\eta/\mathcal{R}T$ [2], and the Nernst equation $V_{eq} = \phi_{eq} + \frac{\mathcal{R}T}{F}\ln\left(\frac{k_O c_{R,eq}}{k_R c_{O,eq}}\right)$. For concentration-dependent Tafel expressions for the activation and concentration-overpotential follow as

$$\eta = b\ln\left(\frac{j}{j_*}\frac{c_{eq}}{c}\right) = b\ln\left(\frac{j}{j_*}\right) + b\ln\left(\frac{c_{eq}}{c}\right). \qquad (2.10)$$

---

[1] Taking the derivative of the porous electrode equation Eq. (3.B.96) with respect to x and inserting Eq. (3.B.97) gives $d^2 c/d\,(x/L)^2 = M^2 c$ with $M^2 = J_* e^{\eta/b}/J_D$ which for constant $M^2 \gg 1$ leads to the solution $c = c_0 e^{-Mx/L}$ with effectiveness factor $\mathcal{E} = \frac{\langle c\rangle}{c_0} = \frac{1}{M} = \frac{J_D}{j}$ using Eq. (3.42). For ohmic limitations $M \approx j/2J_\kappa$ and for a binary electrolyte $M = \frac{1+r+\alpha}{2}\frac{j}{J_D}$.

[2] Using for small arguments $e^{\frac{\alpha_O F\eta}{\mathcal{R}T}} \approx 1 + \frac{\alpha_O F\eta}{\mathcal{R}T}$ and using $\alpha_O + \alpha_R = 1$.

Index

Bibliography

[1] J. B. Allen and R. F. Larry. *Electrochemical methods fundamentals and applications*. John Wiley & Sons, 2001.

[2] L. G. Austin. Tafel slopes for flooded diffusion electrodes. *Transactions of the Faraday Society*, 60:1319–1324, 1964.

[3] A. J. Bard, L. R. Faulkner, and H. S. White. *Electrochemical methods: fundamentals and applications*. John Wiley & Sons, 2022.

[4] M. Z. Bazant. Electrochemical Energy Systems, Massachusetts Institute of Technology: MIT OpenCourseWare. https://ocw.mit.edu/. License: Creative Commons BY-NC-SA., 2014. Accessed: 2021.

[5] A. Bhadra and J. W. Haverkort. The optimal electrode pore size and channel width in electrochemical flow cells. *Journal of Power Sources*, 579:233240, 2023.

[6] P. M. Biesheuvel, S. Porada, and J. E. Dykstra. The difference between faradaic and non-faradaic electrode processes. *arXiv preprint arXiv:1809.02930*, 2018.

[7] E. L. J. Coenen and L. J. J. Janssen. Voidage of bulk solution in a tall vertical gasevolving cell. *Journal of applied electrochemistry*, 27(10):1143–1148, 1997.

[8] COMSOL Multiphysics (R) v. 6.2.

[9] Effective diffusivity in porous materials, application id: 978. https://www.comsol.nl/model/effective-diffusivity-in-porous-materials-978. Accessed: 2021.

[10] M. Doyle, T. F. Fuller, and J. Newman. Modeling of galvanostatic charge and discharge of the lithium/polymer/insertion cell. *Journal of the Electrochemical society*, 140(6):1526, 1993.

[11] N. Epstein. On tortuosity and the tortuosity factor in flow and diffusion through porous media. *Chemical engineering science*, 44(3):777–779, 1989.

[12] T. F. Fuller and J. N. Harb. *Electrochemical engineering*. John Wiley & Sons, 2018.

[13] J. W. Haverkort. A theoretical analysis of the optimal electrode thickness and porosity. *Electrochimica Acta*, 295:846–860, 2019.

[14] A. A. Kulikovsky. How important is oxygen transport in agglomerates in a pem fuel cell catalyst layer? *Electrochimica Acta*, 130:826–829, 2014.

[15] A. A. Kulikovsky. *Analytical modelling of fuel cells*. Elsevier, 2019.

[16] C. Lamy and P. Millet. A critical review on the definitions used to calculate the energy efficiency coefficients of water electrolysis cells working under near ambient temperature conditions. *Journal of power sources*, 447:227350, 2020.

[17] X. Liu, F. Peng, G. Lou, and Z. Wen. Liquid water transport characteristics of porous diffusion media in polymer electrolyte membrane fuel cells: A review. *Journal of Power Sources*, 299:85–96, 2015.

[18] T. Maoka. Electrochemical reduction of oxygen on small platinum particles supported on carbon in concentrated phosphoric acid—i. effects of platinum content in the catalyst layer and operating temperature of the electrode. *Electrochimica acta*, 33(3):371–377, 1988.

[19] N. Nagai, M. Takeuchi, T. Kimura, and T. Oka. Existence of optimum space between electrodes on hydrogen production by water electrolysis. *International journal of hydrogen energy*, 28(1):35–41, 2003.

[20] R. Parsons. General equations for the kinetics of electrode processes. *Transactions of the Faraday Society*, 47:1332–1344, 1951.

[21] M. L. Perry, J. Newman, and E. J. Cairns. Mass transport in gas-diffusion electrodes: a diagnostic tool for fuel-cell cathodes. *Journal of the Electrochemical Society*, 145(1):5, 1998.

[22] D. G. L. Plett. ECE4710/5710: Modeling, Simulation, and Identification of Battery Dynamics, 2019.

[23] T. Shinagawa, A. T. Garcia-Esparza, and K. Takanabe. Insight on tafel slopes from a microkinetic analysis of aqueous electrocatalysis for energy conversion. *Scientific reports*, 5(1):13801, 2015.

[24] P. J. Sides. Phenomena and effects of electrolytic gas evolution. In *Modern aspects of electrochemistry*, pages 303–354. Springer, 1986.

[25] K. Stephan. *Heat transfer in condensation and boiling*. Springer, 1992.

[26] M. E. Suss, K. Conforti, L. Gilson, C. R. Buie, and M. Z. Bazant. Membraneless flow battery leveraging flow-through heterogeneous porous media for improved power density and reduced crossover. *RSC advances*, 6(102):100209–100213, 2016.

[27] W. Tiedemann and J. Newman. Maximum effective capacity in an ohmically limited porous electrode. *Journal of The Electrochemical Society*, 122(11):1482, 1975.

[28] B. Tjaden, S. J. Cooper, D. J. L. Brett, D. Kramer, and P. R. Shearing. On the origin and application of the bruggeman correlation for analysing transport phenomena in electrochemical systems. *Current Opinion in Chemical Engineering*, 12:44–51, 2016.

[29] C. W. Tobias. Effect of gas evolution on current distribution and ohmic resistance in electrolyzers. *Journal of the Electrochemical society*, 106(9):833, 1959.

[30] B. Vijayaraghavan, D. R. Ely, Y.-M. Chiang, R. García-García, and R. E. García. An analytical method to determine tortuosity in rechargeable battery electrodes. *Journal of The Electrochemical Society*, 159(5):A548, 2012.

[31] F. Y. Zhang, X. G. Yang, and C. Y. Wang. Liquid water removal from a polymer electrolyte fuel cell. *Journal of the Electrochemical Society*, 153(2):A225, 2005.

Electrolysers, Fuel Cells and Batteries:
Analytical modelling

J.W. Haverkort

Electrochemical engineering deals with electrochemical devices like electrolysers, fuel cells, and batteries. While several excellent books exist in this long-standing and still growing field, their focus is usually on chemistry or phenomenology. In this textbook, we focus on mathematical modelling of the physical phenomena involved. Instead of resorting to numerical modelling, the aim is to derive simplified analytical models that maximise understanding.

Porous electrodes, ion mass transport, and multiphase flow are central themes in this book. Examples include modelling the water saturation in a fuel cell diffusion layer, the gas fraction and current distribution in an alkaline water electrolyser, the potential distribution in a binary electrolyte inside a porous battery electrode, and the concentration distribution in the flow channel of a redox flow battery. This makes for a diverse, challenging, and stimulating journey, for both students and researchers.

J.W. (Willem) Haverkort
Delft University of Technology, Faculty of Mechanical Engineering

After a PhD in computational nuclear fusion plasma physics, I worked for several years in industry, researching a wide variety of fluid flow phenomena. Presently, I am an associate professor at Delft University of Technology. In our group we work on theoretical, computational, and experimental research, increasingly centred around multiphase flow aspects of alkaline water electrolysis.

TUDelft